

**THESE DE DOCTORAT DE
L'UNIVERSITE PIERRE ET MARIE CURIE**

Spécialité

Paléocéanographie / Paléoclimatologie

Ecole Doctorale des Sciences de l'Environnement (ED 129)

Présentée par

M. Nicolas Duprey

Pour obtenir le grade de

DOCTEUR de l'UNIVERSITÉ PIERRE ET MARIE CURIE

Sujet de la thèse

**Variabilité climatique de deux périodes clés de l'Holocène,
c. 7000-6000 et 3500-2500 années BP, dans le Pacifique Sud-Ouest
à partir de l'analyse d'archives biocarbonatées.**

Directeurs de thèse : G. Cabioch et D. Cardinal

Co-directrice de thèse : C.E. Lazareth

Soutenue le **25/10/2012**, devant le jury composé de :

C.E. Lazareth
M. Elliot
Y-M. Paulet
T. Corrège
A. Juillet-Leclerc
A. Saliot

co-Directrice de thèse
Rapporteur
Rapporteur
Examineur
Examineur
Examineur



" Ce manuscrit ne représente que quelques grammes de papier... mais beaucoup de travail, que je voudrais dédier à mes parents, Marie-France et Jean-Louis. Merci à tous les deux pour votre soutien, votre réconfort, vos encouragements et pour cette vie voyageuse, pleine de belles surprises, qui m'ont amenées sur ces pas et fait de moi quelqu'un d'heureux. Parmi ces surprises, il y avait toi, qui m'attendais dans une petite ville au bord de la mer... et qui m'a suivi (à moins que ce ne soit l'inverse) dans pas moins de 5 pays et sur 4 continents pour continuer cette aventure pas banale qui est la nôtre !! Merci Marielle pour ton soutien sans faille, tes critiques au vitriol, tes encouragements et ta patience pendant ces trois ans. Je m'envolerai bientôt vers l'empire du milieu, pour continuer, avec toi, cette belle histoire... "

Remerciements, Acknowledgements, Agradecimientos

Joie, surprise, jubilation, déception, colère (rare...), ennui, partage (beaucoup !), exaltation, curiosité (indispensable), tristesse, émerveillement et enthousiasme (surtout !) se mélangent entre les lignes de ce manuscrit. Trois années, qui composent une tranche de vie bien remplie, se cachent dans les feuilles de cette thèse... En écoutant bien il est d'ailleurs possible d'entendre, au creux de ces pages, quelques uns des milliers de fou-rires, exclamations, chuchotis, ronflements (?), discussions, hurlements (de rage, de joie...) et rires qui ont été échangés avec de nombreuses personnes lors de ces trois années de thèse. Ce sont ces personnes que je voudrais remercier ici. Des photos mettant en scène quelques-unes de ces personnes « sur le terrain », se sont glissées entre les pages de ce manuscrit en guise de remerciements...

Cette thèse n'est pas seulement le résultat de mon travail, mais également de celui de mes encadrants, Guy Cabioch, Claire Lazareth et Damien Cardinal. J'ai une pensée affectueuse pour Guy qui aurait sûrement été très heureux de lire ces lignes, je le remercie pour sa gentillesse et pour m'avoir fait partager ses connaissances et m'avoir fait rêver et rire avec ses anecdotes de bourlingueur du Pacifique-Sud. Je remercie Damien pour ses conseils lors de la rédaction du manuscrit de thèse, en particulier pour m'avoir appuyé dans mon choix de présenter ce manuscrit sous forme d'articles scientifiques. Je tiens tout particulièrement à remercier Claire avec qui nous avons formé une équipe de choc pendant ces trois années, malgré les déceptions (ah ! la scléro...) et une vieille histoire de trocas fluorescents... Merci d'avoir été à l'écoute, disponible et présente... sans avoir été omniprésente ! Merci de m'avoir fait confiance et d'avoir supporté mon entêtement (... j'ai fait des progrès, non ?). Merci pour ton soutien et ta réactivité dans le rush final de la rédaction de ce manuscrit !

Je voudrais également remercier les membres de mon jury Mary Elliot, Yves-Marie Paulet, Thierry Corrège, Anne Juillet-Leclerc et Alain Saliot d'avoir pris le temps d'examiner mon travail malgré leur emploi du temps chargé. Merci également à Anne Lorrain et encore à Thierry Corrège d'avoir accepté de faire partie de mon comité de thèse, ainsi que pour votre accompagnement et pour vos précieux conseils.

Esa increíble aventura empezo en el 2008 cuando entré en su oficina del CIMAR por primera vez...Desde este momento, he sido catapultado en el maravilloso mundo corallino : ayer Cahuita, Matapalo, isla del Coco, ahora Nueva Caledonia...y tal vez mañana, Hong Kong !! ¡Una locura ! Gracias a usted, gracias por haber confiado en mi !! Gracias Carlos Jiménez.

Merci Hans Hartmann grâce à qui j'ai pu m'envoler pour le Costa Rica il y a quelques années... si j'avais su que cela me mènerait là.... ! A San José, La Rochelle ou Banyuls, on finira bien par se croiser un de ces jours !

Un très grand merci à John Butscher pour ta gentillesse, ton soutien infaillible et ton efficacité lors de mon séjour à Nouméa. Merci de m'avoir fait partager ta connaissance de la mer et de la plongée lors de nos sorties dans le lagon. Et merci de m'avoir fait rêver avec tes récits de plongées et de chasse sous marine !

Merci à Cécile Dupouy, Christophe Maes, Christophe Menkes, Jean-Yves Panché, Léocadie Jamet et Philippe Gérard pour leur aide durant la calibration des bénomètres et leurs conseils. Merci à Marie Noël Segura et Catherine Hartmann pour leur aide lors de mes séjours à Nouméa. Et je n'oublie pas Jacob Waneux et Marcel Faubourg, merci pour votre bonne humeur !

Merci à Jean-Christophe Galipaud d'avoir rendu possible ce volet archéo qui me tenait tant à coeur. Merci à Richard Farman, directeur de l'Aquarium des Lagon de Nouméa, d'avoir mis à notre disposition un bassin à l'aquarium pour la calibration des bénomètres. Merci au propriétaire du *Ratua Island Resort* et à Rufino Pineda pour leur contribution à la collecte des fossiles de coraux et de bénomètres du Vanuatu.

Un très grand merci au staff de radiologie de l'hôpital Jean Verdier de prendre soin depuis plusieurs années de ces malades un peu particuliers que sont nos échantillons de bénitiers et de coraux. Merci pour votre disponibilité, pour vos explications et surtout ... pour votre patience ! Merci en particulier à Kitty Vadrot, Linda Eloi et Christophe.

Merci aux reviewers anonymes et aux autres pour la relecture des différentes parties de cette thèse : Henning Kuhnert, Ruth Gingold, Myrtille Pichon, Mercedes Mendez-Millan, ma mère, William Tran Ba, Marielle Dumestre, Gavin Dunbar, Anne Di Piazza, Tina Omuombo, Sandrine Caquineau.

J'ai beaucoup apprécié la disponibilité et la patience de Magloire Madeng-Yogo et de Joël Ughetto lors de mes doutes existentiels...isotopiques ! Merci à vous deux pour vos explications passionnées et passionnantes ! Un grand merci à Marie Balasse pour les analyses isotopiques de bénitiers.

Pour les longues heures passées à explorer ensemble les mystères de la densitométrie par rayons x, pour tes bonnes idées, ta patience, ton enthousiasme et pour le happy end de notre projet « radioactif », merci Hugues !! Je voudrais également remercier ma petite équipe de Bondy : Sandrine Caquineau, Florence Le Cornec, Jessica Cottet, Nathalie Teinturier, Mercedes MendeZ, Naznine Kalfane, Fethiye Cetin et Thierry Pilorge pour leur bonne humeur et pour m'avoir remonté le moral lors des moments difficiles ! Un remerciement particulier à Florence pour m'avoir initié aux « joies » de l'ICPMS. Merci aux bikers de l'IRD Eric Opigez et Rainer Zeiss pour nos longues discussions cyclistes... et autres ! Une pensée particulière pour Laurence Goury à qui j'ai fait rechercher les références biblio les plus improbables sans arriver à la coller ! Merci à Fatima pour tes encouragements !

Merci à mes compagnons de galère thèse Charlene, Antoine et Renato pour les bons moments passés ensemble et pour les discussions passionnées...scientifiques ou non ! *Gracias Renato ! Tu has sido un gran soporte durante esos tres años, y me has ayudado mucho en mi desarrollo científico, aprendí una cosa muy importante, no importa tanto la respuesta sino LA pregunta !*

Merci frangin d'avoir été là pour me remonter le moral et me changer les idées ! Cuidate timoun !

Un grand merci en vrac à tous ceux qui ont contribué de manière plus ou moins directe à cette thèse, en tout cas de manière certaine à des moments de franche rigolade et à des soirées mémorables durant ces trois ans. MERCI : les " anciens " de Noum's : Merci Will' pour ces moments d'anthologie sauveteurs @ Noum's ou @ Paname. Arthur, je n'oublierai pas ce trajet en 206 tunning sur la route à horaire, de nuit, en écoutant Wax Taylor – Florent, à quand la prochaine plongée dans la grotte-siphon de Yaté ? – Nico et à Florentin je n'oublierai pas votre accueil surprise au champagne (avec verres à pied !) à ma descente de l'avion à la Tontouta en plein milieu de la nuit !! Merci Amandine, Roman, Cath, Balder et Julie pour votre gentillesse et votre bonne humeur !! / les chevelux de La Rochelle : Ad' et Kv1, trois ans de thèse et tous tondu ! Heureusement que ça n'a pas duré un an de plus !! / Merci à Mays-Blia et à Tom pour votre générosité et ces bons moments passés autour d'un ti punch à la belle cabresse bien sûr !! Merci à mes colocos Barbara, Isaline et Myrtille pour leur soutien pendant ces deux ans, les filles : vous êtes GÉ-NI-ALES ne changez pas!! / *Thanks Craig Grove for your warm welcome at the NIOZ, I really enjoyed working with you ! You brought a HUGE contribution to this manuscript by teaching me how to use the climate explorer software!! THANKS!! I am indebted to Laura Lehnoff for her help in the Cahuita project, I will invite you to a (french) restaurant, I swear! Thanks Laura!* / les lofteurs de l'IRD, Gaby, Magalie, Christophe, la Tchambé Raid team du trophy entreprise 2010 : Adrien et Dik pour cette aventure décoiffante en décapotable (jaune !), en hélicoptère...et à pied bien sûr !! Merci aux pom'potes de Banyuls : Marine, Nico, Julie et Nath'. Merci aux étudiants de Bondy : Nico Pujol (un p'tit café ?), Tyna, Hassen, Caro, Nejma, Marianna, Douglas, Keila merci !!

Cette étude a été financée grâce au projet HOLBECO (INSU/IFREMER/IRD) et à l'équipe PALEOPROXUS du LOCEAN (IPSL/LOCEAN (UMR 7159), UPMC/CNRS/IRD/MNHN) et contribue à l'ANR EL PASO (n°2010 BLANC 608 01). Cette étude n'aurait pas été possible sans le soutien de la Province Sud de Nouvelle-Calédonie et de l'Aquarium des Lagons de Nouméa.

Résumé de la thèse

Cette étude a pour but de documenter le climat à deux périodes clés de l'Holocène à partir d'archives biocarbonatées.

Le potentiel du bémittier *Tridacna maxima* (géochimie et croissance) comme archive paléoclimatique a été montré. Des spécimens fossiles de cette espèce ont ensuite été utilisés pour documenter la variabilité climatique du Pacifique Sud-Ouest durant la transition Holocène inférieur-Holocène moyen (7.0-6.0 ka BP) et lors de la migration Lapita en Océanie Lointaine (3.5-2.5 ka BP) en complément d'enregistrements issus d'autres bémittiers et d'un corail massif *Porites sp.* Des enregistrements Sr/Ca de *Porites sp.* ont aussi été utilisés comme paléothermomètre.

A 7.0-6.0 ka BP, la phase de réchauffement postglaciaire était terminée et la marge sud-est de la Warm Pool était dans sa position actuelle. L'influence saisonnière de la SPCZ était plus faible qu'actuellement dans le Pacifique S.O., montrant que la SPCZ était située au nord de sa position actuelle. La variabilité El Niño Southern Oscillation (ENSO) était réduite de 20-30% par rapport à la variabilité actuelle.

La période coïncidant avec l'émergence de la culture Lapita, 3.6-3.4 ka BP, est caractérisée par un état moyen de type La Niña sur le Pacifique S.O avec une forte variabilité ENSO. Le climat a donc pu agir comme déclencheur et/ou favoriser la migration Lapita à 3.2-2.7 ka BP. En effet, des conditions climatiques instables peuvent favoriser le développement et l'expansion de populations nomades dépendantes des ressources marines, comme l'était la population Lapita.

Mots-clés: *Tridacna maxima*, Lapita, Holocène, variabilité climatique, Pacifique Sud-Ouest, ENSO.

Thesis abstract

This study aims to document the climate for two key periods of the Holocene from biocarbonated archives.

The giant clam *Tridacna maxima* was validated as a paleoclimatic archive. Fossil specimens of this species were used to document the climatic variability in the Southwest Pacific during the early mid-Holocene – 7.0-6.0 ka BP – and during the Lapita migration over Remote Oceania – 3.5-2.5 ka BP – in addition to $\delta^{18}\text{O}$ records from fossils specimens of giant clams *T. gigas*, *Hippopus hippopus* and fossils massive coral *Porites sp.* Records of Sr/Ca from *Porites sp.* corals also provided paleo-SST records.

The post glacial SST rise was completed at 7.0-6.0 ka BP and the southeastern edge of the WPWP was located in its current location. At that time the seasonal influence of the SPCZ over the SW Pacific was weaker than it is today as a result of the more northerly location of this structure. The El Niño Southern Oscillation (ENSO) variability was 20-30% weaker than today.

The period when the Lapita culture at 3.6-3.4 ka BP, was characterized by a La Niña-like climatic mean state in the SW Pacific. The Lapita migration-phase at 3.2-2.7 ka BP is coincidental with a strong ENSO variability supporting that the climate had a significant role in the Lapita migration. Indeed, unstable climate may have triggered and/or promoted the development and the expansion of nomad foraging population based on marine resources as the Lapita were.

Keywords: *Tridacna maxima*, Lapita, Holocene, climatic variability, Southwest Pacific, ENSO.

TABLE DES MATIÈRES

CHAPITRE I – INTRODUCTION GÉNÉRALE	13
I. CHANGEMENT CLIMATIQUE : UN CONSTAT INQUIÉTANT	14
II. L'HOLOCÈNE : UNE PÉRIODE CLÉ POUR ÉTUDIER LA VARIABILITÉ NATURELLE DU CLIMAT ..	14
III. L'OCÉAN PACIFIQUE : UNE ZONE STRATÉGIQUE POUR LA COMPRÉHENSION DU CLIMAT	16
IV. LE CONTEXTE CLIMATIQUE DU PACIFIQUE SUD-OUEST	18
V. VARIABILITÉ CLIMATIQUE AU COURS DE L'HOLOCÈNE	22
VI. ARCHIVES PALÉOCLIMATIQUES.....	24
VII. PROXIES.....	26
a. Utilisation du $\delta^{18}\text{O}$ chez les coraux et les bânitièrs.....	26
b. Utilisation du $\delta^{13}\text{C}$ et de la sclérochronologie chez les Bânitièrs.....	27
c. Utilisation du rapport Strontium/calcium chez les coraux.....	28
VIII. PROBLÉMATIQUES, OBJECTIFS ET ORGANISATION DE LA THÈSE.....	29
CHAPITRE II – CALIBRATION OF GIANT CLAM <i>TRIDACNA MAXIMA</i> GROWTH INCREMENTS THICKNESS AND SHELL $\delta^{18}\text{O}$ AS PROXIES OF SEA SURFACE TEMPERATURE: IMPLICATIONS FOR PALEOCLIMATOLOGY	33
I. INTRODUCTION.....	36
II. MATERIALS AND METHODS	37
a. <i>Tridacna maxima</i> specimens.....	37
b. Weekly monitoring	39
c. Age determination.....	39
d. Thick and thin section preparation.....	39
e. Sclerochronological profiles	40
f. Oxygen stable isotopes analyses.....	40
III. RESULTS	41
a. Age determination.....	41
b. Shell and growth pattern description	41
c. Temporal resolution of the growth increments.....	44
d. Description of the modern sclerochronological profiles.....	47
e. Relation between growth increment thickness and SST.....	50
f. Fossil sclerochronological record	50
g. Reconstruction of SST mean seasonal cycle from daily growth increments	51
h. Oxygen stable isotope data.....	52
IV. DISCUSSION.....	54
a. Shell deposition cycles in <i>Tridacna maxima</i>	54
b. SST reconstruction from daily growth increments thickness.....	55
c. Oxygen stable isotope as a proxy for SST	57
CHAPITRE III – EARLY MID-HOLOCENE SST VARIABILITY AND SURFACE-OCEAN WATER BALANCE IN THE SOUTHWEST PACIFIC	61
I. INTRODUCTION.....	64
II. CLIMATIC SETTING.....	65
III. MATERIALS AND METHODS.....	68
a. Fossil Material.....	68

b.	<i>Modern Material and SST/SSS Data Sets</i>	69
c.	<i>Dating and Preservation of the Fossil Samples</i>	69
d.	<i>Geochemical Sampling</i>	69
e.	<i>Geochemical Analysis and Data Processing</i>	70
IV.	RESULTS.....	71
a.	<i>Samples Dating and Preservation</i>	71
b.	<i>Coral Growth Stop</i>	72
c.	<i>Coral Records</i>	72
d.	<i>Giant Clam Records</i>	74
e.	<i>Seasonal variability from the coral records</i>	74
f.	<i>ENSO Variability</i>	75
V.	DISCUSSION.....	76
a.	<i>Post-Glacial SST Rise in the Southwest Pacific</i>	76
b.	<i>Short-Lived Contraction of the WPWP Southern Edge at 6.2–6.0 ka BP</i>	76
c.	<i>Early Mid-Holocene Surface-Ocean Water Balance</i>	77
d.	<i>ENSO Variability</i>	79
VI.	CONCLUSION.....	80

CHAPITRE IV – LAPITA MIGRATION AND CLIMATIC VARIABILITY: NEW INSIGHTS FROM GIANT CLAM AND CORAL GEOCHEMICAL RECORDS83

I.	INTRODUCTION.....	86
II.	SOUTHWEST PACIFIC CLIMATE.....	88
a.	<i>Main Climatic features</i>	88
b.	<i>Seasonal patterns</i>	89
c.	<i>Inter-annual variability</i>	90
d.	<i>Modern material and reef environments</i>	91
e.	<i>New Caledonia</i>	91
f.	<i>Vanuatu</i>	92
III.	ARCHAEOLOGICAL SITES AND MATERIAL.....	93
a.	<i>Archaeological material</i>	93
b.	<i>Dating and fossil samples preservation</i>	93
c.	<i>Geochemical sampling</i>	94
d.	<i>Geochemical analyses</i>	98
e.	<i>ENSO variability</i>	98
IV.	RESULTS.....	98
a.	<i>Samples dating and preservation</i>	98
b.	<i>Giant clams</i>	99
c.	<i>Corals</i>	101
d.	<i>$\delta^{18}\text{O}$ versus $\delta^{13}\text{C}$ scatter plot</i>	101
e.	<i>Modern giant clam baseline</i>	102
f.	<i>Fossil giant clams</i>	102
g.	<i>ENSO variability in New Caledonia</i>	103
V.	DISCUSSION.....	103
a.	<i>Interpreting the bulk geochemical records</i>	103
b.	<i>Giant clam isotopic signature : genus, environment or climate ?</i>	105
c.	<i>La Niña-like mean state ca. 3,600-3,400 years BP</i>	106
d.	<i>Strong ENSO amplitude ca. 3,200-2,700 years BP</i>	107
e.	<i>Relation between climate and Lapita migration</i>	107

CHAPITRE V – SYNTHÈSE.....	111
I. OBJECTIFS.....	112
II. POTENTIEL DU BÉNITIÈRE <i>TRIDACNA MAXIMA</i> COMME ARCHIVE PALÉOCLIMATIQUE.....	113
III. VARIABILITÉ CLIMATIQUE DURANT LA TRANSITION HOLOCÈNE INFÉRIEUR – HOLOCÈNE MOYEN : COMPARAISON DONNÉES / MODÈLES	114
IV. PEUPEMENT DE L’OCÉANIE LOINTAINE ~ 3000 ANS BP ET VARIABILITÉ CLIMATIQUE	122
V. QUELLES HYPOTHÈSES POUR LA MIGRATION LAPITA ?	124
VI. PERSPECTIVES.....	125
RÉFÉRENCES BIBLIOGRAPHIQUES	129
ANNEXE I – RÉFLEXIONS SUR LES ANALYSES GÉOCHIMIQUES DE BIO- CARBONATES (CORAL, COQUILLES).....	143
I. ETUDE DE REPRODUCTIBILITÉ DES ANALYSES ISOTOPIQUES	144
II. CAUSES POSSIBLES DES BIAIS SYSTÉMATIQUES POUR LES ANALYSES ISOTOPIQUES (CAS DU $\delta^{18}\text{O}$)	147
III. MATÉRIAUX DE RÉFÉRENCE : CLÉ DE VOÛTE DE LA GÉOCHIMIE.....	149
IV. CONCLUSIONS, PRÉCONISATIONS ET PERSPECTIVES.....	153
ANNEXE II – ARTICLE: DIGITAL CORRECTION OF COMPUTED X-RADIOGRAPHS FOR CORAL DENSITOMETRY	157



Face à face avec un corail multiséculaire. Cette colonie se trouve sur le site où ont été collectés les bémiers utilisés dans le chapitre I. Plongeur: John Butscher, Fausse Passe de Uitoé, Nouvelle-Calédonie, Pacifique Sud-Ouest. Septembre 2010. Crédit photo: N. Duprey.



Chapitre I – Introduction Générale

I. Changement climatique : un constat inquiétant

Le forçage anthropique sur le système climatique est maintenant un fait : les émissions de gaz à effet de serre, comme le dioxyde de carbone ou le méthane, liées aux activités humaines des 150 dernières années, contribuent au réchauffement climatique global. Le dernier rapport du groupe d'experts intergouvernemental sur l'évolution du climat, le GIEC (*IPCC*¹, en anglais), révèle que l'élévation du niveau moyen des mers, ainsi que la fonte des glaciers et des calottes glaciaires, sont étroitement liées au réchauffement du climat (Figure I-1). D'autre part, le réchauffement climatique modifie les systèmes physiques – par ex., recul du permafrost (Marchenko et al. 2007) – et biologiques – par ex., modification de la phénologie² d'espèces animales et végétales (Walther et al. 2002). Bien que les contributions respectives des actions anthropiques et de la variabilité climatique naturelle aux changements climatiques observés restent encore à établir, il est très probable que les activités humaines au cours des trois derniers siècles soient la cause principale de ces changements.

La compréhension du contexte climatique actuel nécessite donc d'étudier la variabilité naturelle du climat (i.e., exempte de forçage anthropique). La paléoclimatologie, c'est-à-dire l'étude des climats du passé, est un outil privilégié pour comprendre la variabilité climatique naturelle. Cet outil, qui permet de documenter le climat et les changements climatiques survenus dans le passé, améliore notre compréhension des paléoclimats et génère des bases de données qui sont utilisables par les climatologues et les modélisateurs. Ces bases de données sont des bancs d'essai pour les modèles climatiques et permettent de s'assurer que ceux-ci reproduisent fidèlement les variations climatiques passées avant de simuler l'évolution future du climat (Kohfeld and Harrison 2000).

Dissocier les forçages naturels des forçages anthropiques est primordial pour mieux appréhender les changements climatiques en cours, ainsi que leurs conséquences.

II. L'Holocène : une période clé pour étudier la variabilité naturelle du climat

La période Holocène, qui correspond au stade interglaciaire en cours et couvre les derniers 10 000 années BP³, est une période clé pour comprendre la variabilité climatique naturelle. En effet, à l'exception de l'insolation, les forçages climatiques naturels agissant durant l'Holocène étaient similaires à ceux opérants aujourd'hui (Wanner et al. 2011). La période Holocène présente des variations climatiques de faible amplitude, opérant à l'échelle millénaire, séculaire et interannuelle (par ex., Koutavas et al. 2006a; Tudhope et al. 2001; Wanner et al. 2011).

¹ IPCC : Intergovernmental Panel on Climate Change

² Étude de l'influence des climats sur les phénomènes biologiques saisonniers végétaux (feuillaison, floraison, etc.) et animaux (migration, hibernation, etc.). Encyclopédie Larousse

³ Before Present, avant le présent, où le présent est défini comme l'année 1950.

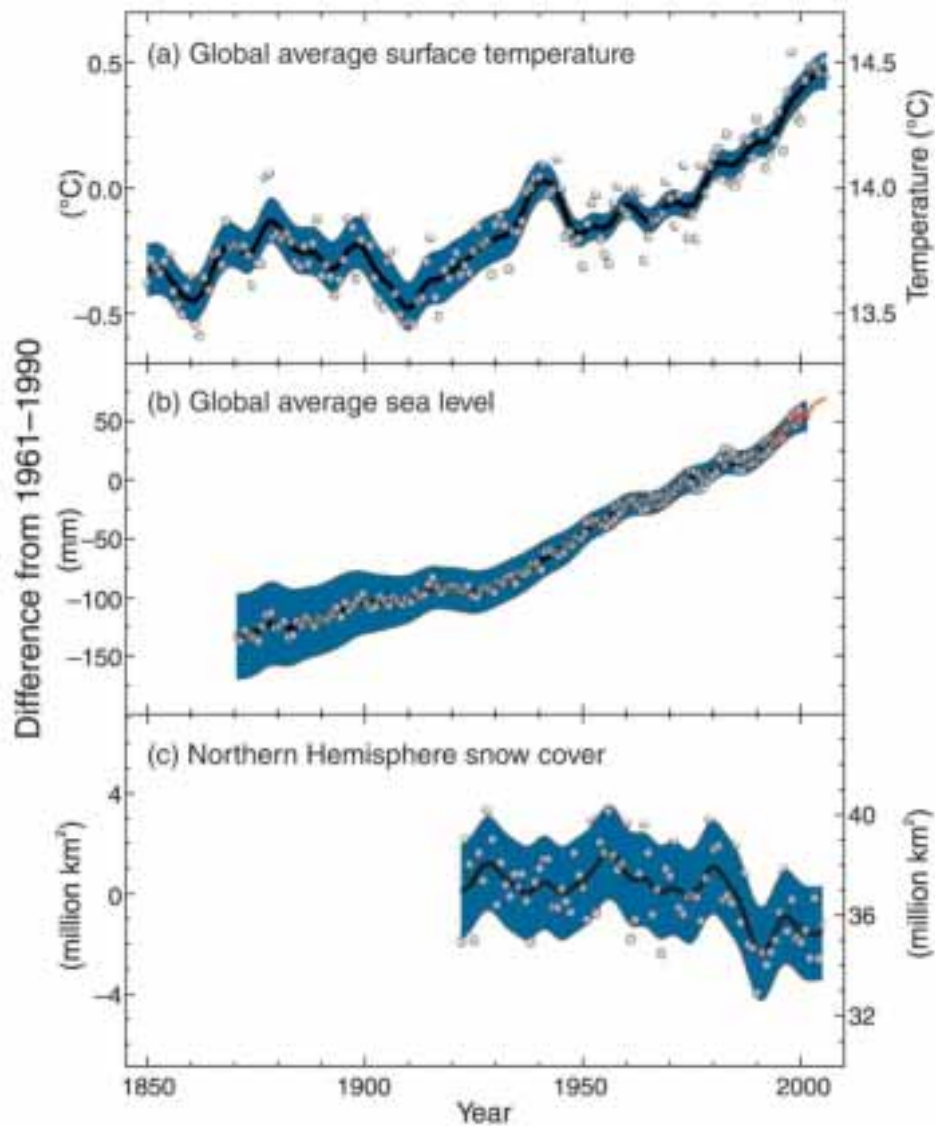


Figure I-1. *Tendance au réchauffement climatique et changements consécutifs observés aux cours des 150 dernières années. a - température moyenne à la surface du globe, b - niveau moyen de la mer à l'échelle du globe selon les données recueillies par les marégraphes (en bleu) et les satellites (en rouge) et c - couverture neigeuse dans l'hémisphère nord en mars – avril. Tous les écarts sont calculés par rapport aux moyennes pour la période 1961-1990. Les courbes lissées représentent les moyennes décennales et les cercles correspondent aux valeurs annuelles. Les zones bleues représentent les intervalles d'incertitude qui ont été estimés à partir d'une analyse poussée des incertitudes connues (a et b) et à partir des séries chronologiques (c). {Figure 1.1 – (Solomon et al. 2007)}.*

Figure I-1. *Global warming trend and related changes during the last 150 years a - global average surface temperature; b - global average sea level from tide gauge (blue) and satellite (red) data; and c - Northern Hemisphere snow cover for March-April. All differences are relative to corresponding averages for the period 1961-1990. Smoothed curves represent decadal averaged values while circles show yearly values. The shaded areas are the uncertainty intervals estimated from a comprehensive analysis of known uncertainties (a and b) and from the time series (c). {Figure 1.1, (IPCC – 2007) (Solomon et al. 2007)}.*

L'amplitude des variations du climat à l'Holocène est similaire aux changements climatiques en cours, bien que les variations climatiques ne soient pas influencées par un forçage anthropique. L'Holocène est donc une période privilégiée pour la compréhension des mécanismes régissant la variabilité climatique naturelle.

L'Holocène est une période clé pour la compréhension de la variabilité climatique naturelle. La variabilité climatique opérant durant cette période est similaire aux changements climatiques observés actuellement et le forçage anthropique y est absent.

III. L'océan Pacifique : une zone stratégique pour la compréhension du climat

Le système climatique global est régi par les fluctuations de taille et de localisation des structures climatiques tropicales de grande échelle. Parmi ces structures se trouvent les corps d'eau de mer chauds tropicaux (*warm pools* en anglais) et les zones de convergences intertropicales (*convergence zones* en anglais). L'océan Pacifique est le plus vaste du globe (166 241 700 km²) et les structures climatiques qui y sont associées – la West Pacific Warm Pool (WPWP⁴), la zone de convergence intertropicale (ITCZ⁵) et la zone de convergence du Pacifique Sud (SPCZ⁶) jouent un rôle central tant dans la circulation atmosphérique globale que dans celle des eaux de surface.

La WPWP s'étend sur plus de 15 millions de kilomètres carrés (27 fois la France) et sur une centaine de mètres de profondeur (Wyrski 1989). La WPWP est située à l'est de la ligne s'étendant des Philippines à la Papouasie Nouvelle-Guinée, excluant l'archipel Indonésien (Figure I-2a). Cette immense étendue d'eau, dont la température moyenne des eaux de surface (SST⁷) dépasse les 28°C, génère le flux convectif le plus intense au monde qui transfère de grandes quantités de chaleur et d'humidité dans l'atmosphère (Graham and Barnett 1995). La convection permanente qui a lieu au-dessus de la WPWP transfère l'énergie issue du rayonnement solaire au niveau de l'équateur vers les pôles, contribuant ainsi à réguler la température globale (Cane and Clement 1999). Les fortes pluies résultant de cette convection, associées à un régime de vent faible, contribuent à maintenir une salinité inférieure à 35⁸ dans la WPWP, ce qui entraîne une forte stratification des eaux de surface, qui est à l'origine de la stabilité de cette structure.

⁴ Afin d'éviter d'éventuelles confusions et pour assurer l'homogénéité du manuscrit, les sigles communément utilisés en océanographie – issus des termes en langue anglaise – ont été adoptés dans le reste du document.

⁵ Inter-Tropical Convergence Zone

⁶ Southwest Pacific Convergence Zone

⁷ Sea Surface Temperature

⁸ échelle PSS-78

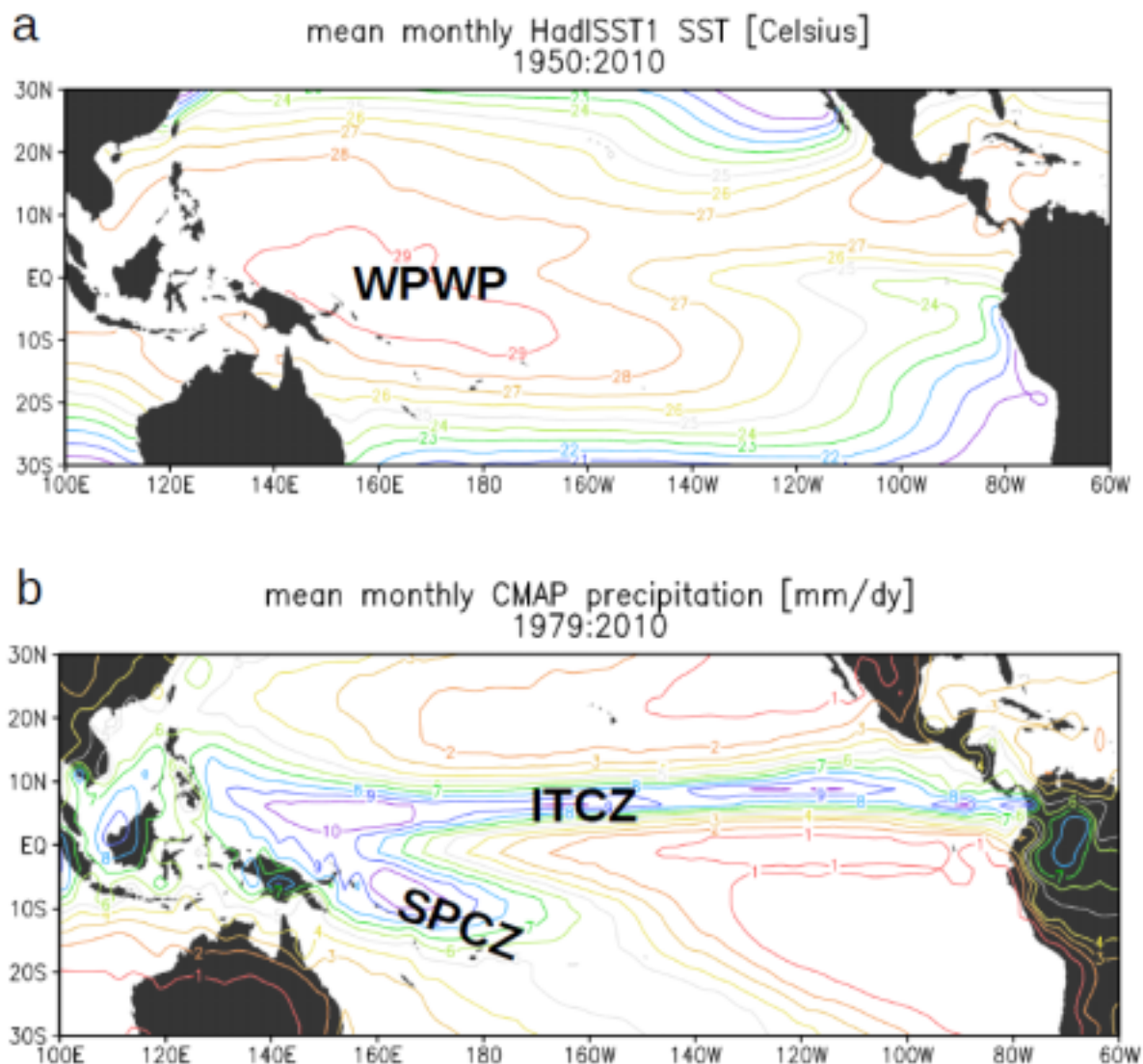


Figure I-2. Localisation des principales structures climatiques du Pacifique **a** - La West Pacific Warm Pool (WPWP). La carte représente la moyenne des températures de surface sur la période 1950-2010 HadISST1 (Rayner et al. 2003). La WPWP est délimitée par l'isotherme 28°C (orange), l'intervalle entre les isothermes vaut 1°C. **b** - La zone de convergence intertropicale (ITCZ en anglais) et la zone de convergence du Pacifique Sud (SPCZ en anglais). La carte représente les isohyètes en mm/jour (écart entre les isohyètes : 1 mm de pluie par jour) sur la période 1979-2010 CMAP (Xie and Arkin 1997). Modifié d'après Climate Explorer : <http://climexp.knmi.nl>.

Figure I-2. Main climatic structures of the Pacific area **a** - West Pacific Warm Pool. The map shows the mean Sea Surface Temperature for the period 1950-2010 HadISST1 (Rayner et al. 2003). The WPWP is delimited by the 28°C isotherm (shown in orange). **b** - Intertropical Convergence Zone (ITCZ) and the South Pacific Convergence Zone (SPCZ). The map shows the isohyets for the period 1979-2010 CMAP (Xie and Arkin 1997). Modified from Climate Explorer : <http://climexp.knmi.nl>.

Suivre les fluctuations de taille et de localisation de la WPWP est donc un enjeu majeur pour la compréhension et la prédiction du climat, et ce en particulier pour la marge Est de la warm pool qui occupe un rôle clé dans la dynamique de El Niño Southern Oscillation – ENSO⁹ (Picaut et al. 2001). Cependant, la température de surface seule ne suffit pas à définir la WPWP dont la masse d'eau possède des caractéristiques complexes (Le Borgne et al. 2002; Maes et al. 2010). Néanmoins, l'isotherme 28°C est communément considéré comme délimitant la WPWP (e.g., Godfrey et al. 1998; Ho et al. 1995; Wyrski 1989).

Ce sont en effet les masses d'eau dont la température de surface atteint la valeur seuil de 28°C qui sont le moteur du processus de convection atmosphérique (Waliser et al. 1993). La zone de convergence intertropicale (ITCZ, Figure I-2b) est une zone d'intense convection de chaleur et d'humidité associée à une pluviométrie très importante. Cette étroite ceinture nuageuse, qui entoure la Terre approximativement au niveau de l'équateur, correspond à la zone de confluence des Alizés des deux hémisphères et à la branche ascendante de la cellule de Hadley¹⁰ (Philander et al. 1996; Waliser and Gautier 1993; Xie and Saito 2001). Au niveau de l'océan Pacifique se trouve une autre structure convective, la zone de convergence du Pacifique Sud (SPCZ). Celle-ci se sépare de l'ITCZ au niveau de la Papouasie Nouvelle-Guinée et s'étend diagonalement dans l'hémisphère sud jusqu'à la Polynésie Française (Figure I-2b). La SPCZ est une des structures climatiques les plus importantes de l'hémisphère sud (Kiladis et al. 1989; Trenberth 1976; Vincent 1994). Dans le Pacifique Sud-Ouest, qui s'étend de la Papouasie Nouvelle-Guinée, à l'ouest, jusqu'aux Iles Fidji, à l'est, en incluant le Vanuatu et la Nouvelle-Calédonie, les variations de SST et de salinité des eaux de surface (SSS¹¹) à l'échelle saisonnière et interannuelle (ENSO) sont étroitement liées aux fluctuations de la marge sud-est de la WPWP et de la SPCZ (Gouriou and Delcroix 2002).

Le Vanuatu et la Nouvelle-Calédonie ont été choisis comme sites d'étude car le climat y est fortement influencé par la WPWP et la SPCZ.

IV. Le contexte climatique du Pacifique Sud-Ouest

Durant l'été austral (janvier, février, mars), la marge sud-est de la WPWP (isotherme 28°C) s'étend jusqu'au nord de la Nouvelle-Calédonie ce qui provoque un réchauffement de l'ensemble du Pacifique Sud-Ouest (Figure I-3a). En été, la SPCZ s'étend vers le sud-ouest, générant des précipitations (P) supérieures à l'évaporation (E) se traduisant par une baisse notable de la SSS sur l'ensemble de la zone (Figure I-3b). Durant l'hiver austral (juillet, août, septembre), la SST diminue suite à la migration de la WPWP vers le nord, qui déplace la marge sud-est de la WPWP au niveau des Îles Salomon (Figure I-3c). A cette période, la

⁹ voir section IV : Le contexte climatique du Pacifique Sud-Ouest

¹⁰ Circulation atmosphérique latitudinale entre la zone dépressionnaire située au niveau de l'équateur et les zones anticycloniques situées approximativement à 30°N et à 30°S.

¹¹ Sea Surface Salinity

SPCZ fusionne avec l'ITCZ dans la zone équatoriale, la balance évaporation / précipitation (E/P) est alors déplacée vers un déficit de précipitation, causant une augmentation de la SSS dans le Pacifique Sud-Ouest (Figures I-3c et I-4d).

Dans le Pacifique Sud-Ouest, l'été austral est caractérisé par une SST élevée et une SSS faible (précipitation > évaporation) et l'hiver austral est caractérisé par une SST faible et une SSS élevée (précipitation < évaporation).

Dans le Pacifique Sud-Ouest, les variations interannuelles de température de surface et des précipitations sont fortement influencées par ENSO (Figure I-4). Ce mode de variabilité climatique entraîne des échanges de chaleur entre l'océan et l'atmosphère à grande échelle ce qui influe sur la température globale (Cane 2005). ENSO se caractérise par l'alternance de phases El Niño (ou phases "chaudes") et La Niña (ou phases "froides") qui affectent le cycle hydrologique et sont associées à des événements climatiques extrêmes tels que : inondations, sécheresses, etc. (Cane 2005; Lyon 2004).

L'alternance des phases El Niño et La Niña s'effectue à l'échelle interannuelle avec une fréquence comprise entre 2.5 et 7 ans environ (Wang and Wang 1996). Lors d'événements El Niño, la WPWP se déplace vers le centre du Pacifique équatorial, entraînant avec elle le système convectif et les précipitations qui y sont associées (Rasmusson and Carpenter 1982). Le Pacifique Sud-Ouest connaît alors une légère baisse de température des eaux de surface, causée par la remontée de la thermocline, et une diminution importante des précipitations qui résulte du réarrangement des centres convectifs et de la circulation de Walker¹² (Delcroix and Picaut 1998; Picaut et al. 1996; Ropelewski and Halpert 1987).

Lors d'événements La Niña, le régime des Alizés est bien établi, grâce à une circulation de Walker renforcée, poussant ainsi les masses d'eau chaudes équatoriales vers l'ouest ce qui génère une convection anormalement forte au-dessus du Pacifique Ouest-Equatorial. Dans le Pacifique Sud-Ouest, la phase La Niña s'accompagne donc d'une hausse des températures de surface et surtout d'une augmentation importante des précipitations (Gouriou and Delcroix 2002).

Les variations de SST et de SSS sont des variables clés pour l'étude du cycle saisonnier ainsi que de la variabilité interannuelle (El Niño Southern Oscillation) dans le Pacifique Sud-Ouest.

¹² Circulation atmosphérique zonale entre la zone dépressionnaire située au niveau de la WPWP et la zone anticyclonique située dans le Pacifique Est tropical.

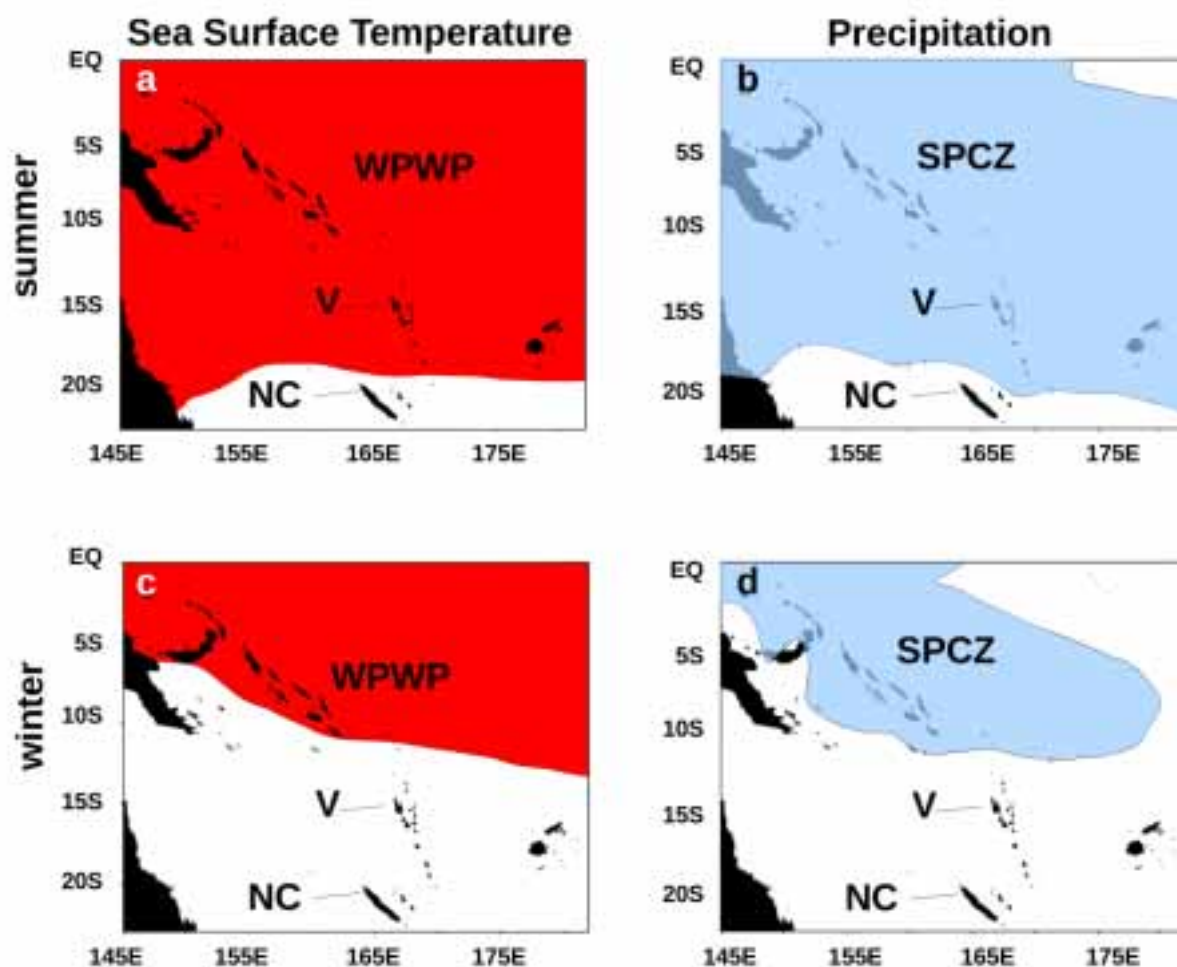


Figure I-3. Variations saisonnières des principales structures climatiques du Pacifique Sud-Ouest. La West Pacific Warm Pool (WPWP) est délimitée par l'isotherme 28°C (aire rouge – HadISST1 moyenne sur la période 1980-2011 (Raymer et al. 2006)). La zone de convergence du Pacifique Sud-Ouest (SPCZ) est délimitée par l'isohyète 6 mm de pluie par jour (aire bleue – CMAP 1980-2010 (Xie and Arkins, 1997)). **a et b** - Configuration des structures climatiques durant l'été austral (janvier, février, mars). **c et d** - Configuration des structures climatiques durant l'hiver austral (juillet, août, septembre). L'archipel du Vanuatu (V) et la Nouvelle-Calédonie (NC) sont représentés sur chaque carte. Modifié d'après Climate Explorer : <http://climexp.knmi.nl>. Cette carte est extraite du chapitre IV.

Figure I-3. Seasonal location of the main climatic features of the Southwest Pacific. The Western Pacific Warm Pool (WPWP) is delimited by the 28°C isotherm (red area - HadISST1 mean 1980-2011 period, (Raymer et al. 2006)). The South Pacific Convergence Zone (SPCZ) is delimited by the 6 mm.d⁻¹ isohyet (blue area - CMAP 1980-2010 (Xie and Arkins, 1997)). **a and b** - Austral summer settings (January, February, March) **c and d** - Austral winter settings (July, August, September). Vanuatu archipelago (V) and New Caledonia (NC) are located on each map. Modified from Climate Explorer : <http://climexp.knmi.nl>. This map is from chapter IV.

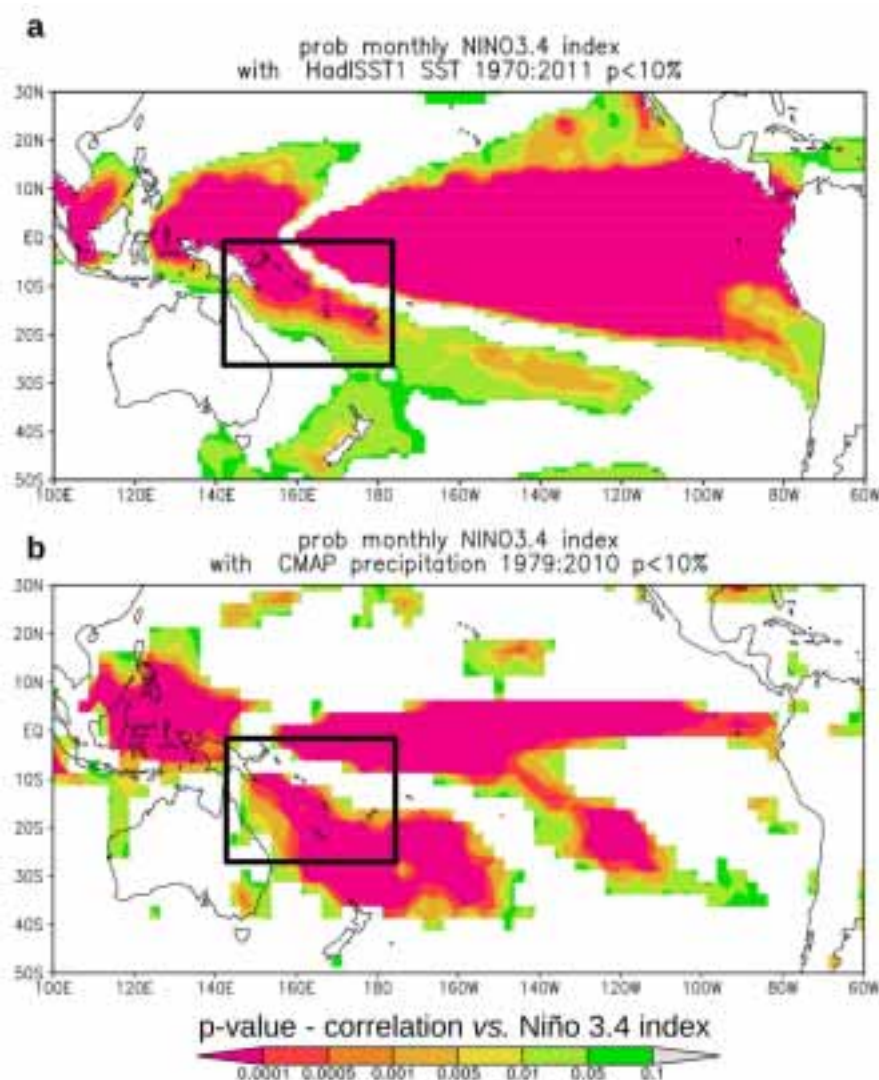


Figure I-4. Influence de El Niño Southern Oscillation (ENSO) sur les températures de surface et sur le régime des précipitations dans le Pacifique **a** - Degré de significativité (p-value) de la corrélation entre l'Index Niño 3.4 et la SST (HadISST1 moyenne sur la période 1970-2011 (Raymer et al. 2006)). **b** - Degré de significativité (p-value) de la corrélation entre l'Index Niño 3.4 et les précipitations (CMAP 1979-2010 (Xie and Arkins, 1997)). Le rectangle noir délimite la zone Pacifique Sud-Ouest (la zone d'étude). Modifié d'après Climate Explorer : <http://climexp.knmi.nl>.

Figure I-4. Influence of the El Niño Southern Oscillation on the SST and on the precipitation regime in the Pacific Ocean. **a** - Degree of significance (p-value) of the correlation between the El Niño 3.4 Index and the SST (HadISST1 mean 1970-2011 period, (Raymer et al. 2006)). **b** - Degree of significance (p-value) of the correlation between the El Niño 3.4 Index and the precipitations (CMAP 1979-2010 (Xie and Arkins, 1997)). The black rectangle shows the Southwest Pacific area (the study area). Modified from Climate Explorer <http://climexp.knmi.nl>.

V. Variabilité climatique au cours de l'Holocène

Les études paléoclimatiques montrent qu'une transition climatique s'est opérée entre l'Holocène inférieur et l'Holocène moyen aux alentours de 7.0-6.0 ka¹³ BP. Cette transition s'accompagne d'un changement d'état climatique moyen dans le Pacifique : l'état moyen de type La Niña opérant à l'Holocène inférieur laisse place à un état moyen de type El Niño (Figure I-5). Cette transition climatique s'accompagne de l'émergence de la variabilité ENSO actuelle (par ex., Gagan et al. 2004; Haug et al. 2001; Koutavas et al. 2006a; Moy et al. 2002; Rodbell et al. 1999; Sandweiss et al. 2001).

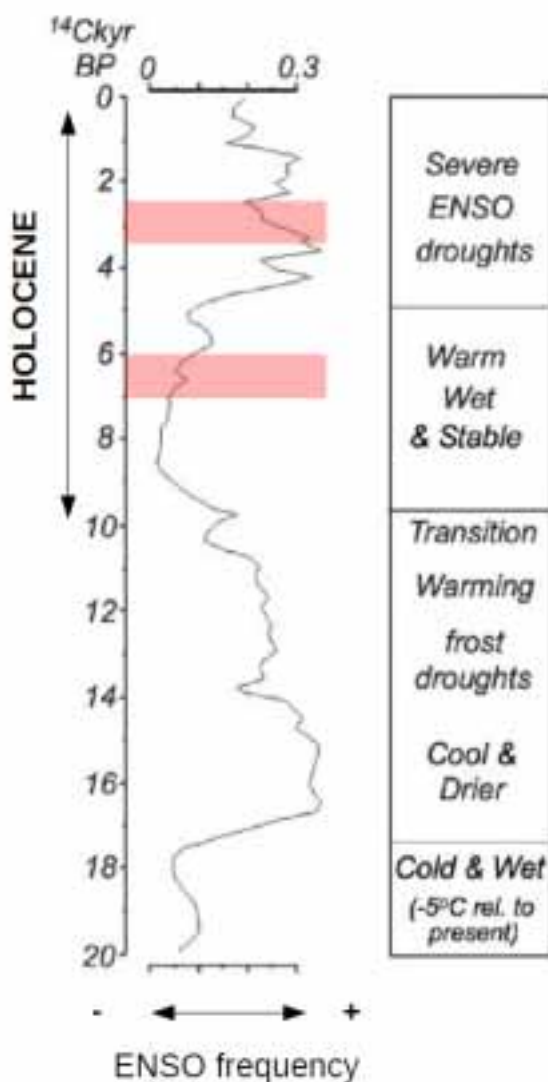


Figure I-5. Evolution de la fréquence des événements El Niño durant l'Holocène d'après des enregistrements de charbons provenant de Papouasie Nouvelle-Guinée (à gauche) et synthèse paléoclimatique (à droite). Les âges sont exprimés en ¹⁴C ka BP. Les auteurs associent la fréquence des feux de forêt, c'est-à-dire la présence de charbons, à une augmentation de la variabilité ENSO. Modifié d'après Haberle et al. (2001).

Figure I-5. El Niño events frequency during the Holocene as indicated by charcoal records from Papua New Guinea (left) and paleoclimatic synthesis (right) issued from these results. Age is expressed as ¹⁴C ka years BP). Authors link the fire frequency (i.e., charcoal abundance) to the increase in ENSO variability. Modified from Haberle et al. (2001).

¹³ Kilo annum : en latin : millier d'années.

La seconde phase remarquable de la période Holocène est caractérisée par le renforcement de l'activité ENSO ca. 3.5-2.5 ka BP dans le Pacifique Tropical – Figure I-5 - (Haug et al. 2001; Koutavas et al. 2006b; Moy et al. 2002; Rodbell et al. 1999; Sandweiss et al. 2001; Tudhope et al. 2001). Cette deuxième transition climatique est particulièrement intéressante car elle s'accompagne de la colonisation de l'Océanie Lointaine (Figure I-6) par la population Lapita (e.g., Denham et al. 2012; Sheppard 2011). La population Lapita est caractérisée par la fabrication d'une poterie incisée à engobe¹⁴ rouge, dite poterie Lapita, présentant des décorations extrêmement riches et variées (Kirch 1997). Des études archéologiques ont révélé que les Lapita avaient un style de vie nomade basé sur l'exploitation des ressources marines et qu'ils étaient capable d'effectuer des trajets maritimes réguliers sur des embarcations pouvant remonter au vent (Gosden and Pavlides 1994; Irwin 2008; Di Piazza et al. 2007; Summerhayes 2007).

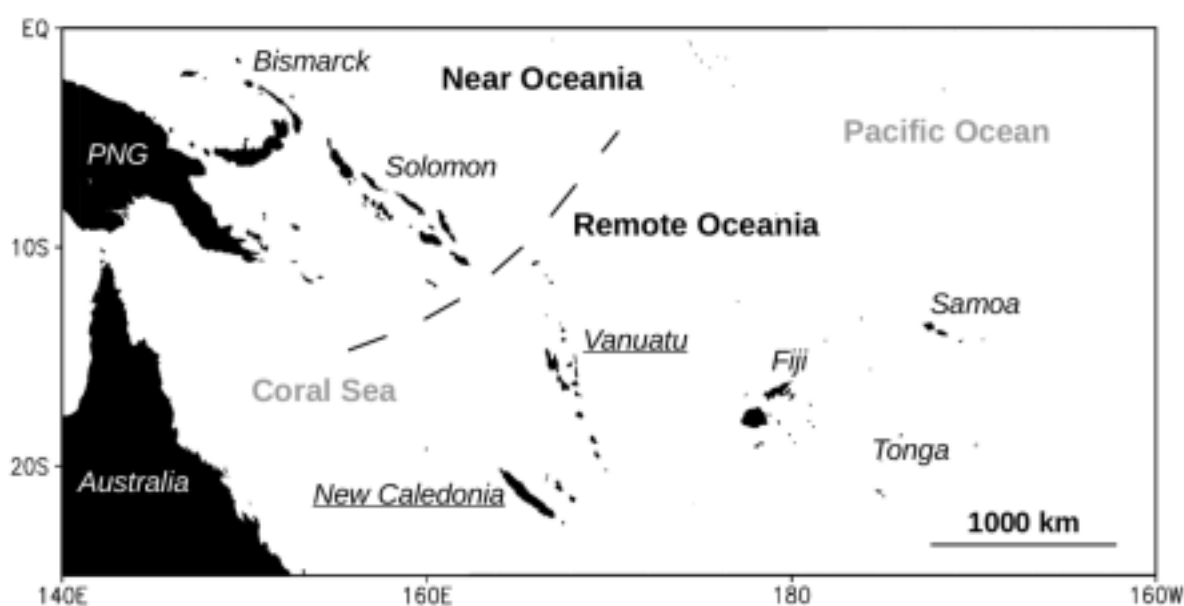


Figure I-6. Carte de la zone Pacifique Sud-Ouest montrant l'emplacement des deux sites étudiés au cours de ma thèse : l'archipel du Vanuatu et la Nouvelle-Calédonie (modifié d'après Climate Explorer : <http://climexp.knmi.nl>). La frontière entre l'Océanie Proche et l'Océanie Lointaine est figurée en pointillés.

Figure I-6. Map of the Southwest Pacific area showing the location of the two study sites of my thesis: the Vanuatu archipelago and New Caledonia (modified from Climate Explorer : <http://climexp.knmi.nl>). The frontier between Near and Remote Oceania is shown by the dashed line.

La migration Lapita survient il y a 3200 ans, alors que la présence humaine est signalée au nord-est de la Papouasie Nouvelle-Guinée (Bismarck) et aux îles Salomon– Figure I-6 – depuis 35 000 ans (Kirch 2000; Sheppard 2011). Cette vague de migration sans précédent s'est étendue sur près d'un dixième de la circonférence du globe terrestre (45000 km)

¹⁴ Matière terreuse dont les potiers recouvrent leur pâte pour en changer la couleur.

jusqu'aux îles Tonga et Samoa, atteintes en moins de cinq siècles (Burley et al. 1999; Denham et al. 2012).

VI. Archives paléoclimatiques

Certains matériaux résultant de processus tels que la sédimentation ou la précipitation de carbonate de calcium "passive" (par ex., spéléothèmes) ou active (par ex., squelette corallien ou coquille de bivalves) intègrent à la fois des marqueurs temporels (par ex., dépôts sédimentaires laminés ou bandes/stries de croissance) et des informations environnementales (par ex., SST) au moment de leur formation (par ex., Anand et al. 2003; Aubert et al. 2009; Corrège 2006). Suivant le matériau considéré, ces informations peuvent être enregistrées durant des périodes s'étendant sur plusieurs dizaines d'années à plusieurs millénaires. Les matériaux remplissant ces conditions sont alors considéré comme des archives climatiques.

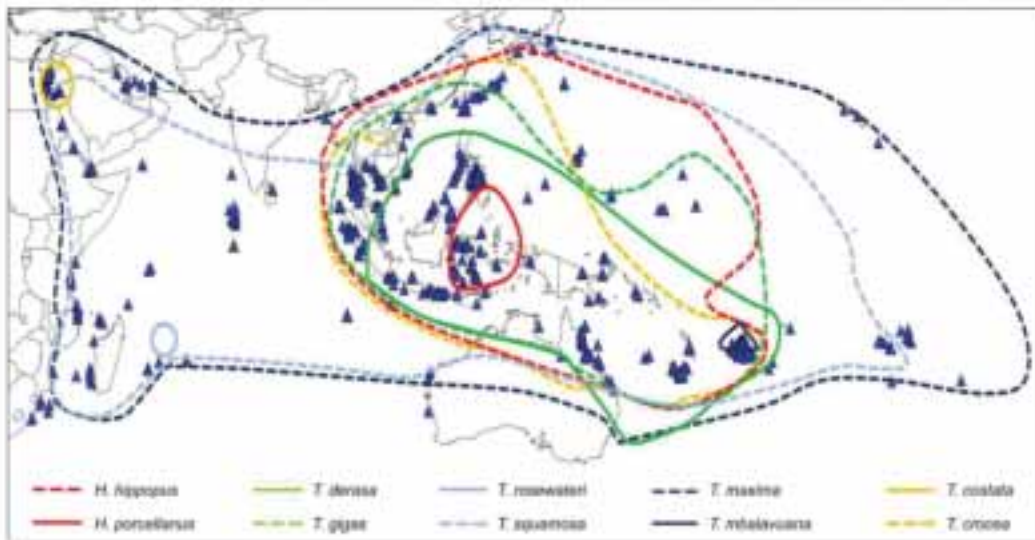
Dans le Pacifique Sud-Ouest, deux types d'archives donnent accès à la variabilité saisonnière et interannuelle : les bénitiers (mollusques bivalves; genres *Tridacna* et *Hippopus*) et les coraux massifs du genre *Porites*. En effet, les bénitiers et les coraux massifs grandissent en précipitant une coquille ou un squelette aragonitique¹⁵ dont la composition et/ou les propriétés varient de manière journalière pour les bénitiers (par ex., Aubert et al. 2009; Sano et al. 2012) ou saisonnière pour les coraux massifs (par ex., Corrège 2006; DeLong et al. 2011). Ces variations périodiques permettent de prélever des échantillons d'aragonite dont la date de déposition est connue. Le taux de croissance de ces organismes est de l'ordre du centimètre par an, ce qui rend possible le prélèvement d'échantillons à une résolution mensuelle ou supérieure. La durée de vie des bénitiers couvre plusieurs décennies et celle des coraux massifs est de l'ordre du siècle. L'ensemble de ces caractéristiques permet d'obtenir, à partir de ces archives, des enregistrements dont la durée et la résolution temporelle sont adéquates à l'étude de la variabilité climatique à l'échelle saisonnière et interannuelle.

Les coraux massifs du genre *Porites sp.* et les bénitiers *Tridacna maxima*, *Tridacna gigas* et *Hippopus hippopus* ont des aires de répartition similaires sur la zone Pacifique (Figure I-7) et les individus fossiles sont abondants sur les terrasses récifales quaternaires émergées des îles du Pacifique Sud-Ouest (par ex., Aharon 1980; Ayling 2006; Taylor 1992). Les coraux massifs, qui contribuent à la formation de récifs coralliens, sont retrouvés plus fréquemment que les bénitiers. En revanche, la coquille très dense de ces derniers résiste mieux aux processus diagénétiques¹⁶ (Aharon 1980; Chappell and A. Polach 1972). De plus, les bénitiers étant une source de nourriture privilégiée des premiers habitants du Pacifique, des coquilles de bénitiers fossiles sont présentes dans les sites archéologiques du Pacifique (Galipaud and Kelly 2007; Kinch 2008; Moir 1989; Seeto et al. 2012).

¹⁵ Aragonite : minéral composé de carbonate de calcium (CaCO₃) dont le système cristallin est orthorhombique.

¹⁶ Diagénèse : ensemble des changements biochimiques et physico-chimiques affectant un sédiment, une roche ou les carbonates biogéniques, après leur dépôt.

a – Distribution of giant clams



b – Distribution of the massive coral *Porites lutea*



Figure I-7. Répartition géographique actuelle **a** - des espèces de bénitiers, adapté de Rosewater (1982; 1965); Lucas (1988); Howard (1988); Zann and Ayling (1988); Gomez and Mingoa-Licuanan (2006) et Richter et al. (2008). Les triangles bleus représentent les données de Reef Check (<http://www.reefcheck.org>), les individus n'ont pas été identifiés au niveau des espèces). Abréviations utilisées pour les genres : T. pour Tridacna, H. pour Hippopus. dans Bin Othman et al. (2010) **b** - du corail massif *Porites lutea*, qui est l'espèce de *Porites* massif la plus largement répandue. D'après <http://coral.aims.gov.au>.

Figure I-7. Present distribution of **a** - giant clams species. Adapted from Rosewater (1965, 1982); Lucas (1988); Howard (1988); Zann and Ayling (1988); Gomez and Mingoa-Licuanan (2002) and Richter et al. (2008). The blue triangles represent Reef Check records and therefore the species are unknown (<http://www.reefcheck.org>). Abbreviation used for genera : T., Tridacna; H., Hippopus **b** - massive coral *Porites lutea*, which is the most common massive *Porites* species. Data from <http://coral.aims.gov.au>.

Dans leurs tissus, les coraux hermatypiques¹⁷ et les bénitiers contiennent, des algues vertes, les zooxanthelles, qui produisent leur énergie à partir de la photosynthèse. Ces zooxanthelles sont en symbiose avec leur hôte: elles lui assurent un apport énergétique en excréant les produits de la photosynthèse et profitent en retour des résidus de la respiration de l'hôte (par ex., Griffiths and Klumpp 1996; Jantzen et al. 2008; Yonge 1975). La photosynthèse nécessite un apport de lumière optimal impliquant que les coraux et les bénitiers sont inféodés aux eaux de surface, rarement en-dessous de 50 mètres pour *Porites sp.* et rarement en dessous de 10-20 mètres pour les bénitiers (Hardy and Hardy 1969). Des variables telles que le taux de croissance et la composition géochimique de ces archives reflètent donc les paramètres environnementaux de la surface de la mer.

Les bénitiers *Tridacna sp.*, *Hippopus sp.* et le corail massif *Porites sp.* sont des archives environnementales adéquates pour la reconstruction des paléoclimats dans la zone Pacifique tropicale.

VII. Proxies

Il est possible d'obtenir des informations sur l'environnement dans lequel se sont développés des bénitiers ou des coraux fossiles en mesurant des paramètres, comme la composition isotopique ou la concentration en éléments traces de leur coquille/squelette, qui reflètent des variables physiques (par ex., la SST) ou chimiques (par ex., la SSS). Ces paramètres sont alors appelés proxies.

a. Utilisation du $\delta^{18}\text{O}$ chez les coraux et les bénitiers

La composition en isotopes stables de l'oxygène ($\delta^{18}\text{O}^{18}$) du squelette corallien et de la coquille du bénitier est en équilibre avec le $\delta^{18}\text{O}$ de l'eau de mer ($\delta^{18}\text{O}_{\text{sw}}$). Lorsque le $\delta^{18}\text{O}_{\text{sw}}$ de l'eau de mer est fortement corrélé à la SSS, comme c'est le cas dans le Pacifique Sud-Ouest, le $\delta^{18}\text{O}$ des archives carbonatées reflète également la salinité du milieu environnant (Juillet-Leclerc et al. 2006; Kilbourne et al. 2004; Morimoto et al. 2002). Lors de la précipitation de la coquille, ou du squelette corallien, le $\delta^{18}\text{O}$ subit un fractionnement qui dépend de la SST (par ex., Aubert et al. 2009; Epstein et al. 1953; Jones et al. 1986; McConnaughey 1989; Weber and Woodhead 1972). Le $\delta^{18}\text{O}$ du squelette corallien et de la coquille du bénitier reflète donc à la fois les variations de SST et de SSS, on parle alors de proxy géochimique. Mesurer ce proxy ($\delta^{18}\text{O}$) permet donc de caractériser un environnement

¹⁷ Les coraux hermatypiques vivent en symbiose avec des zooxanthelles photosynthétiques qui se situent dans leurs tissus à l'inverse des coraux ahermatypiques qui n'en possèdent pas.

$$\delta^{18}\text{O} = \left(\frac{\left(\frac{^{18}\text{O}}{^{16}\text{O}} \right)_{\text{échantillon}}}{\left(\frac{^{18}\text{O}}{^{16}\text{O}} \right)_{\text{standard}}} - 1 \right) \times 1000$$

passé en termes de SST et de SSS : une valeur haute de $\delta^{18}\text{O}$ indique des conditions froides et salées alors qu'une valeur faible de $\delta^{18}\text{O}$ indique des conditions chaudes et peu salées.

b. Utilisation du $\delta^{13}\text{C}$ et de la sclérochronologie chez les Bénéitiers

i. Les isotopes stables du carbone

Chez les bivalves ayant une coquille aragonitique, la composition en isotopes stables du carbone ($\delta^{13}\text{C}$) de la coquille dépend de différents facteurs. Ainsi, la température et la physiologie de l'organisme peuvent influencer la valeur $\delta^{13}\text{C}$ de l'aragonite en induisant un fractionnement isotopique du carbone – on parle dans ce dernier cas “d'effet vital” (Gillikin et al. 2009; Gillikin et al. 2007; Gillikin et al. 2006; Lorrain et al. 2004; McConnaughey et al. 1997; McConnaughey and Gillikin 2008; Tanaka et al. 1986). Le $\delta^{13}\text{C}$ de la coquille dépend également de la proportion de carbone issu de la respiration et de la proportion de carbone fixé par l'activité photosynthétique des zooxanthelles dans la solution à partir de laquelle est précipité la coquille (Gillikin et al. 2009; Gillikin et al. 2007; Gillikin et al. 2006; McConnaughey et al. 1997; Owen et al. 2008; Tanaka et al. 1986; Wanamaker Jr et al. 2007). L'influence respective de la température, des effets vitaux et de la proportion de la respiration et de la photosynthèse dans la composition isotopique de la coquille de bénéitier est encore mal estimée. Ces facteurs ont vraisemblablement une influence modérée sur le $\delta^{13}\text{C}$ de la coquille étant donné que la majeure partie du carbone précipité provient du carbone inorganique dissous dans l'eau de mer – *Dissolved Inorganic Carbon* – DIC (Gillikin et al. 2006; McConnaughey et al. 1997; McConnaughey and Gillikin 2008; Mook and Vogel 1968; Owen et al. 2008). Le $\delta^{13}\text{C}$ reflète donc majoritairement la composition isotopique du DIC.

Le $\delta^{13}\text{C}$ du DIC varie suivant sa source, en effet, le carbone d'origine marine a une signature isotopique plus élevée alors que le carbone issu de la végétation terrestre présente des valeurs faibles de $\delta^{13}\text{C}$. Le carbone provenant du couvert végétal terrestre est présent en milieu marin en particulier au niveau des zones estuariennes où il est acheminé par les rivières et par les fleuves. Le $\delta^{13}\text{C}$ de l'eau de mer va donc refléter la proportion de DIC d'origine marine et de DIC d'origine terrestre. Le $\delta^{13}\text{C}$ du DIC permet donc d'estimer la salinité d'un environnement donné (Fry 2002; Gillikin et al. 2006; Mook 1971; Surge et al. 2001). La valeur du $\delta^{13}\text{C}$ de la coquille des bénéitiers renseigne donc potentiellement sur la salinité du milieu dans lequel c'est développé l'organisme.

ii. La sclérochronologie

La mesure de l'épaisseur des incréments de croissance des bivalves peut également fournir des informations sur l'environnement dans lequel ils se sont développés. L'épaisseur de ces incréments de croissance est influencée par les cycles de SST (infra-journaliers, journaliers, saisonnier etc.), les épisodes de reproduction, les saisons, marées ou bien encore les occurrence de tempêtes (par ex., Pannella and MacClintock 1968; Poulain et al. 2011; Rodland et al. 2008; Rodland et al. 2006; Schöne 2008). Parmi ces facteurs, les variations de SST liées aux cycles journaliers ou saisonniers sont la principale cause de variation de l'épaisseur des incréments de croissance des bivalves, en particulier chez les bénéitiers (Aubert et al. 2009; Schwartzmann et al. 2011; Watanabe and Oba 1999). Il a ainsi été montré, chez

les bénitiers, que l'épaisseur des incréments de croissance journaliers était fortement corrélée à la SST, offrant la possibilité d'obtenir des enregistrements de SST.

c. Utilisation du rapport Strontium/calcium chez les coraux

Depuis les années 1980, le rapport strontium sur calcium (Sr/Ca) du squelette corallien est couramment utilisé comme paléothermomètre (par ex, Beck et al. 1992; Corrège 2006; Schneider and Smith 1982; Swart 1981). Le Sr/Ca est considéré comme un proxy exclusif de la SST, c'est-à-dire que sa valeur n'est, en théorie, pas influencée par d'autres facteurs environnementaux (par ex., la salinité) ou vitaux (i.e. liés à la physiologie de l'organisme). Il est ainsi possible, dans le cas des coraux, de séparer la composante température de la composante salinité du $\delta^{18}\text{O}$ en utilisant la relation entre le Sr/Ca et la température (Kilbourne et al. 2004; Ourbak 2006; Ren et al. 2002). A l'heure actuelle, il n'a pas été trouvé de proxy exclusif de la SST chez les bénitiers. Ainsi, chez les bénitiers, le rapport Sr/Ca de la coquille est sous l'influence de la physiologie de l'organisme qui peut prendre le pas sur la température (cf. effet vitaux), empêchant l'utilisation du Sr/Ca comme paléothermomètre (par ex., Elliot et al. 2009).

Des études, dites de calibration, visent à déterminer s'il existe une relation empirique entre la composition géochimique ou le taux de croissance de ces archives et la SST ou la SSS. Des études de calibration ont permis d'identifier plusieurs proxies de SST et de SSS pour les bénitiers et les coraux. Les relations liant la composition géochimique et l'épaisseur des incréments de croissance (dans le cas des bénitiers) à la SST et/ou à la SSS ont été calibrées pour des coraux massifs *Porites sp.* (e.g., Corrège et al. 2000; Gagan et al. 1998; Lough and Cooper 2011) et pour les bénitiers *Tridacna gigas* (Aharon 1980; Ayling 2006; Elliot et al. 2009; Pätzold et al. 1991; Watanabe et al. 2004; Welsh et al. 2011), *T. squamosa* (Batenburg et al. 2011) et *Hippopus hippopus* (Aubert et al. 2009; Schwartzmann et al. 2011; Watanabe and Oba 1999). Les travaux de Romanek (1985) sur *T. maxima* ont mis en évidence le fort potentiel de cette espèce comme archive paléoclimatique en montrant que le $\delta^{18}\text{O}$ de la coquille variait avec la SST. Cependant il n'a pas été produit d'équation reliant ces deux paramètres.

Le rapport isotopique $\delta^{18}\text{O}$ de la coquille de bénitier et du squelette corallien est un proxy à la fois de la température et de la salinité de la surface de la mer – SST et SSS. Le ratio strontium sur calcium – Sr/Ca – du corail est un proxy de la SST. Dans le cas du corail, le ratio Sr/Ca permet de déconvoluer l'influence de la SST dans le rapport isotopique $\delta^{18}\text{O}$ afin d'obtenir un proxy de la SSS. D'autres proxies permettent de fournir des informations supplémentaires : ainsi le rapport isotopique $\delta^{13}\text{C}$ de la coquille de bénitier peut être utilisé pour caractériser la salinité de l'environnement. Par ailleurs, l'épaisseur des stries de croissance journalière des bénitiers peut apporter des informations sur la SST.

VIII. Problématiques, objectifs et organisation de la thèse

Problématiques – Les changements climatiques observés durant l'Holocène soulèvent plusieurs interrogations :

- Dans quel contexte climatique (état-moyen, variabilité interannuelle et saisonnière) s'est mise en place la variabilité ENSO actuelle durant la transition Holocène inférieur / Holocène supérieur ?
- Dans quel contexte climatique a eu lieu l'augmentation de la variabilité ENSO ca. 3000 années BP ?
- Pourquoi a-t-il fallu attendre près de 30 000 ans avant que les premiers Océaniens entreprennent la traversée des 200 milles nautiques qui séparent l'Océanie Proche de l'Océanie Lointaine ?
- Le renforcement de l'activité ENSO ca. 3.5-2.5 ka BP dans le Pacifique Tropical a-t-il pu avoir un rôle dans la migration Lapita ?

Bien que les nombreux fossiles du bénitier *Tridacna maxima* présents dans le Pacifique Sud-Ouest devraient permettre d'apporter des éléments de réponse aux questions précédentes, certains points doivent être éclaircis avant de pouvoir utiliser cette archive à des fins paléoclimatiques :

- A quelle fréquence sont déposés les incréments de croissance chez *Tridacna maxima* ? Quelle est l'influence de la SST sur les variations d'épaisseur de ces incréments de croissance ? sur le rapport $\delta^{18}\text{O}$ de la coquille ?
- Est-il possible de produire une fonction de transfert reliant l'épaisseur de ces incréments de croissance et la composition isotopique de cette espèce à la SST ? Quelles sont les limitations de ces proxies ?

Dans le Pacifique Sud-Ouest, les reconstructions paléoclimatiques sont trop peu nombreuses et trop dispersées géographiquement pour comprendre les mécanismes associés à l'évolution d' ENSO durant la transition entre l'Holocène inférieur et l'Holocène supérieur, ainsi que pour élucider les modalités du peuplement de l'Océanie Lointaine ca. 3.5-2.5 ka BP. De plus, le bénitier *Tridacna maxima*, susceptible d'apporter des éléments de réponse à ces questions, n'a pas fait l'objet d'une étude de calibration, privant la paléoclimatologie de précieuses informations.

Objectifs – L'objectif général de cette thèse est d'étudier la variabilité climatique de deux périodes clé de l'Holocène en décrivant la position moyenne ainsi que les variations saisonnières et interannuelle (cf. variabilité ENSO) de taille et de localisation de la West Pacific Warm Pool et de la zone de convergence du Pacifique Sud. Les résultats de cette étude ont pour but d'apporter des éléments de réflexion sur la transition climatique s'opérant entre l'Holocène inférieur et l'Holocène moyen et sur le contexte climatique durant la migration Lapita. Cette étude s'appuie sur des enregistrements géochimiques et sur la sclérochronologie


de bénitiers et de coraux fossiles. Une étude de calibration portant sur l'espèce de bénitier *Tridacna maxima* a été effectuée, au préalable, afin de valider l'utilisation du rapport isotopique $\delta^{18}\text{O}$ et de l'épaisseur des incréments de croissance comme proxies de la température de surface de la mer chez cette espèce.

Organisation – Cette thèse se décline en quatre chapitres, dont trois sont rédigés sous forme d'articles scientifiques, en anglais. Le potentiel du bénitier *Tridacna maxima* en tant qu'archive paléoclimatique est étudié dans le chapitre II. Pour comprendre la réponse de la WPWP et de la SPCZ lors la transition climatique s'opérant entre l'Holocène inférieur et l'Holocène moyen [chapitre III] et pour savoir si la migration Lapita, survenant aux alentours de ca. 3.2 ka BP, a coïncidé avec un contexte climatique particulier [chapitre IV], les variations saisonnières et interannuelles de la température et de la salinité de la surface de la mer ont été étudiées dans la zone Pacifique Sud-Ouest. Ce manuscrit se termine par une synthèse [chapitre V] qui reprend les résultats obtenus au cours de ma thèse en les plaçant dans le contexte climatique Holocène.

Remarque : Afin d'éviter les redondances, les références bibliographiques ont été compilées en une seule liste placée à la fin de ce manuscrit. En annexe de cette thèse se trouve une réflexion sur la fiabilité des analyses géochimiques effectuées au cours de ma thèse et sur les améliorations méthodologiques à apporter. Un article scientifique méthodologique, écrit durant ma thèse, dans le cadre d'un projet mené en parallèle, y figure également.



Prélèvement d'eau de mer dans le bassin des bénitiers durant l'expérience de calibration. Aquarium des Lagons, Nouméa, (de g. à d.) Cécile Dupouy et Claire Lazareth. Novembre 2009. Crédit photo: N. Duprey.



**Chapitre II – Calibration of giant clam *Tridacna maxima*
growth increments thickness and shell $\delta^{18}\text{O}$ as proxies of
sea surface temperature: implications for
paleoclimatology**

Le chapitre suivant sera soumis à la revue *Coral Reefs* durant le premier semestre 2013.

Auteurs (dans l'ordre):

Duprey Nicolas,
Lazareth Claire E.,
Butscher John,
Dupouy Cécile,

RÉSUMÉ

Cette étude a pour but d'établir un lien entre la largeur des incréments de croissance et la composition isotopique de l'espèce de bénitier *Tridacna maxima* avec la température de surface de la mer (SST). Trois spécimens de *T. maxima* ont été collectés, vivants, sur le récif barrière de Nouvelle-Calédonie, marqués avec de la calcéïne puis élevés en aquarium de septembre 2008 à juin 2010. L'observation, en lumière transmise, de lames minces issues de la coquille de ces bénitiers révèle des incréments de croissance simples et complexes. Ces incréments, de taille micrométrique, sont déposés journalièrement. Les incréments infra-journaliers qui caractérisent les incréments complexes reflètent vraisemblablement les phases d'ouverture et de fermeture des valves de *T. maxima*. L'épaisseur des incréments journaliers est corrélée positivement à la SST, ce qui a permis d'établir une fonction de transfert reliant ces deux variables. Cette équation a été appliquée à un profil sclérochronologique obtenu sur un *T. maxima* fossile de Nouvelle-Calédonie, daté aux environs de 3000 années BP. L'étude de ce fossile suggère que la SST était plus élevée qu'actuellement et que l'amplitude saisonnière était réduite à cette époque. Cependant des anomalies de croissance ont été observées sur les individus actuels, qui altèrent la réponse du taux de croissance aux variations de la SST. L'impact de ces anomalies sur la reconstruction de SST peut être réduit en travaillant avec des profils sclérochronologiques obtenus sur différents individus dont les périodes de vie se recoupent. La composition en isotopes stables de l'oxygène ($\delta^{18}\text{O}_{\text{shell}}$) de la coquille de l'un des trois spécimens actuels de *T. maxima* a été analysée à une résolution hebdomadaire. Le $\delta^{18}\text{O}_{\text{shell}}$ est fortement corrélé avec les variations saisonnières de la SST. Une fonction de transfert reliant le $\delta^{18}\text{O}_{\text{shell}}$ et la composition isotopique de l'eau de mer ($\delta^{18}\text{O}_{\text{sw}}$) à la SST a été établie :

$$\delta^{18}\text{O}_{\text{shell}} - \delta^{18}\text{O}_{\text{sw}} = -3.56 \times \text{SST} + 20.5$$

L'écart-type des résidus de la régression (1σ) est de $\pm 1.23^\circ\text{C}$, le $\delta^{18}\text{O}_{\text{shell}}$ de *T. maxima* peut donc être utilisé comme un paléothermomètre.

ABSTRACT

Giant clam *Tridacna maxima* sclerochronology and shell geochemical composition' response to sea surface temperature (SST) variations was investigated. Three modern *T. maxima* were collected in New Caledonia, stained with calcein and grew in a seawater-fed aquarium from September 2008 to June 2010. Thin sections of the *T. maxima* outer layer, viewed under transmitted light, revealed simple and complex daily growth increments. The sub-daily growth layers that composed the complex daily growth increments most likely reflected the opening and closing behavior (i.e., gaping) of the giant clam. Growth increment thickness is positively correlated to SST and transfer function linking SST to the growth increment thickness was produced. This equation was used on the sclerochronological profile of a fossil *T. maxima* specimen, dated ca. 3000 years BP, from New Caledonia, revealing higher mean SST than today and reduced seasonal amplitude. However, growth anomalies, that may alter the response of growth to SST, were observed on the *T. maxima* growth increments profiles. Such anomalies can be avoided using overlapping sclerochronological profiles in paleo-SST reconstructions. One of the three modern *T. maxima* was sampled at a weekly resolution for oxygen stable isotope composition ($\delta^{18}\text{O}_{\text{shell}}$). $\delta^{18}\text{O}_{\text{shell}}$ correlates well with the seasonal SST cycle. An equation linking $\delta^{18}\text{O}_{\text{shell}}$ and oxygen stable isotope composition of seawater ($\delta^{18}\text{O}_{\text{sw}}$) to the SST was produced :

$$\delta^{18}\text{O}_{\text{shell}} - \delta^{18}\text{O}_{\text{sw}} = -3.56 \times \text{SST} + 20.5$$

The standard deviation (1σ) of the residuals was $\pm 1.23^\circ\text{C}$, showing that *T. maxima* $\delta^{18}\text{O}_{\text{shell}}$ can be used as a paleo-thermometer.

I. Introduction

The geochemical composition of massive corals has been widely used to assess the past climatic variability (Ayling et al. 2006; Beck 1997; Beck et al. 1992; Corrège 2006; Corrège et al. 2000; Gagan et al. 1998). However, the use of massive corals as a paleoclimatic archive is sometimes hampered because of the poor preservation state of the porous coral skeleton which is prone to diagenesis (e.g., Nothdurft and Webb 2008). Therefore, interpreting coral geochemical data in terms of climatic variability is sometimes critical (Enmar et al. 2000; Hendy et al. 2007; McGregor and Gagan 2003; Muller et al. 2001; Quinn and Taylor 2006).

The dense shell of giant clams is less prone to diagenetic alteration, offering the opportunity to open windows over the past climate, as far as 400,000 years ago (Aharon and Chappell 1986; Ayling 2006; Chappell and A. Polach 1972). The current distribution of the two existing giant clam genera – *Tridacna* and *Hippopus* – overlaps the distribution of the massive coral, *Porites* sp., (Bin Othman et al. 2010). Moreover, fossil giant clams and coral colonies are commonly found together on uplifted reef terraces (Aharon 1980; Ayling 2006). Additionally, giant clams were heavily targeted as a food source during the prehistoric period (e.g., Galipaud and Kelly 2007; Seeto et al. 2012) so that abundant and well dated specimens are commonly unearthed from archaeological sites in the Indo-Pacific area (Faylona et al. 2011; Seeto et al. 2012). Therefore, giant clams are a promising alternative (or a complementary) archive to massive corals for paleoclimatic reconstructions.

The giant clam shell is secreted in oxygen isotopic equilibrium with seawater (e.g., Aharon 1991; Aubert et al. 2009; Jones et al. 1986; Watanabe and Oba 1999). The shell oxygen isotopic composition ($\delta^{18}\text{O}_{\text{shell}}$) reflects thus the SST and the SSS conditions experienced by the giant clam during its life. Transfer functions linking ($\delta^{18}\text{O}_{\text{shell}} - \delta^{18}\text{O}_{\text{sw}}$) and SST were obtained for the *Tridacna* and *Hippopus* genera (Aharon 1980; Aubert et al. 2009; Watanabe and Oba 1999). Nevertheless, despite the density of their shell, giant clams may be affected by diagenesis, precluding any paleoenvironmental reconstruction from shell geochemical analysis (Faylona et al. 2011). In such circumstances, the study of the shell growth increments (i.e., sclerochronology) can potentially replace geochemical studies. Indeed, the thickness of the bivalve growth layers and the rhythm of deposition of these layers are controlled by physiological, e.g., reproduction, ontogeny, disease and environmental factors, e.g., tidal cycle, water temperature, storm events, food availability (reviews in Rhoads and Lutz 1980; Richardson 2001; Schöne 2008). Previous studies showed that *Tridacna gigas*, *T. maxima*, *T. squamosa*, and *Hippopus hippopus* deposit daily growth increments, potentially providing high-resolution paleoclimatic or paleoenvironmental archives (Aharon and Chappell 1986; Aubert et al. 2009; Bonham 1965; Henocque 1980; Pannella and MacClintock 1968; Pätzold et al. 1991; Schwartzmann et al. 2011; Watanabe and Oba 1999). The daily growth increment thickness of *H. hippopus* varies seasonally, being thicker in summer and thinner in winter (Aubert et al. 2009; Schwartzmann et al. 2011; Watanabe and Oba 1999). Higher growth rate was also observed during summer for *T. gigas* and *T. maxima* (Ambariyanto 1997; Lucas et al. 1989). In addition, it was shown that the seasonal variations in *H. hippopus* daily growth increments thickness are related to the SST variations (Aubert et al. 2009; Schwartzmann et

al. 2011; Watanabe and Oba 1999). Tridacnidae's high-resolution (daily) sclerochronology appears thus as a promising tool for past-SST reconstruction.

The giant clam *Tridacna maxima* has the largest distribution area compared to those of the other giant clam species (Bin Othman et al. 2010). It is also abundant on the uplifted reef terraces of the West Pacific (Aharon and Chappell 1986) and it generally dominates in the archaeological giant clam assemblages (Faylona et al. 2011; Moir 1989). *T. maxima* is thus a potential archive for paleoclimatic or paleoenvironmental reconstructions. Nevertheless, at the exception of the early work of Jones et al. (1986), the potential of *T. maxima* as a paleoclimatic archive has not been investigated. The aim of this study is to investigate the growth increments thickness and the shell $\delta^{18}\text{O}$ variations of *T. maxima* as potential recorder of SST changes. This was done through an aquarium growing experiment, which lasted 1.5 yrs, in New Caledonia. Potential application of sclerochronology as a proxy for SST was tested on a fossil *T. maxima* shell recovered in an archaeological site.

II. Materials and methods

a. *Tridacna maxima* specimens

Three *Tridacna maxima* giant clam specimens were collected on 22/09/2008, at 2.5 meters depth, on the outer crest of the barrier reef surrounding New Caledonia main island (*Fausse Passe de Uitoé*, 22°17'S; 166°11'E - Figure II-1). The three giant clams were living in a sub-tidal environment, with a semidiurnal tidal regime. The tide amplitude in New Caledonia is generally inferior to 1.6 m. Each giant clam was carefully removed from the reef with the coral piece it was fixed to. The *T. maxima* specimens, T-02-08, T-03-08, and T-05-08, were then placed in an open-air seawater-fed aquarium for a 1.5 year-long calibration experiment (*Aquarium des Lagons*, Nouméa, New Caledonia - Figure II-1). The water level in the aquarium was kept at approximately 60 cm height during all the experiment. To produce sclerochronological profiles and geochemical time-series, specimens T-02-08 and T-03-08 were stained on 23/02/2009, in a 75 ppm calcein solution for two hours. To ensure that the staining procedure did not affect the giant clam growth, the third specimen, T-05-08, was not stained. From the staining date, the three giant clams were visited once a week and specific giant clam's behavior, meteorological conditions or any peculiar event was reported. Specimen T-02-08 was collected alive the 03/06/2010. Specimens T-03-08 and T-05-08 were found dead on 17/12/2009 and on 12/11/2009 respectively. Because the aquarium was checked once a week, the death dates of T-03-08 and T-05-08 are comprised in the time interval 09-17/12/2009 and 05-12/11/2009 respectively. To study the potential of fossil *Tridacna maxima* shells for paleoenvironmental and paleoclimatic reconstructions, a sclerochronological study was done on a fossil *T. maxima* shell. The fossil specimen was unearthed from an archaeological site in Bourail, New Caledonia (21.38°S, 165.26°E; Figure II-1b). The conventional radiocarbon date for this specimen was 3236 ± 32 years BP. This age was corrected for the marine reservoir effect using the CALIB marine04 database using a deltaR value of -3 ± 9 years (Petchey et al. 2008; Reimer et al. 2009). The calibrated age of this specimen is 3.2-2.9 ka cal. BP (2σ).

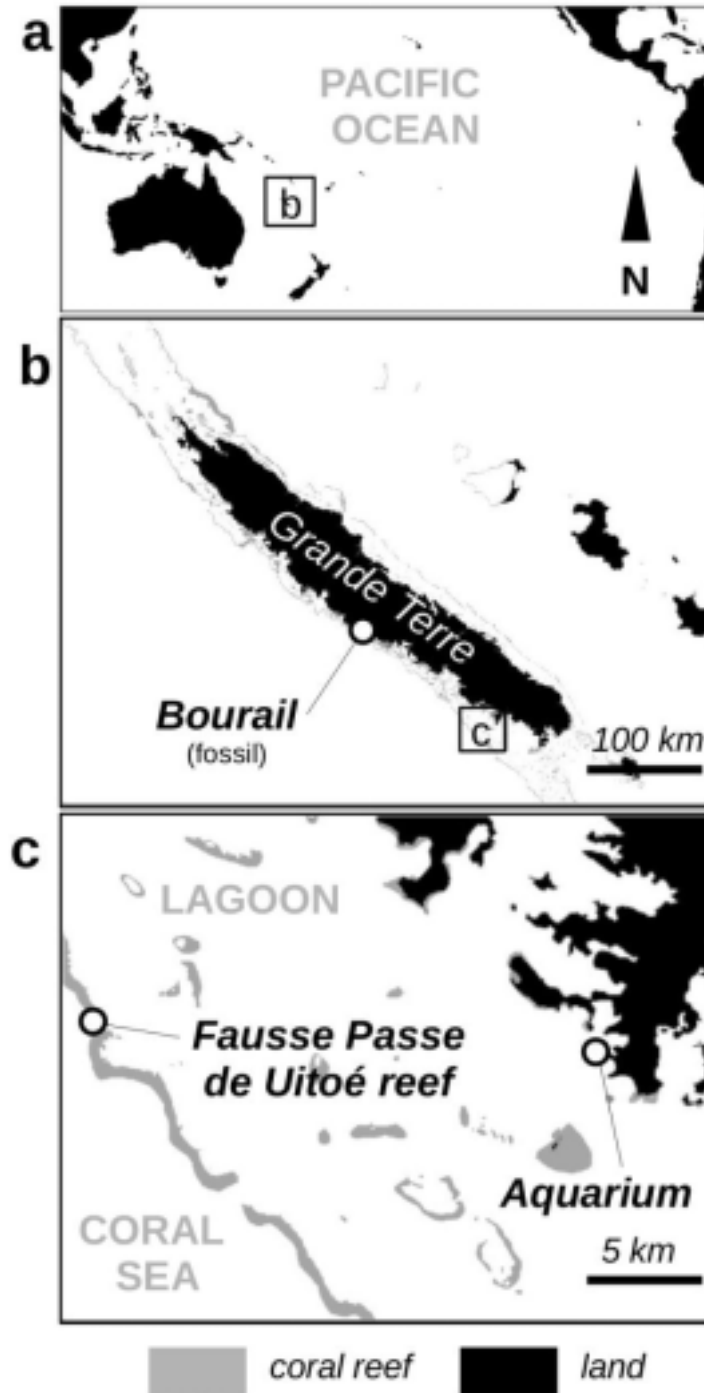


Figure II-1. Location of the study sites. **a** - Location of New Caledonia in the Pacific area **b** - Location of the archaeological site, on the “Grande Terre”, where the fossil *Tridacna maxima* specimen was recovered **c** - Detail of the southwest lagoon of New Caledonia showing the collection site of the three modern *T. maxima* specimens (Fausse Passe de Uitoé Reef) and the location of the aquarium where the three specimens were grown. Map sources : Pacific area map modified from climate explorer (<http://climexp.knmi.nl>), maps b and c were modified from maps provided by the Service de cartographie de l’Institut de Recherche pour le Développement (IRD), Bondy, France.

b. Weekly monitoring

To determine the relation between sea surface temperature (SST) and i) growth increment thickness variations and ii) oxygen stable isotope composition of *Tridacna maxima* shell ($\delta^{18}\text{O}_{\text{shell}}$), the SST in the aquarium was recorded hourly, using a TidbiT[®]-logger. In addition, aquarium seawater samples were collected weekly from February 2009 to June 2010 for oxygen stable isotope ($\delta^{18}\text{O}_{\text{sw}}$) measurements. The seawater samples for isotopic analysis were filtered on Millipore[®] filters (0.45 μm) and stored at 4°C in 50 ml glass flasks until analyzed. Air bubbles were carefully avoided from the seawater flasks to prevent oxygen exchange between seawater and air after the sampling.

c. Age determination

The growth increment thickness variations and the isotopic composition of the giant clams might be influenced by ontogenic effects (Green and Craig 1999; Jones et al. 1986; McKoy 1980; McMichael et al. 1974; Munro and Heslinga 1983; Smith 2011), so that the age of each specimen must be estimated prior to interpret the sclerochronological and geochemical data produced. Molluscan age can be determined using the Von Bertalanffy Growth Function (VBGF) growth model; $L_t = L_\infty * (1 - e^{-K*t})$ where L_t is the shell length at time t , L_∞ the asymptotic growth constant and K the growth constant (Bertalanffy 1957; Bertalanffy 1938). Various VBGF functions for *Tridacna maxima* are available in the literature, but none was produced for New Caledonian populations.

An average VBGF function was thus calculated by averaging the L_∞ and K coefficients from previous studies (Table II-1). The resulting averaged VBGF function is :

$$L_t = 28.6 \pm 1.7 * (1 - e^{-0.09 \pm 0.02 * t}) \text{ (VBGF}_{\text{ave.}})$$

Table II-1 : Compilation of Von Bertalanffy Growth Function parameters (L_{inf} and K) obtained from *Tridacna maxima* giant clam populations and the averaged parameters used in this study (VBGF_{ave}).

Reference	L_{inf} (cm)	K
McKoy, 1980	30.5	0.082
Munro and Heslinga, 1983	30.5	0.112
McMichael, 1975	27.5	0.074
Green and Craig, 1999	27.8	0.065
Smith, 2011	26.9	0.118
VBGF_{ave}	MEAN	0.090
	sd	0.024

d. Thick and thin section preparation

The shell of the Tridacnidae is aragonitic with two types of microstructures : crossed-lamellar for the outer layer and the hinge area and prismatic for the inner layer (Bonham 1965; Carter 1980; Pätzold et al. 1991). The outer layer of *Tridacna maxima* is deposited at a higher growth rate (i.e., thicker growth increments) than the other shell parts (Figure II-2). The outer

shell layer is thus the most suitable part for growth increments counting and measurements and for high-resolution geochemical analyses. *T. maxima* valves have generally five scaled-ridges (Rosewater 1965), the central one being often better preserved on fossil specimens. The sclerochronological and the geochemical studies presented here were based thus on the outer layer of the central ridge of modern and fossil specimens (Figure II-2a). Shells were cut from the shell edge to the umbo following the center of the central ridge using a Buehler® precision saw. Then, a 1 cm-thick section was removed from the shell of each modern and fossil specimen (Figure II-2). The side of the thick section in contact with the center of the central ridge was glass-mounted using epoxy resin and cut to obtain a thin section. The remaining of the thick section was used for the geochemical analyses. Thin sections were ground on polishing-disks of decreasing abrasiveness, down to \varnothing 15 μm , with frequent visual checks under a microscope until growth increments appeared. Then, the thin sections were polished with successive diamond suspensions (down to \varnothing 1 μm) before microscopic observations.

e. Sclerochronological profiles

The thin sections were studied using an optical microscope under transmitted light. The calcein staining was visualized under reflected UV light. Thin sections were digitized using the free geographic information system software (GIS) QuantumGIS® (<http://qgis.org/>). In a first step, thin sections were photographed at a 40x magnification and pictures were assembled. That way, a global view of the thin sections was obtained and used to locate transects along which growth increments were counted. Transects were drawn following the growth direction, approximately at three millimeters from the outer surface of the shell (i.e., the surface in contact with seawater in living giant clams – Figure II-2b), where the growth increments are the thickest. In a second step, pictures focusing on this three millimeter shell band were taken at a 100x magnification and added to the virtual thin section so micrometric growth increments could be identified easily and accurately measured along the transects. All photographs were scaled before added into the GIS-thin section so the growth increments thickness can be measured directly on the virtual thin sections. For the modern specimens, sclerochronological profiles were obtained on the shell part deposited while they were in the aquarium (i.e., from September 2008 to death). This part could be easily identified due to the abrupt change in the shell aspect that accompanied the transfer of the three modern specimens from the reef to the aquarium (see section : III-b *Shell and growth pattern description*). A composite profile was then obtained by averaging the three modern sclerochronological profiles. The sclerochronological profile of the fossil giant clam was measured from the last deposited increment toward the umbo until bioerosion prevented growth increments observation. This resulted in a 110 mm-long sclerochronological profile. To determine whether natural cycles (tides, seasons, etc.) influence giant clam growth increments deposition, spectral analyses were done on the modern composite and the fossil sclerochronological profiles. The spectral analysis was made using the PAST® software (Hammer et al. 2001).

f. Oxygen stable isotopes analyses

The giant clam specimen T-02-09 was selected for oxygen stable isotope analyses because it had a longest lifetime than the two other giant clams. Shell samples were milled on the thick

section of the central ridge, so sclerochronological and isotopic profiles are comparable. Shell samples were collected along a 24 mm-long section that encompasses the section deposited when the specimen was in the aquarium. Fifty-eight samples were milled at 0.5 mm steps in the outer shell layer following growth increment's shape using a micromilling device (MicroMill New Wave[®]). Each carbonate sample weighted ~ 50 to 100 µg. The $\delta^{18}\text{O}_{\text{shell}}$ and $\delta^{18}\text{O}_{\text{sw}}$ were analyzed on a GV IsoPrime[®] mass-spectrometer coupled to a Multiprep carbonate Gilson[®] at the LOCEAN laboratory (University of Paris 6). The analytical precision (1σ) on the shell and water oxygen isotopic measurements was 0.08‰ vpdb (10 runs of homemade calcitic standard) and 0.1‰ smow (10 runs of homemade water standard). To assign time to each isotopic sample, a photograph of the micro-milled thick section was integrated into the virtual GIS-thin section. The picture and the GIS-thin section were superimposed so that the thick section's contours matched those of the GIS-thin section. That way, each micro-milled groove was replaced in the sclerochronological profile and time was thus assigned to each $\delta^{18}\text{O}_{\text{shell}}$ sample.

III. Results

a. Age determination

Lengths of the three *T. maxima* specimens, T-02-09, T-03-09, and T-05-09 were measured at the end of the experiment. Then, the averaged Von Bertalanffy Growth Function was used to estimate the age of each giant clam specimen. Specimens T-02-08, T-03-08, and T-05-08 were respectively 14 ± 6 years-old (shell length : 204 mm), 14 ± 6 years-old (shell length : 207 mm) and 13 ± 5 years-old (shell length : 201 mm). The fossil specimen was 12.5 ± 5 years-old (shell length of 194 mm). According to previous studies, these specimens have reached the adult phase and thus their sexual maturity (Jameson 1976; Jones et al. 1986; LaBarbera 1975; Raymakers et al. 2003).

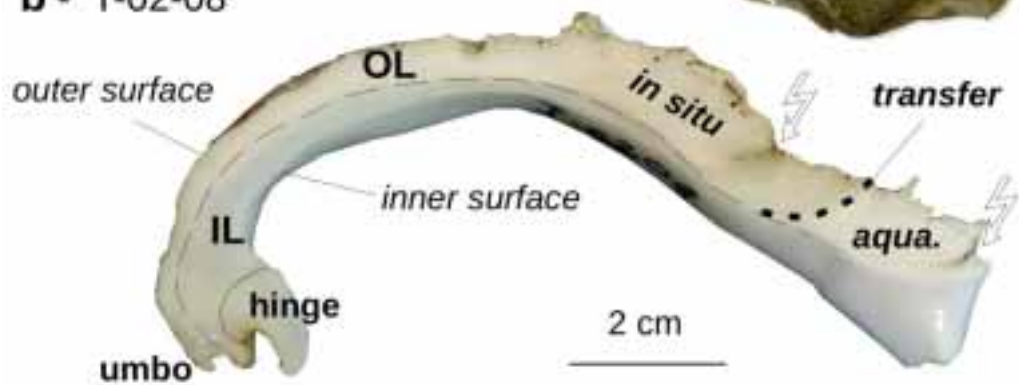
b. Shell and growth pattern description

Thick sections – An abrupt change in the shell aspect occurs at 1-2 cm from the shell edge of the three modern specimens. Most the outer shell layer is greenish and translucent, except the last 1-2 cm where the shell becomes white and opaque (Figures II-2b-d). A similar observation was reported for a *Tridacna squamosa* shell transferred from the field into an aquarium (Batenburg et al. 2011). Consequently, the aspect change observed on the *T. maxima* specimens is interpreted as reflecting the transfer of the specimens from the natural environment (i.e., greenish and translucent shell), to the aquarium (e.g., white and opaque shell). Specimens T-02-08 and T-03-08 present scars indicating disturbed shell deposition (Figures II-2b-c). For T-02-08, two scars are visible, one before and one after the specimen's transfer to the aquarium (Figure II-2b). For T-03-08, the scar occurred while the specimen was in its natural environment (Figure II-2c). The fossil specimen has a homogeneous outer shell layer (Figure II-2e).

a - Central ridge sampling



b - T-02-08



c - T-03-08



d - T-05-08



e - FOSSIL



Figure II-2 (previous page). *Thick sections of the central ridge cut in the modern Tridacna maxima specimens. Dotted black lines indicate the shell color transition related to the transfer of the specimens from the reef (in situ) to the aquarium (aqua.) the 22/02/2009. The thunderbolts show the scars associated to a growth stop. a - Global view of a Tridacna maxima valve before the extraction of the central ridge. Ridges are numbered from I to V. The part of the central ridge (III) to be extracted is shown in grey. b - Specimen T-02-08 : outer layer (OL), inner layer (IL) and hinge area c - Specimen T-03-08 d - Specimen T-05-08 e - Fossil specimen.*

Thin sections – The fluorescent calcein line resulting from the 23/02/2009 staining procedure is clearly visible under reflected UV light, providing an accurate tie-point to establish the sclerochronological and the geochemical time-series. Micrometric growth increments are observed on the three modern specimen thin sections (Figure II-3a). *Tridacna maxima* micrometric growth increment appears, under transmitted light, as a couple of one translucent layer and one opaque layer. The transition between the translucent and the opaque layer is sharp and the opaque layer thickness represents on average 55 to 85% of the total increment width (Figure II-3b). Each couple indicates a cycle of shell deposition composed of two-phases, with a higher deposition during the “opaque phase” of the cycle. Such banding pattern matches the definition of “simple growth increments” as proposed by Panella and MacClintock (1968) for *Tridacna squamosa*. Consequently, *T. maxima* shell growth increment was defined, and measured, as a couple of one translucent layer and one opaque layer (under transmitted light). Each growth increment was measured from the sharp transition between the opaque and the translucent layers, following the shell growth direction (Figure II-3b).

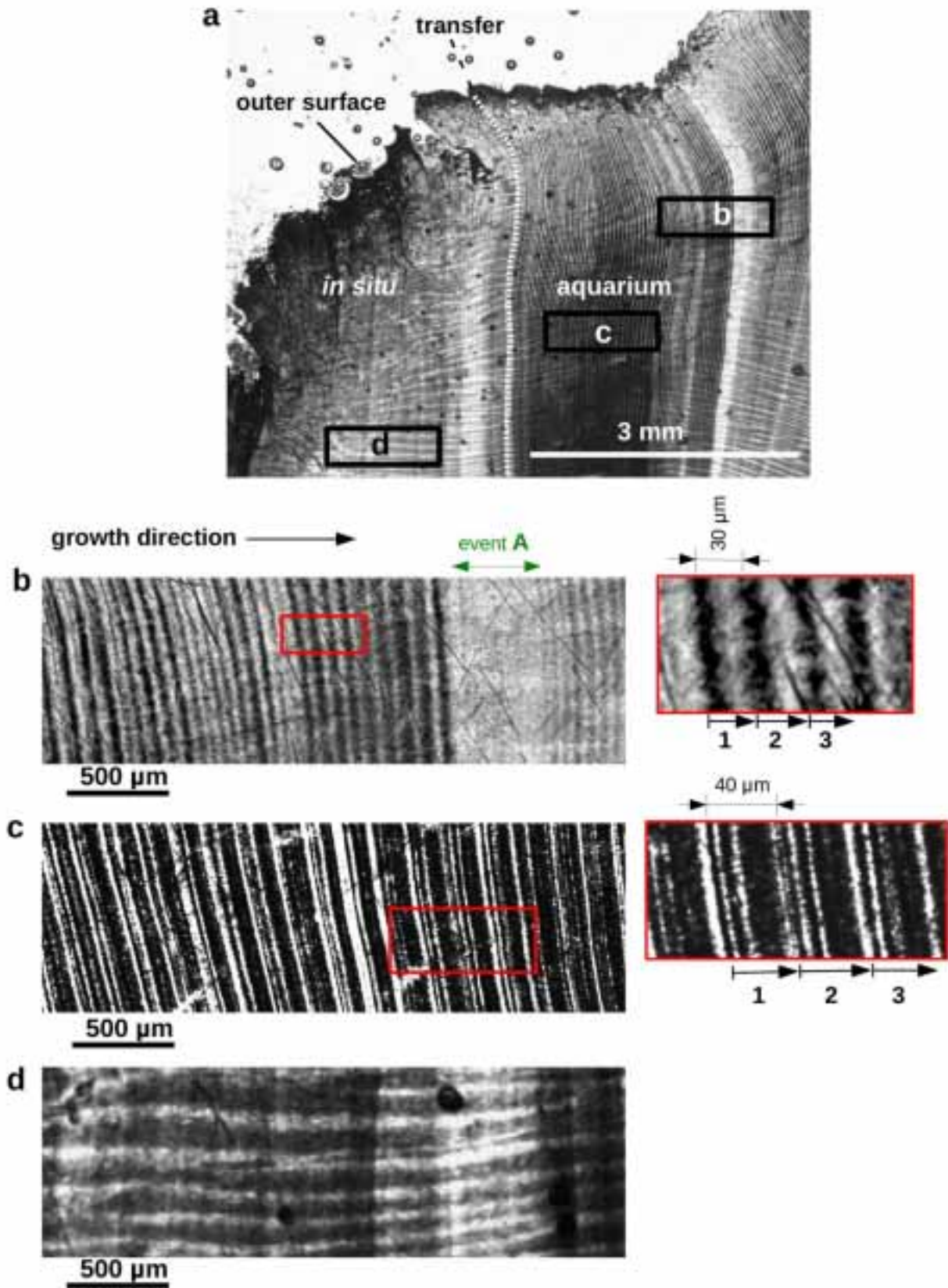
Most micrometric growth increments observed are simple growth increments. However, some growth increments, present an opaque layer splitting into thin couples of opaque and translucent sub-layers of variable thickness (Figure II-3c). Up to four couples of sub-layers are observed (Figure II-3c). Transitions between each of these sub-layers present various degrees of sharpness. This complex banding pattern is similar to the “complex growth increments” described by Panella and MacClintock (1968) in *Tridacna squamosa* shell. The boundaries of each complex growth increment were identified in the deep part of the outer layer, where the growth layers display a simple pattern. Once identified, growth increment boundaries were projected on the transect and then measured following the shell growth direction (Figure II-3c).

Figure II-3 (next page). *Details of the GIS-thin section of the shell of the Tridacna maxima specimen T-02-08, viewed under transmitted light a - View of the thin section showing different growth patterns at a x100 magnification. The white dotted line shows the transition between the greenish and translucent shell to the white and opaque shell, transition related to the transfer of the specimen from the reef to the aquarium (22/02/2009). Areas b, c, and d are enlarged below. b - Simple growth increment, i.e., daily increment, succession. Three daily increment are enlarged in the red insert (right). Arrows show how the measurements were done, ticks delimits one daily increment. The anomalous growth event A occurring in December 2008 is shown by the dark green arrow (see text for details). c - Complex daily growth increments, three are enlarged in the red insert (right). Arrows show how the growth thickness measurements were done, ticks delimits one daily increment. d - Blurry banding pattern characterizing the shell deposited in situ. On these parts, the crossed-lamellar microstructure of the outer layer appears as a banding pattern parallel to the growth direction, obscuring the daily growth increment pattern.*

The shell aspect change observed on the thick sections of the three modern specimens, as a response to the transfer into the aquarium, is associated to an abrupt change in the micrometric banding pattern. The greenish and rather translucent outer shell layer, deposited *in situ*, is characterized by a blurry micrometric banding pattern (Figure II-3d) that turns abruptly into a clear and continuous micrometric banding pattern after the transfer of the specimen into the aquarium. The transfer of the modern giant clam into the aquarium on 22/09/2008 is thus identifiable with precision in the three giant clam thin sections and can be used as a tie-point to assign time to the sclerochronological profile. The banding pattern of the three modern specimens became almost invisible in the last millimeter of growth, i.e., at the shell edge. The fossil specimen has a well-preserved banding pattern (except in the bio-eroded part) with the same simple and complex increment pattern as observed in the modern specimens.

c. Temporal resolution of the growth increments

To determine the deposition rhythm of “simple” and “complex” growth increments and potential cycles in the *Tridacna maxima* shell growth, time must be assigned to the sclerochronological profiles. Two tie-points are available for the modern specimens. The first tie-point is the fluorescent calcein line that indicates the 23/02/2009. The second tie-point is the shell aspect change reflecting the transfer of the individuals from the natural environment to the aquarium (22/09/2008). T-02-08’ shell has two scars indicating growth disturbances (Figure II-2a). Microscope observations of the scar located after the specimen transfer into the aquarium revealed the presence of filamentous forms of bio-eroders on the shell deposition surface (i.e, the part corresponding to the shell edge before the growth disturbance occurs).



Bio-eroders settlement on the shell edge indicates that the giant clam mantle was not fully extended during that period and that shell deposition had ceased for an unknown period. Consequently, growth increments were counted independently on each side of the scar. Growth increments preceding the scar were counted from the calcein staining (23/02/2009) toward the scar (Figure II-4). For the shell portion following the scar, growth increments were counted from the last visible increment backward toward the scar, assuming that this increment was deposited during the period May-June 2010 (Figure II-4). The sclerochronological profile of specimen T-03-08 was obtained by counting growth increments from the calcein staining (23/02/2009) toward the last visible growth increment (i.e., in the growth direction) and from the calcein staining backward in the direction of the shell color change (Figure II-4). For the specimen T-05-09 (not stained), the sclerochronological profile starts from the shell color change (22/09/2008) and continues toward the last visible increment (Figure II-4).

The number of increments between the calcein staining and the shell color change is 153 for T-02-08 and 133 for T-03-08 for a corresponding number of solar days (24 hours) of 154 and a corresponding number of lunar days (24.8 hours) of 160. This suggests that *Tridacna maxima* growth increment deposition occurs following a ~ 24 h frequency. Consequently, *T. maxima* growth increments will be termed daily increments. The sclerochronological record of specimen T-03-08 shows that in *T. maxima*, the number of days recorded may be underestimated by 7%.

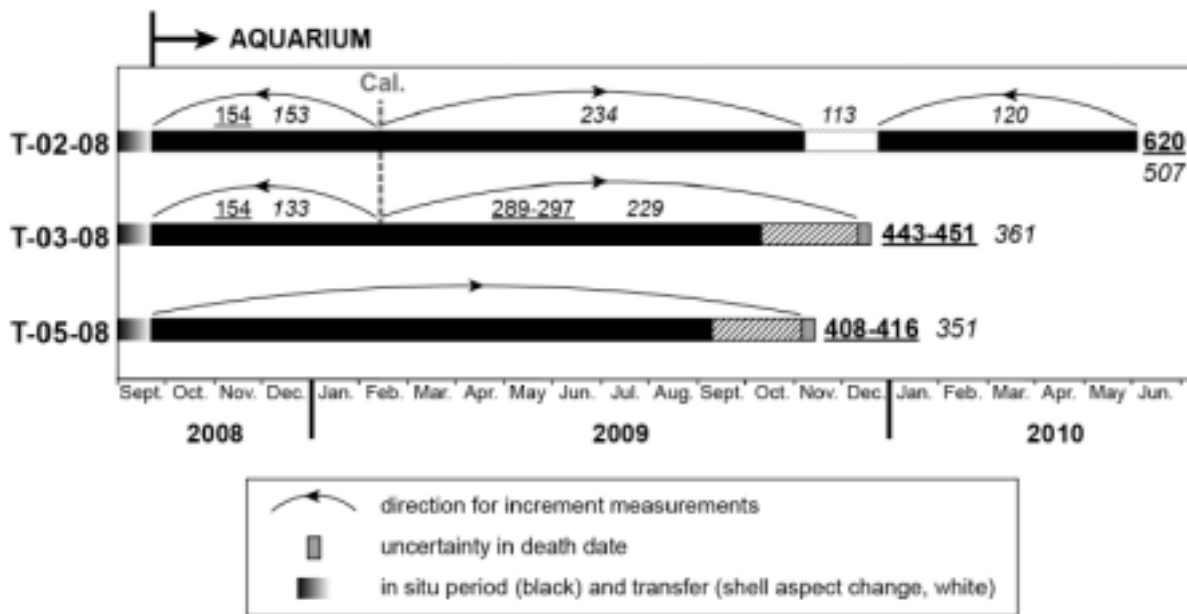


Figure II-4. Life history of the three modern *Tridacna maxima* specimens during the calibration period. On the figure are shown the number of days (underlined) and number of counted growth increments (non-underlined and *italic*). The calcein staining is indicated by a vertical grey dotted line and by “Cal.”.

d. Description of the modern sclerochronological profiles

Time was assigned to the daily increments to obtain sclerochronological time-series. The growth increment corresponding to the calcein staining was defined as day 23/02/2009 in the profiles of specimens T-02-08 and T-03-08. Date was then incremented at a daily step, backward until the shell color change (i.e., transfer into the aquarium) and forward until the scar for the specimen T-02-08 and until the last visible increment for the specimen T-03-08 (i.e., before the death of the specimen – see also Figure II-4). For the specimen T-02-08, the part of the shell deposited after the growth stop (i.e., scar) was anchored in time assuming that the last visible increment corresponded to the death of the animal. This assumption implies some imprecision's in the sclerochronological profile time assignation, considering that no increment are visible in the last deposited part of the shell. For specimen T-05-08 (not stained), date was incremented from the color change toward the last visible increment.

The sclerochronological profile of specimen T-02-08 spans 22/09/2008 to 14/10/2009 and 03/02/2010 to 03/06/2010. Approximately four months are missing in this record, from October 2009 to February 2010 (cf. scar – Figure II-4). The sclerochronological profiles of T-03-08 and T-05-08 span 14/10/2008 - 09/10/2009 and 22/09/2008 - 08/09/2009 respectively (Figure II-4). According to the counting procedure, T-03-08 and T-05-08 sclerochronological records stopped in September and October 2009, respectively, whereas these specimens died in December 2009 and November 2009. T-03-08 and T-05-08 sclerochronological records are thus shorter by about three and two months than the lifetime of the giant clams. This mismatch is beyond the 7% precision previously observed (cf. above section III-c *Temporal resolution of the growth increments*) suggesting that the specimens T-03-08 and T-05-08 had ceased growth three or two months before dying.

The three sclerochronological profiles share a common period : September 2008 to September 2009. A composite profile was constructed by averaging the three sclerochronological profiles for the common period and the T-02-08 profile was used to complete the record beyond September 2009. The three specimens ceased growth between September and October 2009 resulting in a gap in the sclerochronological records (Figures II-4 and II-6). On the spectral analysis of the composite profile, a significant frequency peak occurs at $0.00277 \text{ days}^{-1}$, indicating a ~ 360 day cycle that confirms a daily increment deposition. No peak occurs at around 15 days, excluding a tidal influence on shell growth (Figure II-5).

The mean daily increment thickness of the *Tridacna maxima* specimens, T-02-09, T-03-09, and T-05-09 are $35 \pm 21 \mu\text{m}$, $36 \pm 17 \mu\text{m}$, and $42 \pm 17 \mu\text{m}$ over the period September 2008 to September 2009. The sclerochronological profiles of the three specimens present similar seasonal variations (Figure II-6). The seasonal variations in the daily growth increments thickness are due to a change in the thickness of both the opaque and the translucent layers. However, opaque layers remain generally wider than the translucent ones. Linear regressions between the three sclerochronological profiles for the common period (22/09/08 – 08/09/2009) show that the three profiles are well correlated (Table II-1). The sclerochronological profile of T-02-09 presented the lowest correlation coefficient with the others profiles. This specimen is characterized by higher daily growth variability than the two other specimens, which probably explains the lowest correlation.

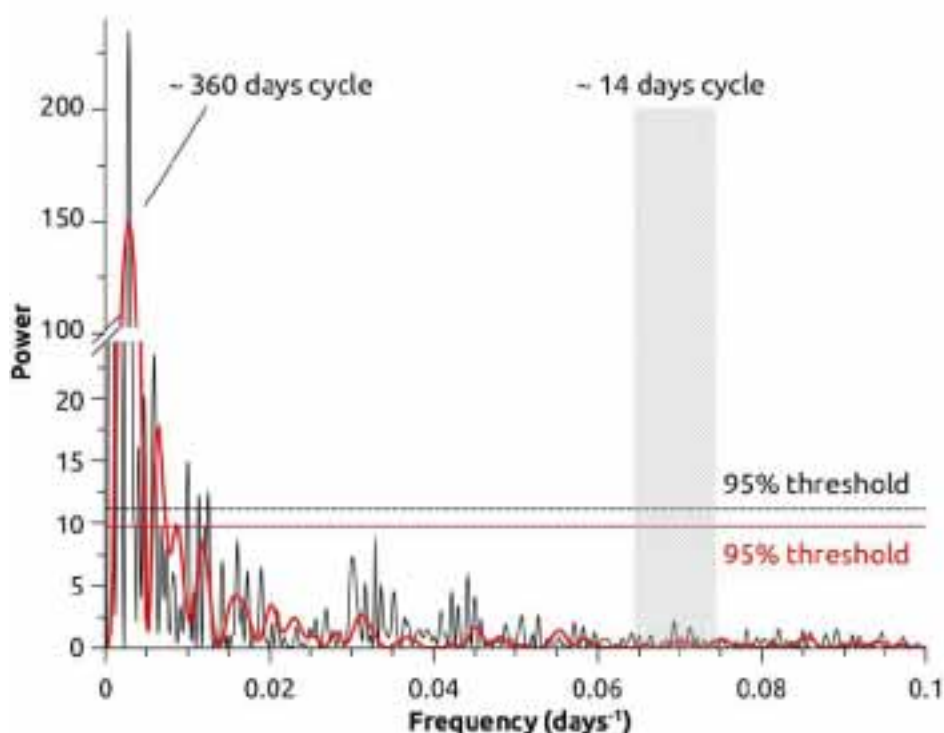


Figure II-5. Spectral analysis of the modern composite (red) and of the fossil (black) sclerochronological profiles.

Table II-1 : Pearson correlation coefficient (R) between the sclerochronological profiles of the three modern giant clams for the period : 22/09/2008 to 31/10/2009. * p-value < 0.01.

	T-03-08	T-05-08	composite
T-02-08	0.37*	0.47*	0.77*
T-03-08		0.72*	0.83*
T-05-08			0.91*

Sclerochronological profiles of the three specimens follow SST changes rather accurately (Figure II-6). Nevertheless, on the T-02-08 profile, a severe growth reduction is observed in mid-November 2008 (Figure II-6a). Daily increment thickness passes within six days from 45 μm to 8 μm , and stays at around 8 μm for 20 days before to resume growth again, up to the values preceding the anomalous growth event. This event will be termed “event A”. On the thin section, this event is characterized by a very discrete, almost translucent daily banding pattern (Figure II-3b). An anomalous growth event is also visible in the T-05-08 profile at the beginning of March 2009. The daily growth started to decrease and reached 20 $\mu\text{m}\cdot\text{d}^{-1}$ by mid-March (Figure II-6c).

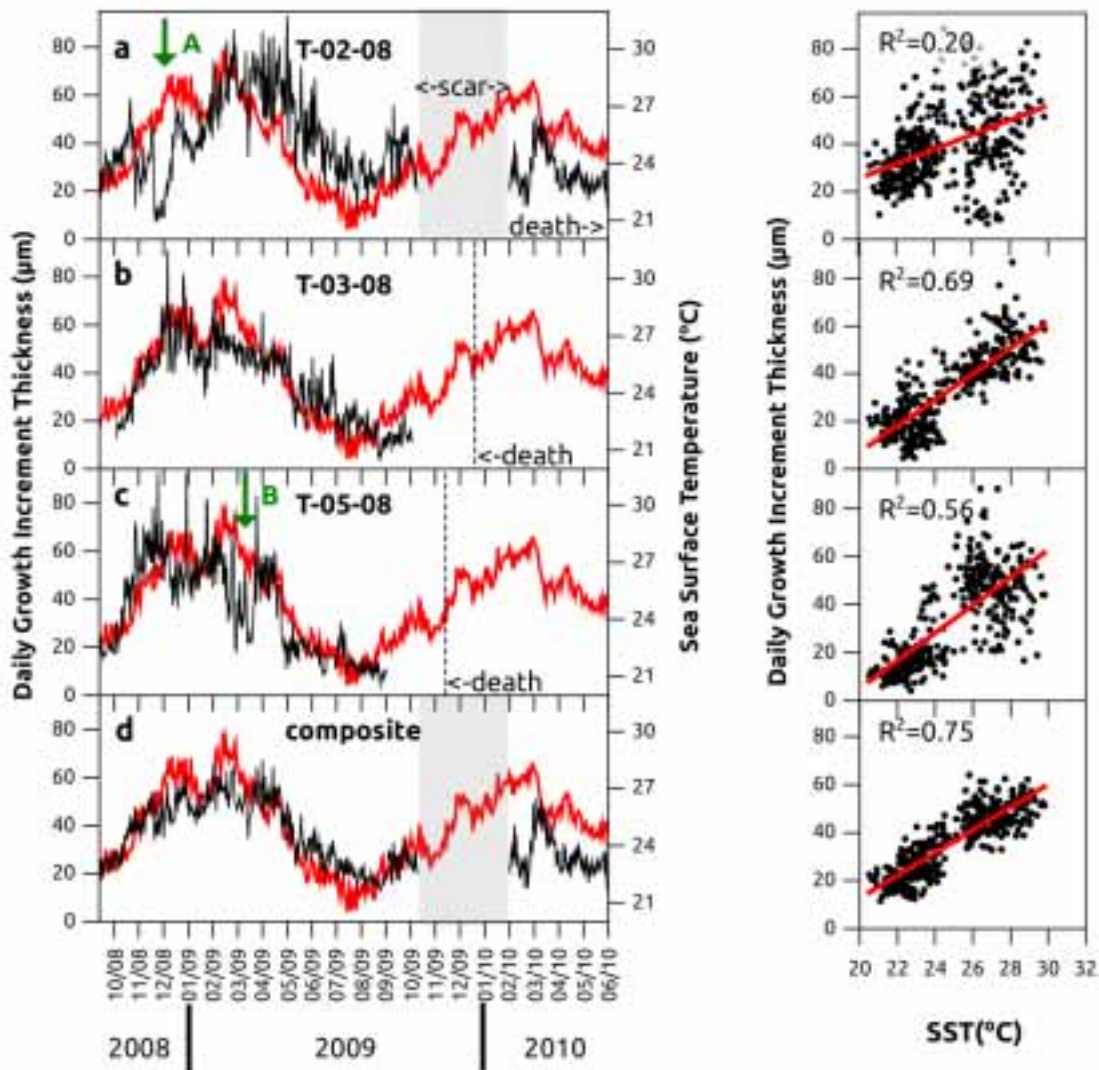


Figure II-6. Sclerochronological profiles of the three modern *Tridacna maxima* shells (black) together with the SST variations (red). Regressions between daily increment thickness and SST are shown on the right of each profile. The R^2 values are significant at a 95% threshold. **a** to **c** - T-02-08, T-03-08, and T-05-08. **d** - Composite profile. For T-02-08 and the composite profile, regressions did not include the data after the scar. Dotted lines indicate the date of death of the specimens. Anomalous growth events A and B are shown by green arrows (see text for details).

From mid-March, growth is characterized by daily increments with highly variable thicknesses. Normal growth resumes at the beginning of April. This oscillating growth event, termed thereafter “event B”, lasted one month. The composite profile (i.e., average of the three sclerochronological profiles) matches well the SST variations from September 2008 to September 2009 (Figure II-6d). The mean daily growth rate calculated from the composite profile is $37 \pm 16 \mu\text{m.d}^{-1}$. The mean summer (January to March : JFM) growth increment thickness for this profile is $51 \pm 6 \mu\text{m}$, the mean winter (July to September : JAS) value is $21 \pm 5 \mu\text{m}$. In New Caledonia today, giant clam *Tridacna maxima* growth is thus on average 58% higher in summer than in winter.

e. Relation between growth increment thickness and SST

The individual and the composite sclerochronological profiles are significantly correlated to the SST measured in the aquarium on the period September 2008 to September 2009 (Figure II-6). Apart from T-02-08, the R^2 are higher than 0.5. The highest regression coefficient is found for the composite profile ($R^2 = 0.75$, $p < 0.001$), with the resulting equation :

$$\text{SST} = 0.151 \times \text{growth} + 19.15 \quad (1)$$

where SST is the sea surface temperature in degree Celsius and growth is the composite *T. maxima* daily growth increments thickness (micrometer). The standard deviation of the residuals is 1.3°C (1σ).

f. Fossil sclerochronological record

The sclerochronological profile of the Late Holocene *Tridacna maxima* presents five cycles of alternating periods of thick and thin growth increments (Figure II-7). According to the observations made on the modern sclerochronological profiles, these cycles have presumably a yearly frequency and thicker and thinner growth increments most likely correspond to summer and winter periods. Winter periods are better defined than summer periods, they were thus used as tie-points for cycles numbering. After the cycle V, no cycle is visible and the daily growth increments decrease until the death of the specimen. Consequently, the sclerochronological study and the spectral analysis focused on cycles I to V. Time was arbitrarily assigned to the fossil record by attributing a date to each growth increment. Growth increments present a clear Gaussian shape during the transition from cycle II to III, the lowest growth increment thickness was thus set as August, 15th which is the center of the coldest month observed today in New Caledonia. Then, dates were incremented to the preceding and following months, toward each extremity of the record. The mean daily growth increment thickness recorded from cycle I to V is $48 \pm 12 \mu\text{m}$. The mean summer (JFM) growth increment thickness is $53 \pm 13 \mu\text{m}$ and the mean winter (JAS) value is $44 \pm 11 \mu\text{m}$. The difference between summer and winter growth for the fossil specimen is 26%. The spectral analysis revealed a significant (95%) frequency at ca. $0.00277 \text{ days}^{-1}$ corresponding to the annual cyclicity (Figure II-5). The daily increment deposition of the fossil *T. maxima* is thus confirmed. No tidal influence appears in the spectral analysis (Figure II-5).

g. Reconstruction of SST mean seasonal cycle from daily growth increments

Past SST seasonal cycle is a key parameter to study climate changes and paleo-SST seasonal cycles are a valuable benchmark against which to evaluate climate models. Such information may be obtained from the sclerochronological profiles of *Tridacna maxima*. The daily sclerochronological profiles of the modern (composite 09/2008-09/2009) and the fossil data were averaged into monthly time-series. For the 5 year-long fossil data, monthly values were calculated by averaging all daily growth values corresponding to months of January, to February, etc. The mean-seasonal growth cycles were then converted into SST using equation 1 (Figure II-8).

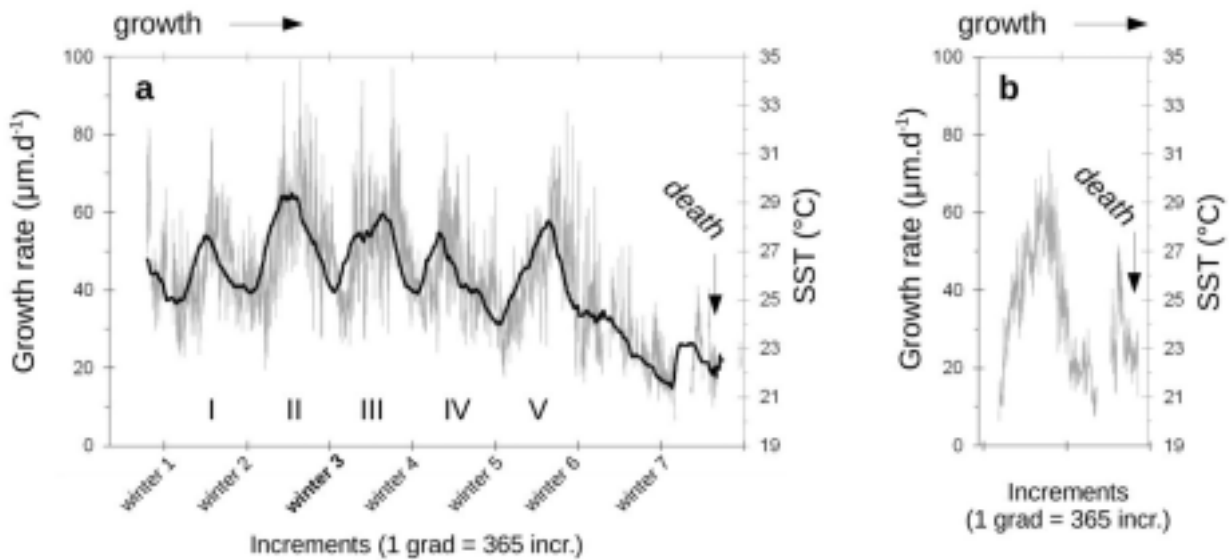


Figure II-7. Sclerochronological profiles and equivalent SST values (equation 1) versus time of **a** - the fossil (black curve is a 30 points running average) and **b** - the modern *Tridacna maxima* (composite) from New Caledonia.

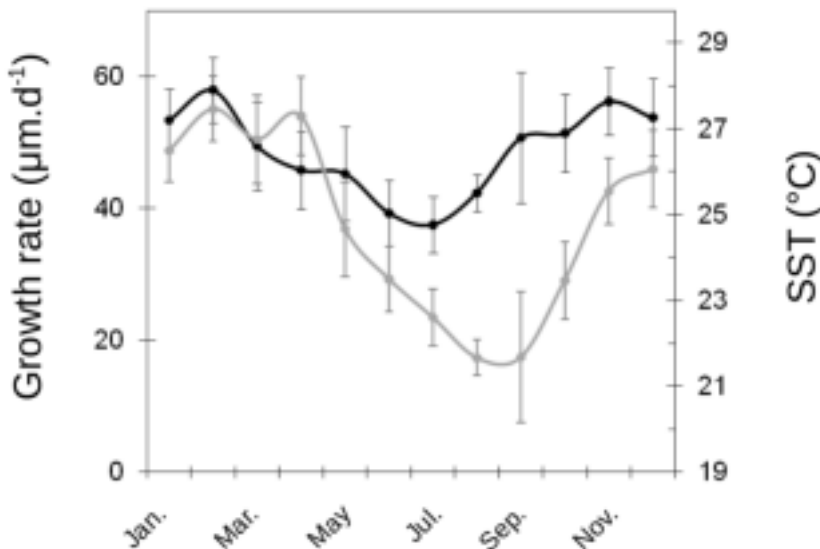


Figure II-8. Reconstructed mean seasonal SST cycle based on the sclerochronological profiles from modern (grey) and fossil (black) *Tridacna maxima* specimens. Error bars represent one standard deviation.

The SST record reconstructed from the modern sclerochronological data present mean, summer, and winter values comprised within the standard deviation interval of the SST value recorded by the logger for the period 09/2008-09/2009 (Table II-2). The modern sclerochronological record underestimates the annual amplitude by 18%. The fossil record presents a mean SST value higher by ~ 2°C than the two modern mean SST values (Table II-2).

Table II-2. Instrumental sea surface temperature (SST – °C) recorded in the aquarium (logger) and reconstructed SST from the modern and the fossil *Tridacna maxima* sclerochronological profiles. Modern data encompass the period September 2008 to September 2009. JFM: January to March - summer; JAS: July to September – winter.

	logger	modern	fossil
<i>mean ± sd</i>	24.8 ± 2.4	24.5 ± 2.4	26.5 ± 1.9
<i>JFM</i>	27.7 ± 0.9	26.9 ± 0.9	27.2 ± 1.9
<i>JAS</i>	22.2 ± 0.8	22.3 ± 0.8	25.7 ± 1.7
<i>amplitude</i>	5.5	4.5	1.5

The reconstructed SST records from the fossil and the modern specimens displayed similar summer SST values whereas the mean winter value recorded by the fossil is ~ 3°C higher than the modern mean winter values. The fossil SST seasonal amplitude is lower than the amplitude recorded by the modern specimen by 70% (Table II-2).

h. Oxygen stable isotope data

The $\delta^{18}\text{O}_{\text{shell}}$ time-series obtained on the giant clam T-02-08 has approximately a weekly resolution. The $\delta^{18}\text{O}_{\text{shell}}$ profile displays a clear seasonal pattern whereas the $\delta^{18}\text{O}_{\text{sw}}$ profile remains around 0.24 ± 0.18 ‰ vpdb during the calibration period (Figure II-9). The $(\delta^{18}\text{O}_{\text{shell}} - \delta^{18}\text{O}_{\text{sw}})$ profile displays a clear seasonal pattern. Data corresponding to the January to March (July to September) months were averaged to obtain summer (winter) mean values. Mean summer value was -1.51 ± 0.10 ‰ vpdb and mean winter value was -0.39 ± 0.17 ‰ vpdb (Figure II-10). The annual amplitude (JFM minus JAS) is 1.12‰ vpdb. The isotopic composition $(\delta^{18}\text{O}_{\text{shell}} - \delta^{18}\text{O}_{\text{sw}})$ of the shell deposited after the growth stop of September 2009 is poorly correlated to SST (Figure II-10), probably because of the peculiar event that disturbed shell deposition (i.e., scar) evidenced by the sclerochronological study (Figure II-6a). Those data were thus excluded from the following calculation. The $(\delta^{18}\text{O}_{\text{shell}} - \delta^{18}\text{O}_{\text{sw}})$ is significantly anti-correlated to SST (Figure II-10). The equation that links $(\delta^{18}\text{O}_{\text{shell}} - \delta^{18}\text{O}_{\text{sw}})$ to SST for that period is :

$$\text{SST} = -3.56 \times (\delta^{18}\text{O}_{\text{shell}} - \delta^{18}\text{O}_{\text{sw}}) + 20.5 \quad (2)$$

where $(\delta^{18}\text{O}_{\text{shell}} - \delta^{18}\text{O}_{\text{sw}})$ is expressed in ‰ vpdb and SST is the sea surface temperature in degree Celsius. The standard deviation of the residuals is 1.23°C (1σ) and the regression coefficient is $R^2 = 0.70$ (p<0.05).

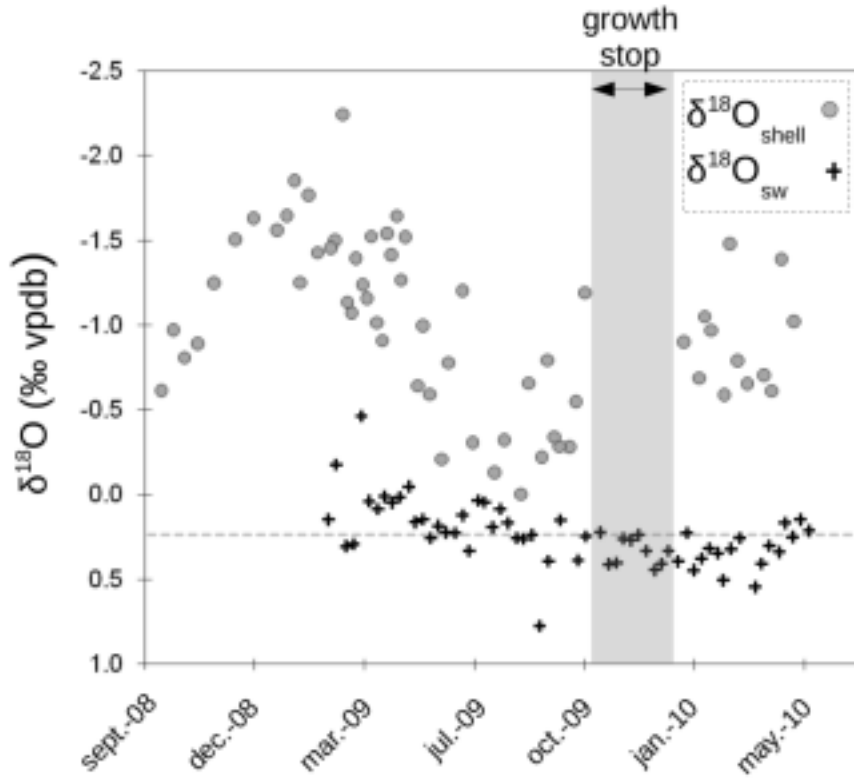


Figure II-9. Oxygen stable isotope composition of *Tridacna maxima* specimen T-02-08 ($\delta^{18}O_{shell}$) and aquarium seawater $\delta^{18}O_{sw}$. The grey dashed line represents the averaged $\delta^{18}O_{sw}$ value.

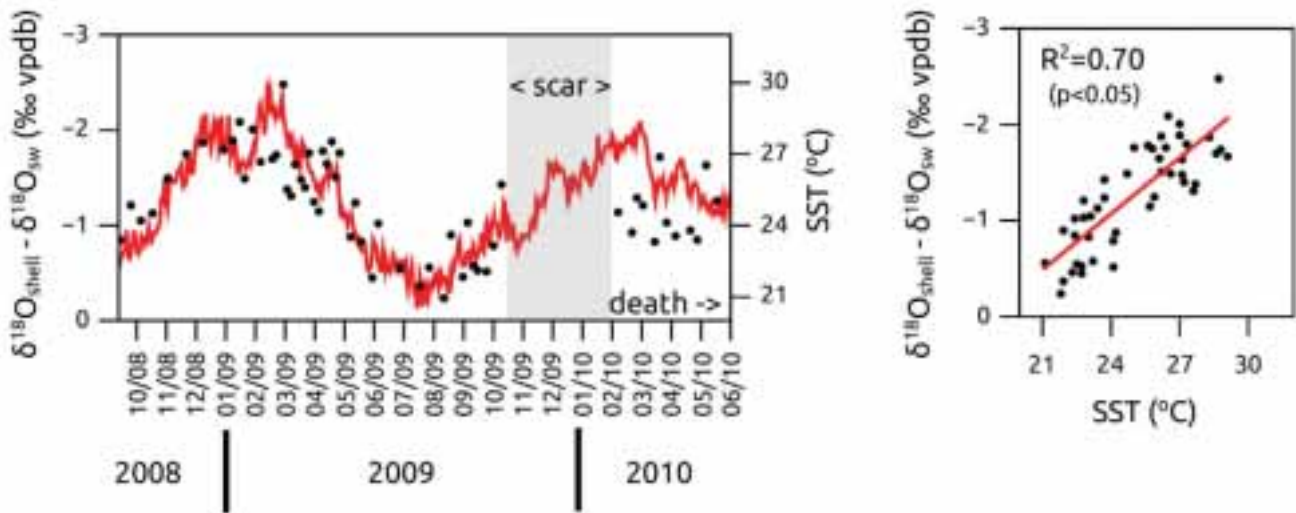


Figure II-10. Seasonal variation of $(\delta^{18}O_{shell} - \delta^{18}O_{sw})$ from the *Tridacna maxima* specimen T-02-08 (black dots) and SST (red curve) and regression of $(\delta^{18}O_{shell} - \delta^{18}O_{sw})$ against SST. The data after the scar are excluded from the regression.

IV. Discussion

a. Shell deposition cycles in *Tridacna maxima*

Thin sections of the three modern *Tridacna maxima* revealed micrometric growth pattern that reflect shell deposition cycles occurring at different frequencies. The main growth increment pattern, composed of couples of translucent and opaque layers, records the ~ 24 hour cycle. A more discrete growth increment pattern was observed in some of the daily growth increments, evidencing sub-daily deposition cycles.

Influence of the tidal cycle – The three modern giant clams *Tridacna maxima* were collected in a sub-tidal environment and then grown in an aquarium with a constant water level. However, tidal regime may still influence the properties of the seawater : dissolved organic carbon, suspended matter, particulate organic carbon, biomass and salinity (Cadée 1982; Weber and Woodhead 1971). Such changes might influence giant clam growth. Nevertheless, no tidal frequency occurred in the spectral analysis of the sclerochronological profile of the modern specimens : tidal regime did not influence the *T. maxima* growth in the environmental context of this study. This is in agreement with previous studies that revealed that giant clams growth increments reflect solar days (Aubert et al. 2009; Henocque 1980; Sano et al. 2012; Schwartzmann et al. 2011; Watanabe and Oba 1999).

Daily variation in shell deposition rate – *Tridacna maxima* daily increments are characterized by an opaque layer being thicker than the translucent one, characterizing thus a higher deposition rate. In bivalves, shell-forming tissues are located on the mantle; consequently, shell deposition occurs when valves are open and the mantle extended along the shell margins, bringing the shell-forming tissues in contact with the internal surface of the shell (Pannella and MacClintock 1968; Schöne 2008; Wheeler 1992).

Moreover, in giant clams, mantle expansion also permits an optimal lightening of the zooxanthellae located in the mantle of the animal, enhancing the photosynthetic production of the symbionts, which ultimately benefit their host (e.g., Griffiths and Klumpp 1996; Jantzen et al. 2008; Yonge 1975). As a consequence, the thick opaque layer of a daily increment, characterizing fast shell deposition rate, is most likely deposited during day-time, when the valves are opened and the mantle fully extended. At the opposite, phases of lower shell deposition rate, leading to the thin translucent layer, may occur at night, when giant clam valves are partially closed and mantle contracted. This indicates that, although reduced, shell deposition occurs also at night. These assumptions are supported by a study performed on *Hippopus hippopus* that showed that this giant clam species has its valves open during the day and partially closed during the night (Schwartzmann et al. 2011). Consequently, in *T. maxima*, daily increment thickness and the geochemical composition of the shell deposited within a day, reflects both night-time and day-time conditions with a greater influence of day-time conditions.

Sub-daily deposition cycles – The *Tridacna maxima* shell growth pattern is also characterized by a sub-daily pattern, forming complex growth increments (Figure II-3b). By analogy with the day/night depositional cycles, it may be inferred that the opaque layers may reflect high

shell deposition rate that occurs when the valves are open and the mantle fully extended, allowing optimal photosynthetic performances. Thin translucent increments, in turn, indicate periods of low shell deposition rate while valves are partially closed and the mantle partially retracted. This sub-daily banding might thus be related to sub-daily rhythms in shell deposition, itself related to sub-daily gaping behavior in *Tridacna maxima*.

b. SST reconstruction from daily growth increments thickness

The daily increments of the three modern *Tridacna maxima* specimens from New Caledonia recorded the seasonal variations of the sea surface temperature (SST) from September 2008 to September 2009. Seventy five percent of the composite daily increment thickness variations were explained by the SST, the *T. maxima* shell growth is thus strongly influenced by SST. A transfer function, linking the growth increments thickness and the SST was calculated (1). This equation may apply to fossil sclerochronological profiles and would potentially provide paleo-SST records. However, the reliability of this equation relies on the coupling between growth increment thickness and SST that may be disrupted by various environmental or physiological factors.

Ontogenic influence may biases the relation between growth increment thickness and SST, indeed, *Tridacna maxima* growth follows an asymptotic trend (Green and Craig 1999; McKoy 1980; McMichael et al. 1974; Munro and Heslinga 1983; Smith 2011). This implies that the equation linking growth increment thickness to SST may change during the bivalve's life, because the growth increments thickness decreases with the age of the specimen. Consequently, equation 1, that link daily shell growth to SST, may not be applicable in the earliest parts of the shell. In this study, this ontogenic effect was avoided by studying three modern specimens that have the same age.

Observation of the modern *Tridacna maxima* sclerochronological profiles revealed that decoupling between the growth increment thickness and SST variations occurred during the period of experiment. The first growth anomaly was only observed on the T-02-08 shell. It lasted approximately one month and occurred before the weekly observation program started (event A). This event is characterized by a very discrete daily banding pattern (Figure II-3a). This section has an aspect similar to that of the night-time shell deposition and is thus interpreted as reflecting slow shell deposition phases, which occur when the valves are partially closed. In giant clams, the energy brought by the photosynthetic symbionts and, to a lesser extent, by filter feeding, is allocated to growth, reproduction, or energy storage. Thus, a shell deposition decrease, as observed during event A, indicates that less energy was allocated to growth, which traduces a reorganization of the giant clam energy budget, possibly in response to various stressing factors (e.g., reproduction, disease, predators, bio-erosion, storms etc.).

Spawning-related growth slowdown has been described in various bivalve shells (e.g., Kanazawa and Sato 2008; Rhoads and Lutz 1980; Schöne 2008). In giant clams, reproduction requires a lot of energy, which is thus transferred from growth to reproduction (Hean and Cacho 2003; Klumpp and Griffith 1994; Lucas 1994). Growth decrease, without any other identifiable cause, like bio-erosion or environmental stress, has been interpreted as spawning-

related in *Hippopus hippopus* (Aubert et al. 2009). For recall, all *Tridacna maxima* specimens studied here have reached sexual maturity. In addition, the “event A” observed in the T-02-08 shell does not correlate with any peculiar SST variation and this growth anomaly mimics what has been observed in *H. hippopus*. Consequently, “event A”, in the sclerochronological profile of T-02-08, is most probably linked to a spawning event.

The second independent growth anomaly (event B - Figure II-3c) occurred in T-05-08, just after the summer SST maxima. Event B probably indicates a temperature-induced physiological disorder. However, the growth of the two other giant clams was not affected by this SST peak suggesting inter-individual differences in *T. maxima* SST tolerance. Inter-individual differences are also revealed by the sclerochronological profile of specimen T-02-08 which. This specimen presents a higher growth rate and higher daily increments thickness variability than the two others specimens during the calibration period, which cannot be related to any peculiar SST variations. These observations show that, although SST is the main factor influencing *T. maxima* growth, other factors, intrinsic to the individual, e.g., physiological or genetic, may also play a role in the shell deposition rate of *T. maxima*.

The three sclerochronological profiles of the modern *Tridacna maxima* specimens displayed a simultaneous growth stop in September/October 2009. A change in the three giant clam behaviors was observed on November 2009. The three giant clams had their mantle retracted and had a poor response to shading and touching stimuli. Two specimens even died in the three following months and the sole specimen that survived this peculiar event presents a well pronounced scar (Figure II-2a). The simultaneity of these growth stops suggests that they have a common origin. During the weekly monitoring it has been reported that five *Porites sp.* colonies were introduced in the aquarium from the 19/08/2009 to the 27/08/2009. These coral specimens were not part of the calibration experiment. The introduction of these coral colonies might have brought some infectious agent inside the aquarium that would have caused the death of two of the *T. maxima* specimens. Norton et al. (1993) reported cases of juvenile and adult clams mortalities by the bacterial parasite *Rickettsial sp.* Interestingly, the authors also mentioned that one of the symptoms of a *Rickettsial sp.* infestation is a retraction of the giant clam mantle, as observed here, suggesting that such an infection occurred in the aquarium, in September 2009. A scar, similar to the one visible on specimen T-02-08 shell during the peculiar September 2009 event, is visible in the shell of the same specimen and in the shell of specimen T-03-08. These scars are located on the shell portion deposited while the specimens were still on the reef (Figures II-2a and II-2b). This reveals that similar growth stops also occur in the natural environment, most likely under adverse conditions.

This study on *Tridacna maxima* shell growth showed that 1) adverse conditions, such as a *Rickettsial sp.* (or others) infestation, may generate a simultaneous growth stop in a *T. maxima* population that can lead to a scar formation in some specimens, 2) *T. maxima* can cease growth for four months when facing adverse conditions, 3) the sensitivity level of individual *T. maxima* specimens to adverse conditions is variable, 4) scars in *T. maxima* shell indicate potentially prolonged growth stop and possibly a population die-off, 5) in a shell portion overgrowing a scar, the relation between the growth increment thickness and SST can be

disrupted for a period up to four months and 6) replicated and overlapping sclerochronological profiles are necessary for accurate SST reconstruction.

Composite *Tridacna maxima* sclerochronological profiles can thus provide information on past SST, with a precision of about 1.3°C. To investigate further the potential of fossil *Tridacna maxima* specimen for past-SST reconstruction, the sclerochronological profile of the fossil specimen was converted into SST using equation 1. The mean seasonal cycle was reduced by about 70% compared to the modern *T. maxima* specimen record (Figure II-8). The low seasonal amplitude recorded by the fossil giant clam is beyond the difference of amplitude recorded by the modern giant clam compared to the instrumental SST record (Table II-2). This suggests that the seasonal SST cycle was significantly reduced 3,000 years ago. The record of the fossil specimen revealed that the SST may have been about 2°C higher 3,000 years ago, due to warmer winters. It is beyond the scope of this study to interpret the fossil data in terms of paleoclimate and paleoenvironment, however, this study demonstrates that *Tridacna maxima* sclerochronology is an interesting alternative to stable isotopic studies to obtain information about the average, minimum, and maximum past SSTs.

Moreover, the seasonality in *Tridacna maxima* daily increment thickness change provides additional information about the seasonal SST amplitude. This point is of prime interest because SST amplitude is a key variable to investigate the climatic system, e.g., in response to an orbitally-induced insolation change as it occurred during the Holocene (e.g., Braconnot et al. 2000; Sun et al. 2005). In an archeological context, sclerochronology may help to determine seasonal patterns in human harvesting habits (Lutz and Clark 1984; Rhoads and Pannella 1970). However, although this goal could not be achieved in this study because of the dramatic ontogenic growth decrease observed in the last years of the 3000 year-old *Tridacna maxima* specimen, it would be possible to get such information with younger specimens.

c. Oxygen stable isotope as a proxy for SST

This is the first time that an equation linking ($\delta^{18}\text{O}_{\text{shell}} - \delta^{18}\text{O}_{\text{sw}}$) and SST is produced for *Tridacna maxima* (equation 2). This study showed that SST can be reconstructed using the ($\delta^{18}\text{O}_{\text{shell}} - \delta^{18}\text{O}_{\text{sw}}$) values with a precision of $\pm 1.23^\circ\text{C}$. The precision of *Tridacna maxima* $\delta^{18}\text{O}_{\text{shell}}$ equation is similar to the range reported for *Hippopus hippopus*; 1°C - 1.4°C (Aubert et al. 2009; Watanabe and Oba 1999). The equation produced for *Tridacna maxima* has a similar slope than that published for *Hippopus hippopus* records (Aubert et al. 2009; Watanabe and Oba 1999) and that of a composite record including various giant clam species (Aharon and Chappell 1986). This observation suggests that giant clam $\delta^{18}\text{O}_{\text{shell}}$ records SST variation independently of the genus. The main difference between these equations is the y-intercept (Figure II-11). Y-intercept is generally the main source of uncertainties for transfer functions linking geochemical proxies and SST (e.g., Sr/Ca in corals, see Corrège 2006). The causes of these uncertainties may be related to the carbonate sampling method, i.e., micromilling (Aubert et al. 2009; this study) versus freezing microtome sampling technique (Watanabe and Oba 1999) and on the instrumental datasets used for the calibration, e.g., *in situ* measurements (this study) versus local datasets (Aubert et al. 2009; Watanabe and Oba

1999). Moreover, the use of calcitic standards (e.g., NB19), to correct the isotopic fractionation occurring during the phosphoric acid dissolution of the carbonate samples, may be inappropriate for aragonitic samples like the giant clam shell. Indeed, it has been demonstrated that the fractionation coefficients of the aragonite and of the calcite versus the phosphoric acid temperature were different, although still subject to uncertainties (Gilg et al. 2007; Kim et al. 2007). This point may be a major cause of systematic biases among laboratories, possibly leading to the observed differences in the y-intercept of the SST proxy transfer functions.

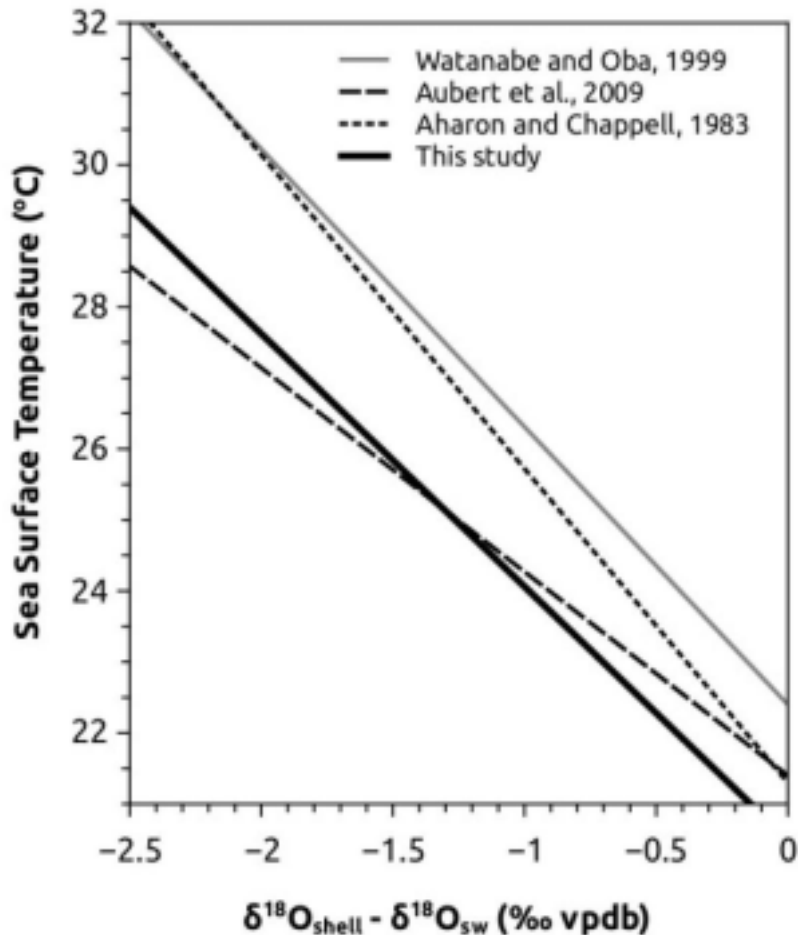


Figure II-11. $(\delta^{18}O_{shell} - \delta^{18}O_{sw})$ and SST empirical transfer functions produced for giant clams, *Hippopus* sp. and *Tridacna* sp. genus. $(\delta^{18}O_{shell} - \delta^{18}O_{sw})$ data produced in this study is shown by black dots.

However, systematic analytical biases may not affect the slope of the equation linking $(\delta^{18}O_{shell} - \delta^{18}O_{sw})$ and SST. An averaged SST/ $(\delta^{18}O_{shell} - \delta^{18}O_{sw})$ slope was thus calculated from both *Tridacna* and *Hippopus* genera data; this returns a mean slope of $-3.82 \pm 0.75^{\circ}\text{C}.\text{‰ vpdb}^{-1}$ (Aharon 1980; Aubert et al. 2009; Watanabe and Oba 1999; this study). The standard deviation of $0.75^{\circ}\text{C}.\text{‰ vpdb}^{-1}$ associated to this slope shows that *Tridacnidae* $(\delta^{18}O_{shell} - \delta^{18}O_{sw})$ is a reliable proxy for past climate reconstruction and gives the opportunity to work with the abundant fossils of this species, in particular with those found in the archaeological deposits of the Pacific islands (Moir 1989).



Collecte d'un b nitier Tridacna maxima fossile, datant de la transition Holoc ne inf rieur / Holoc ne moyen, sur les terraces r cifales quaternaires de Espiritu Santo (Vanuatu). Jean-Christophe Galipaud – Octobre 2009. Cr dit photo: Claire E. Lazareth.



Chapitre III – Early mid-Holocene SST variability and surface-ocean water balance in the Southwest Pacific

Ce chapitre est publié dans la revue *Paleoceanography*.

Auteurs (dans l'ordre) :

Duprey Nicolas,
Lazareth Claire E.,
Corrège Thierry,
Le Cornec Florence,
Maes Christophe,
Pujol Nicolas,
Madeng-Yogo Magloire,
Caquineau Sandrine,
Soares Derome Caroline,
Cabioch Guy.

Citation :

Duprey, N., C. E. Lazareth, T. Corrège, F. Le Cornec, C. Maes, N. Pujol, M. Madeng-Yogo, S. Caquineau, C. Soares Derome, and G. Cabioch (2012), Early mid-Holocene SST variability and surface-ocean water balance in the southwest Pacific, *Paleoceanography*, 27(4).

Étapes du processus de publication :

reçu : 23 mai 2012;
révisé : 28 septembre 2012;
accepté : 2 octobre 2012;
publié : 17 novembre 2012.

RÉSUMÉ

Des enregistrements de Sr/Ca, $\delta^{18}\text{O}$ et de $\delta^{18}\text{O}_{\text{sw}}$ ont été obtenus à partir de fossiles de coraux massifs *Porites sp.* (6.7–6.5 ka BP) et d'un bénitier *Tridacna maxima* (6.2–6.0 ka BP) datant de la transition Holocène inférieur / Holocène moyen. Les données de Sr/Ca, $\delta^{18}\text{O}$ et de $\delta^{18}\text{O}_{\text{sw}}$ sont ici considérées comme des proxies de la température (SST) et de la salinité (SSS) de surface de l'océan. Les enregistrements géochimiques issus des fossiles ont été comparés à des enregistrements similaires obtenus à partir de spécimens actuels de coraux *Porites sp.* et de bénitiers *Tridacna maxima*.

Les SST reconstruites à partir des coraux fossiles et du corail actuel sont similaires ce qui implique que la position de la marge sud-est de la Western Pacific Warm Pool (WPWP) était analogue à sa position actuelle aux alentours de 6.7–6.5 ka BP. Le réchauffement post-glaciaire du Pacifique Sud-Ouest était donc achevé durant la transition Holocène inférieur/moyen.

Les coraux et le bénitier fossiles ont enregistré des conditions plus salées que l'actuel dans le Pacifique Sud-Ouest en lien avec 1) un découplage entre le régime des précipitations et la SPCZ due à une position plus septentrionale de cette dernière et 2) une intensification du transport de chaleur vers la zone extra-tropicale due à un renforcement de la circulation de Hadley.

L'enregistrement de $\delta^{18}\text{O}$ obtenu à partir de la colonie corallienne couvrant la plus longue période de temps montre que l'amplitude de El Niño Southern Oscillation (ENSO) était réduite de 20-30% comparé à la variabilité ENSO de la période 1928-1992. Cette observation est en accord avec la tendance à une réduction de l'activité ENSO durant la première partie de l'Holocène mise en évidence à partir d'autres reconstruction paléoclimatiques. Cependant, le découplage entre la SPCZ et le régime des précipitations, mit en évidence précédemment, a pu également contribuer à réduire l'amplitude du signal ENSO enregistré dans le corail fossile.

ABSTRACT

We present early mid-Holocene records of Sr/Ca, $\delta^{18}\text{O}$ and $\delta^{18}\text{O}_{\text{sw}}$ from marine archives collected in Vanuatu: two *Porites sp.* corals (6.7–6.5 ka BP) and a *Tridacna maxima* giant clam (6.2–6.0 ka BP). Sr/Ca, $\delta^{18}\text{O}$, and $\delta^{18}\text{O}_{\text{sw}}$ were used as proxies for sea surface temperature (SST) and sea surface salinity (SSS). The fossil geochemical records were compared to modern *Porites sp.* and *T. maxima* records.

Reconstructed mean SSTs from the two fossil *Porites sp.* and from the modern coral are similar, implying that the Western Pacific Warm Pool (WPWP)' southern edge had reached its modern location by 6.7–6.5 ka BP. The post-glacial SST rise in the Southwest Pacific was thus completed by the early mid-Holocene.

The two early mid-Holocene corals and the giant clam recorded saltier conditions than modern related to 1) a decoupling between the precipitation regime and the SPCZ due to a northerly position of this climatic feature and 2) an increase of the moisture transport to the extra-tropics, driven by a strengthened or extended Hadley cell.

The longest $\delta^{18}\text{O}$ coral profile displays an El Niño Southern Oscillation (ENSO) signal reduced by 20–30% compared to the period 1928–1992, in concordance with the reduced ENSO variability observed in the Pacific area during the first half of the Holocene. However, the decoupling between the SPCZ and the precipitation regime may have also contributed to the weak ENSO signal recorded in the early mid-Holocene coral $\delta^{18}\text{O}$ profile.

I. Introduction

The transition from the early Holocene to the mid-Holocene (~ 7.0–6.0 ka BP) was accompanied by a progressive, but significant, change of the climate mean-state which took place at the millennial timescale. The early Holocene, which started at around 11 ka BP, was characterized by a cold post-glacial climate that warmed progressively until reaching temperature higher than modern ones during the Holocene Thermal Maximum, at around 9.0–5.0 ka BP (see the review proposed by Renssen et al. 2012). During the first part of the Holocene the summer insolation in the Northern Hemisphere was higher than present conditions as a response to the orbital forcing (Berger and Loutre 1991). This strong insolation resulted in higher monsoon activity in Africa (deMenocal et al. 2000) and in Asia (Zhang et al. 2011). During the mid-Holocene period, that started ca. 7.0–6.0 ka BP, the boreal summer insolation decrease (Berger and Loutre 1991) and the monsoon regimes weakened (Wang et al. 2005; Wanner et al. 2008; Zhang et al. 2011).

Superimposed to these changes, occurring at the millennial time-scale, the mid-Holocene also witnessed the strengthening of the more prominent high frequency climatic variability mode: the El Niño Southern Oscillation – ENSO (e.g., Gagan et al. 2004; Haberle et al. 2001; Koutavas et al. 2006b; Moy et al. 2002; Sandweiss et al. 2001; Tudhope et al. 2001; Vargas et al. 2006). ENSO is associated with dramatic changes in the precipitation regime and sea surface temperature (SST) throughout the world, leading to ecological and socio-economical disasters (e.g., Cane 2005; Lyon 2004; McPhaden et al. 2006). The heart of this climatic oscillation is nested in the Pacific Ocean; however ENSO' influence extends beyond the Pacific boundaries and reaches remote areas through strong teleconnections (Ambrizzi et al. 1995; Diaz et al. 2001; Kiladis et al. 1989). Improving predictability of the ENSO evolution represents a major challenge for the coming decades; this goal requires refining our understanding of the links between ENSO variability and the changes in the climatic mean-state as well as improving climate simulations based on numerical models. Early mid-Holocene climatic changes present the same order of magnitude as the ongoing climate changes. Documenting such changes will provide thus invaluable clues to understand the mechanisms involved in the climate dynamic. However, the spatial and the temporal resolution of the early mid-Holocene paleoclimatic reconstructions are still insufficient to fulfill such an objective.

The Southwest (SW) Pacific area is a key-region of the Pacific Ocean to track past climate changes. Indeed, the SW Pacific climate is governed by two major climatic structures that influence the global climate: the Western Pacific Warm Pool (WPWP) and the South Pacific Convergence Zone (SPCZ). ENSO strongly influences the position and size of both the WPWP and SPCZ at the interannual timescale (e.g., Vincent 1994). The WPWP can be defined as the permanent body of warm seawater located to the east of a line between the Philippines and Papua New Guinea (PNG), excluding the warm waters within the Indonesian Archipelago. This warm water body causes a strong atmospheric convection over the SW Pacific, influencing the global distribution of heat and water evaporation [Cane and Clement, 1999]. To date, the exact definition of the spatial extent of the WPWP has been elusive as the warm pool margins are not solely defined by a specific SST front, but rather by distinct

hydrological features and ecosystem dynamics (Le Borgne et al. 2002; Maes et al. 2010; Picaut et al. 2001). Nevertheless, the WPWP area is usually defined as the water body enclosed within the 28°C SST isotherm (Wyrski 1989). The SPCZ is the largest extension of the Inter-Tropical Convergence Zone – ITCZ (Kiladis et al. 1989; Trenberth 1976; Vincent 1994). The SPCZ is a band of low-level convergence, cloudiness and precipitation, present all year long, characterized by warm SST and low sea surface salinity (SSS). The SPCZ is generally defined as the maximum precipitation tongue extending southeastward from PNG and the Solomon Islands down to the south of French Polynesia.

SSS and SST thus represent key-variables to assess the variability of these climatic features in terms of location and activity. The geochemical composition of massive coral skeleton and giant clam shell is sensitive to changes occurring in the surrounding seawater. Past changes in sea surface conditions can thus be assessed from the geochemical composition of coral and giant clam fossil specimens. The strontium calcium (Sr/Ca) ratio of coral skeleton is now widely used as a paleothermometer (e.g., Beck et al. 1992; Corrège 2006; Schneider and Smith 1982; Swart 1981). Concerning giant clams, the Sr/Ca composition of the shell is influenced by vital effects, hampering the use of this ratio as a paleothermometer (Elliot et al. 2009).

Stable oxygen isotopes composition ($\delta^{18}\text{O}$) of coral skeleton and giant clam shell is a function of both temperature and oxygen isotopic composition of the surrounding water ($\delta^{18}\text{O}_{\text{sw}}$) (McConnaughey 1989). In regions dominated by strong atmospheric convection, as in the SW Pacific area, the $\delta^{18}\text{O}_{\text{sw}}$ is a reliable proxy of SSS since both SSS and $\delta^{18}\text{O}_{\text{sw}}$ depend on the surface-ocean water balance, i.e., the evaporation/precipitation balance (Juillet-Leclerc et al. 2006; Kilbourne et al. 2004; Morimoto et al. 2002). Obtaining Sr/Ca and $\delta^{18}\text{O}$ profiles from coral and giant clam can thus provide useful information on the size and location of the WPWP and of the SPCZ.

Early mid-Holocene SST and $\delta^{18}\text{O}_{\text{sw}}$ monthly resolved data sets have been reconstructed from Sr/Ca and $\delta^{18}\text{O}$ records obtained from two fossil *Porites sp.* coral colonies and a fossil *Tridacna maxima* giant clam from Vanuatu archipelago (SW Pacific). These data are compared to modern records based on a *Porites sp.* colony from Vanuatu and a modern specimen of *T. maxima* from New Caledonia (SW Pacific). Based on these comparisons, the early mid-Holocene climate variability in the SW Pacific is documented, focusing first on the post-glacial SST evolution in this area and its implications in terms of WPWP' southern edge location. Then, the surface-ocean water balance variability is investigated to study the seasonal influence of the SPCZ in the SW Pacific area. Finally ENSO variability is presented and discussed.

II. Climatic Setting

The climate in the SW Pacific (Figure III-1) is mainly influenced by the seasonal extension of the WPWP southern edge and of the SPCZ (Figure III-2). During the austral summer, the WPWP and the SPCZ move southward, bringing warmer and fresher waters in this region

(linked to precipitation increase). The northward migration of the WPWP and the SPCZ during the austral winter results in cooler and saltier (less precipitation) waters. In Vanuatu, seasonal variations of SSS and SST are thus anti-correlated (Figure III-3). Because of its southern location compared to Vanuatu, New Caledonia is less influenced by the WPWP southern edge and by the SPCZ. This explains the differences with the Vanuatu SST and SSS data in terms of mean values and seasonal cycle amplitude (Figure III-3).

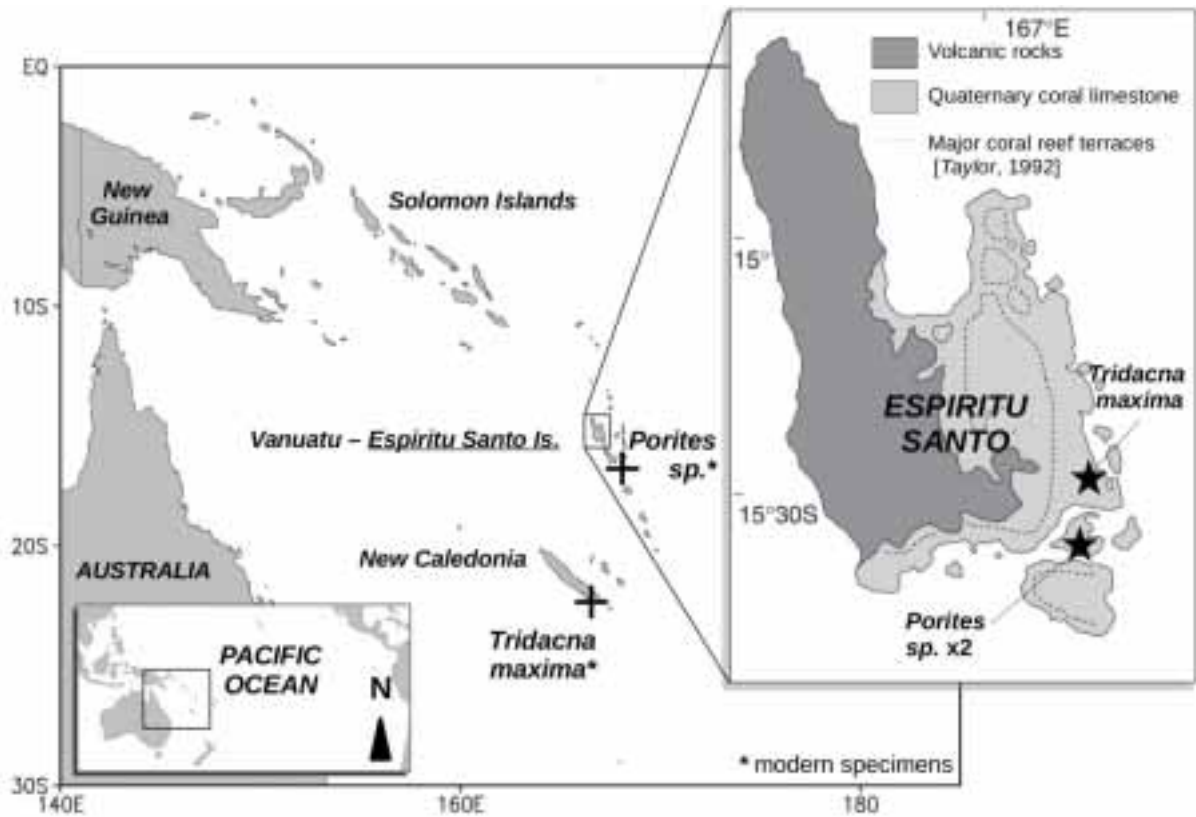


Figure III-1. Location of New Caledonia and of the Vanuatu archipelago in the Southwest Pacific. Crosses: sampling sites of the modern specimens. The insert shows a detailed map of the Espiritu Santo Island with the collection sites of the fossil material (stars). Uplifted coral reef data is from Taylor (1992).

In the SW Pacific, interannual climatic variability is influenced by ENSO. During an El Niño event, the southern edge of the WPWP and the SPCZ both move northward of their mean position, resulting in cooler and saltier conditions in Vanuatu. During a La Niña event, the WPWP and the SPCZ migrate southward of their mean position, bringing warmer and fresher conditions. An anomalous decrease (increase) in SST associated with an anomalous decrease (increase) in SSS indicates thus La Niña (El Niño) phase of ENSO. In the SW Pacific area, precipitation, and thus SSS, variations present a higher correlation with ENSO than SST (Figure III-2).

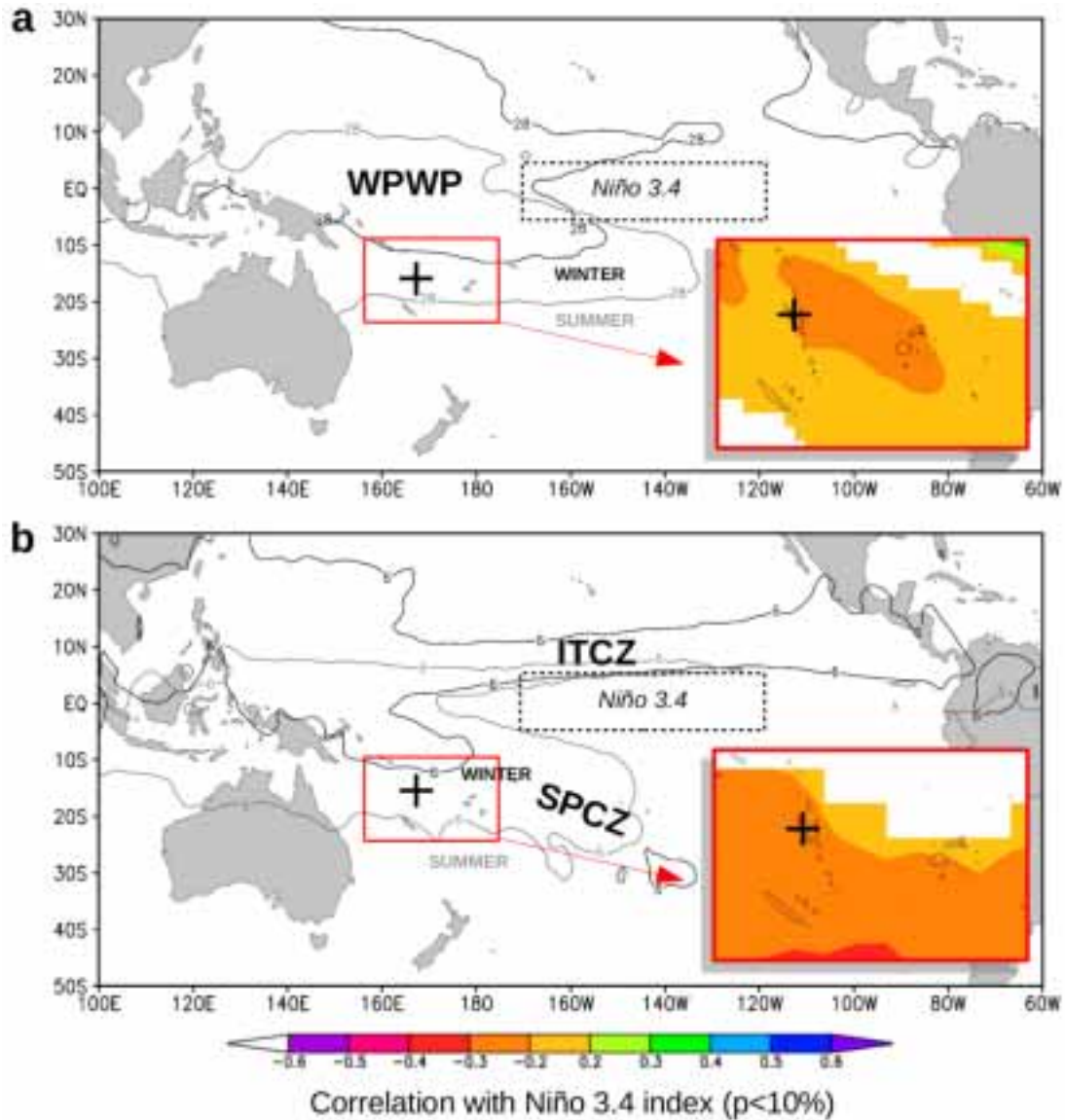


Figure III-2. Seasonal location of the main climatic features of the Pacific Ocean: (a) The Western Pacific Warm Pool (WPWP). The gray (black) curve represents the 28°C isotherm in winter (summer) (HadISST1 mean 1980–2011 period, (Rayner et al. 2003)). The insert shows the Pearson correlation coefficient (r) between the SST data set (same as above) and the SST in the El Niño 3.4 box for the SW Pacific area. (b) The Inter-Tropical Convergence Zone (ITCZ) and the South Pacific Convergence Zone (SPCZ). The gray (black) curve represents the 4 mm.d⁻¹ isohyet in winter (summer) (CMAP 1980–2010). The insert shows the Pearson correlation coefficient (r) between the precipitation data set (same as above) and the SST in the El Niño 3.4 box for the SW Pacific area. Black cross: Vanuatu archipelago. Modified from Climate Explorer (<http://climexp.knmi.nl>).

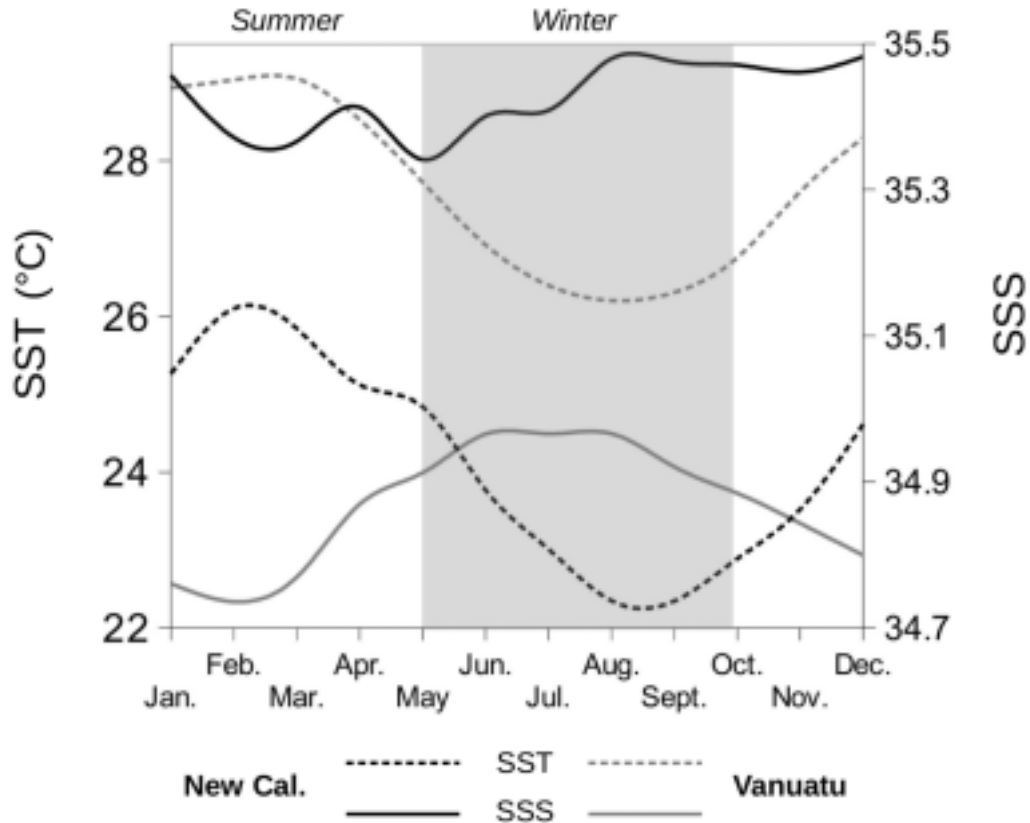


Figure III-3. Instrumental SST and SSS data. The modern SST and SSS conditions in New Caledonia were recorded by a thermo-salinograph located on the Fausse Passe de Uitoé reef (22.28°S, 166.98°E), from 1992 to 2009. Data were provided by the Réseau d'observation des stations côtières of the Institut de Recherche pour Développement (IRD Nouméa, New Caledonia). Vanuatu SSS data for the 1949 to 2008 period came from a 2°x2° grid, centered on 16°S, 165.5°E (Gouriou and Delcroix 2002). SST data was selected for the period 1970–2011 on a 3°x3° grid, centered on 15.5°S, 164.5°E – HadISST1.1 (Rayner et al. 2003).

III. Materials and Methods

a. Fossil Material

For this study, fossil corals and giant clams that grew in a shallow fringing reef environment were targeted. Fossil specimens were collected on uplifted fringing reef areas of Espiritu Santo Island (15.35°S, 167.18°E), the main island of the Vanuatu archipelago. Two fossil *Porites* sp. colonies, Psp-06-09 and Psp-07-09, were collected on an islet (Ratua Island) located in the southeast of Espiritu Santo (Figure III-1). The length of the colonies was 29 cm and 35 cm along the growth axis. Psp-07-09 is composed of two slabs. One of these slabs presents a growth stop, marked with a one-millimeter layer of altered skeleton, causing a temporal hiatus. The left valve of a *Tridacna maxima* giant clam was recovered on the Southeast part of Espiritu Santo Island (Figure III-1). This sample, labeled T-10-09, measured 25.5 cm along the antero-posterior axis and 16.5 cm along the dorso-ventral axis.

b. Modern Material and SST/SSS Data Sets

To define a modern baseline against which to compare the fossil records, a *Tridacna maxima* and a *Porites sp.* modern colony were collected in New Caledonia and in Vanuatu respectively. These two sites were described in terms of averaged values and seasonal variations of instrumental SST and SSS.

New Caledonia – A modern *Tridacna maxima* was collected alive in 2008, on the Fausse Passe de Uitoé reef (22.28°S, 166.98°E – New Caledonia – Figure III-1). This giant clam (T-02-08) grew then in a seawater-fed aquarium at the Aquarium des Lagons (Nouméa, New Caledonia) for 13 months. The seawater feeding the aquarium was continuously pumped from a coastal fringing reef nearby the aquarium. Modern conditions in New Caledonia were characterized using SST and SSS records extending from 1992 to 2009. These data were measured on the clam collection site (Fausse Passe de Uitoé reef) and were provided by the *Réseau d'observation des stations côtières of the Institut de Recherche pour le Développement* (IRD-Nouméa, New Caledonia).

Vanuatu – A modern living *Porites sp.* colony (VA-EPI) was collected in 2007 on a fringing reef of the Epi Island in Vanuatu (Figure III-1). The $\delta^{18}\text{O}$ record from a modern *Porites lutea* that grew from 1928 to 1992 on Espiritu Santo (Kilbourne et al. 2004) was also used to assess possible changes in ENSO variability during the early mid-Holocene. Modern SSS conditions in Vanuatu were taken from the data set compiled by Gouriou and Delcroix (2002), on a 2°x2° grid centered on 16°S–165.5°E, for the 1949–2008 period. The HadISST1.1 data set was used to characterize the modern SST in Vanuatu (Rayner et al. 2003). Data were selected for the period 1970–2011 on a 3°x3° grid, centered on 15.5°S 164.5°E.

c. Dating and Preservation of the Fossil Samples

Fossil samples were dated using conventional ^{14}C measurements and dates were calibrated using the Marine09 database (Reimer et al. 2009). The DeltaR value used for the Vanuatu area was 29 ± 28 years according to Petchey et al. (2008). The coral samples and the fossil giant clam shell were screened for their mineralogical composition and micro-structure preservation before geochemical analysis to ensure they were well-preserved. Mineralogical analyses were carried out using X-ray diffraction (XRD) on a Siemens® D500 device (Cu-K α , 40 kV, 30 mA) with a scan velocity of two seconds at a step size of 0.02° 2 θ . Minerals were identified by comparison with the reference JCPDF database (Joint Committee of Powder Diffraction File). The preservation state of the fossil specimens was evaluated by comparing Scanning Electronic Microscopy (SEM) images of modern and fossil specimens of coral and giant clams. Samples were sputter-coated with platinum and observed on a Cambridge® S360 device at 15 kV.

d. Geochemical Sampling

Coral samples - Corals were cut in 10 mm thick slabs parallel to the major growth axis. X-radiographs revealed the annual density banding. A couple of high- and low-density bands was assumed to represent one year of coral growth (Knutson 1972). Before sampling, coral slabs were cleaned in milli-Q water in an ultrasonic bath and oven-dried at 40°C. Coral slabs

were sampled continuously along the main growth axis with a step of 1 mm with a diamond drill-bit using a three-axis positioning system.

Giant clam samples – The central ridge of the modern (T-02-09) and of the fossil (T-10-09) *Tridacna maxima* left valves were cut off with a diamond saw. For oxygen stable isotope analyses, samples were obtained using a Micro-Mill device (New Wave®). Samples were milled following growth increments in the outer shell layer, every 0.25 mm (modern) and 0.80 mm (fossil). The modern giant clam was sampled on the part of the shell deposited from September 2008 to October 2009 while the specimen was in the aquarium.

e. **Geochemical Analysis and Data Processing**

Strontium/Calcium – The Strontium (Sr) and Calcium (Ca) concentrations of coral samples VA-EPI, Psp-06-09, and Psp-07-09 were determined following the method detailed by Le Cornec and Corrège (1997). Analyses were made using an inductively coupled plasma mass spectrometer (ICP-MS; Agilent 7500 CX®). The certified reference material JCp-1 (coral material) from the Geological Survey of Japan (Hathorne et al. 2010; Inoue et al. 2004; Okai et al. 2002) was used to validate the accuracy of the analyses. Analytical reproducibility (1σ) on coral Sr/Ca measurements was $0.05 \text{ mmol.mol}^{-1}$, based on 30 runs of a home-made coral standard on a six-month period. Time was assigned to the coral geochemical profiles based on both Sr/Ca ratio and density banding. Considering that today lower (higher) SST is found in August (February) in Vanuatu, the highest (lowest) Sr/Ca values were arbitrary set as August (February - Figure III-3). Each so-obtained time series was then mathematically re-sampled at a monthly resolution by linear interpolation. To avoid any data smoothing that could result from the interpolation process, the re-sampling was made by interpolating six points between each Sr/Ca minima/maxima pairs, assuming that coral growth is linear within six-month periods.

$\delta^{18}\text{O}$ - The oxygen stable isotope samples of the modern *Porites sp.* (VA-EPI), the fossil *Porites sp.* (Psp-07-09), and the two *Tridacna maxima* (T-02-08 and T-10-09) were analyzed on a GV IsoPrime® mass-spectrometer at LOCEAN (Paris 6 University), whereas fossil *Porites sp.* Psp-06-09 was analyzed on a GV Optima® mass-spectrometer at EPOC (Bordeaux I University). Both instruments were coupled to a Multiprep carbonate Gilson®. To ensure the inter-spectrometer comparison, 70 duplicates samples of Psp-07-09 were analyzed on both equipments. Results are expressed as $\delta^{18}\text{O}$ (standardized against Vienna Pee Dee Belemnite - vpdb). The analytical precision (1σ) on oxygen isotopic determinations, based on 10 runs of the reference material NBS-19, was 0.08‰ vpdb within one day, for both spectrometers. Time was assigned to the $\delta^{18}\text{O}$ profiles based on the tie-points determined previously from the Sr/Ca ratio and the density banding. Each time series was mathematically re-sampled as previously described.

$\delta^{18}\text{O}_{\text{sw}}$ – The $\delta^{18}\text{O}_{\text{sw}}$ values were calculated from the coral Sr/Ca and the $\delta^{18}\text{O}$ records using the equation established by Juillet-Leclerc and Schmidt (2001): $\delta^{18}\text{O}_{\text{aragonite}} - \delta^{18}\text{O}_{\text{sw}} = 0.45 - 0.20 \cdot \text{SST}$ (Sr/Ca was converted into SST using the mean equation for *Porites sp.* (Corrège 2006). Mean seasonal cycles of Sr/Ca and $\delta^{18}\text{O}_{\text{sw}}$ were calculated for all coral records by averaging each monthly re-sampled value (e.g., average of all January values, all February

values, etc.). Most of the monthly $\delta^{18}\text{O}_{\text{sw}}$ values, excluding the seasonal peak values, were averaged to obtain a mean surface ocean water balance. Seasonal extremes below the mean surface ocean water balance reflect a freshening of the superficial waters and extremes above the mean define a salinity increase in the superficial waters.

ENSO frequency band-pass filtering – The $\delta^{18}\text{O}$ profiles of the modern coral of Kilbourne et al. (2004) and of the continuous fossil coral record Psp-06-09 were band-pass filtered as described by Tudhope et al. (2001). This process extracts the 2.5- to 7-yr frequency of the signal (i.e., the dominant mode of modern ENSO - (Trenberth 1976). First, the modern coral $\delta^{18}\text{O}$ record was compared with to the 2.5–7 years band-pass filtered El Niño 3.4 index (Kaplan et al. 1998) to ensure that the ENSO variability was faithfully recorded. Second, the ENSO variability was quantified by calculating the standard deviation of the modern and fossil band-pass filtered $\delta^{18}\text{O}$ time series. To assess possible changes in ENSO variability during the early mid-Holocene compared to modern conditions, the standard deviation of the 25-yr long fossil ENSO record was compared to the standard deviation of the modern ENSO record calculated on different time periods lasting approximately 20 years: 1928–1950, 1951–1970, and 1971–1992.

IV. Results

a. Samples Dating and Preservation

The two *Porites sp.* colonies were dated at 6.7–6.5 ka BP (see Table 1 for ^{14}C ages). The fossil *Tridacna maxima* was dated at 6.2–6.0 ka BP. XRD analyses revealed that the three coral samples (modern and fossils one) and the fossil giant clam are composed of 100% aragonite. Comparison of SEM images of modern and fossil specimens revealed that the fossil material is well-preserved. Indeed, the fossil corals present unaltered primary aragonite needles and the centers of calcification are affected neither by dissolution nor by secondary aragonite deposition (Figure III-4a and 4b). The crossed-lamellar aragonitic micro-structure of the giant clam outer shell layer is also well-preserved (Figure III-4c and 4d).

Table 1. Main geochemical characteristics of the samples presented in this study^a

Archive	<i>Tridacna maxima</i>		<i>Porites sp.</i>		
Reference	T-02-09	T-10-09	VA EPI	Psp-06-08	Psp-07-08
Date ^{14}C (yr. BP \pm uncert.)	modern	5737 \pm 27	modern	6208 \pm 35	6220 \pm 32
Date cal (yr. BP – 2 σ range)	—	6.2–6.0	—	6.7–6.5	6.7–6.5
Location	New Caledonia	Vanuatu	Vanuatu	Vanuatu	Vanuatu
Record length (yr.)	1	6	7	25	19
$\delta^{18}\text{O}$ (vpdb ‰)	–1.04 \pm 0.53	–0.99 \pm 0.33	–4.68 \pm 0.21	–4.35 \pm 0.16	–4.29 \pm 0.28
$\delta^{18}\text{O}_{\text{sw}}$ (vpdb ‰)	—	—	0.01 \pm 0.05	0.27 \pm 0.05	0.28 \pm 0.04
Se/Ca (mmol mol ⁻¹)	—	—	8.99 \pm 0.08	9.01 \pm 0.08	9.03 \pm 0.08

^aGeochemical mean values are calculated from monthly re-sampled time series.

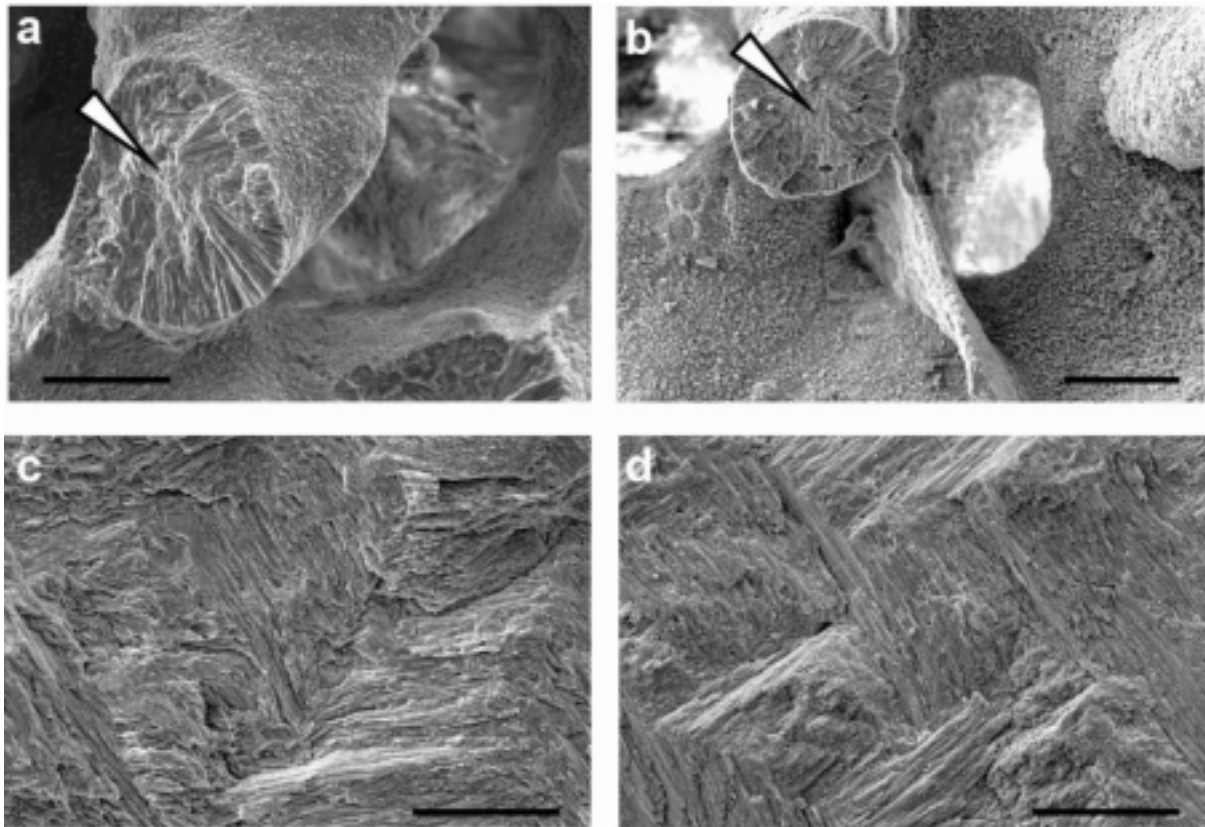


Figure III-4. Microstructural comparison between modern and fossil (this study) corals and giant clam (SEM images, scale: 50 μ m). Massive coral *Porites* sp. specimens: (a) modern coral VA EPI; (b) early mid-Holocene coral Psp-07-09, with arrow indicating center of calcification. Giant clam *Tridacna maxima* specimens: (c) modern giant clam T-02-09; (d) early mid-Holocene giant clam T-10-09 (scale 50 μ m).

b. Coral Growth Stop

A one-millimeter layer of altered skeleton, interpreted as a growth stop, was observed on one slab of the fossil Psp-07-09 #2. On this particular section of the skeleton, sponge chips were observed (SEM study). This confirms that this part of the colony suffered tissue loss during a short period. The density banding pattern, $\delta^{18}\text{O}$, $\delta^{18}\text{O}_{\text{sw}}$, and Sr/Ca records of this slab present annual variations, except for a 4-cm part that overgrew the growth stop. Time could not be assigned for the geochemical profiles in that 4-cm thick section, these data are not included in the study (shaded area in Figure III-5).

c. Coral Records

Comparison of the density banding and of the geochemical profiles revealed that the Psp-06-09 record is 25 years long and the Psp-07-09 record is 19 years long. The $\delta^{18}\text{O}$ reproducibility obtained from the samples analyzed twice, i.e., on the two different mass spectrometers, is good (mean relative error = 3%, $n = 48$), excluding analytical bias that could have been due to the use of two different equipment. Psp-06-09 and Psp-07-09 $\delta^{18}\text{O}$ records have a similar

mean $\delta^{18}\text{O}$ (Table 1). The modern coral VA-EPI from Vanuatu recorded a 7 year period (1999 to 2006 - Figure III-5). The Sr/Ca composition of the modern coral reflects the mean SST, which was $27.7 \pm 1.1^\circ\text{C}$ for the 1970–2011 period (SSS was 34.9 ± 0.3 – 1949–2008, based on the PSS-78 scale). The fossil Sr/Ca mean values are similar to the modern mean ($9.00 \text{ mmol.mol}^{-1}$). The skeletal Sr/Ca, $\delta^{18}\text{O}$, and $\delta^{18}\text{O}_{\text{sw}}$ time series generated from the fossil corals (Psp-06-09 and Psp-07-09) all display seasonal variations (Figure III-5). The Sr/Ca records of the modern and of the two early mid-Holocene corals have a mean value of $9.00 \text{ mmol.mol}^{-1}$ (Table 1, Figure III-5). The two fossil $\delta^{18}\text{O}$ ($\delta^{18}\text{O}_{\text{sw}}$) records have similar mean values and are ^{18}O -enriched by $+0.3\text{‰}$ vpdb ($+0.3\text{‰}$ vpdb) compared to the modern record (Table 1, Figure III-5).

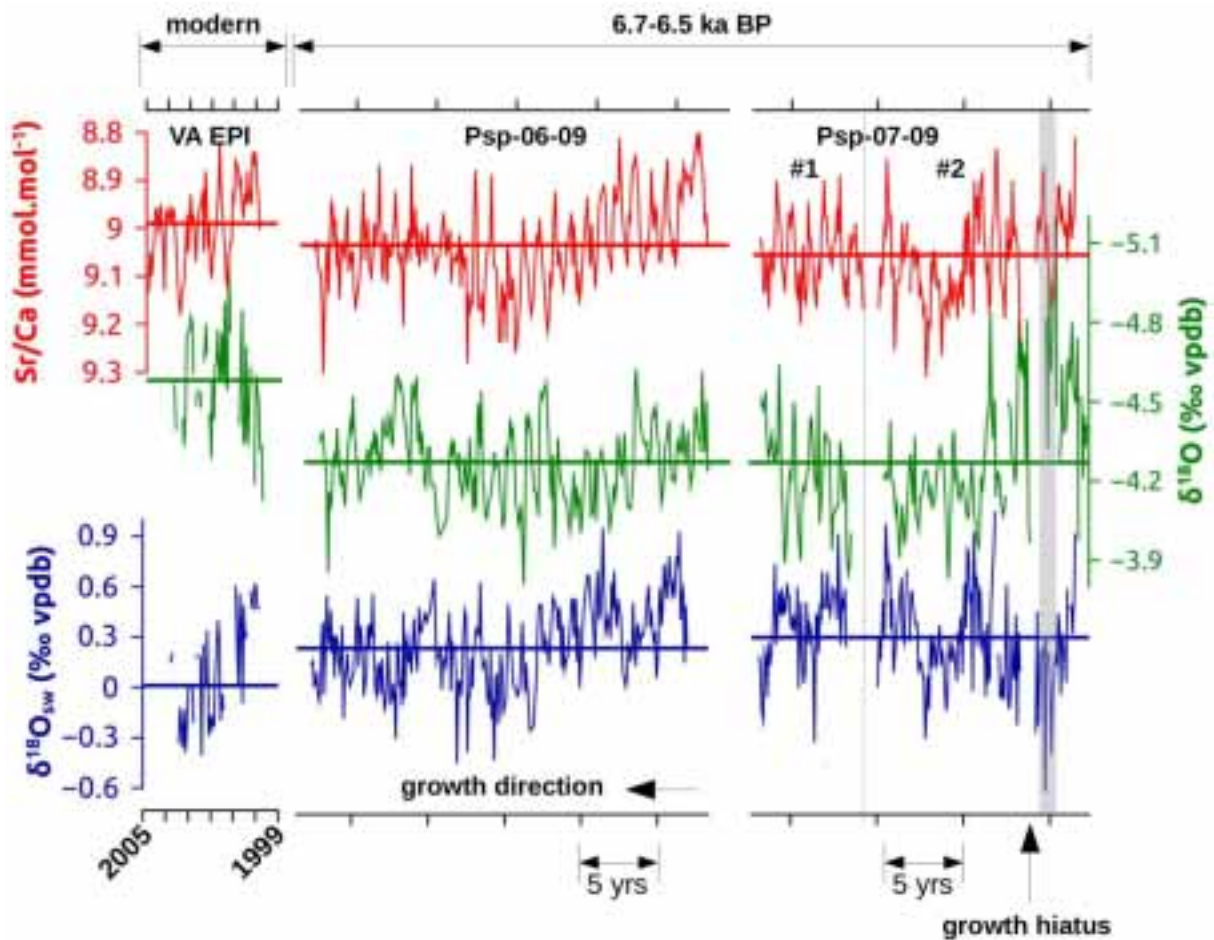


Figure III-5. Monthly resolved geochemical data obtained from the modern and the two fossil *Porites* sp. corals from Vanuatu: Sr/Ca (red), $\delta^{18}\text{O}$ (green) and $\delta^{18}\text{O}_{\text{sw}}$ (blue). The thick horizontal line represents the average value of each record. The growth hiatus of the colony Psp-07-09 is shown by the black arrow and the shaded area indicates the anomalous part of the record not included in the study (cf. text). Note that both Sr/Ca-axis and $\delta^{18}\text{O}$ -axis are inverted.

d. Giant Clam Records

The $\delta^{18}\text{O}$ composition of the modern *Tridacna maxima* from New Caledonia shows one annual cycle corresponding to the 13 months spent in the aquarium – September 2008 to October 2009 (Figure III-6a). The mean $\delta^{18}\text{O}$ composition of this specimen is $-1.04 \pm 0.53\text{‰}$ vpdb. This value reflects the mean SST and SSS conditions in New Caledonia today: average SST and SSS values recorded in the period 1992–2009 are $24.1 \pm 1.6^\circ\text{C}$ and 35.4 ± 0.22 (based on the PSS-78 scale) respectively. The $\delta^{18}\text{O}$ composition of the modern *T. maxima* is used as a baseline for modern conditions against which to compare the $\delta^{18}\text{O}$ composition of the early mid-Holocene *T. maxima*. The $\delta^{18}\text{O}$ record from the fossil *T. maxima* is characterized by four clear annual cycles and two less defined cycles (Figure III-6b). The 6.2–6.0 ka BP *T. maxima* record from Vanuatu has a mean $\delta^{18}\text{O}$ value of -0.99‰ vpdb which is similar to the modern specimen from New Caledonia (Table 1).

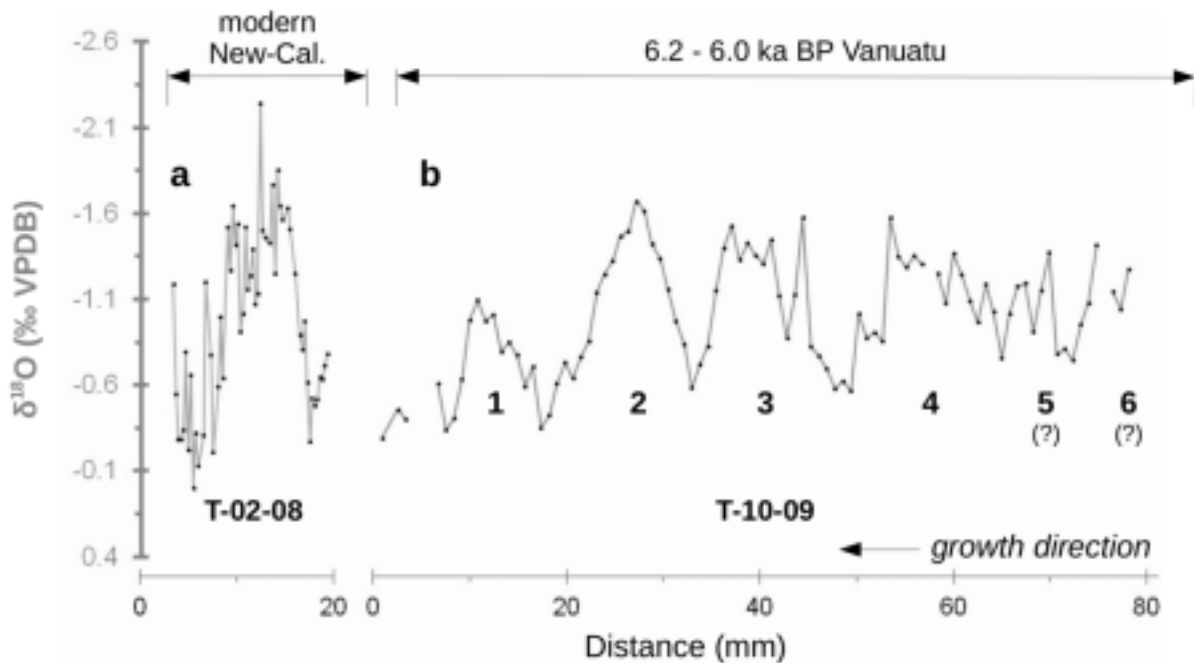


Figure III-6. $\delta^{18}\text{O}$ records obtained from the modern and the fossil *Tridacna maxima* giant clams as a function of distance (zero corresponds to the animal death). The $\delta^{18}\text{O}$ axis is inverted. (a) Record obtained from the modern *T. maxima* T-02-09 collected in New Caledonia and (b) record of the 6.2–6.0 ka BP *T. maxima* collected in Vanuatu.

e. Seasonal variability from the coral records

The modern coral Sr/Ca record (Figure III-7a) displays seasonal variations that reflect well the instrumental SST variations measured in Vanuatu (Figure III-3). The modern coral recorded low $\delta^{18}\text{O}_{\text{sw}}$ values oscillating around 0‰ vpdb during most part of the year, excepted of a $\delta^{18}\text{O}_{\text{sw}}$ peak reaching 0.3‰ vpdb in October (Figure III-7a). The $\delta^{18}\text{O}_{\text{sw}}$ data recorded well the SSS signal with low salinity conditions all year long, excepted in winter, that reflect well the seasonal patterns observed today in Vanuatu (Figure III-3).

The two early mid-Holocene coral records display almost identical seasonal Sr/Ca and $\delta^{18}\text{O}_{\text{sw}}$ variations. The two early mid-Holocene Sr/Ca records have amplitudes similar to that of the modern Sr/Ca record (Figure III-7). The $\delta^{18}\text{O}_{\text{sw}}$ cycle recorded by the fossil coral is characterized by a rather flat profile centered on 0.3‰ vpdb with a positive peak reaching 0.5‰ vpdb in February and a negative peak reaching 0.0‰ vpdb in August (Figure III-7b and 7c). Unlike the modern coral records, the two early mid-Holocene coral colonies revealed saltier summer and fresher winter conditions. The consistency of the Sr/Ca and the $\delta^{18}\text{O}_{\text{sw}}$ profiles in the two fossil records indicates that the synchronous seasonal variation of SST and SSS is a robust feature of the early mid-Holocene.

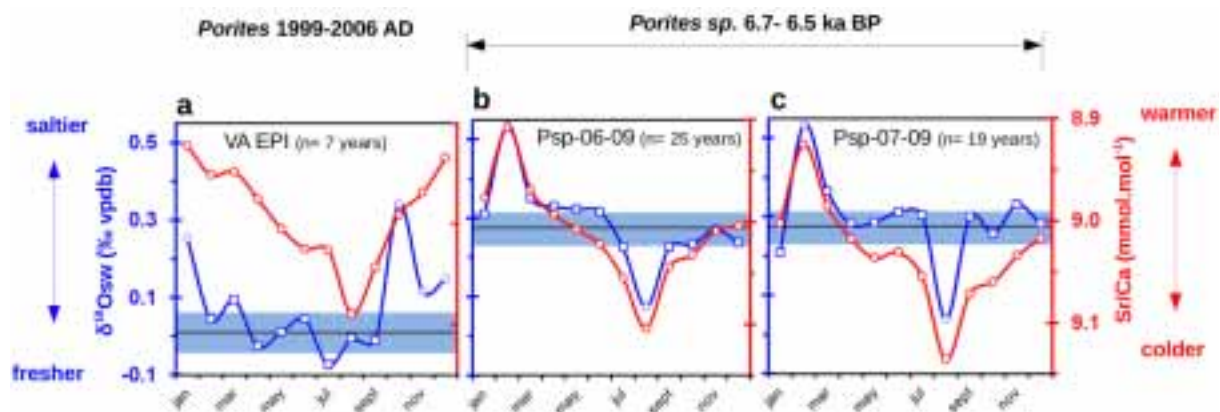


Figure III-7. Seasonal variations of Sr/Ca (red) and $\delta^{18}\text{O}_{\text{sw}}$ (blue) from corals collected in Vanuatu. The average $\delta^{18}\text{O}_{\text{sw}}$ (black line and 1 standard deviation interval in blue) was calculated by averaging the data points represented by the squares (i.e., extremes not included), **a** – modern coral record, and **b & c** – 6.7– 6.5 yrs BP fossil coral colonies.

f. ENSO Variability

The ENSO-filtered $\delta^{18}\text{O}$ data of the modern coral (Kilbourne et al. 2004) correlates well with the ENSO-filtered El Niño 3.4 index (Figure III-8a), indicating that the Vanuatu modern coral recorded faithfully the ENSO variations. The amplitude of the filtered 25-years long $\delta^{18}\text{O}$ profile of the fossil coral Psp-06-09 is slightly lower than the modern record (Figure III-8b). The standard deviation of the 25-yr long fossil record is equal to 0.067 ‰ vpdb. This value was compared to the standard deviation of the modern ENSO-filtered $\delta^{18}\text{O}$ record calculated over three distinct periods: 1928–1950 (sd = 0.081), 1951–1970 (sd = 0.088) and 1971–1992 (sd = 0.097). The variability of the early mid-Holocene record is respectively 17%, 24%, and 31% lower than the modern ENSO signal recorded during these three periods.

V. Discussion

a. *Post-Glacial SST Rise in the Southwest Pacific*

The mean Sr/Ca values of the two fossils and of the modern coral colonies from Vanuatu indicate that the early mid-Holocene mean SST was similar to its modern value (Figure III-5). Considering the analytical error on strontium calcium analyses ($\pm 0.05 \text{ mmol.l}^{-1}$) and the average coral Sr/Ca versus temperature slope – $\pm 0.0607 \text{ mmol.l}^{-1}.\text{°C}^{-1}$ (Corrège 2006) – the accuracy of the Sr/Ca paleothermometer is $\pm 1\text{°C}$ within the analytical settings of this study. Mean SST gridded instrumental data is $\sim 28\text{°C}$ in Vanuatu implying that the reconstructed early mid-Holocene mean SST was between 27 and 29°C.

In the SW Pacific area, SST reconstructions from coral Sr/Ca and $\delta^{18}\text{O}$ giant clam archives revealed cooler conditions than present until ca. 7.0 ka BP (Abram et al. 2009; Aharon 1980; Beck 1997). Cooler SSTs in the early Holocene are supposedly linked to the delayed SW Pacific postglacial SST rise (Beck 1997; Gagan et al. 2004). Our results show that the post-glacial SST rise was completed by the early mid-Holocene in the SW Pacific. This observation is in agreement with the slightly warmer SST reported from other coral records from New Caledonia (Montaggioni et al. 2006) and in the Australian Great Barrier Reef (Gagan et al. 2004; Gagan et al. 1998). All these coral records, support the hypothesis of a moderate warming of the equatorial Western Pacific during the “Holocene Thermal Maximum” (ca. 8–7 ka BP), as it is also suggested by marine sediment records (Stott et al. 2004) and by global atmosphere-ocean-vegetation model simulations (Renssen et al. 2012).

b. *Short-Lived Contraction of the WPWP Southern Edge at 6.2–6.0 ka BP*

The 6.2–6.0 ka BP *Tridacna maxima* record revealed that the SW Pacific experienced slight SST fluctuations during the post-glacial stabilization of the SST around its present values. Because the modern New Caledonian giant clam and the fossil Vanuatu giant clam mean $\delta^{18}\text{O}$ values are similar, they may have grown in similar environmental conditions. Considering that New Caledonia surface water is on average $\sim 3.5\text{°C}$ cooler and ~ 0.5 saltier compared to the Vanuatu ones (Figure III-3), conditions in the Vanuatu region at around 6.2–6.0 ka BP were most likely cooler and saltier than today. However, a SST drop of $\sim 3.5\text{°C}$ at 6.2–6.0 ka BP is very unlikely considering that the two fossil coral records from Vanuatu showed mean SST values similar to modern ones at 6.7–6.5 ka BP. This SST drop is thus most likely overestimated. The two fossil coral $\delta^{18}\text{O}$ records revealed that the seawater was enriched in the heavier oxygen isotope by $+0.3\text{‰}$ vpdb indicating saltier than present mean conditions at 6.7–6.5 ka BP (Figure III-7). Assuming that the $\delta^{18}\text{O}_{\text{sw}}$ recorded by the fossil corals remain unchanged at 6.2–6.0 ka BP, such seawater ^{18}O -enrichment would have shifted the giant clam shell $\delta^{18}\text{O}$ value in the same proportion, because giant clam aragonite is deposited in isotopic equilibrium with seawater. Considering an average $\delta^{18}\text{O}$ versus SST slope of $0.26\text{‰}.\text{°C}^{-1}$ for Tridacnidae shells (Aharon 1980; Aubert et al. 2009; Watanabe and Oba 1999), the SST change in the early mid-Holocene would account for an apparent SST cooling of about 1°C . In addition, the equations linking giant clam $\delta^{18}\text{O}$ to SST show that the accuracy of this proxy is between $\pm 1\text{°C}$ and $\pm 1.4\text{°C}$ (Aubert et al. 2009; Watanabe and Oba 1999). This accuracy of giant clam $\delta^{18}\text{O}$ as a temperature proxy must also be considered and could explain this

overestimated SST change. The SST negative anomaly recorded by the fossil giant clam is thus most probably around $2 \pm 1^\circ\text{C}$.

This value is consistent with the $1\text{--}2^\circ\text{C}$ cooling observed ca. 6.0 ka BP at the margins of the IPWP by Abram et al. (2009). According to Lea et al. (2000) and Stott et al. (2004), the SST in the western equatorial Pacific during the Holocene presented weak variations around the modern SST values. Colder conditions observed at the southern edge of the WPWP at 6.2–6.0 ka BP are thus probably not related to a cooling trend of the WPWP, but rather to a short-lived contraction or northward migration of the WPWP. This suggests that the southern edge of the WPWP retracted below its actual boundaries at that time. Such fluctuation of the WPWP' southern edge during the Holocene is also suggested by the planktonic foraminifera $\delta^{18}\text{O}$ record from the Ocean Drilling Program sediment core 828A, collected offshore Vanuatu (Martinez et al. 1997). Interestingly, the timing of this event matches the global cooling event reported at around 6.3 ka BP (see the review in Wanner et al. 2011). However, additional mid-Holocene paleo-SST records in the Vanuatu region are needed to confirm the timing of such a northward shift of the WPWP at 6.2–6.0 ka BP and to determine to which extent the SW Pacific cooling may be linked to this global cold event.

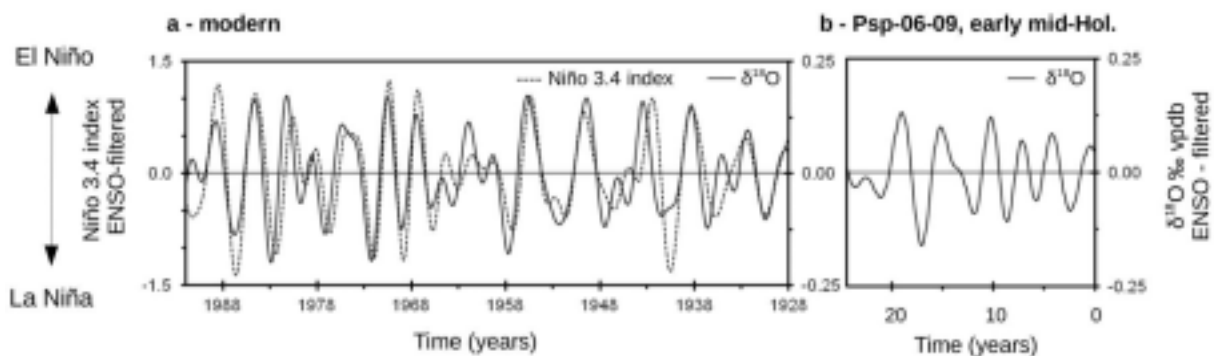


Figure III-8. Comparison of modern versus early mid-Holocene ENSO amplitudes. (a) ENSO-filtered modern coral $\delta^{18}\text{O}$ data (data from Kilbourne et al. 2004) and El Niño 3.4 Index. (b) Porites sp. Psp-06-09 ENSO-filtered $\delta^{18}\text{O}$ data.

c. Early Mid-Holocene Surface-Ocean Water Balance

The post-glacial stabilization of SST around its present value in the SW Pacific at 6.7–6.5 ka BP was accompanied by change of the surface-ocean water balance compared to modern conditions. The modern coral record from Vanuatu displays a low average $\delta^{18}\text{O}_{\text{sw}}$ value (0.0‰ vpdb) that reflects the strong influence of ^{18}O -depleted waters brought by the SPCZ-related precipitation (Figure III-3). The modern coral record shows a positive $\delta^{18}\text{O}_{\text{sw}}$ peak in October linked to a reduction in precipitation input (Figure III-7a). Indeed, Vanuatu is not influenced by the SPCZ in winter (Figure III-2b) and the increased easterlies in winter induce a strong evaporation that contributes to enrich the surface seawater with the heavier oxygen

isotope. This $\delta^{18}\text{O}_{\text{sw}}$ peak reflects a higher SSS in agreement with the instrumental record (Figure III-3). As such, any change of the surface-ocean water balance (i.e., SSS) would be recorded in the early mid-Holocene coral $\delta^{18}\text{O}_{\text{sw}}$ profiles.

The early mid-Holocene corals recorded an average $\delta^{18}\text{O}_{\text{sw}}$ composition enriched by about +0.3‰ vpdb compared to the modern seawater (Figure III-7). The early mid-Holocene average $\delta^{18}\text{O}_{\text{sw}}$ composition is similar to the modern winter value, suggesting that the average surface-ocean water balance at ca. 6.7–6.5 ka BP was shifted toward modern winter-like conditions, i.e., when the SPCZ is not affecting the Vanuatu region (Figure III-2b). Such a dramatic reduction of SPCZ-related precipitation input indicates that the SPCZ was most likely located northward from its present location and possibly merged with the inter tropical convergence zone. Moreover, the seasonal $\delta^{18}\text{O}_{\text{sw}}$ cycle reveals that the early mid-Holocene summers were characterized by saltier conditions whereas fresher conditions would have been expected regarding the southward summer migration of the SPCZ observed today (Figure III-2b). This supports the assumption of a northerly located SPCZ during the early mid-Holocene.

However, these results seem in contradiction with numerical climate simulations at 6 ka BP that evidenced a southward shift, and intensification, of the SPCZ (Brown et al. 2008; Brown et al. 2007; Chiang et al. 2009). It may be argued that saltier conditions recorded by the fossil corals during the early mid-Holocene summers may reflect the occurrence of seasonal upwelling that could have counter-balanced the SSS dilution due to SPCZ-related precipitation in the SW Pacific. Nevertheless, the water masses located beneath the thermocline are characterized by higher SSS and lower SST than superficial waters (Maes and Varillon 2011), so that a seasonally easterlies-driven upwelling regime in the SW Pacific would have led to opposite reconstructed SSS and SST variations. Consequently, the dramatic precipitation deficit and dry summers during the early mid-Holocene strongly suggest that the precipitation regime was decoupled from the SPCZ during the early mid-Holocene. Fossil coral records would thus reflect local variations of the precipitation regime rather than variations of the SPCZ location or intensity.

The northerly located SPCZ during the early mid-Holocene as demonstrated in this study is consistent with the northward location of the ITCZ during the early mid-Holocene evidenced from sediment proxy data (Haug et al. 2001) and from coupled ocean-atmosphere model simulations (Braconnot et al. 2007). This suggests a synchronous northward displacement of both the ITCZ and the SPCZ during the early mid-Holocene, explaining the high SSS observed in the Western Pacific during the first half of the Holocene (Figure III-9). These observations evidence that the Pacific Ocean convective features experienced an important northward re-organization during the early mid-Holocene, possibly in response to the orbital forcing.

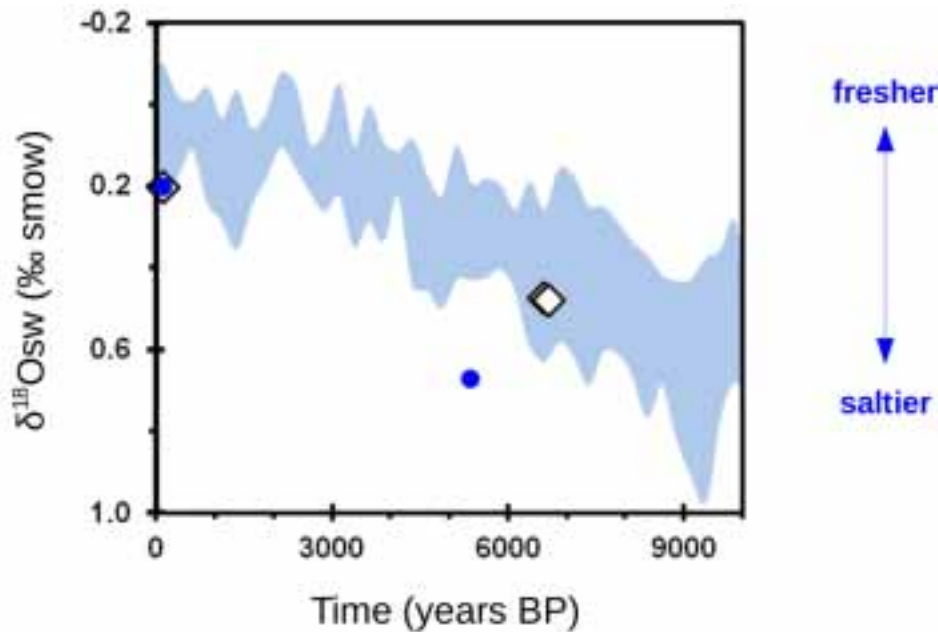


Figure III-9. Holocene $\delta^{18}O_{sw}$ evolution in the Western Pacific area – Diamond: coral data (this study), Blue dots: coral data from Gagan et al. (1998) Blue area – foraminifer’s data from sediment cores ODP806B, MD70, MD76 and MD81. The blue area represents one standard deviation interval of the mean values calculated from the four sedimentary records (Lea et al. 2000; Stott et al. 2004).

However, the northward location of the SPCZ solely cannot explain the salinity recorded in summer by the early mid-Holocene corals. Indeed, this summer $\delta^{18}O_{sw}$ value reaches 0.5‰ vpdb which indicates even drier conditions than recorded today during winter (0.3‰ vpdb – Figure III-7), when Vanuatu is not affected by the SPCZ. This suggests that evaporation had also played a significant role in the surface ocean water balance during the early mid-Holocene. An average surface-ocean water balance shifted toward evaporation during the mid-Holocene was shown from a Australian Great Barrier Reef coral record (Gagan et al. 1998). Increased evaporation in the early mid-Holocene is also supported by the similar or warmer conditions than today recorded by early mid-Holocene fossil corals from PNG, GBR, and New Caledonia (Abram et al. 2009; Gagan et al. 2004; Gagan et al. 1998; Montaggioni et al. 2006). Moreover, general circulation model simulations indicate a strengthening, or an extension, of the Hadley cell as a response of a slight warming of the tropical zone (Lu et al. 2007; Rind 2000). Stronger, or extended, Hadley cell would enhance the poleward water vapor transport, and thus the poleward heat flux, increasing the evaporation in the tropics. This suggests a stronger coupling between the tropics and the extra-tropical regions during the early mid-Holocene as compared to the modern era.

d. ENSO Variability

Since coral $\delta^{18}O$ is sensitive to both SST and SSS variations, it is a reliable proxy to study the ENSO variability. Indeed, a synchronous increase (decrease) in SST and decrease (increase)

in SSS influences the coral $\delta^{18}\text{O}$ in the same way, resulting in enhanced interannual coral $\delta^{18}\text{O}$ variations as observed in the modern Vanuatu coral record (Figure III-8a). The early mid-Holocene coral from Vanuatu recorded an ENSO variability that was in average 20–30% lower than the variability recorded by the modern coral for the period 1928–1992 (Figure III-8b). Several factors may have caused the ENSO variability to weaken during the early mid-Holocene. On the one hand, previous studies suggested that ENSO teleconnections may not be stationary (e.g., Diaz et al. 2001; Stahle et al. 1998; Vargas et al. 2006). Consequently, a change in the ENSO teleconnections over the Pacific area during the early mid-Holocene may result in a reduced ENSO signal in the SW Pacific fossil corals records. On the other hand, the decoupling between the precipitation and the SPCZ in the SW Pacific, evidenced from the early mid-Holocene coral records, may also have contributed to a reduced ENSO signal in the $\delta^{18}\text{O}$ coral record. Indeed, the strength of the ENSO signal in the coral $\delta^{18}\text{O}$ record relies on the tight coupling between the SPCZ and the precipitation. The decoupling of the SPCZ and the precipitation regime observed during the early mid-Holocene would have lead to a disruption between the ENSO variability and coral $\delta^{18}\text{O}$ variations, leading to a weaker ENSO signal in the $\delta^{18}\text{O}$ record.

Non stationary ENSO teleconnections in the SW Pacific, or a decoupling between the precipitation and ENSO would thus appear as locally reduced ENSO variability while stronger ENSO variability prevails in the regions where ENSO is tightly linked to, i.e., the WPWP, the Pacific cold tongue or western South America. However, paleo reconstructions from PNG charcoal and coral records revealed a significant reduction of the ENSO variability during the early mid-Holocene (Haberle et al. 2001; Tudhope et al. 2001). Moreover, mollusks, archeological and sedimentary records from South America and the cold tongue area evidenced a reduced ENSO variability during the early and the early mid-Holocene (Koutavas et al. 2006b; Moy et al. 2002; Sandweiss et al. 2001; Vargas et al. 2006). Weak ENSO variability during the first half of the Holocene is also observed in ocean-atmosphere coupled model runs. All those evidences strongly suggest that the reduced ENSO variability recorded by the early mid-Holocene Vanuatu coral reflects a real ENSO trend, although the role of the forcing involved in the ENSO variability decrease are still greatly debated (Braconnot et al. 2012; Chiang et al. 2009; Clement et al. 2000; Liu et al. 2000; Roberts 2007; Zheng et al. 2008). Consequently, the reduced amplitude of the ENSO signal in the early mid-Holocene coral $\delta^{18}\text{O}$ record reflect both 1) a global weaker ENSO variability and 2) the decoupling between the precipitation and the SPCZ.

VI. Conclusion

Monthly resolved $\delta^{18}\text{O}$ records from two 6.7–6.5 ka BP *Porites sp.* colonies and from a 6.2–6.0 ka BP *Tridacna maxima* opened a window on the SW Pacific climate during the early mid-Holocene. The post-glacial SST rise was found to be completed by about 6.7–6.5 ka BP with conditions as warm, or slightly higher, than today suggesting a weak Holocene Thermal Maximum in that region. Cooler conditions were recorded at 6.2–6.0 ka BP, possibly related to a short-lived contraction of the WPWP southern edge. Early mid-Holocene *Porites sp.*

records revealed drier than modern conditions, caused by a northward mean position of the SPCZ and an increased moisture transport in the extra tropics related to a strengthened or extended Hadley circulation. Such configuration strongly suggests that the climatic mean state was La Niña-like during the early mid-Holocene period.

One of the early mid-Holocene corals recorded a lower ENSO variability than the modern one. This reflects the reduced ENSO variability evidenced by previous studies during the first half of the Holocene, although the decoupling between the SPCZ and the precipitation regime in the SW Pacific may also have contributed to the reduced ENSO signal observed in our coral record. The combined use of corals and of a giant clam improves the temporal and spatial coverage of early mid-Holocene data in the SW Pacific area. The information brought by our study provides an benchmark against which to test climate models and should help constraining the SPCZ behavior in simulations of past and modern climate conditions.

Acknowledgments. We thank Richard Farman and the Aquarium des Lagons of Nouméa (New Caledonia) for the raceway facilities. We also thank the owner of the Ratua Island resort and Jean-Christophe Galipaud for their help in the fossils collection, Rufino Pineda for the logistical help in Espiritu Santo, and John Butscher for the logistical help in New Caledonia. We are also grateful to the radiology staff of Jean Verdier Hospital (Bondy, Seine Saint Denis, France) for coral slabs x-radiographs. Thanks are extended to Hugues Boucher for the data processing. Marielle Dumestre, Joël Ughetto also contributed to many helpful discussions. The authors are grateful to Gavin Dunbar and to an anonymous reviewer for their corrections and comments, which help improving that manuscript. This study was done in the framework of the HOLBECO project, supported by the French INSU-EC2CO program (managed by the IFREMER Institute). This work is dedicated to our esteemed and dearly missed colleague Guy Cabioch.



Découpe d'une tranche dans une colonie de corail massif Porites sp. avec la scie lapidaire du "dock", au centre IRD de Nouméa. Guy Cabioch, octobre 2010. Crédit photo: N. Duprey.



Chapitre IV – Lapita migration and climatic variability: new insights from giant clam and coral geochemical records

Ce chapitre sera soumis à la revue *Palaeogeography Palaeoclimatology Palaeoecology* courant 2013.

Auteurs (dans l'ordre):

Duprey Nicolas,
Galipaud Jean-Christophe,
Cabioch Guy,
Lazareth Claire E.

RÉSUMÉ

Afin d'explorer la relation entre la migration Lapita dans l'Océanie Lointaine, survenue ca. 3200 années BP, et le climat, la composition isotopique globale ou "bulk" ($\delta^{18}\text{O}$ et $\delta^{13}\text{C}$) de bénitiers a été analysée. Huit spécimens appartenant aux genres *Tridacna* et *Hippopus* ont été collectés sur des sites archéologiques Lapita au Vanuatu et en Nouvelle-Calédonie. Les enregistrements isotopiques "bulk" de $\delta^{18}\text{O}$ et $\delta^{13}\text{C}$, intégrant des périodes comprises entre 3 et 10 ans, ont été utilisés respectivement comme proxies des conditions de température/salinité et de l'influence estuarienne ou océanique. La composition en strontium/calcium (Sr/Ca) d'une colonie de corail massif *Porites sp.*, contemporaine de la migration Lapita, a été également analysée et interprétée comme un indicateur des paléotempératures de l'eau de mer de surface. Ces données ont été comparées à des enregistrements similaires obtenus à partir de bénitiers et de coraux actuels afin d'évaluer dans quelle mesure les conditions passées ont pu différer des conditions actuelles. Les enregistrements de Sr/Ca du corail fossile indiquent que les conditions ca. 3600-3400 années BP étaient plus chaudes qu'actuellement dans le Pacifique Sud-Ouest. Ceci est en accord avec les conditions chaudes et peu salées enregistrées par un bénitier fossile sur cette même période. Ceci suggère des conditions du type La Niña sur le Pacifique Sud-Ouest ca. 3600-3400 années BP. Cinq bénitiers fossiles, datés dans l'intervalle ca. 3200-2700 années BP, présentent deux compositions isotopiques distinctes, le premier groupe est appauvri en isotopes lourds du carbone et de l'oxygène par rapport au second. La différence entre ces deux groupes est supérieure aux valeurs trouvées sur des bénitiers actuels vivants sur un récif frangeant ou sur un récif barrière. Les bénitiers fossiles ont donc enregistré, sur cette période, à la fois des conditions peu salées et des conditions plus froides et plus salées alternant à l'échelle interannuelle. Dans le Pacifique Sud-Ouest, ce mode de variabilité est caractéristique d'El Niño Southern Oscillation, ce qui suggère fortement que l'activité ENSO était forte ca. 3200-2700 years BP. La migration Lapita ca. 3200 années BP s'est donc déroulée dans un contexte climatique caractérisé par une forte variabilité ENSO, indiquant que le climat a pu agir comme élément déclencheur et/ou favoriser cette migration. En effet, des conditions climatiques instables ont pu favoriser le développement et l'expansion de populations nomades dépendantes des ressources marines, comme l'était la population Lapita.

ABSTRACT

To explore further the possible influence of the climate on the Lapita migration, ca. 3,200 years BP, bulk oxygen ($\delta^{18}\text{O}$) and carbon ($\delta^{13}\text{C}$) isotopic composition of eight shells of *Tridacna* and *Hippopus*, giant clams, unearthed on Lapita archaeological sites (Southwest Pacific – SW), were analyzed. Shell $\delta^{18}\text{O}$ and $\delta^{13}\text{C}$ are proxies for sea surface temperature/sea surface salinity – SST/SSS – and dissolved inorganic carbon source – estuarine vs. oceanic. Bulk samples encompassed time periods ranging from 3 to 10 years. A fossil massive coral *Porites sp.*, contemporaneous of that period, was also analyzed for Strontium/Calcium – Sr/Ca – considered as a proxy for SST. These records were compared to modern equivalents, to assess whether past climatic conditions had changed. The Sr/Ca ratio of the fossil coral indicated that conditions were warmer than they are today in the Southwest Pacific, ca. 3,600 to 3,400 years BP, in agreement with a giant clam record that evidenced warm and wet conditions during that period. This suggests that La Niña-like conditions were most likely operating in the SW Pacific at that time. Five giant clams, all dated within the interval ca. 3,200 to 2,700 years BP, presented two different isotopic composition : one group is strongly depleted in the heavier isotopes of both carbon and oxygen whereas the other is enriched in carbon and oxygen heavy isotopes. This reveals that, during that interval, conditions were alternatively warmer and fresher with a rather estuarine environment and colder and saltier with a more oceanic environment, at the interannual timescale. The difference in the isotopic composition of the two groups is beyond the range of isotopic values recorded by modern giant clams living in different reefs environments (fringing and barrier reefs). In the SW Pacific, such interannual variability is characteristic of El Niño Southern Oscillation, suggesting that the fossil giant clams recorded a strong ENSO variability ca. 3,200 to 2,700 years BP. The Lapita migration, ca. 3,200, occurred thus in parallel with a strong ENSO variability suggesting that climate had most likely played a role in the triggering of the Lapita migration. Indeed, unstable climate may have favored the development and the expansion of nomad foraging populations relying on marine resources, as the Lapita were.

I. Introduction

Pacific colonization started with a first human settling phase reported in Near Oceania (PNG, Solomon Islands, and the Bismarck Archipelago) ca. 45,000-42,000 years BP¹⁹ (O’Connell and Allen 2004). The easternmost advance of this migration phase was the Bismarck Archipelago, reached ca. 40,000 years BP (Groube et al. 1986; Leavesley et al. 2002; O’Connell and Allen 2004). There is no evidence of further eastward expansion for the next 35,000 years, until the emergence of the Lapita culture in the Bismarck archipelago ca. 3,470-3,250 years BP (Denham et al. 2012; Kirch 1997). There are strong archaeological evidence that the Lapita culture emerged in foraging populations relying on marine and land resources (Gosden and Pavlides 1994; Summerhayes 2007). It is commonly thought that the Lapita people were voyaging routinely across the islands of Near Oceania with canoes able to sail windward (Irwin 2008; Di Piazza et al. 2007). The Lapita resumed the eastward colonization of the Pacific ca. 3,200 years BP, from the Bismarck archipelago (Denham et al. 2012). The Lapita spread in less than five centuries over the hitherto uninhabited archipelagos of Remote Oceania (east of the Salomon islands, i.e., islands of Santa Cruz, Vanuatu, New-Caledonia, Fiji, etc.), as far as the western Polynesian archipelagos of Samoa and Tonga, reached by 2,850 years BP (Burley et al. 1999; Denham et al. 2012).

This unprecedented 4,500 km-migration event was characterized by phases of rapid eastward expansion with pauses in-between (Sheppard 2011). Digital navigation simulations, using instrumental winds and currents records, were used to provide information on the feasibility of eastward voyages across the Pacific. Such simulations revealed that the Samoa and Tonga archipelagos can potentially be reached from the Bismarck Archipelago by drifting/downwind sailing canoes (Anderson et al. 2006; Avis et al. 2007) and windward sailing canoes (Irwin 2008; Di Piazza et al. 2007), like the ones used by the Lapita people.

This is quite surprising then, that the Lapita migration occurred so lately in the Holocene (ca. 3,300 years BP) whereas human occupation is reported in Near Oceania ca. 40,000 years BP. Many questions rise regarding the factors that have triggered the late, intriguing, Lapita migration. Climate may have played a significant role in the Lapita migration : whereas relatively stable La Niña conditions prevailed during the Holocene, a strengthening of the El Niño Southern Oscillation variability was reported ca. 4,000-3,000 years BP, concomitantly to the Lapita migration (Haberle et al. 2001; Haug et al. 2001; Koutavas et al. 2006b; Moy et al. 2002; Rodbell et al. 1999; Sandweiss et al. 2001; Tudhope et al. 2001).

Many works documented climate-driven prehistoric human settlement and migration patterns (Dolukhanov 1997; van Geel et al. 1996; Gribchenko and Kurenkova 1997; Gupta et al. 2006; Huntley 1999; Tyson et al. 2002; Yesner 2001). Unstable climate greatly increases population vulnerability; indeed, unpredictable and highly variable climate hampers the development and the continuity of animal domestication and agriculture (Gupta 2004; Richerson et al. 2001) and could increase wildfires frequency (Haberle et al. 2001), potentially leading to large-scale

¹⁹ Compte tenu de l'échelle de temps à laquelle c'est déroulée la migration Lapita, les dates, exprimées en milliers d'années, sont plus adaptées et remplacent donc, dans ce chapitre, la notation en kilo annum (ka).

migrations. Moreover, increased climatic variability may have favored the emergence of disease epidemics, like malaria for instance, which development is favored during El Niño events (Poveda et al. 2001; Zhou et al. 2004). However, to date, the Southwest (SW) Pacific climate during the late-Holocene is poorly documented, so the potential role played by the climate in the Lapita migration in Remote Oceania remains obscure. To investigate whether the Lapita migration coincided with a peculiar climatic context, the Southwest Pacific climate variability ca. 3,000 years BP was studied.

Fossil *Tridacna* and *Hippopus* giant clams and massive coral *Porites* sp. geochemical records have been widely used for past climatic reconstructions in the western Pacific because their geochemical composition reflects changes occurring in the surrounding environment (e.g., Aharon 1980; Ayling et al. 2006; Beck 1997; Corrège et al. 2004; Gagan et al. 1998). Both fossil giant clams and massive corals are widely found in the SW Pacific area. Moreover, because giant clams were particularly targeted by the prehistoric gatherers as a food source, entire valves of *Tridacna* or *Hippopus* genus are commonly found on Lapita archaeological sites (Galipaud and Kelly 2007; Moir 1989; Seeto et al. 2012). Giant clams and massive corals provide thus an opportunity to document further the relation between climate variability and Lapita migration.

The Strontium-Calcium ratio (Sr/Ca) of coral skeleton is a reliable proxy for SST (Beck et al. 1992; Corrège 2006; Schneider and Smith 1982; Swart et al. 1991). Stable oxygen isotope composition ($\delta^{18}\text{O}$) of giant clam shell is deposited in equilibrium with the oxygen stable isotope composition of seawater ($\delta^{18}\text{O}_{\text{sw}}$), as such, giant clam $\delta^{18}\text{O}$ is a proxy for both sea surface temperature – SST – and sea surface salinity – SSS – (Aharon 1980; Aubert et al. 2009; Jones et al. 1986; McConnaughey 1989; Watanabe and Oba 1999). High $\delta^{18}\text{O}$ values indicate colder and saltier conditions whereas low $\delta^{18}\text{O}$ values are associated to warmer and fresher conditions.

In bivalves, the carbon stable isotopes composition ($\delta^{13}\text{C}$) of the shell is affected by several factors, including the SST and the organism physiology that may cause a fractionation of the stable carbon isotope (Gillikin et al. 2009; Gillikin et al. 2007; Gillikin et al. 2006; Lorrain et al. 2004; McConnaughey et al. 1997; McConnaughey and Gillikin 2008; Tanaka et al. 1986). Information is however still lacking to fully understand the mechanisms linking these factors to the shell $\delta^{13}\text{C}$. In marine bivalves, the stable carbon isotope ($\delta^{13}\text{C}$) fractionation due to vital effect seems limited and it is believed that the shell $\delta^{13}\text{C}$ composition reflects mostly the seawater Dissolved Inorganic Carbon – DIC – (Gillikin et al. 2006; McConnaughey et al. 1997; McConnaughey and Gillikin 2008; Mook and Vogel 1968; Owen et al. 2008). So, shell $\delta^{13}\text{C}$ may reflect mostly the DIC isotopic composition. Because fluvial DIC is often isotopically lighter than oceanic DIC, the shell $\delta^{13}\text{C}$ would thus reflect the proportion of fluvial/estuarine versus oceanic DIC source in the environment : low (high) $\delta^{13}\text{C}$ values would reflect a greater (lower) fluvial/estuarine (oceanic) DIC input which potentially reflect higher (lower) precipitation. In an estuarine environment the DIC isotopic composition is correlated to SSS permitting thus to use the shell $\delta^{13}\text{C}$ as an indirect proxy for SSS (Gillikin et al. 2006; McConnaughey et al. 1997; McConnaughey and Gillikin 2008; Mook and Vogel 1968; Owen et al. 2008).

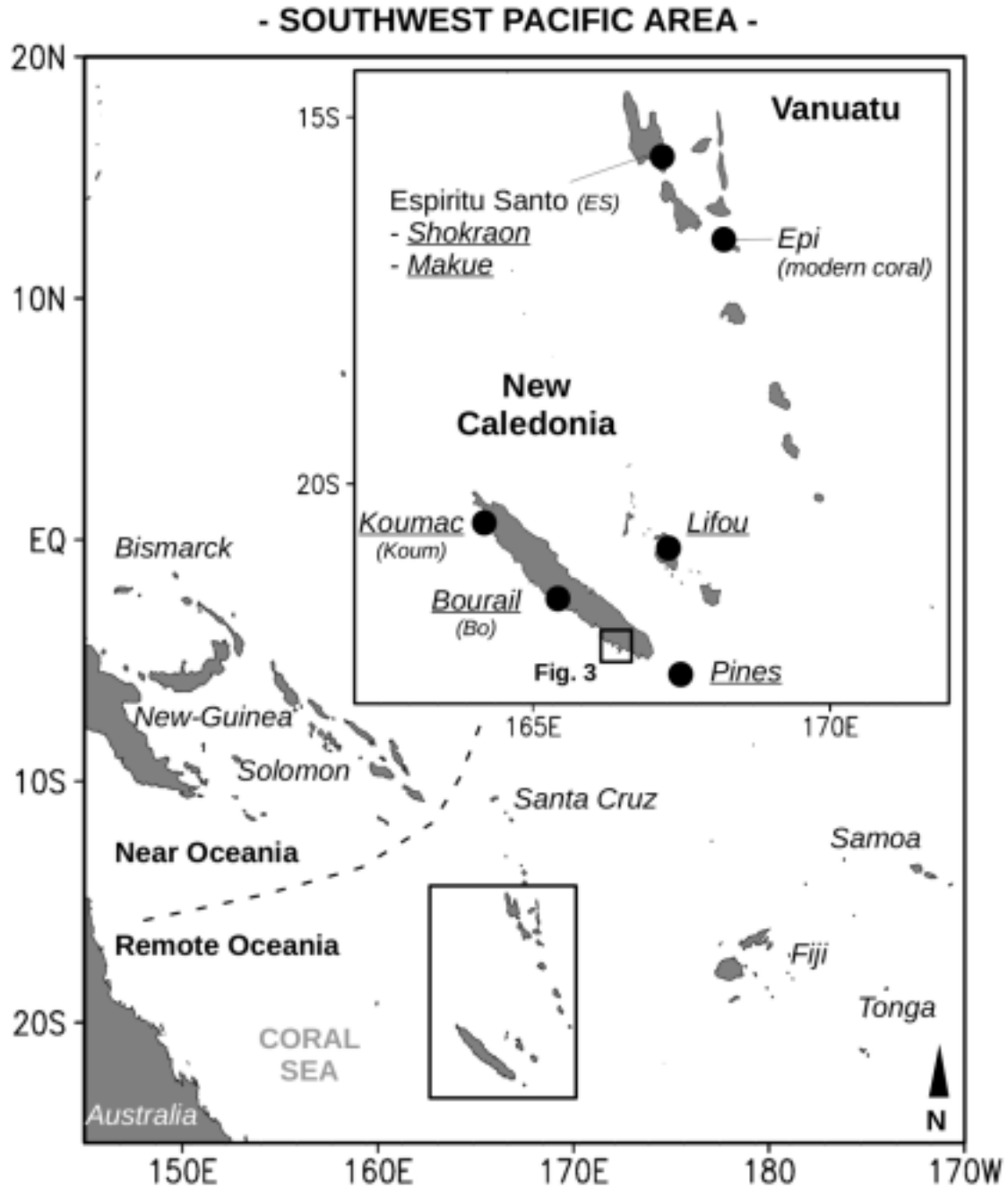
To document the climatic variability during the Lapita migration, fossil *Tridacna* and *Hippopus* giant clams were collected on Lapita archaeological sites in Vanuatu and New Caledonia – Southwest Pacific – and analyzed for oxygen bulk isotopic composition ($\delta^{18}\text{O}$ and $\delta^{13}\text{C}$). In addition, a fossil massive coral *Porites sp.*, contemporaneous to the Lapita period, was collected on an uplifted reef terrace of the Espiritu Santo Island (Vanuatu) and analyzed for its Sr/Ca composition. To document the climatic variability ca. 3000 years BP, the fossil records were compared to $\delta^{18}\text{O}$ and $\delta^{13}\text{C}$ records of modern *Tridacna* and *Hippopus* giant clams from New Caledonia and to a Sr/Ca record of a modern *Porites sp.* coral from Vanuatu. Then, the possible link between the climate variability and the Lapita migration ca. 3000 years BP is discussed.

II. Southwest Pacific climate

a. Main Climatic features

In the South West Pacific (Figure IV-1), the climate variability is mainly driven by changes in the size and the location of two main climatic features, the West Pacific Warm Pool (WPWP) and the South Pacific Convergence Zone (SPCZ). The WPWP is the permanent warm seawater body located to the east of a line between the Philippines and the Papua New Guinea (PNG), excluding the warm waters from the Indonesian Archipelago. The WPWP is commonly defined by the 28°C SST isotherm (Wyrski 1989), although a more accurate definition would integrate hydrological features and ecosystem dynamics criterion (Le Borgne et al. 2002; Maes et al. 2010). The SPCZ is a band of low-level convergence, cloudiness and precipitation, present all year-long, which is generally defined as the maximum precipitation tongue extending south-eastward from Papua New Guinea and the Solomon Islands to the south of French Polynesia (Kiladis et al. 1989; Trenberth 1976; Vincent 1994).

Figure IV-1 (next page). *Map of the Southwest Pacific area. The insert focuses on the Vanuatu archipelago and New Caledonia. Black dots show the location mentioned in the text, Lapita archaeological sites are underlined. The reference of the site used in the text is given in parenthesis when abbreviated.*



b. Seasonal patterns

In the SW Pacific, the austral summer is characterized by reduced easterlies and by warm and wet conditions related to the southward expansion of the southern edge of the WPWP and of the SPCZ (Figures IV-2a and IV-2b). The SST rises whereas the SSS diminishes due to important precipitations. The austral winter is characterized by strengthened easterlies and by cool and dry conditions related to the northward migration of the WPWP southern edge and of the SPCZ (Figures IV-2c and IV-2d). In winter, SST decreases and SSS raises in response to reduced precipitations.

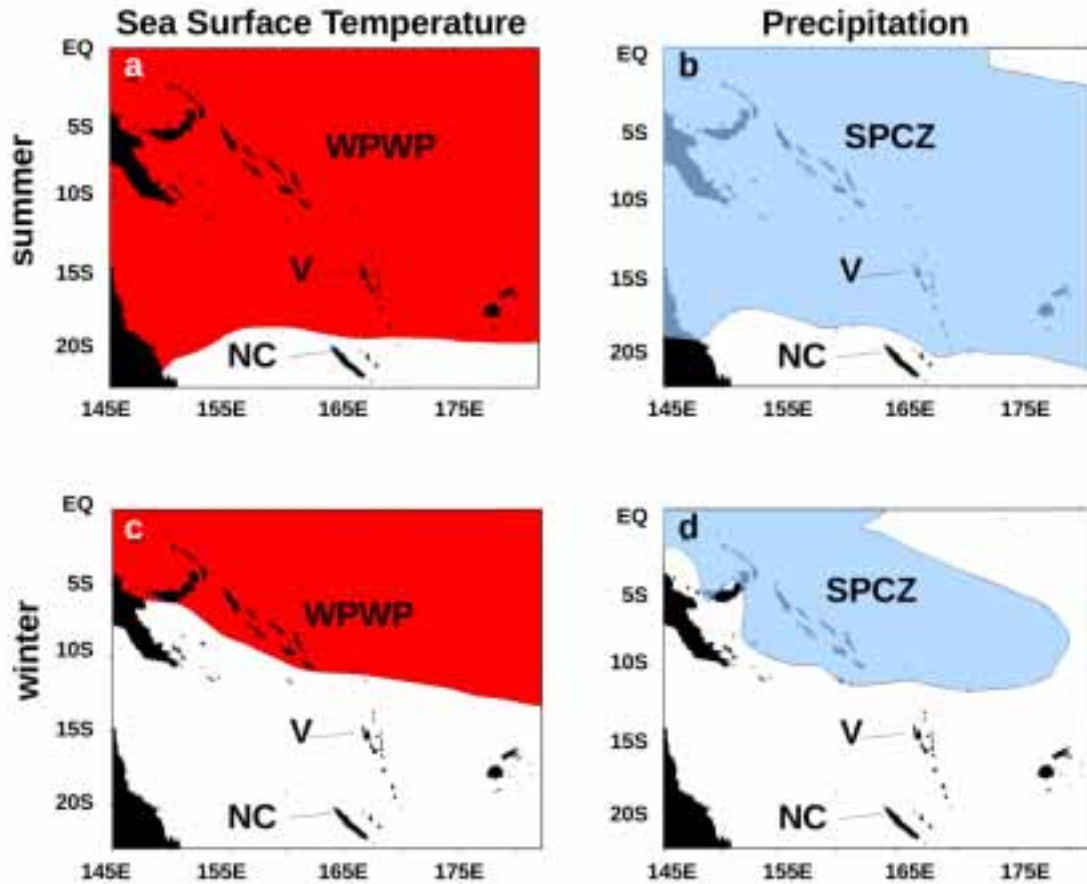


Figure IV-2. Seasonal location of the main climatic features of the Southwest Pacific. The Western Pacific Warm Pool (WPWP) is delimited by the 28°C isotherm (red area - HadISST1 mean 1980-2011 period, (Raymer et al. 2006)). The South Pacific Convergence Zone (SPCZ) is delimited by the 6 mm.d⁻¹ isohyet (blue area - CMAP 1980-2010 (Xie and Arkins, 1997)). **a** and **b** - Austral summer settings (January, February, March) **c** and **d** - Austral winter settings (July, August, September). Vanuatu archipelago (V) and New Caledonia (NC) location are shown on each map. Modified from Climate Explorer (<http://climexp.knmi.nl>).

c. Inter-annual variability

The El Niño Southern Oscillation (ENSO), characterized by a 2 to 7 years periodicity, is the main mode of variability affecting the Pacific at the inter-annual time-scale (Wang and Wang 1996). The neutral climatic mean-state is characterized by a moderate zonal sea level pressure (SLP) gradient across the Pacific Ocean that drives moderate easterlies wind regime; this wind circulation is the lower branch of the Walker circulation. During a La Niña phase of ENSO, the zonal SLP gradient increases and the easterlies wind regime strengthens across the Pacific Ocean. In the SW Pacific, during a La Niña phase, the WPWP and the SPCZ move south-eastward, leading to warmer and fresher conditions around the SW Pacific islands (Gouriou and Delcroix 2002). The El Niño phase of ENSO is characterized by a collapse of the Walker circulation, causing the wind regime to reverse from an easterly to a westerly

regime. In El Niño-phase, the southern edge of the WPWP and the SPCZ both move northward of their mean position, resulting in cooler and saltier conditions in the SW Pacific islands. An anomalous increase (decrease) in SST associated to an anomalous decrease (increase) in SSS indicates thus La Niña (El Niño) phase of ENSO in the SW Pacific region (Gouriou and Delcroix 2002).

d. Modern material and reef environments

This study is based on isotopic data from fossil giant clams and a massive coral colony from New Caledonia and Vanuatu – Southwest Pacific – (Figure IV-1). To interpret these data in terms of paleoenvironmental conditions, the geochemical composition of modern specimens, living in various modern reef environments was analyzed. SST and SSS dataset were used to characterize these modern reef environments.

e. New Caledonia

The New Caledonia main island, *Grande Terre*, is surrounded by a barrier reef delimiting a shallow lagoon with platform reefs. Some important sections of the *Grande Terre* shore are lined by fringing reefs. Four *Tridacna maxima* were collected alive the September 22th, 2008 on the outer barrier reef surrounding the *Grande Terre* (*Fausse passe de Uitoé* reef; n°1 on Figure IV-3) and a recently dead specimen was collected (September 23th, 2009), inside the lagoon, on the *Larégnère islet* reef (lagoon platform reef; n°2 on Figure IV-3). Two *Hippopus hippopus* were collected live on *Larégnère* reef on September 22th, 2008 (lagoon platform reef; n°3 on Figure IV-3). Finally, an *H. hippopus* specimen collected in 2003, on *Ducos Island* fringing reef, studied by Aubert et al., (2009), was added to this study. Living specimens collected for that study were part of a growing experiment designed to calibrate geochemical and sclerochronological proxies (chapitre I). The living giant clam specimens were grown in open-air, seawater fed aquarium from September 2008 to June 2010 (*Aquarium des lagons*, Nouméa – n°4 on Figure IV-3). The *H. hippopus* specimen studied by Aubert et al. (2009) also grew in the same aquarium from May 2003 to July 2004. The seawater of the aquarium was directly pumped from a lagoon fringing reef nearby. It was thus considered that the geochemical composition of the shell deposited while the giant clams were in the aquarium represented a “lagoon fringing reef-like” environment, whereas the geochemical composition of the shell deposited *in situ* was considered to reflect barrier or platform reef, depending on the site. At the end of the experiment, the shell of the giant clams collected alive had thus recorded two types of successive environments – barrier reef / lagoon fringing reef – and – lagoon platform reef / lagoon fringing reef. These environments are characterized in terms of average SST and SSS in Table IV-1.

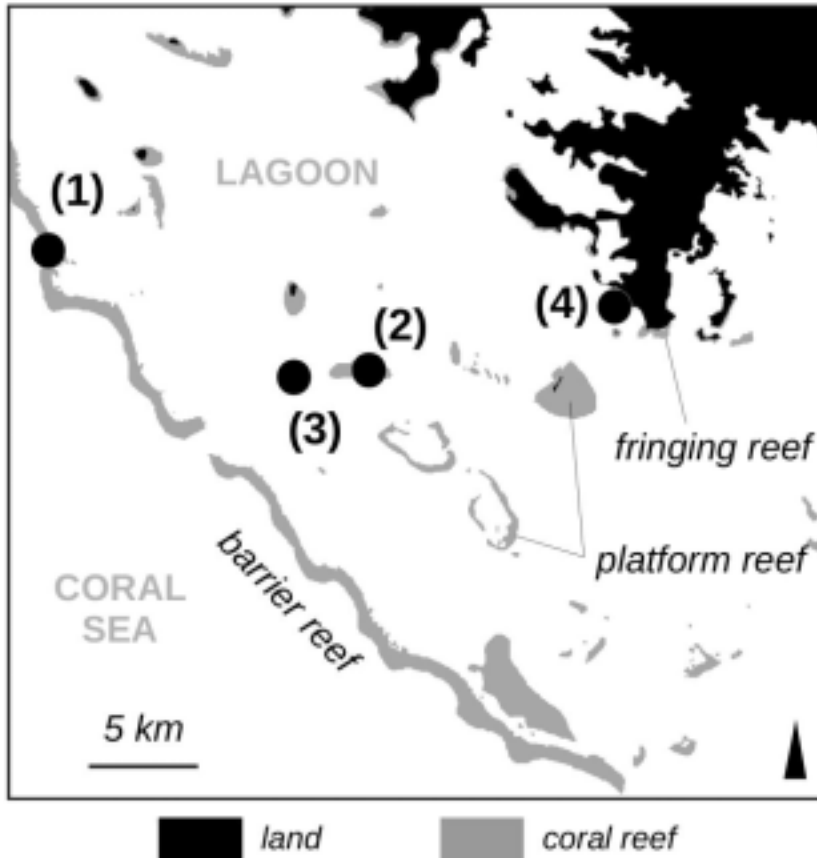


Figure IV-3. Location of the modern reef environments where the modern giant clam specimens grew (1) Uitoé reef (barrier reef); (2) Larégnère Islet (platform-reef), (3) Larégnère reef (platform-reef) and (4) Aquarium of Nouméa (lagoon fringing reef-like). Note the barrier reef complex (grey) that delimits the lagoon area from the Coral Sea. Map background : Service de cartographie de l'Institut de Recherche pour le Développement (IRD), Bondy, France.

Table IV-1 : Instrumental records of sea surface temperature (SST – °C) and sea surface salinity (SSS) characterizing the three modern reef environments studied. Results are given \pm 1 standard deviation. NC : New Caledonia; VA : Vanuatu.

marine environment	location	station	type of data	source	SST	SSS ²⁰
Lagoon fringing reef	NC	Anse Vata 22.3°S, 166.4°E	in situ logger	Réseau d'observation des stations côtières of the Institut de Recherche pour le Développement - IRD	24.7 \pm 2.2 (1997-2010)	35.3 \pm 0.7 (1977-2005)
Barrier reef		Fausse Passe de Uitoé 22.3°S, 167°E			24.1 \pm 1.6 (1992-2009)	35.4 \pm 0.2 (1992-2009)
Open-ocean fringing reef	VA	3° x 3° grid, centered on 15.5°S, 164.5°E	satellite	HadISST1 -Rayner et al., 2003	27.7 \pm 1.1 (1970-2011)	-
		2° x 2° grid, centered on 16°S, 165.5°E		Gouriou and Delcroix, 2002	-	34.9 \pm 0.3 (1949-2008)

f. Vanuatu

Vanuatu Archipelago is composed of 83 islands located at 15°S, 166°W (Southwest Pacific). Most of Vanuatu islands are surrounded by fringing reefs characterized by an open-ocean context due to the absence of barrier reefs. A modern *Porites sp.* colony, VA-EPI, was

²⁰ based on the PSS-78 scale

collected on August 2007 on a fringing reef of the Epi Island (Figure IV-1). This colony was used to characterize the Sr/Ca signature of coral living in a modern fringing reef in an oceanic context. This environment is characterized in terms of average SST and SSS in Table IV-1.

III. Archaeological sites and material

a. Archaeological material

In New Caledonia, four fossils were collected on the west coast of the *Grande Terre*, on two coastal archaeological sites, Koumac and Bourail-Nessadiou, and two fossils were collected on two sites on nearby islands, Isle of Pines –Vatcha – and Lifou Island – Gaxapo – (Figure IV-1). In Vanuatu, two fossil giant clams were collected on two archaeological sites located on Espiritu Santo Island – Shokraon – and on Aoré Island – Makué – (Figure IV-1). Each site is described in terms of archaeological context, past marine environment, and potential freshwater input from the available literature and personal field experience in Table IV-2. Each fossil giant clam is referenced by two letters indicating the genus and the species (Hh : *Hippopus hippopus*, Tg : *Tridacna gigas*, Tm : *Tridacna maxima*) followed by an indication of the archaeological site where the specimen was collected (e.g., Bo : Bourail, ES : Espiritu Santo, etc.).

b. Dating and fossil samples preservation

Fossil samples were dated using conventional ^{14}C measurements and dates were corrected for the Marine Reservoir Effect (MRE) using the Marine09 database (Reimer et al. 2009). The offset between the MRE and the local atmosphere-ocean ^{14}C (Delta R) is responsible for uncertainties in the radiocarbon ages; the Delta R values used here were 29 ± 28 years for the Vanuatu specimens and -3 ± 9 years for the New Caledonia specimens (Petchey et al. 2008).

Fossil clam shells and coral skeleton can be altered (diagenesis) through time. Various types of diagenesis can occur, like dissolution or precipitation of new material (i.e., secondary aragonite in coral skeleton pores). Such processes might modify the archive's geochemistry, resulting in biased paleoenvironmental records (e.g., Muller et al. 2001; Nothdurft and Webb 2008). Moreover, the giant clam valves are frequently found associated to cooking structures in the Lapita archeological sites (Galipaud and Kelly 2007). When removed live from the sea, giant clams maintain their valves tightly closed suggesting that Lapita might have exposed the recently harvested giant clams to fire to collect the meat. Such treatment might have caused the biogenic aragonite to transform into the more stable calcium carbonate calcite polymorph (Foster et al. 2008; Gaffey et al. 1991). Consequently, shell mineralogical composition and microstructure preservation must be checked on each fossil specimen prior to any chemical analysis.

Mineralogical X-ray diffraction (XRD) analyses were done using a Siemens[®] D500 device (Cu-K α , 40 kV, 30 mA) with a scan velocity of two seconds at a step size of 0.02° 2 θ . Minerals were identified by comparison with the reference JCPDF database (Joint Committee of Powder Diffraction File). To examine the micro-structural preservation of the fossil

specimens, small shell and coral pieces were cut, sputter-coated with platinum and observed using a Scanning Electronic Microscopy (SEM) Cambridge S360 device at 15 kV.

Table IV-2 : Description of archaeological sites in which the fossil giant clam specimens were collected and of the marine environment in which they grew (NC : New Caledonia; VA : Vanuatu).

site	location	archeological context	excavations	marine environment at 3000 years BP	potential freshwater input	Genus specie	specimen	comments
<i>Koumac</i>	NC	unknown	1981 (Galipaud 1996; Sand 2010).	mangrove and lagoon fringing reef	river	<i>Tridacna maxima</i>	TmKoum	whole valve
						<i>Hippopus hippopus</i>	HhBo	broken valve
<i>Bourail-Nessadiou</i>	NC	Lapita	1979 D. Frimigacci	mangrove and lagoon fringing reef	river	<i>Tridacna maxima</i>	TmBo	whole valve
						<i>Tridacna maxima</i>	TmBo2	whole valve
<i>Lifou (Gaxapo)</i>	NC	Lapita	2008 F. Wadra	open-ocean fringing reef	freshwater resurgences	<i>Tridacna maxima</i>	TmLifou	whole valve
<i>Isle of Pines (Vatcha)</i>	NC	Lapita	1978 D. Frimigacci	open-ocean fringing reefs / shallow lagoon	freshwater resurgences	<i>Hippopus hippopus</i>	HhPines	broken valve
<i>Shokraon</i>	VA	Early-Lapita	2000 JC. Galipaud	open-ocean fringing reef	river	<i>Tridacna gigas</i>	TgES	broken valve
<i>Makué</i>	VA	Early-Lapita	(Galipaud and Kelly, 2007)	open-ocean fringing reef	river	<i>Hippopus hippopus</i>	HhES	broken valve

c. Geochemical sampling

i. Giant clams

The central ridge of each modern and fossil giant clam was cut off from the valves using a diamond saw (Figure IV-4). Each central ridge was sampled along a single transect perpendicular to the growth direction and encompassing the shell deposited during the entire life of the specimen, using a Micro-Mill device – New Wave[®]. This method is termed bulk-sampling.

For the *Tridacna maxima* specimens, the shell deposited during the early life of the animal is usually highly bio-eroded and it was thus not sampled (Figure IV-4a). To avoid any fractionation due to the heat generated during the milling process and to obtain a fine-sized

and homogeneous carbonate powder, the drilling device was parameterized as follow : drilling speed : 50%, scan speed : 15 $\mu\text{m}\cdot\text{s}^{-1}$, depth per pass : 30 μm , with a number of pass ranging from 2 to 8 depending on the transect length. With such settings, enough material was obtained to analyze, at least, three replicates for each giant clam specimen (stable isotopes analyzes).

Tridacna maxima specimens were sampled on the outer shell layer (Jones et al. 1986). For the modern specimens, the shell section deposited *in situ* and the section deposited in the aquarium were bulk-sampled independently. The transition between the two environments is clearly visible in the outer layer of the shell : most of the shell is greenish and translucent and it turns abruptly white and opaque on the last centimeter of growth (Figure IV-4a).

Hippopus hippopus specimens were bulk sampled in the shell inner layer (Aubert et al. 2009; Watanabe and Oba 1999). Unlike the modern *T. maxima* specimens, the modern *H. hippopus* did not reflect the environmental change (i.e., *in situ* to aquarium) in the inner layer of the shell (Figure IV-4b). Consequently, it was not possible to sample independently the shell deposited in the two environments. The entire inner shell layer was thus sampled, averaging the geochemical signature of both environments.

In *Tridacna gigas*, the hinge and the inner layer have a similar $\delta^{18}\text{O}$ composition (Elliot et al. 2009). Consequently, the fossil *Tridacna gigas* shell was sampled in the hinge and the inner layer to obtain a duplicate of the shell $\delta^{18}\text{O}$ composition.

ii. Coral sample

The two coral colonies were sliced parallel to the main growth axis to obtain a 10 mm-thick slab for each colony. The annual density banding was revealed by x-radiographs of the coral slabs (Knutson 1972). Before sampling, the slabs were cleaned in an ultrasonic bath with milli-Q water and oven-dried at 40°C. A diamond drill-bit coupled to a three-axis positioning system was used to collect carbonate samples at a 1 mm step, along a transect parallel to the growth axis, for strontium and calcium analyzes.

iii. Estimation of the time period averaged in the bulk records

The Von Bertalanffy Growth Function (VBGF) was used to i) determine the age of the giant clams collected and ii) determine the period averaged in each bulk sample. Various VBGF are available both for *Tridacna maxima* (Green and Craig 1999; McKoy 1980; McMichael et al. 1974; Munro and Heslinga 1983; Smith 2011) and *Hippopus hippopus* (Beckvar 1981; Munro and Heslinga 1983; Shelley 1989)

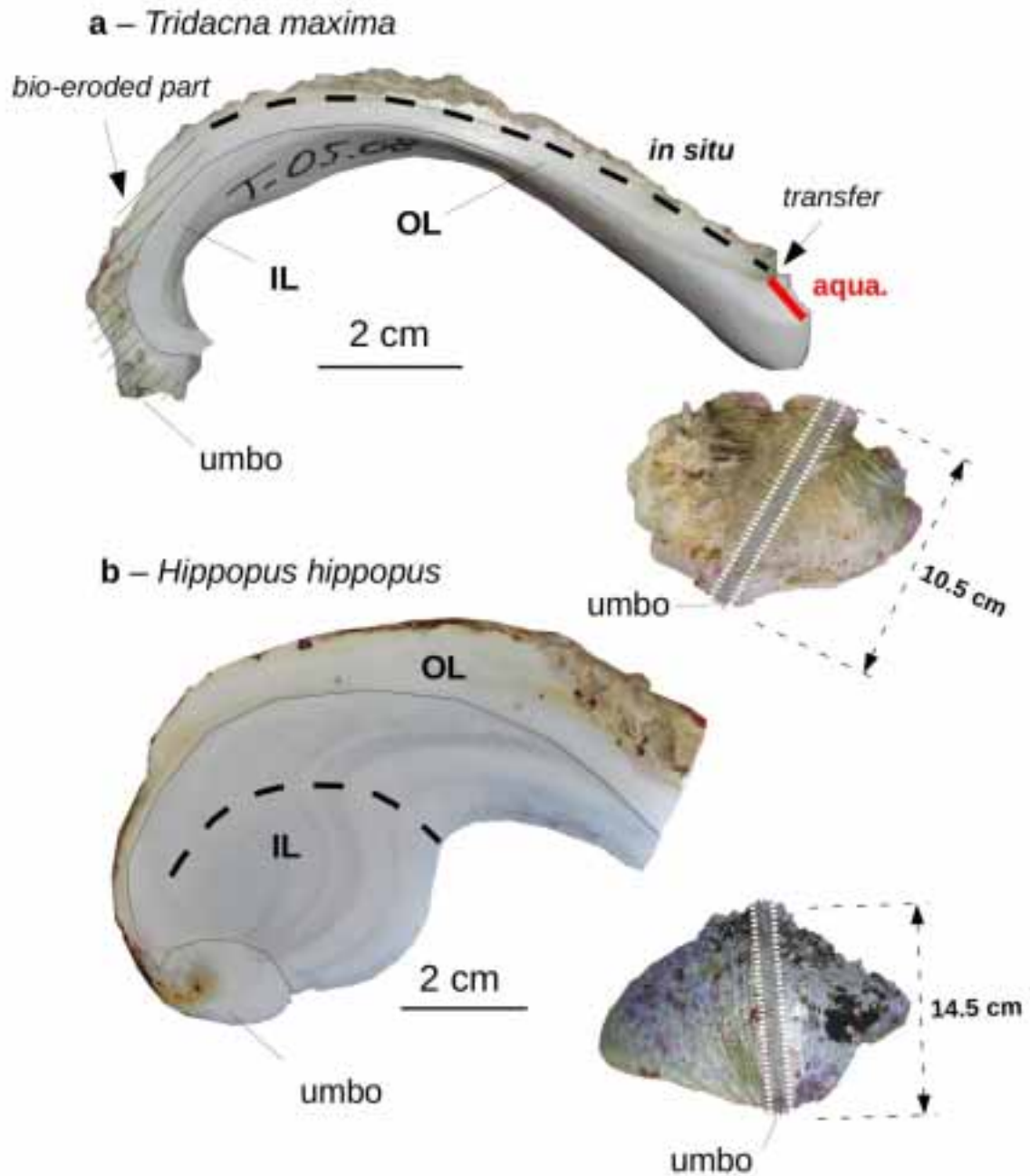


Figure IV-4. Bulk sampling design for the giant clams **a** - *Tridacna maxima* : the shell was sampled following the growth axis (dashed black line) in the outer layer – OL, note the color of the shell before and after the transfer of the specimen into the aquarium (red). **b** - *Hippopus hippopus* : the shell was sampled following the growth axis (dashed line) in the inner layer – IL. The shell part cut for the bulk sampling is represented by the white dotted rectangles on the whole shell images.

Ages of modern and fossil specimens were determined using an average equation (VBGF_{ave.}- Tables IV-3 and IV-4). However, the VBGF could not be applied to the specimens presenting incomplete, i.e., broken, valves because the shell length could not be measured (fossil *T. gigas* and *H. hippopus*). In such case, ages were determined by counting the translucent and opaque growth layers visible in the hinge or in the inner layer (e.g., *H. hippopus* in Figure IV-4b) assuming that they reflect yearly growth (e.g., Aharon 1980; Aubert et al. 2009).

Table IV-3 : Compilation of Von Bertalanffy Growth Function parameters (L_{inf.} and K) obtained from *Tridacna maxima* giant clam populations and the averaged parameters used in this study (VBGF_{ave.}).

Reference	L _{inf.} (cm)	K
McKoy, 1980	30.5	0.082
Munro and Heslinga, 1983	30.5	0.112
McMichael, 1975	27.5	0.074
Green and Craig, 1999	27.8	0.065
Smith, 2011	26.9	0.118
VBGF_{ave.}	MEAN 28.6	0.090
	sd 1.7	0.024

Table IV-4 : Compilation of Von Bertalanffy Growth Function parameters (L_{inf.} and K) obtained from *Hippopus hippopus* giant clam populations and the averaged parameters used in this study (VBGF_{ave.}).

Reference	L _{inf.} (cm)	K
Munro and Heslinga, 1983	40	0.213
Beckvar, 1981	40	0.1
Shelley, 1989 - Iris Point	34.7	0.205
Shelley, 1989 - Pionner Bay	41.5	0.155
VBGF_{ave.}	MEAN 39.1	0.168
	sd 3.0	0.052

For the *Tridacna gigas* and *Hippopus hippopus* specimens, the bulk sampling integrated the entire lifetime of the specimens. For the *T. maxima* specimens, the strong bio-erosion observed in the earliest parts of specimens prevented sampling the entire lifetime, so the time period averaged in each bulk sample is necessarily shorter than the lifetime of the specimen. No annual growth layer are visible in the *T. maxima* shells so the mean annual growth rate of *T. maxima* was estimated by measuring the shell deposited from the transfer of the specimens from the barrier reef to the aquarium (Sept. 2008) to the death of the animal (Oct. 2009). This annual growth rate was then used to determine the time period averaged in the bulk record sampled in the shell deposited *in situ*. However, considering that giant clams annual growth rate decreases with age (Shelley 1989), the period calculated is an estimation of the maximum period recorded by each *T. maxima* bulk sample.

d. Geochemical analyses*i. Stable isotopes*

The oxygen and carbon stable isotopes composition was analyzed on a Thermo Delta V Advantage[®] mass-spectrometer coupled to a Thermo Kiel IV carbonate device at the *Service de Spectrométrie de Masse Isotopique du Museum National d'Histoire Naturelle* (Paris, France). Results are expressed as $\delta^{18}\text{O}$ and $\delta^{13}\text{C}$ (standardized against Vienna Pee Dee Belemnite – vpdb). Analytical reproducibility (1σ) on isotopic determinations was 0.04‰ vpdb for $\delta^{18}\text{O}$ and 0.01‰ vpdb for $\delta^{13}\text{C}$. These values are based on 32 runs of a homemade calcitic standard during the period of analysis (4 days).

ii. Strontium/Calcium

The Strontium (Sr) and Calcium (Ca) concentrations of the coral samples were analyzed using an inductively-coupled plasma mass spectrometer (ICP-MS; Agilent 7500 CX[®]), following the method of Le Cornec and Corrège (1997). Analytical precision on Sr/Ca was assessed using the certified reference material JcP-1²¹ (coral material) from the Geological Survey of Japan (Hathorne et al. 2010; Inoue et al. 2004; Okai et al. 2002). Analytical reproducibility (1σ) on coral Sr/Ca measurements was 0.05 mmol.mol⁻¹, based on 30 runs of a home-made coral standard over a six months period.

e. ENSO variability

ENSO variability in the SW Pacific is characterized by periods of high SST and low SSS named La Niña phases alternating with periods of low SST and high SSS referred as El Niño phases. These events occur every 2 to 7 years. Considering that the giant clam bulk $\delta^{18}\text{O}$ records obtained in this study integrated time periods comprised between 3 to 11 years, they may have recorded the interannual variations of the SST and the SSS related to the ENSO variability. The amplitude of the La Niña/El Niño events in the giant clam $\delta^{18}\text{O}$ signature can thus be quantified by calculating the standard deviation of the modern and of the fossil bulk records.

IV. Results**a. Samples dating and preservation**

All samples are composed of 100% aragonite (XRD results). The aragonitic microstructure of the giant clam shells and the primary aragonite needles and centers of calcification of the coral sample are well preserved, without dissolution or secondary aragonite (SEM observations). The conventional (i.e., non-calibrated) age of the fossil *Porites sp.* coral colony was $3,583 \pm 36$ years BP. Non-calibrated radiocarbon ages of the archaeological giant clam specimens are reported in Table IV-5.

²¹ The certified value for the Sr/Ca ratio was : 8.82 mmol.mol⁻¹.

Table IV-5 : Uncalibrated radiocarbon ages of the archeaeological giant clam specimens presented in this study.

Reference	age ¹⁴ C uncal. ± uncert.
TmKoum	2,648 ± 33
HhBo	3,120 ± 24
TmBo	3,236 ± 32
TmBo2	3,198 ± 33
TmLifou	3,064 ± 23
HhPines	3,047 ± 24
TgES	3,172 ± 24
HhES	3,625 ± 30

Calibrated radiocarbon dates of the giant clam specimen HhES and of the fossil *Porites sp.* colony from Vanuatu fall within the interval (2σ) 3,600-3,400 years BP (Table IV-6). Calibrated dates of giant clam specimens HhBo, TmBo, HhPines, TmBo2 and TmLifou are comprised in the interval 3,200 – 2,900 years BP. Specimen TmKoum is younger : 2,500-2,300 years BP (Table IV-6).

b. Giant clams

Hippopus hippopus – Ages of the modern and the fossil *H. hippopus* specimens are reported in Tables IV-6 and IV-7. Because the bulk sampling procedure included the entire inner layer, the period captured by the bulk sampling corresponds to the age of the *H. hippopus* specimens.

Tridacna sp. – Modern *T. maxima* ages are reported in Table IV-6. The three modern *T. maxima* specimens that grew in the aquarium deposited around 10 mm of shell during the 13 months period. The annual growth rate in the outer of the shell layer was thus $\sim 10 \text{ mm.yr}^{-1}$. This growth rate value was used to determine the time period averaged in the bulk record sampled in the part of the shell deposited *in situ*. The longest *in situ*-bulk transect was 7 cm-long, which correspond to a maximum time period of 7 years. Considering that the four modern *T. maxima* specimens were collected in 2009, the bulk samples integrated a time period spanning the decade of the 2000's. Time periods included in the fossil specimens' bulk samples are reported in Table IV-7.

Table IV-6 : Characteristics of the giant clams specimens collected on modern reef environments (New Caledonia).

Genus specie	Reef environment	Specimen	height (cm)	length (cm)	Age (yr)	Record length (years)	$\delta^{13}\text{C}\text{‰}$ vpdb	$\delta^{18}\text{C}\text{‰}$ vpdb	mean $\delta^{13}\text{C}\text{‰}$ vpdb	mean $\delta^{18}\text{C}\text{‰}$ vpdb
<i>Tridacna maxima</i>	Lagoon/ Fringing reef (aquarium)	T-02-08	12.6	20.4	14±6	1	1.45±0.01	-0.47±0.05		
		T-03-08	16	20.7	14±6	1	1.41±0.01	-0.72±0.05	1.46±0.06	-0.72±0.25
		T-05-08	13.5	20.1	13±5	1	1.52±0.01	-0.96±0.02		
	Platform reef	T-04-08	9.5	16.7	9±3.8	< 7	1.58±0.02	-0.46±0.05	1.58±0.02	-0.46±0.05
	Barrier reef	T-01-08	13.4	18.7	12±5	< 7	1.34±0.01	-0.20±0.01		
		T-02-08	12.6	20.4	14±6	< 3	1.50±0.02	-0.09±0.01	1.45±0.08	-0.16±0.05
		T-03-08	16	20.7	14±6	< 5	1.51±0.00	-0.14±0.02		
T-05-08		13.5	20.1	13±5	< 7	1.44±0.00	-0.19±0.00			
<i>Hippopus hippopus</i>	Platform reef and lagoon/ Fringing reef (aquarium)	H-06-08	19.8	29	8±4		1.66 ± 0.00	-0.34±0.02		
		H-07-08	15.4	22	5±2		1.51±0.01	-0.49±0.06	1.46±0.22	-0.48±0.14
		Hh N5 04	18	26	4		1.22±0.01	-0.61±0.03		

Table IV-7 : Characteristics of the giant clams specimens collected on the archaeological sites of Vanuatu (VA) and New Caledonia (NC). Hh : *Hippopus hippopus*; Tm : *Tridacna maxima*; Tg : *Tridacna gigas*. Specimens are classified in three groups according to their isotopic signature (see section IV- d).

	Spec.	Reef env.	Date ^{14}C calib. (ka BP)	height (cm)	length (cm)	Age (yr)	Record Length (yr.)	$\delta^{13}\text{C}\text{‰}$ vpdb	$\delta^{18}\text{C}\text{‰}$ vpdb	mean $\delta^{13}\text{C}\text{‰}$ vpdb	mean $\delta^{18}\text{C}\text{‰}$ vpdb
Fossils #1 (NC)	HhBo	Lagoon fringing reef	3.0-2.8	n/a	n/a	7	7	2.53±0.01	-0.68±0.02		
	TmBo	Lagoon fringing reef	3.2-2.9	11.6	19.4	13±5	< 9	2.29±0.02	-0.50±0.02	2.61±0.36	-0.56±0.10
	HhPines	Open ocean fringing reef	2.9-2.7	n/a	n/a	11	11	3.00±0.02	-0.51±0.02		
Fossils #2 (NC)	TmBo2	Lagoon fringing reef	3.1-2.9	9.2	15.5	9±3	<4	2.09±0.00	-1.80±0.01		
	TmKoum	Lagoon fringing reef	2.5-2.3	8.4	14.2	8±3	<3	2.13±0.01	-1.50±0.02	2.06±0.09	-1.58±0.19
	TmLifou	Open ocean fringing reef	2.9-2.8	12.6	~ 20	~ 13	<6	1.95±0.00	-1.45±0.01		
Fossils #3 (VA)	HhES		3.6-3.4	n/a	n/a	3	3	1.89±0.02	-2.27±0.01	1.89±0.02	-2.27±0.01
	TgES	Open ocean fringing reef	3.1-2.8	10.7	n/a	10	10	2.32±0.08	-1.99±0.28	2.32±0.08	-1.99±0.28

The hinge of the *T. gigas* specimen presents 10 couplets of opaque and translucent bands, i.e., 10 years. Considering that the bulk samples milled in the hinge and in the inner layer integrated the entire life of the animal, the bulk sample was assumed to average a 10 years period (Table IV-7). Because of the small size of the giant clam shells studied here and because marks of tool-uses were absent (Moir 1990), it was assumed that all the archaeological giant clams specimens were harvested on nearby reefs for consumption. Considering that the time periods included in the giant clam bulk isotopic composition ranged from 3 to 11 years (Tables IV- 6 & 7), they most probably reflects the interannual environmental variability of the giant clams collection sites (Table IV-2).

c. Corals

The length of the modern and of the fossil *Porites sp.* records were determined by cross-checking the annual density growth bands (Knutson 1972) and the Sr/Ca annual cycles. The modern coral VA-EPI from Vanuatu recorded 7 years (1999 to 2006) and the fossil record spans 22 years. Both records were averaged to obtain a bulk Sr/Ca composition. The mean Sr/Ca value of the fossil *Porites sp.* colony is $8.80 \pm 0.09 \text{ mmol.mol}^{-1}$ and the mean Sr/Ca value of the modern coral colony from Vanuatu is $8.99 \pm 0.08 \text{ mmol.mol}^{-1}$ (Figure IV-5). This value is significantly lower ($p < 0.001$, Mann-Whitney) by $0.18 \text{ mmol.mol}^{-1}$ than the modern Vanuatu coral.

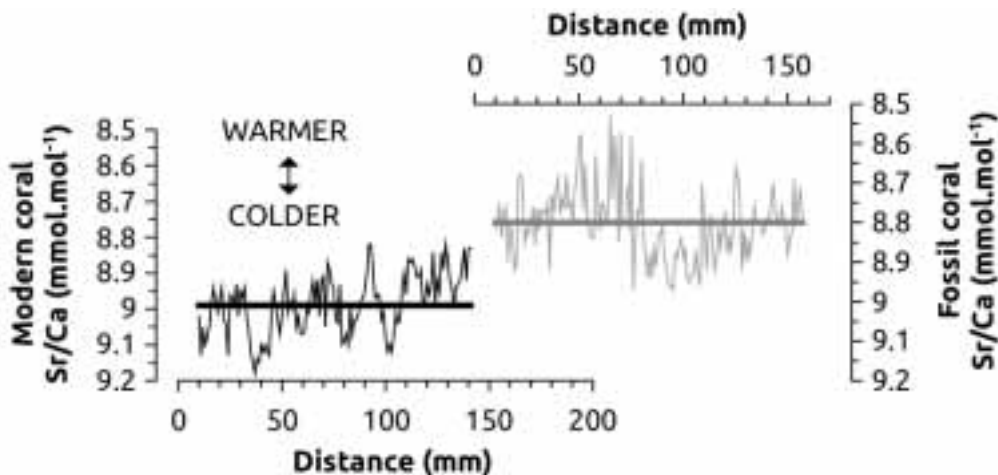


Figure IV-5. Strontium/Calcium profiles and mean values of the modern (black) and the fossil (grey) *Porites sp.* corals. Note that the y axis is reversed.

d. $\delta^{18}\text{O}$ versus $\delta^{13}\text{C}$ scatter plot

Modern and fossil giant clams $\delta^{18}\text{O}$ was plotted against $\delta^{13}\text{C}$ to i) determine to which extent the modern giant clam records reflect the different reef environments in which they grew, ii) find out if the giant clam genus has an influence on the isotopic records and iii) to characterize the past environments in which the fossil specimens grew. Four groups, one modern and three fossils, with distinct isotopic compositions emerged from this scatter plot (Figure IV-6).

e. Modern giant clam baseline

A mean isotopic composition ($\delta^{18}\text{O}$ and $\delta^{13}\text{C}$) for the *modern* group was calculated by averaging the data of all the modern giant clams : mean $\delta^{13}\text{C}$ composition is $1.47 \pm 0.12\text{‰}$ vpdb, and mean modern $\delta^{18}\text{O}$ composition is $-0.42 \pm 0.27\text{‰}$ vpdb. The giant clams' $\delta^{18}\text{O}$ composition presents significant differences depending on the environmental settings. The *Tridacna maxima* specimens that grew on the barrier reef have a $\delta^{18}\text{O}$ composition enriched by $+0.26\text{‰}$ vpdb compared to the mean modern $\delta^{18}\text{O}$ composition ($-0.42 \pm 0.27\text{‰}$ vpdb). The *T. maxima* specimens that grew in the aquarium present a $\delta^{18}\text{O}$ composition depleted by -0.30‰ vpdb compared to the *modern* group (Table IV-7). The *T. maxima* specimen that grew on the lagoon platform reef and the three *H. hippopus* specimens that grew on both the lagoon platform reef and in the aquarium, present intermediate or similar $\delta^{18}\text{O}$ values (Table IV-7).

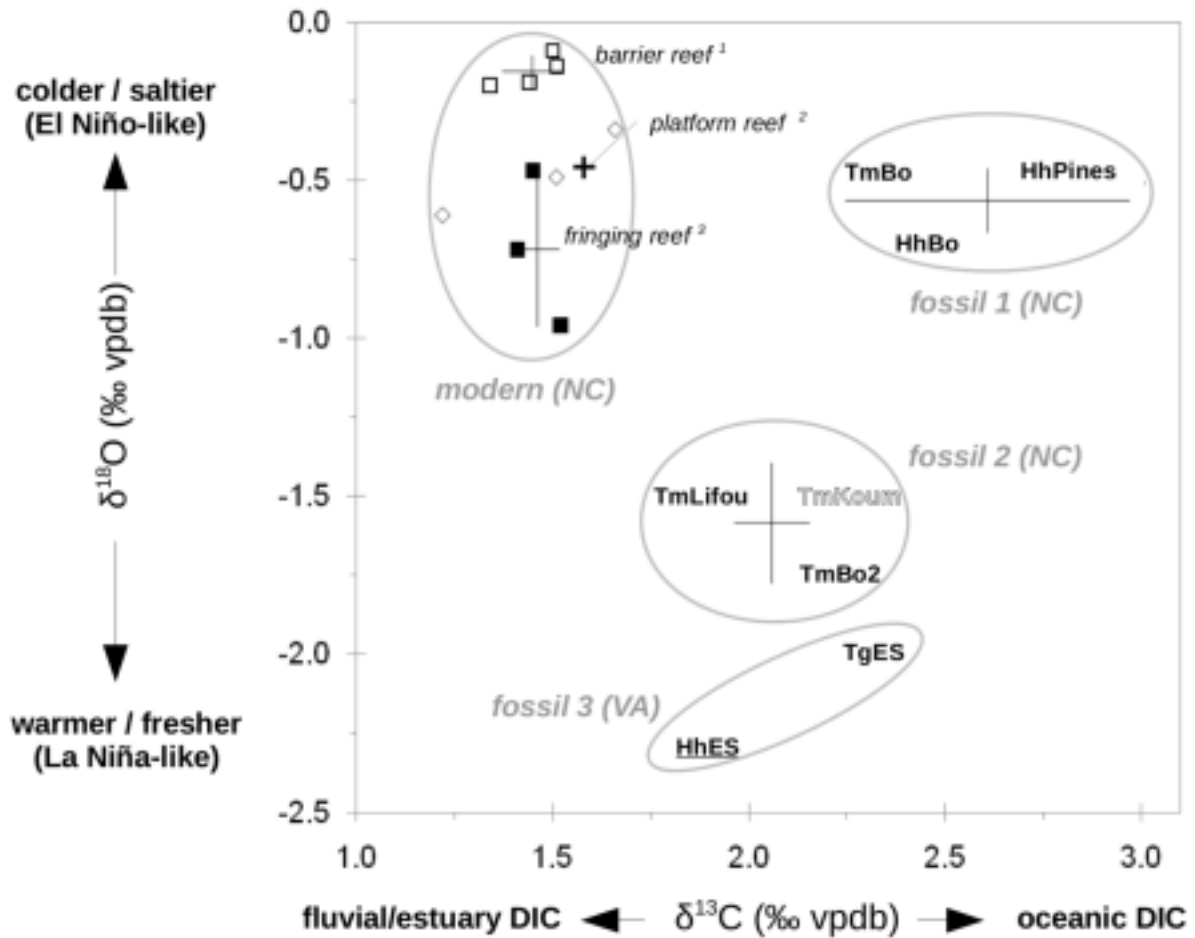
f. Fossil giant clams

Group fossil 1 – This group includes three specimens from New Caledonia, dated at 3,200-2,700 years BP, one *Tridacna maxima* – TmBo – and two *Hippopus hippopus* – HhBo and HhPines (Figure IV-6). These specimens have the same $\delta^{18}\text{O}$ composition than the *Modern* group and present a $\delta^{13}\text{C}$ composition enriched by $+1\text{‰}$ vpdb compared to the modern mean value.

Group fossil 2 – The second group of fossil specimens is composed by three *Tridacna maxima* from New Caledonia; TmLifou, TmKoum, and TmBo2 (Figure IV-6). These specimens present a $\delta^{18}\text{O}$ composition depleted by -1‰ vpdb and a $\delta^{13}\text{C}$ composition enriched by $+0.5\text{‰}$ vpdb compared to the *modern* group. These specimens are contemporaneous to the *group fossil 1* (3,200-2,700 years BP) except the specimen TmKoum that post-dates the other fossil specimens (2,500-2,300 years BP).

Group fossil 3 – The two fossil giant clams from Vanuatu compose the third group (Figure IV-6). Specimens of this group present the lowest $\delta^{18}\text{O}$ values of all the giant clam records. The *Hippopus hippopus* – HhES – dated ca. 3,600-3,400 years BP, has a $\delta^{18}\text{O}$ composition depleted by -1.85‰ vpdb compared to the modern group. The *Tridacna gigas* specimen – TgES – dated ca. 3,200-2,700 years BP, has a $\delta^{18}\text{O}$ composition depleted by -1.57‰ vpdb compared to the *modern* group. The $\delta^{13}\text{C}$ composition of specimens from *groups fossil 3* and *fossil 2* are similar. Both groups have a $\delta^{13}\text{C}$ composition enriched by $+0.5\text{‰}$ vpdb compared to the modern group from New Caledonia (Figure IV-6).

Figure IV-6 (next page). $\delta^{18}\text{O}$ versus $\delta^{13}\text{C}$ stable isotope bulk composition of the giant clam specimens. *Tridacna maxima* modern specimens from the three different modern reefs environment : barrier reef (empty squares), platform-reef (black cross) and lagoon fringing reef (black squares). *Hippopus hippopus* specimen records (empty diamond) integrated both platform and lagoon fringing reef environments. The isotopic composition of the fossil specimens from New Caledonia (*fossil 1* and *fossil 2*) and from Vanuatu (*fossil 3*) is plotted using their reference's name (Hh : *Hippopus hippopus*, Tg : *Tridacna gigas*, Tm : *Tridacna maxima*). Note that the error on isotopic determinations is smaller than the label. Fossil specimens are comprised between 3,200-2,700 years BP, except HhEs : 3,600-3,400 years BP (underlined) and TmKoum 2,500-2,300 years BP (thick letters).



g. ENSO variability in New Caledonia

The modern bulk $\delta^{18}\text{O}$ records, that encompass the period 2000-2009, present a standard deviation of 0.27 ‰ vpsdb (Figure IV-7). The standard deviation of the the fossil bulk $\delta^{18}\text{O}$ records was calculated by pooling the records of groups *fossil 1* and *fossil 2* which only include records from New Caledonia. The period considered here is 3,500-2,500 years BP. The standard deviation of the fossil bulk $\delta^{18}\text{O}$ records is 0.57 ‰ vpsdb, twice the modern standard deviation (Figure IV-7). Fossil $\delta^{18}\text{O}$ values are more negative that the modern $\delta^{18}\text{O}$ values, reflecting warmer and fresher conditions than modern ones.

V. Discussion

a. Interpreting the bulk geochemical records

The bulk sampling method was used in this study to generate a consequent amount of paleoclimatic data from many fossil specimens. A similar sampling method was used successfully in paleoclimatic studies using massive coral colonies (Abram et al. 2009). In the present study, the bulk sampling provided interannually resolved record which included time periods comprised between 3 to 11 years. Such resolution is requested to study the ENSO variability which frequency peaks around 2-7 years (e.g., Trenberth 1976; Tudhope et al. 2001).

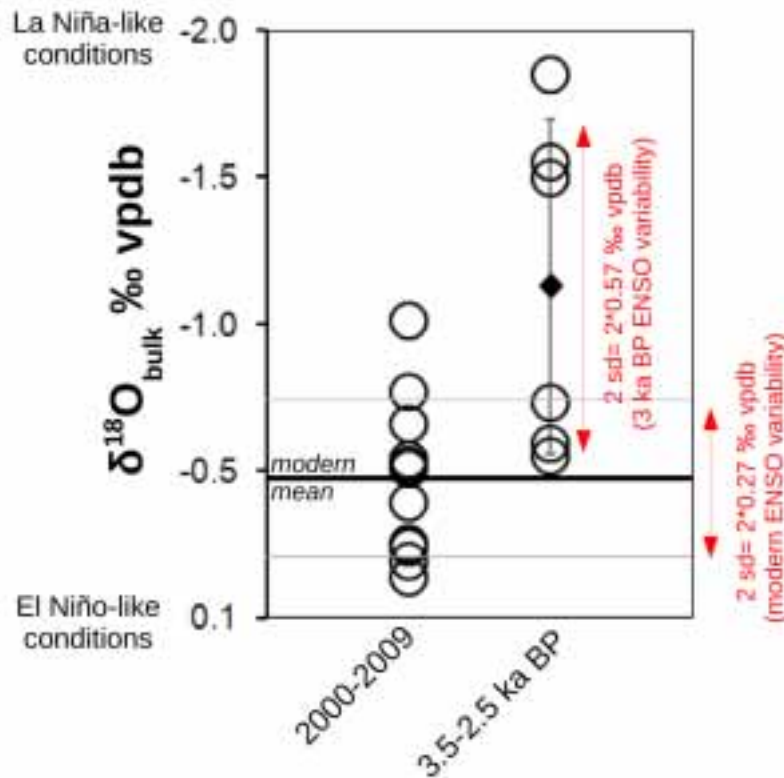


Figure IV-7. Modern (2000-2009) and fossil (3,500-2,500 years BP) giant clam *Tridacna maxima* bulk $\delta^{18}\text{O}$ records. The black diamond is the mean fossil $\delta^{18}\text{O}$ value. Note that the y-axis is inverted so that low $\delta^{18}\text{O}$ indicates warm and fresh conditions whereas high $\delta^{18}\text{O}$ values indicates cool and salty conditions.

Interpreting bivalve's bulk data require careful consideration. Indeed, giant clams' growth is positively correlated to SST, i.e., more shell is deposited during warm periods (e.g., summer) than during cold periods (e.g., winter). Consequently, warm periods tend to be over-represented in the bulk samples (Aharon 1980; Aubert et al. 2009; Jones et al. 1986). This bias implies that bulk records cannot be directly compared to instrumental records. However, in this study, the same bulk sampling method was used on modern and fossil specimens. Consequently, both datasets are comparable assuming that SST affects fossil and modern giant clam's growth similarly.

The shell geochemical composition may also be influenced by ontogenic effects. Jones et al. (1986) evidenced, from the shell isotopic composition of a 28 years-old *Tridacna maxima*, that the growth of this species is characterized by a linear growth until age 10 and that growth sharply decreased beyond age 10. They also observed that the shell isotopic composition of *T. maxima* varied depending on the life-stage of the animal. These authors revealed that the shell deposited after \sim age 10 had a $\delta^{18}\text{O}$ composition enriched by $+0.27\text{‰ vpdb}$, compared to the shell deposited in the first 10 years. These authors interpreted the change in the $\delta^{18}\text{O}$ record as reflecting the transition from the juvenile to the adult phase (supposed to occur around age 10). However, more recent studies showed that *T. maxima* reaches its sexual maturity at

around two years-old (Raymakers et al. 2003), suggesting that the geochemical composition change observed in the 28 years-old *T. maxima* specimen would rather reflects a transition from the adult toward the senescent phase.

Considering that the modern and fossil *Tridacna maxima* specimens studied here are between ~ 8 and ~ 15 year-old, bulk samples might include shell deposited during the senescent phase, potentially biasing the environmental signature of the isotopic record. Regarding the $\delta^{18}\text{O}$ signature, the difference observed between pairs of groups – *fossil 2* and *3* – versus – *modern* and *fossil 1* – is superior by a factor three to the isotopic difference between adult and senescent shell isotopic composition as reported by Jones et al (1986) (Figure IV-6). Thus, a potential bias due to ontogenetic trends cannot explain the anomalous negative $\delta^{18}\text{O}$ composition of groups *fossil 2* and *3*.

On the $\delta^{13}\text{C}$ record of the 28 years-old *T. maxima* specimen, a linear decrease of about 0.04‰ $\text{vpdb}\cdot\text{year}^{-1}$ is observed along the 28 year-long record with no particular trend beyond age 10 (Jones et al. 1986). Considering that the longest bulk record produced in this study encompass a time-period of about 11 years (Table IV-6) and assuming a linear $\delta^{13}\text{C}$ ontogenic decrease of about 0.04‰ $\text{vpdb}\cdot\text{year}^{-1}$, the ontogenic bias in the $\delta^{13}\text{C}$ record would be less than 0.2‰ vpdb . This value is lower than the inter-group differences previously described which range from 0.5 to 1.0‰ vpdb . This evidences that the differences observed in the bulk isotopic composition of the four groups cannot be explained by the ontogenetic trend only.

b. Giant clam isotopic signature : genus, environment or climate ?

The giant clam data presented in this study shows no relation between the shell isotopic $\delta^{18}\text{O}$ and $\delta^{13}\text{C}$ composition and the giant clam's genus (Figure IV-6). The differences, observed in the giant clams' shell isotopic composition, were thus assumed to reflect environmental changes rather than genus-specific isotopic signature. However, there is no agreement between the isotopic composition of groups *fossil 1* and *fossil 2* and the reef environment surrounding the archaeological sites where fossils were collected (Table IV-6). The best example is shown on Figure IV-6 by the three giant clams specimens (TmBo, TmBo2 and HhBo) collected on the same archaeological site of Bourail (characterized by a lagoon fringing reef environment); that are distributed in groups *fossil 1* (TmBo and HhBo) and *fossil 2* (TmBo2). As such, the various environments cannot explain solely the differences observed between the groups, implying that these differences reflect changes affecting the climatic-mean state.

Oxygen stable isotopes – Stable oxygen isotope composition ($\delta^{18}\text{O}$) of giant clam shell is commonly used as a proxy for both sea surface temperature – SST – and sea surface salinity – SSS – (Aharon 1980; Aubert et al. 2009; Jones et al. 1986; McConnaughey 1989; Watanabe and Oba 1999). Cold (warm) and salty (fresh) conditions are reflected by high (low) $\delta^{18}\text{O}$ values. In New Caledonia, the $\delta^{18}\text{O}$ composition of modern giant clams reflects the reef environment : the $\delta^{18}\text{O}$ composition of specimens living on the barrier reef presents higher values than specimen living in a lagoon fringing reef or in a platform reef, in agreement with the SST and SSS gradients observed in these two reef environments (Table IV-1).

Carbon stable isotopes – Interpretation of stable carbon isotope composition ($\delta^{13}\text{C}$) of giant clam shell is not straightforward and it implies a careful study of the context in which the organism developed. In giant clams, the stable carbon isotope ($\delta^{13}\text{C}$) fractionation due to vital effect seems limited and it is believed that the shell $\delta^{13}\text{C}$ composition reflects mostly the seawater dissolved inorganic carbon (DIC) composition (McConnaughey and Gillikin 2008). Considering that fluvial DIC is often isotopically lighter than oceanic DIC, shell $\delta^{13}\text{C}$ sensitivity to DIC could be used as an indirect proxy for SSS, and thus precipitations (e.g., Gillikin et al. 2006; Mook and Vogel 1968). However, the modern bulk $\delta^{13}\text{C}$ records of giant clams collected in a fringing reef environment show no significant difference with those of specimens collected on a barrier reef. All the modern giant clams from New Caledonia have a $\delta^{13}\text{C}$ composition depleted by - 0.5 to - 1.5‰ vpdb compared to the fossil giant clams (Figure IV-6). This shift may be related to the anthropogenic ^{12}C input in the atmosphere and in the ocean resulting from the fossil fuel massive burning that occurred for the last 150 years (Suess effect). The order of magnitude of the ^{13}C -depletion observed between modern and fossil giant clam records is similar to the $\delta^{13}\text{C}$ shift attributed to the Suess effect observed in marine bivalves shell or sclerosponges (e.g., Böhm et al. 1996; Butler et al. 2010; Swart et al. 2010). This supports that the ^{13}C -depletion recorded by the modern giant clams reflects most likely the Suess effect. Consequently, the modern $\delta^{13}\text{C}$ records cannot be considered as a reliable baseline against which to compare fossil $\delta^{13}\text{C}$ records in terms of SSS. However, fossil $\delta^{13}\text{C}$ records that are not affected by this phenomenon are still comparable.

c. La Niña-like mean state ca. 3,600-3,400 years BP

The *Porites sp.* colony and the giant specimen HhES from Vanuatu witnessed the climatic conditions ca. 3,600-3,400 years BP. Specimen HhES, included in group *fossil 3*, present a very low $\delta^{18}\text{O}$ value compared to the giant clam specimens from New Caledonia (NC), indicating that Vanuatu has experienced warmer and fresher conditions than NC at that time (Figure IV-6). Fresher conditions are also supported by the lower shell $\delta^{13}\text{C}$ values of group *fossil 3* compared to the specimens of group *fossil 1* (group *modern* is omitted due to anthropogenic ^{12}C contamination). This suggests that giant clam HhES was exposed to a higher fluvial or estuarine DIC concentration than the giant clams from NC, reflecting most probably a higher precipitation regime in Vanuatu than in NC ca. 3,600-3,400 years BP. Warmer and fresher conditions in Vanuatu than in NC ca. 3,600-3,400 years BP is consistent with the differences observed today between these two locations ($\sim 3.6^\circ\text{C}$ and ~ 0.5 SSS). This supports that the modern SST and SSS latitudinal gradients between Vanuatu and NC were already in place 3,000 years ago.

The fossil *Porites sp.* colony presents a lower Sr/Ca ratio than the modern colony suggesting that Vanuatu has experienced warmer conditions than today at that time (Figure IV-5). The equivalent SST anomaly using Corrège (2006)' equation is $+3 \pm 1^\circ\text{C}$ compared to Vanuatu current conditions. Such SST anomalies were already reported in Papua New-Guinea corals during the Holocene (Abram et al. 2009). These authors hypothesized that warm anomalies at the edges of the WPWP were related to a phase of expansion of the WPWP. The warm anomaly, recorded in Vanuatu, could have been thus related to a southward migration of the WPWP southern edge and of the SPCZ, as suggested by the warm and wet conditions

recorded ca. 3,600-3,400 years BP by the giant clam HhES. Such configuration of the WPWP, in the SW Pacific, strongly suggests that La Niña-like conditions were most likely operating in the SW Pacific ca. 3,600-3,400 years BP, in agreement with other paleoclimatic studies in the Pacific area, which reported that a La Niña-like mean-state prevailed during the Holocene until ca. 4,000 years BP (Haug et al. 2001; Koutavas et al. 2006b; Moy et al. 2002; Rodbell et al. 1999; Sandweiss et al. 2001).

d. Strong ENSO amplitude ca. 3,200-2,700 years BP

Five giant clams collected in New Caledonia – NC – (*fossil 1* and *fossil 2*) and giant clam specimen TgES, from Vanuatu, provide records of the period 3,200-2,700 years BP. Group *fossil 1* falls within the mean $\delta^{18}\text{O}$ composition of the modern specimens (*modern*), it was assumed thus, that those giant clams grew under SST and SSS conditions similar to the modern ones (Figure IV-6). The $\delta^{18}\text{O}$ composition of the other group (*fossil 2*) is closer to the $\delta^{18}\text{O}$ composition of the Vanuatu giant clam (*fossil 3*). This indicates that these specimens grew in a warmer and fresher environment than observed today in NC, close to the warm conditions found in Vanuatu ca. 3,200-2,700 years BP. These results are supported by the $\delta^{13}\text{C}$ records: group *fossil 1* presented high shell $\delta^{13}\text{C}$ values compared to those of group *fossil 2* suggesting that the former experienced higher estuarine/fluvial DIN input, reflecting most likely a strong precipitation input ca. 3,200-2,700 years BP. The contrasted bulk isotopic signatures suggest that, in NC, the SST/SSS conditions changed within a 4 to 11 years period, from near modern NC conditions to fresher and warmer conditions, with temperature being similar or slightly warmer than experienced today in Vanuatu.

This observation implies that important latitudinal migrations of the southern edge of the WPWP and of the SPCZ occurred at the inter-annual timescale ca. 3,200-2,700 years BP. In the SW Pacific, the inter-annual variability in size or location of these climatic features is strongly linked to ENSO (Gouriou and Delcroix 2002). The fossil giant clam's isotopic records are thus reflecting the ENSO activity ca. 3,200-2,700 years BP. The ENSO variability recorded by the archaeological giant clams is 50% higher than the ENSO variability recorded by the modern giant clams for the 2000's decade (Figure IV-7). In addition, the records available seem to suggest that the ENSO variability ca. 3,000 years BP was skewed toward the La Niña-phase (Figure IV-7). An increase in ENSO amplitude and frequency is observed in many places around the Pacific ca. 3,000 years BP (Haug et al. 2001; Koutavas et al. 2006b; Moy et al. 2002; Rodbell et al. 1999; Sandweiss et al. 2001), however, this is the first time that such an increase in ENSO amplitude is evidenced in the Southwest Pacific. Interestingly, the giant clam specimen from New Caledonia dated at 2,500-2,300 years BP recorded warm and fresh conditions and fluvial/estuarine influence, suggesting that strong La Niña conditions were still operating during the post-Lapita era (TmKoum, *fossil 2* – Figure IV-6).

e. Relation between climate and Lapita migration

Coral and giant clam records from Vanuatu evidenced that a La Niña-like mean-state was operating in the Southwest Pacific ca. 3,600-3,400 years BP. Other paleoclimatic reconstructions showed that stable conditions were prevailing in the Pacific during the

Holocene, until ca. 4,000 years BP (Haug et al. 2001; Koutavas et al. 2006b; Moy et al. 2002; Rodbell et al. 1999; Sandweiss et al. 2001). The ca. 3,600-3,400 years BP period encompasses the emergence of the Lapita culture on the Bismark Archipelago ca. 3,470-3,250 years BP; (Denham et al. 2012). The stable climatic conditions prevailing in the Pacific suggests that conditions were favorable for human population development in Near Oceania until ca. 3,600-3,400 years BP. This may explain why the Lapita migration did not occur earlier whereas archaeological evidences suggested that Lapita people already matched the requirements for long-term maritime voyaging, i.e., navigation skills and upwind sailing canoes (Gosden and Pavlides 1994; Irwin 2008; Di Piazza et al. 2007; Summerhayes 2007).

Lapita settlement in Vanuatu ca. 3,250-3,100 years BP and in Fiji ca. 3,130-3,010 years BP (Denham et al. 2012), coincided with a period of strengthened ENSO amplitude evidenced from the archaeological giant clams records of New Caledonia and Vanuatu. This observation is in agreement with other studies from the West Pacific reporting a increase in the ENSO amplitude (Tudhope et al. 2001) and in the ENSO frequency (Haberle et al. 2001). Continental records from Vanuatu and New Caledonia indicates prevailing drier ca. 3,250-2,500 years BP, suggesting that the SW Pacific area experienced severe droughts, most likely related to strong El Niño events at that time (Wirrmann et al. 2011a; Wirrmann et al. 2011b; Wirrmann et al. 2006). This last observation seems contradictory with the archaeological giant clam's records that tends to indicate a shift of the ENSO variability toward La Niña-phase. This point should be investigated further by increasing the number of giant clams records to elucidate whether this observation reflects a real climatic trend toward the La Niña-phase or if this trend is due to the relatively limited fossil giant clam specimens available.

This study and the previous paleoclimatic reconstruction indicate that an abrupt increase in the ENSO amplitude occurred synchronously to the Lapita migration, supporting the hypothesis that climate had played a significant role in the triggering of the Lapita migration. Indeed, unstable climate may have favored the development and the expansion of nomad foraging populations relying on marine resources.



Deux Tridacna maxima en milieu naturel, Fausse Passe de Uitoé, Nouvelle-Calédonie, Pacifique Sud-Ouest. Septembre 2010. Crédit photo: N. Duprey.



Chapitre V – Synthèse

I. Objectifs

L'objectif principal de ce travail de thèse a été de documenter la variabilité climatique du Pacifique Sud-Ouest à deux périodes clés de l'Holocène : 7.0-6.0 et 3.5-2.5 ka BP. Pour cela, j'ai d'abord étudié le potentiel du bénitier *Tridacna maxima* comme archive paléoclimatique. Une fois cette étape réalisée, il a été possible d'utiliser des spécimens fossiles de *T. maxima*, en complément d'autres espèces (*T. gigas*, *Hippopus hippopus*) et de coraux massifs *Porites sp.*, à des fins paléoclimatiques. La prise de conscience, il y a quelques décennies, de l'influence des activités anthropiques sur le système climatique global s'est accompagnée d'un essor sans précédent de l'étude du climat. La compréhension et la prédiction du climat sont les objectifs principaux de la climatologie qui s'appuie d'une part sur l'étude du climat du passé, la paléoclimatologie et d'autre part sur la modélisation numérique.

La paléoclimatologie repose sur l'analyse d'archives climatiques diverses (par ex., carottes de sédiments, de glaces, de coraux) qui fournissent des enregistrements de nature variée (par ex., humidité, précipitation, température de l'eau, de l'air) à des échelles temporelles (du siècle dernier au Paléozoïque) et des résolutions temporelles diverses (millénaire à saisonnière). Décoder les informations enregistrées par ces diverses archives requiert une étude préalable, dite de calibration, qui a pour but de lier, de façon empirique une variable mesurée dans l'archive (par ex., composant géochimique, pollinique, écailles de poissons), à un paramètre de l'environnement (par ex., humidité, précipitation, température de l'eau, de l'air), on parle alors de proxy.

Dans le Pacifique tropical, les paramètres océanographiques clefs permettant de comprendre le climat sont la température (SST²²) et la salinité (SSS²³) de surface de la mer (par ex., Gouriou and Delcroix 2002; Picaut et al. 1996). La compréhension de la variabilité climatique dans cette région nécessite d'atteindre une échelle temporelle assez fine, idéalement interannuelle à saisonnière. Accéder à cette résolution temporelle est essentielle car c'est à cette échelle que s'exerce le mode de variabilité le plus fort du système climatique, El Niño Southern Oscillation (ENSO), qui influe fortement la zone Pacifique (Philander 1990; Trenberth 1976). Malheureusement, les données instrumentales de SST et de SSS remontent très rarement avant 1950. En revanche, la paléoclimatologie permet de pallier ce manque grâce à des enregistrements indirects de SST et de SSS, obtenus à partir d'archives telles que les coraux et les bénitiers. Si les études de calibration sont abondantes pour les coraux, en particulier sur le genre *Porites sp.* (par ex., Corrège et al. 2000), elles le sont moins pour les bénitiers. C'est notamment le cas de l'espèce *Tridacna maxima*, pour laquelle il n'existe aucune étude de calibration à l'heure actuelle bien qu'elle possède actuellement la plus grande aire de répartition et que de nombreux fossiles de cette espèce soient présents sur les anciennes terrasses coralliennes et sur les sites archéologiques du Pacifique (Aharon 1980; Moir 1989; bin Othman et al. 2010). C'est pourquoi un des premiers objectifs de mon travail de thèse a été d'étudier le potentiel de *T. maxima* en tant qu'archive paléoclimatique.

²² Sea Surface Temperature

²³ Sea Surface Salinity

Cet objectif a été réalisé en deux étapes. Dans un premier temps, trois spécimens vivants de *T. maxima* ont été placés durant 1 an et 8 mois dans un aquarium dont la température (SST) et la composition isotopique de l'eau ($\delta^{18}\text{O}_{\text{sw}}$) ont été mesurées respectivement à une fréquence horaire et hebdomadaire. Après avoir été analysés, les profils sclérochronologiques²⁴ ainsi que la composition en isotopes stables de l'oxygène de ces bénitiers ($\delta^{18}\text{O}_{\text{arag.}}$) ont été mis en relation avec la SST pour calibrer ces proxies.

Une fois les profils sclérochronologiques et la composition isotopique calibrés, il est devenu possible d'accéder aux enregistrements de SST contenus dans les valves des bénitiers *Tridacna maxima*. Ces enregistrements peuvent être complétés par des enregistrements similaires obtenus à partir de valves de *T. gigas* ou d'*Hippopus hippopus* ou encore de coraux massifs du genre *Porites sp.* Ces enregistrements, de résolution interannuelle à saisonnière, sont particulièrement précieux pour mieux comprendre la variabilité climatique dans le Pacifique Sud-ouest. La variabilité climatique de deux périodes de l'Holocène mérite une attention particulière, l'une vers 7.0-6.0 ka BP, l'autre vers 3.5-2.5 ka BP.

La transition de l'Holocène inférieur vers l'Holocène moyen (~ 7.0-6.0 ka BP) s'accompagne en effet de l'émergence de la variabilité ENSO actuelle. L'amplitude de la variabilité ENSO durant l'Holocène inférieur est modérée puis elle augmente graduellement au cours de la deuxième partie de l'Holocène. La fréquence et l'amplitude de la variabilité ENSO augmente brusquement il y a 3000 ans (~ 3.5-2.5 ka BP) pour atteindre une fréquence et une amplitude qui n'ont pas d'équivalent au cours de la première partie de l'Holocène (Haug et al. 2001; Koutavas et al. 2006b; Moy et al. 2002; Rodbell et al. 1999; Sandweiss et al. 2001). Documenter l'état moyen du système climatique du Pacifique Sud-Ouest lors de ces deux périodes particulières est primordial pour comprendre les changements survenus dans l'activité ENSO en absence de tout forçage anthropique. Dans le Pacifique Sud-Ouest, l'état-moyen climatique est caractérisé par les variations de la marge sud-est de la West Pacific Warm Pool (WPWP²⁵) et de la zone de convergence du Pacifique Sud (SPCZ²⁶) qui gouvernent respectivement les variations interannuelles et saisonnières de la SST et de la SSS – c'est-à-dire la balance évaporation / précipitation – (Gouriou and Delcroix 2002). La SST et la SSS sont donc des paramètres-clés pour étudier les fluctuations de la taille et de la localisation de la WPWP et de la SPCZ.

II. Potentiel du bénitier *Tridacna maxima* comme archive paléoclimatique

L'étude de la composition isotopique de la coquille de *Tridacna maxima* s'est également révélée prometteuse. Cette étude, portant sur un spécimen actuel collecté en Nouvelle-Calédonie, a permis de mettre en évidence que la coquille aragonitique de *Tridacna maxima* est précipitée en équilibre isotopique avec l'eau de mer (chapitre II). Les variations

²⁴ Sclérochronologie: du grec "sklero", dur et "chronos", le temps. C'est l'étude des parties dures des êtres vivants, ici à des fins paléoclimatiques.

²⁵ West Pacific Warm Pool

²⁶ South Pacific Convergence Zone

saisonniers de $\delta^{18}\text{O}_{\text{arag}}$ sont donc le résultat des variations saisonnières de la SST et du $\delta^{18}\text{O}_{\text{sw}}$. Le $\delta^{18}\text{O}_{\text{sw}}$ étant gouverné par la balance évaporation/précipitation, c'est donc un proxy de la SSS. Le $\delta^{18}\text{O}_{\text{arag}}$ reflète donc à la fois la SST et la SSS. Une fonction de transfert empirique reliant le paramètre ($\delta^{18}\text{O}_{\text{arag}} - \delta^{18}\text{O}_{\text{sw}}$) à la SST a pu être établie, validant l'utilisation de *T. maxima* comme archive climatique (chapitre II).

L'étude sclérochronologique de trois bénitiers modernes de Nouvelle-Calédonie a permis de montrer (i) que les stries d'accroissement du bénitier *Tridacna maxima* étaient déposées à une fréquence journalière et (ii) que l'épaisseur des stries journalières était positivement corrélée à la SST (chapitre II). Les stries d'accroissement enregistrent donc les variations saisonnières de SST. J'ai ensuite établi une fonction linéaire empirique reliant l'épaisseur des stries à la SST permettant une estimation des extremums saisonniers et de l'amplitude saisonnière. Cependant, l'épaisseur des stries d'accroissement n'est pas seulement fonction de la température de l'eau. Elle résulte également d'un ensemble de facteurs physico-chimiques (nutriments, salinité, turbidité, marées) et physiologiques (reproduction, maladie, ontogénie) (par ex., Aubert et al. 2009; Pannella 1976; Pannella and MacClintock 1968; Poulain et al. 2011; Rhoads and Pannella 1970; Schöne 2008; Schwartzmann et al. 2011). Ces facteurs peuvent altérer la relation reliant la SST à l'épaisseur des stries de croissance et donc réduire la fiabilité des stries d'accroissement de *T. maxima* comme proxy de la SST. En effet, notre étude a mis en évidence des arrêts de croissance ainsi que des périodes durant lesquelles la relation linéaire entre SST et épaisseur des stries d'accroissement était altérée, vraisemblablement en réponse à des facteurs non-climatiques (chapitre II). L'interprétation de l'épaisseur des stries d'accroissement de *Tridacna maxima* en termes de paléo-SST nécessite un examen approfondi des profils sclérochronologiques afin de détecter des anomalies ou des arrêts de croissance. L'utilisation de profils obtenus sur différents individus ayant enregistré la même période de temps permet de s'affranchir des anomalies de croissance individuelles et fait ressortir les variations climatiques saisonnières, permettant ainsi de compléter et de recouper les informations obtenues à partir de l'analyse géochimique de la coquille de *T. maxima* (chapitre II).

La composition en isotopes stables de l'oxygène ($\delta^{18}\text{O}_{\text{arag}}$) de *T. maxima* est un proxy fiable de la salinité et de la température des eaux de surface. L'étude des stries d'accroissement de *T. maxima* fournit un proxy complémentaire de la température, notamment dans le cas de fossiles affectés par des altérations diagénétiques.

III. Variabilité climatique durant la transition Holocène inférieur – Holocène moyen : comparaison données / modèles

Température de surface de l'eau de mer – En analysant deux coraux massifs fossiles du genre *Porites sp.* et un bénitier fossile collectés au Vanuatu, j'ai pu obtenir des enregistrements de SST et de SSS pour la période 7.0-6.0 ka BP. Les températures de surface reconstruites à partir des coraux sont similaires aux températures actuelles (Figure V-1a). La marge sud-est de la WPWP, définie par l'isotherme 28°C, atteignait donc le Vanuatu (15°S) à cette période.

Ceci indique que la phase de réchauffement post-glaciaire était terminée lors de la transition Holocène inférieur - Holocène moyen et que la WPWP était dans une configuration similaire à celle observée actuellement. Ces résultats sont cohérents avec les simulations obtenues à partir des modèles couplés océan-atmosphère-végétation du programme Paleoclimate Modelling Intercomparison Project phase II – PMIP II (Figure V-3). En effet, dans la région Pacifique Sud-Ouest les températures de surface moyenne simulées à 6000 ans BP ne présentent pas de différence avec les températures actuelles. Les modèles utilisés dans le cadre du programme PMIP-II reproduisent bien les valeurs moyennes de SST dans le Pacifique Sud-Ouest.

Les variations saisonnières de SST sont un paramètre-clés pour comprendre les forçages climatiques opérant à l'échelle saisonnière ainsi que pour évaluer les modèles numériques. Les coraux fossiles ont enregistré une amplitude saisonnière de la SST similaire à celle enregistrée par les coraux actuels (Figure V-2). Ceci implique que les variations latitudinales saisonnières de la marge sud-est de la WPWP avaient la même amplitude qu'actuellement. Cependant, le contraste saisonnier de l'insolation était plus faible durant la transition Holocène inférieur-Holocène moyen qu'il ne l'est actuellement (Berger and Loutre 1991). L'insolation est le forçage majeur dans les modèles numériques. Par exemple, les modèles du projet PMIP II suivent les variations d'insolation et reproduisent une variation amplitude saisonnière de SST réduite dans le Pacifique Sud-Ouest (Braconnot et al. 2000; Liu et al. 2000). Les modèles ne reproduisent pas les variations saisonnières de SST observées dans les enregistrements coralliens. Ceci souligne probablement les difficultés des modèles à reproduire les variations saisonnières de SST dans cette zone. D'avantage de données paléoclimatiques sont nécessaire afin de mieux caractériser et de mieux comprendre les variations saisonnières de SST dans le Pacifique Sud-Ouest.

Balance évaporation / précipitation – L'étude des enregistrements coralliens datant de la transition Holocène inférieur – Holocène moyen a permis de mettre en évidence, d'une part, des conditions plus salées dans le Pacifique Sud-Ouest indiquant un déficit de précipitations (Figure V-1b) et d'autre part un cycle hydrologique saisonnier inversé montrant une influence réduite de la SPCZ durant l'été austral (Figure V-2). Dans le Pacifique Sud-Ouest le régime des précipitations était donc découplé de la SPCZ. Ceci implique que la position moyenne de la SPCZ était au nord de sa position actuelle, en accord avec d'autres études montrant que la zone de convergence intertropicale (ITCZ) était située au nord de sa position actuelle durant l'Holocène inférieur, en réponse à une insolation supérieure de l'hémisphère nord liée à la configuration orbitale (Figures V-1c et V-1d). Cette information suggère que l'ITCZ et la SPCZ ont un comportement analogue en réponse au forçage orbital. Le déplacement de l'ensemble des structures convectives du Pacifique au cours de l'Holocène inférieur aurait maintenu l'essentiel des précipitations dans l'hémisphère nord, causant ainsi l'augmentation de salinité observée dans le Pacifique Sud-Ouest dans la première moitié de l'Holocène. D'autre part une intensification du transport de chaleur vers la zone extra-tropicale due à un renforcement de la circulation de Hadley a pu augmenter significativement l'évaporation dans la zone tropicale, contribuant à l'augmentation de la salinité observé dans les enregistrements fossiles (Gagan et al. 1998).

Figure V-1 (page suivante). *Mise en perspective des enregistrements de SST et de SSS obtenus au cours de ma thèse dans le contexte climatique Holocène. La transition Holocène inférieur – Holocène moyen et la période correspondant à la migration Lapita sont figurées en grisé.*

a - SST enregistrée par les coraux étudiés dans ma thèse. Les données sont normalisées par rapport à la moyenne du corail moderne (chapitres III et IV). La courbe en gris foncé est un lissage Gaussien de 25 mois.

b - Reconstruction de la composition en isotopes stables de l'oxygène de l'eau de mer ($\delta^{18}O_{sw}$). $\delta^{18}O_{sw}$ reconstruit à partir de carottes de sédiments collectées dans la WPWP en bleu. L'enveloppe représente l'intervalle correspondant à un écart-type des données issues de Stott et al. (2004) et de Lea et al. (2000). Losanges blancs : $\delta^{18}O_{sw}$ reconstruit à partir des coraux fossiles du Vanuatu étudiés dans ma thèse (les barres d'erreur représentent un écart-type - chapitre III).

c - Teneur en Titane (%) de la carotte sédimentaire ODP 1002 prélevée dans le bassin de Cariaco – moyenne glissante de 3 points – (Haug et al. 2001). La teneur en titane reflète les apports terrigènes issus du ruissellement des eaux de pluies. Une teneur élevée est interprétée comme indiquant un régime de précipitations fort et une position moyenne de l'ITCZ vers le nord.

d - Insolation reçue par la Terre aux mois de janvier et de juillet, aux latitudes 15N, 15S, 65N et 65S (Berger and Loutre 1991). Cette figure illustre les changements d'insolation entre les deux hémisphères et les changements dans l'amplitude du contraste saisonnier au sein de chaque hémisphère.

e - Composition en isotopes stables de l'oxygène ($\delta^{18}O$) de la stalagmite D4 collectée dans la grotte Dongge (Chine) (Yuan et al. 2004). Le $\delta^{18}O$ reflète les précipitations issues de la mousson asiatique (Asian Monsoon A.M.), un appauvrissement en $\delta^{18}O$ est interprété comme indiquant des précipitations abondantes et une mousson forte, caractérisée par une position moyenne de l'ITCZ vers le nord.

f - Evolution du gradient zonal de SST dans le Pacifique. La SST est reconstruite à partir du rapport Magnésium/Calcium de foraminifères. Courbe rouge : SST dans la WPWP (carottes sédimentaires MD70, MD 71 et MD 81 (Stott et al. 2004) et ODP 806B (Lea et al., 2000). La courbe représente l'intervalle correspondant à un écart-type. Courbe bleue : SST dans la cold tongue, Pacifique Est (carottes sédimentaires V21-30 et V19-28 (Koutavas et al. 2006a). Les flèches verticales bleues illustrent le gradient zonal de SST dans le Pacifique aux deux périodes étudiées.

g - Densité de charbons issus de carottes sédimentaires lacustres collectées en Papouasie Nouvelle-Guinée et en Indonésie (Haberle et al. 2001). Les charbons reflètent la fréquence de feu de forêts. Les auteurs associent la fréquence des feux de forêts à la fréquence des événements ENSO.

→ The english version of this caption is on page 118.

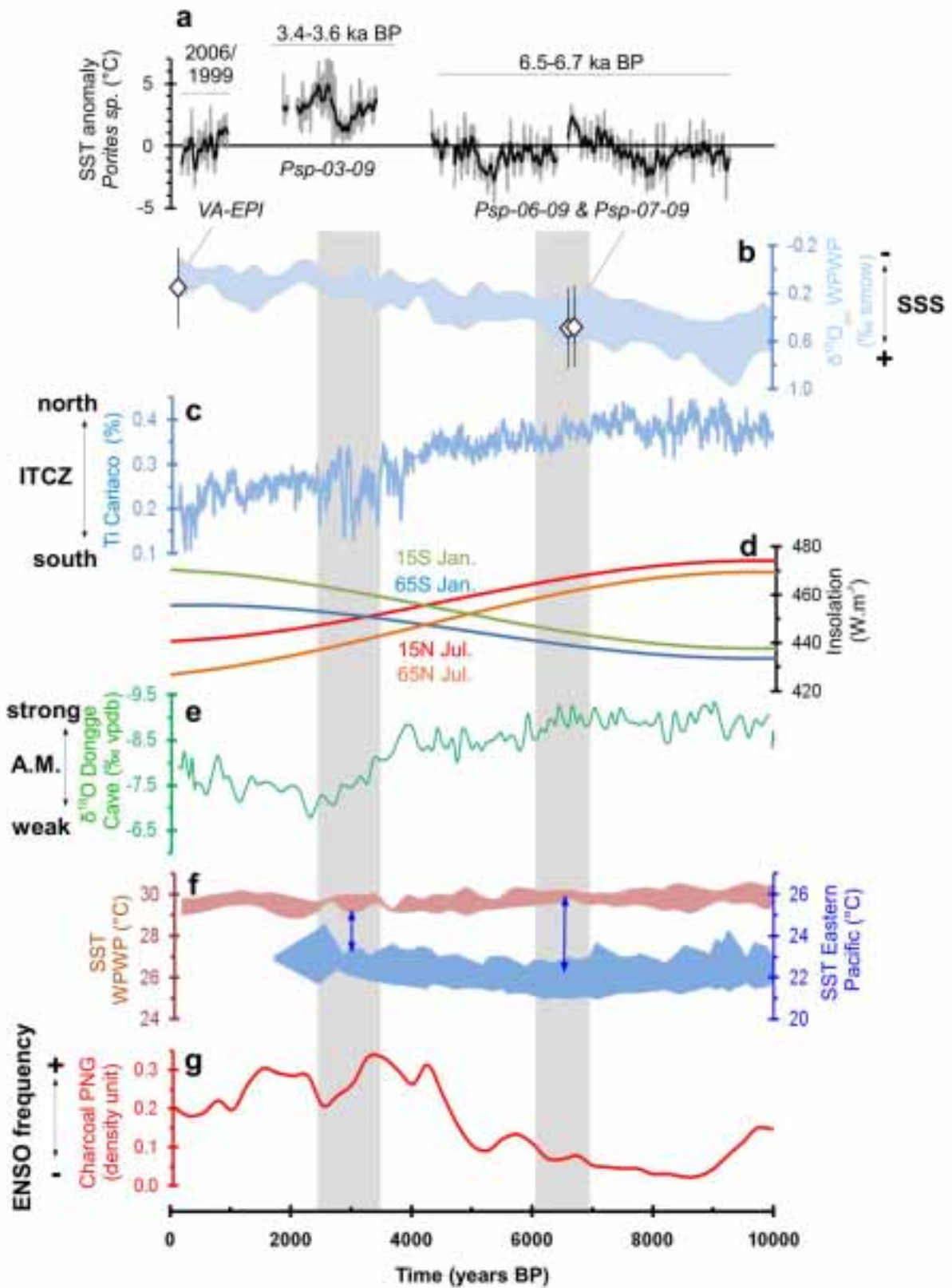


Figure V-1. SST and SSS records obtained in this work included in the Holocene climatic context. The two periods studied are highlighted by the dashed areas.

a - SST anomalies calculated from the strontium calcium ratio of the fossil coral colonies studied during my thesis (data were normalized with the mean of the modern coral - chapters III and IV). Dark grey curve is the 25-months Gaussian filtered data.

b - Reconstruction of the oxygen stable isotopes composition of seawater ($\delta^{18}O_{sw}$). Blue area : $\delta^{18}O_{sw}$ data from the WPWP area, the area represents one standard deviation calculated from the data of Stott et al. (2004) and Lea et al. (2000). Empty diamonds: $\delta^{18}O_{sw}$ data from the Southwest Pacific area, error bars represent one standard deviation (chapter III).

c - Titanium content (%) of the sediment core ODP 1002 collected in the Cariaco basin (3-points running mean) (Haug et al., 2001). Higher Ti content reflects greater terrigenous input from riverine runoff and is interpreted to indicate greater precipitation and a more northerly mean latitude of the ITCZ.

d - Earth insolation during January and July at latitudes 15N, 15S, 65N and 65S (Berger, 1978). This figure shows the inter-hemispheric insolation contrast evolution and the seasonal insolation contrast evolution for each hemisphere.

e - Oxygen stable isotopes composition ($\delta^{18}O$) of stalagmite D4 collected in Dongge Cave, China (Yuan et al., 2004). $\delta^{18}O$ reflect the asian monsoon (A.M.) precipitation regime, ^{18}O -depletion is interpreted as reflecting abundant precipitation and strong monsoon, characterised by a northerly located ITCZ.

f - Pacific zonal SST gradient evolution. SST data are reconstructed from foraminifers' magnesium calcium ratio. Red curve : WPWP SST from sediment cores MD70, MD71 et MD 81 (Stott et al., 2004) and ODP 806B (Lea et al. 2000). Curves represent the one standard deviation interval. Blue curve : cold tongue SST (Eastern Pacific) from sediment cores V21-30 and V19-28 (Koutavas et al. 2006). Vertical blue arrows indicate the zonal gradient across the Pacific Ocean for the two periods studied.

g - Charcoal density from lacustrine sediment records collected in Papua New Guinea and in Indonesia (Haberle et al. 2001). Charcoal density reflects the fire frequency. Authors related the fire frequency to the ENSO events frequency.

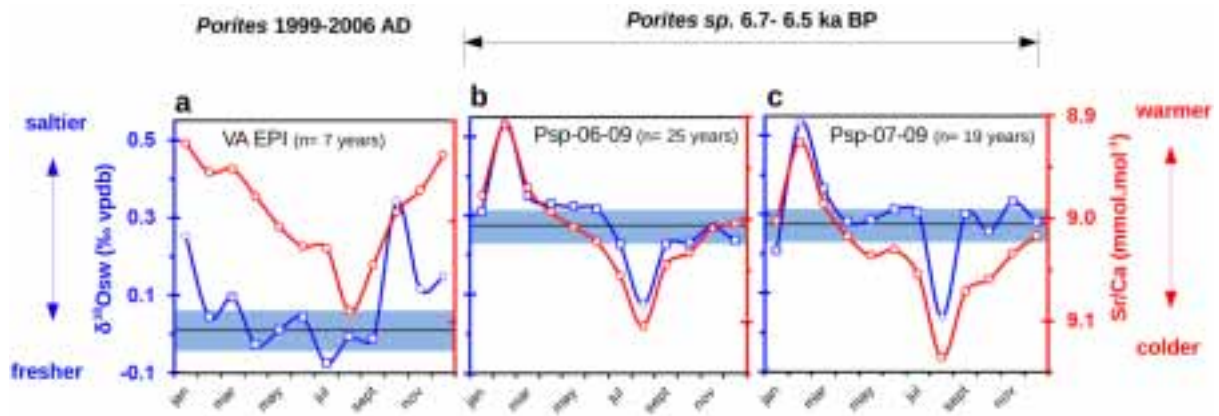


Figure V-2. Variations saisonnière du Sr/Ca (rouge) et du $\delta^{18}O_{sw}$ (bleu) dans les coraux collectés au Vanuatu. Les valeurs moyennes de $\delta^{18}O_{sw}$ (ligne noire) et l'intervalle correspondant à plus ou moins un écart-type (bleu) ont été calculés à partir des points représentés par des carrés (i.e., les extrêmes saisonniers n'ont pas été inclus). **a** – enregistrement d'un corail actuel **b** et **c** – enregistrements obtenus à partir des coraux datés à 6.7-6.5 années BP.

Figure V-2. Seasonal variations of Sr/Ca (red) and $\delta^{18}O_{sw}$ (blue) from corals collected in Vanuatu. The average $\delta^{18}O_{sw}$ (black line and 1 standard deviation interval in blue) was calculated by averaging the data points represented by the squares (i.e., extremes not included), **a** – modern coral record, and **b** & **c** – 6.7– 6.5 yrs BP fossil coral colonies.

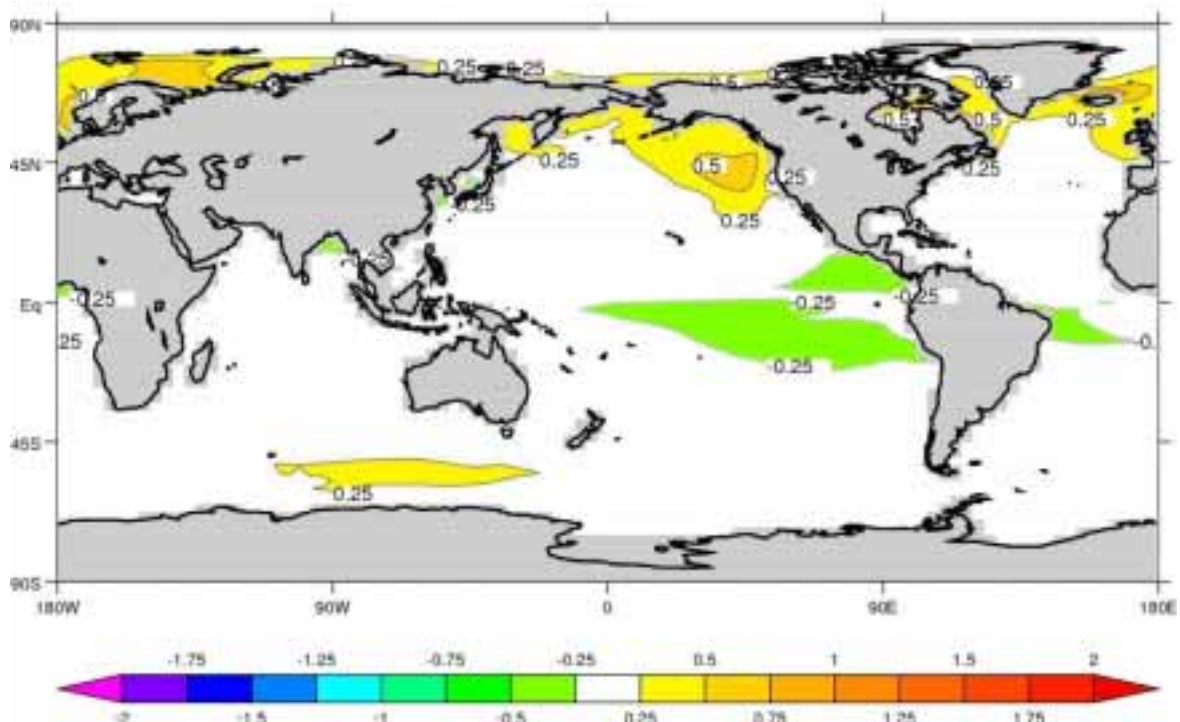


Figure V-3. Carte de synthèse du programme PMIP2/MOTIF : différence entre la SST moyenne annuelle simulée par six modèles de type océan-atmosphère-végétation et la SST instrumentale actuelle. Unité Kelvin. source : <http://pmip2.lsce.ipsl.fr/database/map>.

Figure V-3. Synthesis map of PMIP2/MOTIF programme: difference between annual mean SST simulated by six ocean-atmosphere-vegetation models and instrumental SST. Units : Kelvin. source : <http://pmip2.lsce.ipsl.fr/database/map>.

Les simulations du programme PMIP-II montrent des changements importants dans le régime des précipitations dans la zone Pacifique Sud-Ouest (Figure V-4). Les modèles montrent un déficit de précipitation au nord de l'emplacement actuel de la SPCZ à 6000 ans BP et un excès de précipitation au niveau de l'axe Papouasie Nouvelle Guinée- Salomon-Vanuatu-Fidji. Ceci suggère que les modèles place la SPCZ au sud de sa position actuelle à 6000 ans BP. Ces résultats sont en contradiction avec les enregistrements obtenus dans le cadre de ma thèse qui indiquent, au contraire, un déficit de précipitation sur le Vanuatu en réponse à un déplacement de la SPCZ au nord de sa position actuelle (Chapitre III). Ces résultats contradictoires indiquent soit une interprétation erronée des enregistrements paléoclimatiques, soit un biais dans la modélisation de la dynamique de la SPCZ. A l'heure actuelle les données paléoclimatiques concernant la variabilité de la SPCZ au cours de l'Holocène sont insuffisantes pour pouvoir trancher entre ces deux hypothèses.

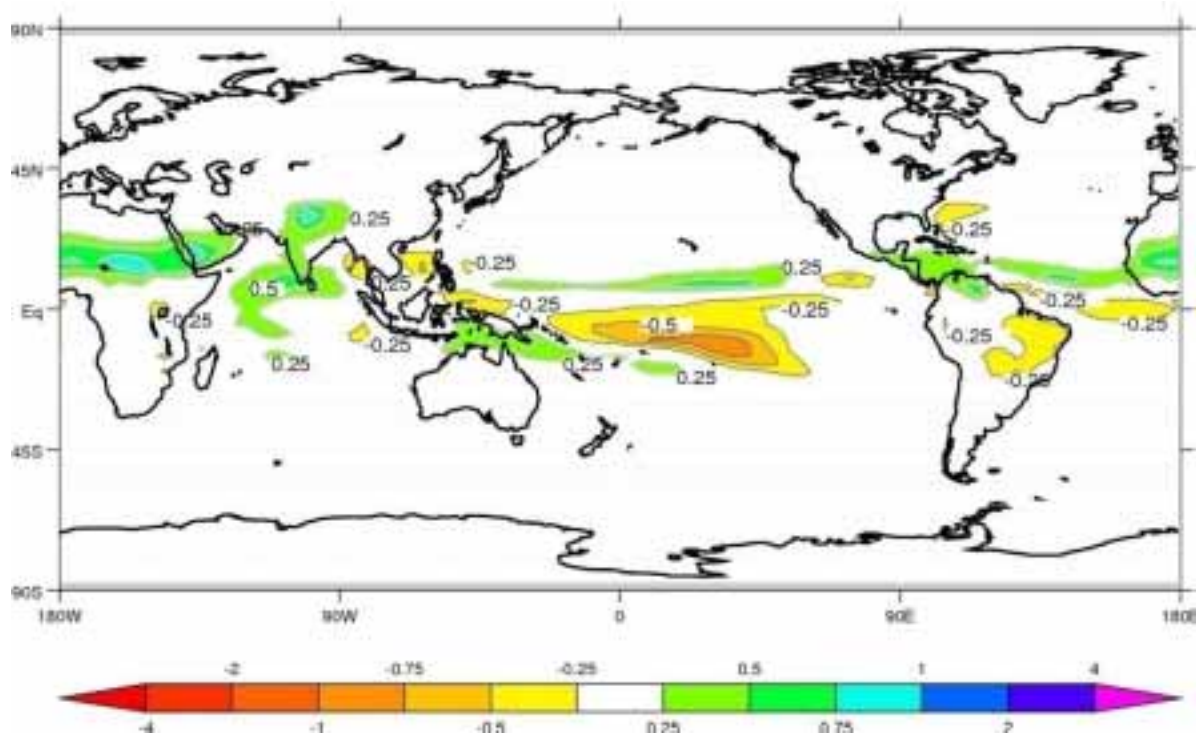


Figure V-4. Carte de synthèse du programme PMIP2/MOTIF : différence entre les précipitations moyennes annuelles simulées par six modèles de type océan-atmosphère-végétation et les précipitations instrumentales actuelles. Unité mm.jour^{-1} . Source : <http://pmip2.lsce.ipsl.fr/database/map>.

Figure V-4. Synthesis map of PMIP2/MOTIF programme: difference between annual mean precipitation simulated by six ocean-atmosphere-vegetation models and instrumental precipitation. Units : mm.day^{-1} . Source : <http://pmip2.lsce.ipsl.fr/database/map>.

Variabilité ENSO – L'enregistrement de $\delta^{18}\text{O}$ obtenu à partir d'un corail fossile datant de la transition Holocène inférieur – Holocène moyen montre que l'amplitude d'El Niño Southern Oscillation (ENSO) était réduite de 20-30% comparé à la variabilité ENSO de la période 1928-1992 (Chapitre III). L'ordre de grandeur de la réduction de la variabilité ENSO observé dans notre enregistrement corallien est en accord avec les études paléoclimatiques précédentes

(Figure V-5) ainsi qu'avec les simulations des modèles couplés océan-atmosphère (Zheng et al. 2008).

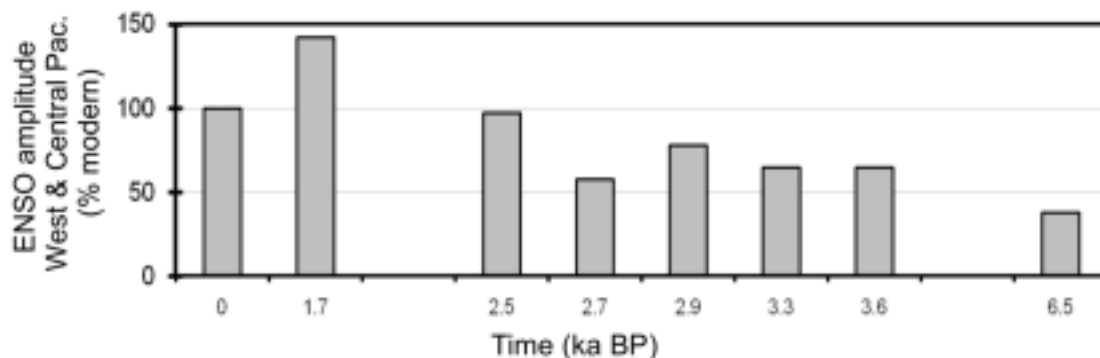


Figure V-5. Amplitude de ENSO enregistrée par des colonies de coraux massifs en Papouasie Nouvelle-Guinée (Tudhope et al. 2001) et dans le Pacifique central (Woodroffe 2003; Woodroffe and Gagan 2000).

Figure V-5. ENSO amplitude recorded by fossil massive corals from Papua New Guinea (Tudhope et al., 2001) and from the Central Pacific (Woodroffe et al., 2003; Woodroffe and Gagan, 2000).

Les mécanismes liés à la diminution de l'activité ENSO soient encore sujet à discussion (par ex., Chiang et al. 2009; Luan et al. 2012; Marzin and Braconnot 2009; Roberts 2007). Cependant, un des mécanismes ayant pu contribuer à la baisse de l'activité ENSO durant transition Holocène inférieur – Holocène moyen pourrait être lié au changement de configuration orbital. En effet, durant l'Holocène inférieur, le forçage orbital augmente le contraste thermique entre les deux hémisphères ainsi qu'entre les continents et les océans. Ceci génère un renforcement des alizés dans l'hémisphère sud et de la mousson asiatique dans l'hémisphère nord (Figure V-1e). La mousson asiatique renforce à son tour le régime des alizés, via la circulation de Walker, durant l'été boréal. L'action de ces deux facteurs a pu contribuer à empêcher le développement d'évènements El Niño durant l'Holocène inférieur (Marzin and Braconnot 2009). Cependant, dans le cas des enregistrements coralliens obtenus dans le Pacifique Sud-Ouest, le découplage entre la SPCZ et le régime des précipitations, mit en évidence précédemment doit également être considéré. En effet, le découplage entre la SPCZ et les précipitations a pu également contribuer à réduire l'amplitude du signal ENSO enregistré dans le corail fossile.

Les comparaisons données - modèles à 6000 ans BP dans le Pacifique Sud-Ouest ont permis de mettre en évidence que i) les modèles ne reproduisent pas les variations saisonnières de SST ii) les modèles et les données ne sont pas cohérent en ce qui concerne la position moyenne de la SPCZ iii) les données confirment l'ordre de grandeur de la baisse de ENSO simulée par les modèles. Ces conclusions mettent en avant i) l'incapacité des modèles à reproduire certains aspects de la variabilité climatique Holocène, ainsi que ii) le manque de données paléoclimatiques concernant les changements de position et d'intensité de la SPCZ ainsi que les variations saisonnières de SST cours de l'Holocène. Ces derniers points sont des axes de recherche prometteurs qui mériteraient d'être approfondis dans les années à venir.

IV. Peuplement de l'Océanie Lointaine ~ 3000 ans BP et variabilité climatique

Les bénitiers collectés sur les sites archéologiques Lapita ainsi que le corail fossile ont permis d'étudier le climat du Pacifique Sud-Ouest à deux périodes clés de la migration Lapita. Au cours de la première période, qui s'étend de 3.6 à 3.4 ka BP, la culture Lapita apparaît dans les îles Bismarck (Denham et al. 2012; Kirch 1997). La deuxième période, de 3.2 à 2.7 ka BP, correspond à la phase de migration de la population Lapita : c'est durant ce laps de temps que les premiers navigateurs colonisent l'Océanie Lointaine jusqu'aux îles Tonga et Samoa, soit un périple de près de 4500 km à travers l'Océan Pacifique (Burley et al. 1999).

L'enregistrement Sr/Ca du corail fossile étudié au cours de ma thèse révèle que la période de 3.6 à 3.4 ka BP est caractérisée par des conditions plus chaudes que actuellement, ce qui suggère une expansion de la marge sud-est de la WPWP dans le Pacifique Sud-Ouest. Cette observation est en accord avec les conditions chaudes et humides enregistrées par les bénitiers fossiles datés de cette époque (chapitre IV). Des conditions anormalement chaudes et humides sont caractéristiques, dans le Pacifique Sud-Ouest, des phases La Niña. Dans le Pacifique Sud-Ouest, les phases La Niña sont associées à un régime de vent d'est – les Alizés – bien établi. Le Pacifique Sud-Ouest a vraisemblablement connu un régime de vent dominé par des Alizés forts avant la migration Lapita. Les reconstructions paléoclimatiques précédemment publiées montrent également que le climat de la zone Pacifique était caractérisé par des conditions de type La Niña et par une variabilité ENSO faible jusqu'aux environs de 4.0-3.0 ka BP (chapitres III et IV; Gagan et al. 2004; Haug et al. 2001; Koutavas et al. 2006a; Moy et al. 2002; Rodbell et al. 1999; Sandweiss et al. 2001).

L'étude des bénitiers provenant des sites archéologiques Lapita a montré que la région Pacifique Sud-Ouest a connu, durant l'intervalle 3.2-2.7 ka BP, une alternance de périodes présentant des conditions similaires à la période actuelle et de périodes plus chaudes, accompagnées d'un excès de précipitations (Figure V-6). Les positions de la marge sud-est de la WPWP et la SPCZ ont donc fluctué entre une position proche de leur emplacement actuel et une position située plus au sud. Cette variabilité interannuelle accrue reflète vraisemblablement l'occurrence de phases de type La Niña prononcées, indiquant une forte amplitude de la variabilité ENSO. Bien que les enregistrements disponibles suggèrent une variabilité dominée par des événements La Niña (conditions plus chaudes et excès de précipitations), il est possible que les occurrences d'événements El Niño (conditions froides et déficit de précipitations) n'aient pas été représentées dans l'effectif de bénitiers fossiles étudiés (n=8). Des études sédimentaires et palynologiques menées au Vanuatu et en Nouvelle-Calédonie ont montré l'existence de conditions plus sèches et plus froides il y a ~ 3000 ans, révélant que le Pacifique Sud-Ouest a également connu des phases El Niño à cette époque (Wirmann et al. 2011a; Wirmann et al. 2011b; Wirmann et al. 2006). A l'inverse des phases La Niña, qui sont caractérisées par un régime de vents d'Est, les phases El Niño sont associées à des vents d'Ouest. Il est donc très probable que le régime des vents ait été très variable au moment de la migration Lapita.

Les données paléoclimatiques disponibles dans la zone Pacifique montrent une augmentation de la fréquence d'ENSO il y a ~ 3000 ans (Figure V-5). Par ailleurs, la diminution de la mousson asiatique (Figure V-1e) associée à la réduction du gradient zonal de SST le long du Pacifique équatorial lors de l'Holocène supérieur auraient réduit l'intensité de circulation de Walker (Figure V-1f). La circulation de Walker réduite aurait permis une augmentation de l'amplitude (Figure V-3c) et de la fréquence d'évènements ENSO, qui atteint des valeurs élevées dans le Pacifique-Ouest ~ 3000 années BP (Figure V-1g et V-5). La coïncidence de ce changement dans la variabilité ENSO, qui n'a pas d'équivalent au cours de l'Holocène, et de la migration Lapita il y a 3000 ans, soulève de nombreuses questions.

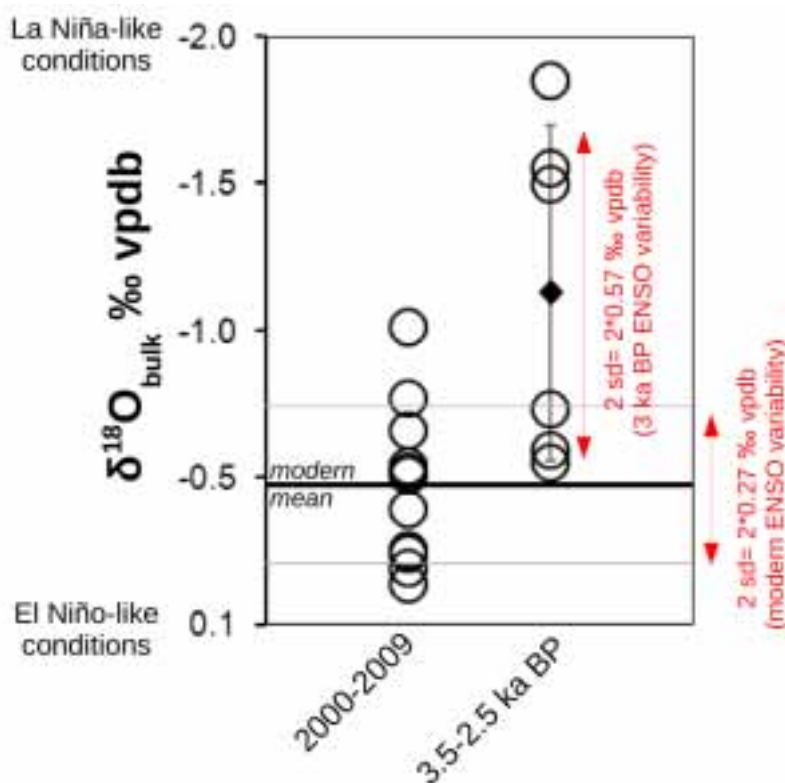


Figure IV-6. Enregistrements de $\delta^{18}O$ “bulk” obtenus à partir de bécitiers *Tridacna maxima* actuels (2000-2009) et fossiles (3500-2500 ans BP). Le losange noir est la moyenne des enregistrements fossiles. Remarque : l’axe des ordonnées est inversé : les conditions chaudes et humides sont donc indiquées par des valeurs faibles de $\delta^{18}O$, et les conditions froides et sèches correspondent aux valeurs élevées de $\delta^{18}O$.

Figure IV-6. Modern (2000-2009) and fossil (3,500-2,500 years BP) giant clam *Tridacna maxima* bulk $\delta^{18}O$ records. The black diamond is the mean fossil $\delta^{18}O$ value. Note that the y-axis is inverted so that warm and wet conditions correspond to low $\delta^{18}O$ values and cool and dry conditions are indicated by high $\delta^{18}O$ values.

V. Quelles hypothèses pour la migration Lapita ?

L'un des aspects intrigant de la migration Lapita vers l'Océanie Lointaine est son déroulement survenant relativement tard au cours de l'Holocène – ca. 3000 ans BP. En effet, des études archéologiques ont montré que les populations présentes depuis 35 000 ans en Papouasie Nouvelle-Guinée, dans les îles Salomon et les îles Bismarck possédaient *a priori* les connaissances nécessaires en matière de navigation à voile ainsi que des pirogues capable de remonter au vent (Gosden and Pavlides 1994; Irwin 2008; Di Piazza et al. 2007; Summerhayes 2007). Ces connaissances auraient été suffisantes pour mener à bien des voyages d'explorations vers l'est du Pacifique avant la migration Lapita. Cependant la prise de risque des explorateurs lors de tels voyages à la voile doit également être considérée. De tels voyages ont vraisemblablement été entrepris dans le but d'assurer la survie de la population et/ou lors que la prise de risque était minimale. Les conditions climatiques stables mises en évidence avant la migration Lapita (Chapitre III & IV) ont sûrement été propice au développement des populations présentes depuis 35 000 ans dans cette zone sans pour autant encourager les voyages d'explorations vers l'est (Groube et al. 1986; Leavesley et al. 2002; O'Connell and Allen 2004). De plus, le régime des alizés qui dominait vraisemblablement à cette époque a pu restreindre l'accessibilité des îles de l'Océanie Lointaine à la voile. En revanche, l'augmentation de la fréquence (Haberle et al. 2001 - Figure V-1g) et de l'amplitude (chapitre IV; Tudhope et al. 2001) de la variabilité ENSO à partir de 4000 ans BP ont pu rendre les populations de l'Océanie Proche plus vulnérables aux aléas climatiques. Un régime climatique instable a pu empêcher le développement et le maintien de l'élevage et de l'agriculture (Gupta 2004; Richerson et al. 2001) et entraîner une augmentation de la fréquence des feux de forêts en zone tropicale (Haberle et al. 2001). En effet, lors d'un événement El Niño, le déplacement de la WPWP vers le centre du Pacifique, consécutif à la baisse du régime des alizés, s'accompagne du déplacement du centre de convection vers l'est, générant d'importantes sécheresses dans la zone Pacifique Ouest (par ex., Haberle et al. 2001; Lyon 2004; Picaut et al. 1996). Des conditions instables auraient donc favorisé un mode de vie nomade, basé, dans le cas des Lapita, sur l'exploitation des ressources marines. Des simulations démographiques de la migration Lapita tendent à appuyer l'hypothèse que les Lapita aient pu être des "gitans de la mer", du moins pendant les premiers temps de la migration (Di Piazza and Pearthree 1999). De plus, les changements de régime de vents associés à une activité ENSO forte, survenant de manière régulière et donc relativement prédictible, ont pu être mis à profit par ces "gitans de la mer" pour accroître leur domaine d'exploration dans un premier temps, puis, dans un second temps, pour assurer des échanges réguliers entre les différentes îles de l'Océanie Lointaine et établir des colonies stables.

La migration Lapita vers l'Océanie Lointaine, ca. 3000 années BP, a coïncidé avec la transition depuis des conditions climatiques stables, dominées par des conditions du type La Niña, vers un régime instable caractérisé par une variabilité ENSO accrue. L'instabilité climatique liée à ENSO a probablement rendu les populations en place plus vulnérables aux aléas climatiques, forçant ainsi les habitants de l'Océanie Proche à privilégier un mode de vie nomade, basé sur les ressources marines. La variabilité du régime des vents associée à l'activité ENSO a également pu faciliter la migration Lapita.

VI. Perspectives

Cette thèse a permis de compléter nos connaissances sur l'évolution de la variabilité climatique dans le Pacifique Sud-Ouest au cours de l'Holocène. En retour, cette thèse a également soulevé plusieurs questions, en particulier en ce qui concerne l'influence de la SPCZ sur le Pacifique Sud-Ouest.

- Quelles ont été les variations latitudinales de la SPCZ aux échelles millénaire, décennale, interannuelle et saisonnière aux différentes périodes de l'Holocène ?
- Comment a évolué l'amplitude saisonnière de la SST durant l'Holocène ?
- A quelle période de l'Holocène la SPCZ a-t-elle atteint sa configuration actuelle ?
- Quelle a été la réponse climatique des différents archipels composant l'Océanie Lointaine (Fidji, Tonga, Samoa) à la modification du régime ENSO ca. 3.0 ka BP ?

Les enregistrements paléoclimatiques de l'Holocène obtenus sur les coraux fossiles lors de ma thèse viennent étoffer la base de données déjà existante pour la région Pacifique. L'ajout de ces nouvelles données complète en particulier la série d'enregistrements coralliens obtenus dans le Pacifique Sud-Ouest (Vanuatu et Nouvelle-Calédonie) au cours de différentes études effectuées en partenariat avec l'Institut de Recherche pour le Développement (IRD). Ces enregistrements, qui s'étendent du Younger-Dryas²⁷ (Corrège et al. 2004) jusqu'à nos jours en passant par l'Holocène inférieur (Beck 1997; Beck et al. 1992; Montaggioni et al. 2006) et l'Holocène supérieur (Corrège et al. 2000) offrent une opportunité unique de répondre aux interrogations précédentes. En effet, ces archives permettraient de documenter la variabilité saisonnière, interannuelle et décennale, des fluctuations de la WPWP et de la SPCZ.

A l'ère de la modélisation climatique, le "patrimoine paléoclimatique" acquis par l'IRD offre une dimension supplémentaire à la paléoclimatologie et mériterait d'être exploré de nouveau. Peu de données sont actuellement disponibles sur les variations de la SPCZ durant l'Holocène et un des défis majeurs pour les années à venir est justement la modélisation de cette structure climatique qui est jusque là peu contrainte malgré son rôle-clé dans le climat du Pacifique Sud-Ouest (par ex., Gouriou and Delcroix 2002). Je me suis aperçu, en effet, que le "patrimoine paléoclimatique" du Pacifique Sud-Ouest n'avait pas été exploité au maximum de son potentiel car, d'une part, les données existantes ne sont pas comparables quantitativement entre elles et, d'autre part, la nature des analyses (isotopes de l'oxygène, éléments traces) diffère d'une étude à l'autre.

La "révision" de ce "patrimoine paléoclimatique" impliquerait dans un premier temps un (ré)examen approfondi de l'intégrité géochimique des fossiles ayant servi à la production de ces enregistrements. Le deuxième handicap de ce patrimoine est l'impossibilité de comparer ces enregistrements de manière quantitative tant pour les enregistrements isotopiques que pour les éléments traces. En effet, l'existence de biais analytiques systématiques d'un laboratoire à l'autre et d'un instrument à l'autre limite fortement la comparaison des enregistrements. L'annexe 1 développe de manière plus approfondie ces difficultés auxquelles

²⁷ Épisode d'intense refroidissement global s'étant produit de 12800 à 11500 BP.

j'ai été confronté lors de ma thèse et des solutions sont proposées pour résoudre ces biais systématiques. Le troisième point-clé de cette ré-analyse est la "standardisation" du type d'analyses effectuées. En effet, la majeure partie des enregistrements disponibles dans la banque de fossiles de l'IRD sont des enregistrements de Sr/Ca et donc de paléo-SST. Or, la SSS est un paramètre-clé pour étudier la variabilité climatique dans cette région. La valorisation de ce "patrimoine climatique" passe donc également par des analyses complémentaires visant à obtenir des enregistrements de la composition en isotopes stables de l'oxygène ($\delta^{18}\text{O}$) des fossiles, en parallèle des enregistrements de Sr/Ca, afin d'extraire l'enregistrement de SSS contenu dans le $\delta^{18}\text{O}$ du corail.

Les travaux réalisés au cours de ma thèse sur la calibration du bénitier *Tridacna maxima* comme archive paléo-climatique ouvrent de nouvelles possibilités concernant l'utilisation de spécimens fossiles de cette espèce dans des reconstructions paléo-climatiques. Il est ainsi envisageable de compléter la ré-analyse du patrimoine-corail de l'IRD par des enregistrements de bénitiers fossiles de l'espèce *Tridacna maxima*.

L'abondance de spécimens fossiles retrouvés lors de fouilles archéologiques offre également une perspective intéressante pour mettre en relation les migrations humaines dans le Pacifique et le climat. Les tendances observées dans cette étude (chapitre IV) montrent une augmentation de la variabilité ENSO et une prédominance d'évènements La Niña. Ces tendances doivent être confirmées ou infirmées en multipliant le nombre d'enregistrements obtenus à partir de bénitiers datés autour de la période Lapita. La grande quantité de bénitiers collectés sur les nombreux sites archéologiques Lapita devrait permettre d'évaluer l'amplitude de la variabilité interannuelle liée à ENSO (par ex., en appliquant la méthode de *bulk sampling* utilisée dans ma thèse – chapitre IV) et ainsi obtenir un panorama de la variabilité climatique sur l'ensemble du Pacifique-Ouest. Ces données devraient également permettre de dater, de manière précise, l'apparition et l'évolution du changement dans la variabilité ENSO au cours de l'Holocène supérieur.

L'étude de la variabilité de la SPCZ au cours de l'Holocène est un enjeu de taille pour la compréhension de la variabilité climatique passée et future. La ré-analyse du "patrimoine paléoclimatique" du Pacifique Sud-Ouest, acquis durant les dernières décennies, permettrait de remplir cet objectif. La possibilité d'utiliser le bénitier *Tridacna maxima* comme archive climatique ouvre de nouvelles possibilités concernant l'utilisation de spécimens fossiles dans des reconstructions paléoclimatiques. Ceci permet en particulier d'utiliser les échantillons archéologiques prélevés dans la zone Indo-Pacifique, durant les fouilles des dernières décennies, pour mettre en relation les peuplements humains et le climat.

Remarque : les enregistrements géochimiques obtenus au cours de ma thèse sur les coraux et les bénitiers (actuels et fossiles) seront à termes disponibles au téléchargement sur le site de la National Oceanic and Atmospheric Administration (NOAA) à partir du lien suivant : <http://www.ncdc.noaa.gov/paleo/datalist.html>.



Prélèvement d'eau de mer près du thermosalinographe (cylindre vertical) de la Fausse Passe Uitoé, Nouvelle-Calédonie. Les données SST et SSS de cet instrument ont été utilisées dans ma thèse. John Butscher, Août 2010. Crédit photo: N. Duprey.



Références bibliographiques

- Abram NJ, McGregor HV, Gagan MK, et al. (2009) Oscillations in the southern extent of the Indo-Pacific Warm Pool during the mid-Holocene. *Quaternary Science Reviews* 28:2794–2803.
- Aharon P (1980) Stable isotope geochemistry of a late quaternary coral reef sequence, New Guinea: application of high resolution data to paleoclimatology. Ph.D thesis, Australian National University.
- Aharon P (1991) Recorders of reef environment histories - stable isotopes in corals, giant clams, and calcareous algae. *Coral Reefs* 10:71–90.
- Aharon P, Chappell J (1986) Oxygen isotopes, sea level changes and the temperature history of a coral reef environment in New Guinea over the last 105 years. *Palaeogeography, Palaeoclimatology, Palaeoecology* 56:337–379.
- Ambariyanto (1997) Effect of nutrient enrichment in the field on the biomass, growth and calcification of the giant clam *Tridacna maxima*. *Marine Biology* 129:635–642.
- Ambrizzi T, Hoskins BJ, Hsu H-H (1995) Rossby wave propagation and teleconnection patterns in the austral winter. *Journal of Atmospheric Sciences* 52:3661–3672.
- Anand P, Elderfield H, Conte MH (2003) Calibration of Mg/Ca thermometry in planktonic foraminifera from a sediment trap time series. *Paleoceanography* 18:1050.
- Anderson A, Chappell J, Gagan M, Grove R (2006) Prehistoric maritime migration in the Pacific islands: an hypothesis of ENSO forcing. *The Holocene* 16:1–6.
- Aubert A, Lazareth CE, Cabioch G, et al. (2009) The tropical giant clam *Hippopus hippopus* shell, a new archive of environmental conditions as revealed by sclerochronological and $\delta^{18}\text{O}$ profiles. *Coral Reefs* 28:989–998.
- Avis C, Montenegro A, Weaver A (2007) Simulating island discovery during the Lapita expansion. *The Journal of Island and Coastal Archaeology* 2:197–209
- Ayling BF (2006) Seasonal paleoclimates of the MIS 5E, 9 and 11 interglacials, using geochemical proxies in *Porites* and *Tridacna*. Ph.D thesis, Australian National University.
- Ayling BF, McCulloch MT, Gagan MK, et al. (2006) Sr/Ca and $\delta^{18}\text{O}$ seasonality in a *Porites* coral from the MIS 9 (339–303 ka) interglacial. *Earth and Planetary Science Letters* 248:462–475.
- Batenburg SJ, Reichert G-J, Jilbert T, et al. (2011) Interannual climate variability in the Miocene: High resolution trace element and stable isotope ratios in giant clams. *Palaeogeography, Palaeoclimatology, Palaeoecology* 306:75–81.
- Beck JW (1997) Abrupt changes in early Holocene tropical sea surface temperature from coral Sr/Ca thermometry. *Nature* 385:705–707.
- Beck JW, Edwards RL, Ito E, et al. (1992) Sea-surface temperature from coral skeletal strontium/calcium ratios. *Science* 257:644–647.
- Beckvar N (1981) Cultivation, spawning, and growth of the giant clams *Tridacna gigas*, *T. derasa*, and *T. squamosa* in Palau, Caroline Islands. *Aquaculture* 24:21–30.
- Berger A, Loutre MF (1991) Insolation values for the climate of the last 10 million years. *Quaternary Science Reviews* 10:297–317.
- Bertalanffy L (1957) Quantitative laws in metabolism and growth. *The Quarterly Review of Biology* 32:217–231.
- Bertalanffy L (1938) A quantitative theory of organic growth (inquiries on growth laws II). *Human biology* 10:181–213.
- Böhm F, Joachimski MM, Lehnert H, et al. (1996) Carbon isotope records from extant Caribbean and South Pacific sponges: Evolution of $\delta^{13}\text{C}$ in surface water DIC. *Earth and Planetary Science Letters* 139:291–303.
- Bonham K (1965) Growth rate of giant clam *Tridacna gigas* at bikini atoll as revealed by radioautography. *Science* 149:300–302.

- Le Borgne R, Barber RT, Delcroix T, et al. (2002) Pacific warm pool and divergence: temporal and zonal variations on the equator and their effects on the biological pump. *Deep Sea Research Part II: Topical Studies in Oceanography* 49:2471–2512.
- Braconnot P, Luan Y, Brewer S, Zheng W (2012) Impact of Earth's orbit and freshwater fluxes on Holocene climate mean seasonal cycle and ENSO characteristics. *Clim Dyn* 38:1081–1092.
- Braconnot P, Marti O, Joussaume S, Leclainche Y (2000) Ocean feedback in response to 6 kyr BP insolation. *Journal of Climate* 13:1537–1553.
- Braconnot P, Otto-Bliesner B, Harrison S, et al. (2007) Results of PMIP2 coupled simulations of the Mid-Holocene and Last Glacial Maximum—Part 2: feedbacks with emphasis on the location of the ITCZ and mid-and high latitudes heat budget. *Climate of the Past* 3:279–296.
- Brown J, Collins M, Tudhope AW, Toniazzo T (2007) Modeling mid-Holocene tropical climate and ENSO variability: towards constraining predictions of future change with palaeo-data. *Climate Dynamics* 30:19–36.
- Brown J, Tudhope AW, Collins M, McGregor HV (2008) Mid-Holocene ENSO: Issues in quantitative model-proxy data comparisons. *Paleoceanography* 23 - PA3202.
- Burley DV, Nelson DE, Shutler Jr R (1999) A radiocarbon chronology for the Eastern Lapita frontier in Tonga. *Archaeology in Oceania* 59–70.
- Butler PG, Richardson CA, Scourse JD, et al. (2010) Marine climate in the Irish Sea: analysis of a 489-year marine master chronology derived from growth increments in the shell of the clam *Arctica islandica*. *Quaternary Science Reviews* 29:1614–1632.
- Cadée GC (1982) Tidal and seasonal variation in particulate and dissolved organic carbon in the western Dutch Wadden Sea and Marsdiep tidal inlet. *Netherlands Journal of Sea Research* 15:228–249.
- Cane M, Clement AC (1999) A role for the tropical Pacific coupled ocean-atmosphere system on Milankovitch and millennial timescales part II: Global impacts. *geophysical monograph-american geophysical union* 112:373–384.
- Cane MA (2005) The evolution of El Niño, past and future. *Earth and Planetary Science Letters* 230:227–240.
- Carter JG (1980) Environmental and biological controls of bivalve shell mineralogy and microstructure [Mollusca]. Plenum Press. Rhoads, D.C. & Lutz, R.A, New York, pp 69–114
- Chappell J, A. Polach H (1972) Some effects of partial recrystallisation on ¹⁴C dating Late Pleistocene corals and molluscs. *Quaternary Research* 2:244–252.
- Chiang JCH, Fang Y, Chang P (2009) Pacific Climate Change and ENSO Activity in the Mid-Holocene. *Journal of Climate* 22:923–939.
- Clement AC, Seager R, Cane MA (2000) Suppression of El Niño during the mid-Holocene by changes in the Earth's orbit. *Paleoceanography* 15:731–737.
- Le Cornec F, Corrège T (1997) Determination of uranium to calcium and strontium to calcium ratios in corals by inductively coupled plasma mass spectrometry. *Journal of Analytical Atomic Spectrometry* 12:969–973.
- Corrège, Gagan MK, Beck JW, et al. (2004) Interdecadal variation in the extent of South Pacific tropical waters during the Younger Dryas event. *Nature* 428:927–929.
- Corrège T (2006) Sea surface temperature and salinity reconstruction from coral geochemical tracers. *Palaeogeography Palaeoclimatology Palaeoecology* 232:408–428.
- Corrège T, Delcroix T, Recy J, et al. (2000) Evidence for stronger El Niño-Southern Oscillation (ENSO) events in a mid-Holocene massive coral. *Paleoceanography* 15:465–470.

- Delcroix T, Picaut J (1998) Zonal displacement of the western equatorial Pacific “fresh pool”. *Journal of Geophysical Research-Oceans* 103:1087–1098.
- DeLong KL, Flannery JA, Maupin CR, et al. (2011) A coral Sr/Ca calibration and replication study of two massive corals from the Gulf of Mexico. *Palaeogeography, Palaeoclimatology, Palaeoecology* 307:117–128.
- deMenocal P, Ortiz J, Guilderson T, Sarnthein M (2000) Coherent high- and low-latitude climate variability during the Holocene warm period. *Science* 288:2198–2202.
- Denham T, Ramsey C, Specht J (2012) Dating the appearance of Lapita pottery in the Bismarck Archipelago and its dispersal to Remote Oceania. *Archaeology in Oceania* 47:39–46.
- Diaz HF, Hoerling MP, Eischeid JK (2001) ENSO variability, teleconnections and climate change. *International Journal of Climatology* 21:1845–1862.
- Dolukhanov PM (1997) The Pleistocene-Holocene transition in northern Eurasia: environmental changes and human adaptations. *Quaternary International* 41:181–191.
- Elliot M, Welsh K, Chilcott C, et al. (2009) Profiles of trace elements and stable isotopes derived from giant long-lived *Tridacna gigas* bivalves: Potential applications in paleoclimate studies. *Palaeogeography Palaeoclimatology Palaeoecology* 280:132–142.
- Enmar R, Stein M, Bar-Matthews M, et al. (2000) Diagenesis in live corals from the Gulf of Aqaba. I. The effect on paleo-oceanography tracers. *Geochimica et Cosmochimica Acta* 64:3123–3132.
- Epstein S, Buchsbaum R, Lowenstam HA, Urey HC (1953) Revised carbonate-water isotopic temperature scale. *Geological Society of America Bulletin* 64:1315–1326.
- Faylona MGP, Lazareth CE, Sémah A-M, et al. (2011) Preliminary study on the preservation of giant clam (*Tridacnidae*) shells from the Balobok Rockshelter archaeological site, south Philippines. *Geoarchaeology* 26:888–901.
- Foster LC, Andersson C, Høie H, et al. (2008) Effects of micromilling on $\delta^{18}\text{O}$ in biogenic aragonite. *Geochemistry Geophysics Geosystems* 9 (4).
- Fry B (2002) Conservative mixing of stable isotopes across estuarine salinity gradients: A conceptual framework for monitoring watershed influences on downstream fisheries production. *Estuaries* 25:264–271.
- Gaffey SJ, Kolak JJ, E. Bronnimann C (1991) Effects of drying, heating, annealing, and roasting on carbonate skeletal material, with geochemical and diagenetic implications. *Geochimica et Cosmochimica Acta* 55:1627–1640.
- Gagan MK, Ayliffe LK, Hopley D, et al. (1998) Temperature and surface-ocean water balance of the mid-Holocene tropical Western Pacific. *Science* 279:1014–1018.
- Gagan MK, Hendy EJ, Haberle SG, Hantoro WS (2004) Post-glacial evolution of the Indo-Pacific Warm Pool and El Niño-Southern Oscillation. *Quaternary International* 118:127–143.
- Galipaud JC (1996) Le rouge et le noir: la poterie Mangaasi et le peuplement des îles de Mélanésie. *Mémoires de Pierre, Mémoires d’Homme: Tradition et Archéologie en Océanie Hommage à José Garanger* 115–125.
- Galipaud JC, Kelly MC. (2007) Makué (Aore Island, Santo, Vanuatu): A new Lapita site in the ambit of New Britain obsidian distribution. *Oceanic explorations: Lapita and western Pacific settlement* 26:151–162.
- Van Geel B, Buurman J, Waterbolk HT (1996) Archaeological and palaeoecological indications of an abrupt climate change in The Netherlands, and evidence for climatological teleconnections around 2650 BP. *Journal of Quaternary Science* 11:451–460.

- Gilg H, Taubald H, Struck U (2007) Phosphoric acid fractionation factors for aragonite between 25 and 72°C with implications on aragonite-calcite oxygen isotope fractionation. *Geochim Cosmochim Acta* 71:A323.
- Gillikin DP, Hutchinson KA, Kumai Y (2009) Ontogenic increase of metabolic carbon in freshwater mussel shells (*Pyganodon cataracta*). *Journal of Geophysical Research* 114:G01007.
- Gillikin DP, Lorrain A, Bouillon S, et al. (2006) Stable carbon isotopic composition of *Mytilus edulis* shells: relation to metabolism, salinity, $\delta^{13}\text{C}$ DIC and phytoplankton. *Organic Geochemistry* 37:1371–1382.
- Gillikin DP, Lorrain A, Meng L, Dehairs F (2007) A large metabolic carbon contribution to the $\delta^{13}\text{C}$ record in marine aragonitic bivalve shells. *Geochimica et Cosmochimica Acta* 71:2936–2946.
- Godfrey JS, Jr RAH, Johnson RH, et al. (1998) Coupled Ocean-Atmosphere Response Experiment (COARE): An interim report. *J Geophys Res* 103:14395–14,450.
- Gomez ED, Mingoa-Licuanan SS (2006) Achievements and lessons learned in restocking giant clams in the Philippines. *Fisheries Research* 80:46–52.
- Gosden C, Pavlides C (1994) Are islands insular? Landscape vs. seascape in the case of the Arawe Islands, Papua New Guinea. *Archaeology in Oceania* 162–171.
- Gouriou Y, Delcroix T (2002) Seasonal and ENSO variations of sea surface salinity and temperature in the South Pacific Convergence Zone during 1976-2000. *Journal of Geophysical Research-Oceans* 107, p14.
- Graham NE, Barnett TP (1995) ENSO and ENSO-related predictability. II: Northern hemisphere 700-mb height predictions based on a hybrid coupled ENSO model. *Journal of climate* 8:544–549.
- Green A, Craig P (1999) Population size and structure of giant clams at Rose Atoll, an important refuge in the Samoan Archipelago. *Coral Reefs* 18:205–211.
- Gribchenko YN, Kurenkova EI (1997) The main stages and natural environmental setting of late Palaeolithic human settlement in Eastern Europe. *Quaternary International* 41:173–179.
- Griffiths CL, Klumpp DW (1996) Relationships between size, mantle area and zooxanthellae numbers in five species of giant clam (Tridacnidae). *Marine Ecology Progress Series* 137:139–147.
- Groube L, Chappell J, Muke J, Price D (1986) A 40,000 year-old human occupation site at Huon Peninsula, Papua New Guinea. *Nature* 324:453–455.
- Gupta AK (2004) Origin of agriculture and domestication of plants and animals linked to early Holocene climate amelioration. *Current Science* 87:54–59.
- Gupta AK, Anderson DM, Pandey DN, Singhvi AK (2006) Adaptation and human migration, and evidence of agriculture coincident with changes in the Indian summer monsoon during the Holocene. *Current Science* 90:1082–1090.
- Haberle SG, Hope GS, Van der Kaars S (2001) Biomass burning in Indonesia and Papua New Guinea: natural and human induced fire events in the fossil record. *Palaeogeography, Palaeoclimatology, Palaeoecology* 171:259–268.
- Hammer Ø, Harper DAT, Ryan PD (2001) PAST-Palaeontological statistics. 25:2009.
- Hardy JT, Hardy SA (1969) Ecology of *Tridacna* in Palau. XXIII:467–472.
- Hathorne E, Adkins J, Asami R, et al. (2010) An inter-laboratory study of coral Sr/Ca and other element/Ca ratios. 10th International Conference on Paleoceanography, ICP 10
- Haug GH, Hughen KA, Sigman DM, et al. (2001) Southward migration of the intertropical convergence zone through the Holocene. *Science* 293:1304–1308.
- Hean RL, Cacho OJ (2003) A growth model for giant clams *Tridacna crocea* and *T. derasa*. *Ecological modelling* 163:87–100.

- Hendy EJ, Gagan MK, Lough JM, et al. (2007) Impact of skeletal dissolution and secondary aragonite on trace element and isotopic climate proxies in *Porites* corals. *Paleoceanography* 22 - PA4101.
- Henocque Y (1980) L'âge du bénitier *Tridacna maxima* (Mollusques—Bivalves) par examen des stries de croissance de sa coquille. *Bulletin de la Société zoologique de France* 105:309–312.
- Ho C-R, Yan X-H, Zheng Q (1995) Satellite observations of upper-layer variabilities in the Western Pacific Warm Pool. *Bulletin of the American Meteorological Society* 76:669–679.
- Huntley B (1999) Climatic change and reconstruction. *Journal of Quaternary Science* 14:513–520.
- Inoue M, Nohara M, Okai T, et al. (2004) Concentrations of trace elements in carbonate reference materials coral JCp-1 and giant clam JCt-1 by inductively coupled plasma-mass spectrometry. *Geostandards and Geoanalytical Research* 28:411–416.
- Irwin G (2008) Pacific seascapes, canoe performance, and a review of Lapita voyaging with regard to theories of migration. *Asian Perspectives-Hong Kong Then Honolulu-* 47:12.
- Jameson (1976) Early life history of *Tridacna maxima* and *Hippopus hippopus*. *Pacific Science* 30:219–233
- Jantzen C, Wild C, El-Zibdah M, et al. (2008) Photosynthetic performance of giant clams, *Tridacna maxima* and *T. squamosa*, Red Sea. *Marine Biology* 155:211–221.
- Jones DS, Williams DF, Romanek CS (1986) Life history of symbiont-bearing giant clams from stable isotope profiles. *Science* 231:46–48.
- Juillet-Leclerc A, Schmidt G (2001) A calibration of the oxygen isotope paleothermometer of coral aragonite from *Porites*. *Geophysical Research Letters* 28:4135–4138.
- Juillet-Leclerc A, Thiria S, Naveau P, et al. (2006) SPCZ migration and ENSO events during the 20th century as revealed by climate proxies from a Fiji coral. *Geophysical Research Letters* 33 (17).
- Kanazawa T, Sato S (2008) Environmental and physiological controls on shell microgrowth pattern of *Ruditapes philippinarum* (Bivalvia: Veneridae) from Japan. *Journal of Molluscan Studies* 74:89–95.
- Kaplan A, Cane MA, Kushnir Y, et al. (1998) Analyses of global sea surface temperature 1856-1991. *Journal of Geophysical Research* 103:567–18.
- Kiladis GN, Vonstorch H, Vanloon H (1989) Origin of the South-Pacific Convergence Zone. *Journal of Climate* 2:1185–1195.
- Kilbourne KH, Quinn TM, Taylor FW, et al. (2004) El Nino-Southern Oscillation-related salinity variations recorded in the skeletal geochemistry of a *Porites* coral from Espiritu Santo, Vanuatu. *Paleoceanography* 19 – PA4002.
- Kim ST, Mucci A, Taylor BE (2007) Phosphoric acid fractionation factors for calcite and aragonite between 25 and 75 C: revisited. *Chemical Geology* 246:135–146.
- Kinch J (2008) From prehistoric to present: giant clam (tridacnidae) use in Papua New Guinea in: early human impacts on megamolluscs. *The Journal of Island and Coastal Archaeology*. Antczak A., Cipriani R., Oxford, pp 164–166.
- Kirch PV (1997) *The Lapita peoples: ancestors of the Oceanic world*. Blackwell Oxford p 353.
- Kirch PV (2000) *On the road of the winds: an archaeological history of the Pacific Islands before European contact*. University of California Press, Berkeley
- Klumpp DW, Griffith CL (1994) Contributions of phototrophic and heterotrophic nutrition to the metabolic and growth requirements of four species of giant clam (Tridacnidae). *Marine Ecology Progress Series* 115:103–115.

- Knutson DW (1972) Coral chronometers: seasonal growth bands in reef corals. *Science* 177:270–272.
- Kohfeld KE, Harrison SP (2000) How well can we simulate past climates? Evaluating the models using global palaeoenvironmental datasets. *Quaternary Science Reviews* 19:321–346.
- Koutavas A, deMenocal PB, Lynch-Stieglitz J (2006a) Holocene trends in tropical Pacific sea surface temperatures and the El Niño–Southern Oscillation. *PAGES News* 14:22–23.
- Koutavas A, Demenocal PB, Olive GC, et al. (2006b) Mid-Holocene El Niño–Southern Oscillation (ENSO) attenuation revealed by individual foraminifera in eastern tropical Pacific sediments. *Geology* 34:993.
- LaBarbera M (1975) Larval and post-larval development of the giant clams, *Tridacna maxima* and *Tridacna squamosa* (Bivalvia: Tridacnidae). *Malacologia* 15:67–79.
- Lea DW, Pak DK, Spero HJ (2000) Climate impact of late quaternary equatorial Pacific sea surface temperature variations. *Science* 289:1719–1724.
- Leavesley MG, Bird MI, Fifield LK, et al. (2002) Buang Merabak: early evidence for human occupation in the Bismarck Archipelago, Papua New Guinea. *Australian Archaeology* 55–57.
- Liu Z, Kutzbach I, Wu L (2000) Modelling climate shift of El Niño variability in the Holocene. *Geophysical Research Letters* 27:2265–2268.
- Lorrain A, Paulet YM, Chauvaud L, et al. (2004) $\delta^{13}\text{C}$ variation in scallop shells: Increasing metabolic carbon contribution with body size? *Geochimica et Cosmochimica Acta* 68:3509–3519.
- Lough JM, Cooper TF (2011) New insights from coral growth band studies in an era of rapid environmental change. *Earth Science Reviews* 108:170–184.
- Lu J, Vecchi GA, Reichler T (2007) Expansion of the Hadley cell under global warming. *Geophys. Res. Lett* 34 – L06805.
- Luan Y, Braconnot P, Yu Y, et al. (2012) Early and mid-Holocene climate in the tropical Pacific: seasonal cycle and interannual variability induced by insolation changes. *Climate of the Past Discussions* 8:505–555.
- Lucas JS (1994) The biology, exploitation, and mariculture of giant clams (Tridacnidae). *Reviews in Fisheries science* 2:181–223.
- Lucas JS (1988) Giant clams: description, distribution and life history. In: Copland JW and L (ed) *Giant Clams in Asia and the Pacific*. ACIAR, Canberra, pp 21–32.
- Lucas JS, Nash WJ, Crawford CM, Braley RD (1989) Environmental influences on growth and survival during the ocean-nursery rearing of giant clams, *Tridacna gigas* (L.). *Aquaculture* 80:45–61.
- Lutz RA, Clark GR (1984) Seasonal and geographic variation in the shell microstructure of a salt-marsh bivalve (*Geukensia demissa* (Dillwyn)). *Journal of Marine Research* 42:943–956.
- Lyon B (2004) The strength of El Niño and the spatial extent of tropical drought. *Geophysical Research Letters* 31 - L21204.
- Maes C, Sudre J, Garçon V (2010) Detection of the eastern edge of the Equatorial Pacific Warm Pool using satellite-based ocean color observations. *SOLA* 6:129–132.
- Maes C., Varillon D (2011) Large-scale climatic and oceanic conditions around Santo in: *The Natural history of Santo*. Bouchet P., Le Guyader H. & Pascal O. (Eds.). Muséum national d’Histoire naturelle, Paris; IRD, Marseille; Pro-Natura international, Paris, 572 p. (Patrimoines naturels 70).
- Marchenko SS, Gorbunov AP, Romanovsky VE (2007) Permafrost warming in the Tien Shan Mountains, Central Asia. *Global and Planetary Change* 56:311–327.

- Martinez J, Deckker PD, Chivas AR (1997) New estimates for salinity changes in the Western Pacific Warm Pool during the Last Glacial Maximum: Oxygen-isotope evidence. *Marine Micropaleontology* 32:311–340.
- Marzin C, Braconnot P (2009) The role of the ocean feedback on Asian and African monsoon variations at 6 kyr and 9.5 kyr BP. *Comptes Rendus Geoscience* 341:643–655.
- McConnaughey T (1989) C-13 and O-18 isotopic disequilibrium in biological carbonates.2. invitro simulation of kinetic isotope effects. *Geochimica Et Cosmochimica Acta* 53:163–171.
- McConnaughey TA, Burdett J, Whelan JF, Paull CK (1997) Carbon isotopes in biological carbonates: respiration and photosynthesis. *Geochimica et Cosmochimica Acta* 61:611–622.
- McConnaughey TA, Gillikin DP (2008) Carbon isotopes in mollusk shell carbonates. *Geo-Marine Letters* 28:287–299.
- McGregor HV, Gagan MK (2003) Diagenesis and geochemistry of *Porites* corals from Papua New Guinea: Implications for paleoclimate reconstruction. *Geochimica et Cosmochimica Acta* 67:2147–2156.
- McKoy JL (1980) Biology, exploitation and management of giant clams (Tridacnidae) in the Kingdom of Tonga. *Fisheries bulletin* 1.
- McMichael DF, Cameron AM, Campbell BM, et al. (1974) Growth rate, population size and mantle coloration in the small giant clam *Tridacna maxima* (Roding), at One Tree Island, Capricorn Group, Queensland. The Great Barrier Reef Committee. p 241-254.
- McPhaden MJ, Zebiak SE, Glantz MH (2006) ENSO as an integrating concept in earth science. *Science* 314:1740–1745.
- Moir BG (1989) A review of tridacnid ecology and some possible implications for archaeological research. *Asian Perspectives* 27:95–121.
- Moir BG (1990) Comparative studies of “Fresh” and “Aged” *Tridacna gigas* shell: Preliminary investigations of a reported technique for pretreatment of tool material. *Journal of Archaeological Science* 17:329–345.
- Montaggioni LF, Le Cornec F, Corrège T, Cabioch G (2006) Coral barium/calcium record of mid-Holocene upwelling activity in New Caledonia, South-West Pacific. *Palaeogeography Palaeoclimatology Palaeoecology* 237:436–455.
- Mook WG (1971) Paleotemperatures and chlorinities from stable carbon and oxygen isotopes in shell carbonate. *Palaeogeography, Palaeoclimatology, Palaeoecology* 9:245–263.
- Mook WG, Vogel JC (1968) Isotopic Equilibrium between Shells and Their Environment. *Science* 159:874–875.
- Morimoto M, Abe O, Kayanne H, et al. (2002) Salinity records for the 1997–98 El Niño from Western Pacific corals. *Geophysical Research Letters* 29:4 PP.
- Moy CM, Seltzer GO, Rodbell DT, Anderson DM (2002) Variability of El Nino/Southern Oscillation activity at millennial timescales during the Holocene epoch. *Nature* 420:162–165.
- Muller A, Gagan MK, McCulloch MT (2001) Early marine diagenesis in corals and geochemical consequences for paleoceanographic reconstructions. *Geophysical Research Letters* 28:4471–4474.
- Munro JL, Heslinga GA (1983) Prospects for the commercial cultivation of giant clams (Bivalvia: Tridacnidae). *Proceedings of the Gulf and Caribbean Fisheries Institute*. pp 122–134
- Norton JH, Shepherd MA, Abdon-Nagutt MR, Lindsay S (1993) Mortalities in the giant clam *Hippopus hippopus* associated with Rickettsiales-like organisms. *Journal of Invertebrate Pathology* 62:207–209.

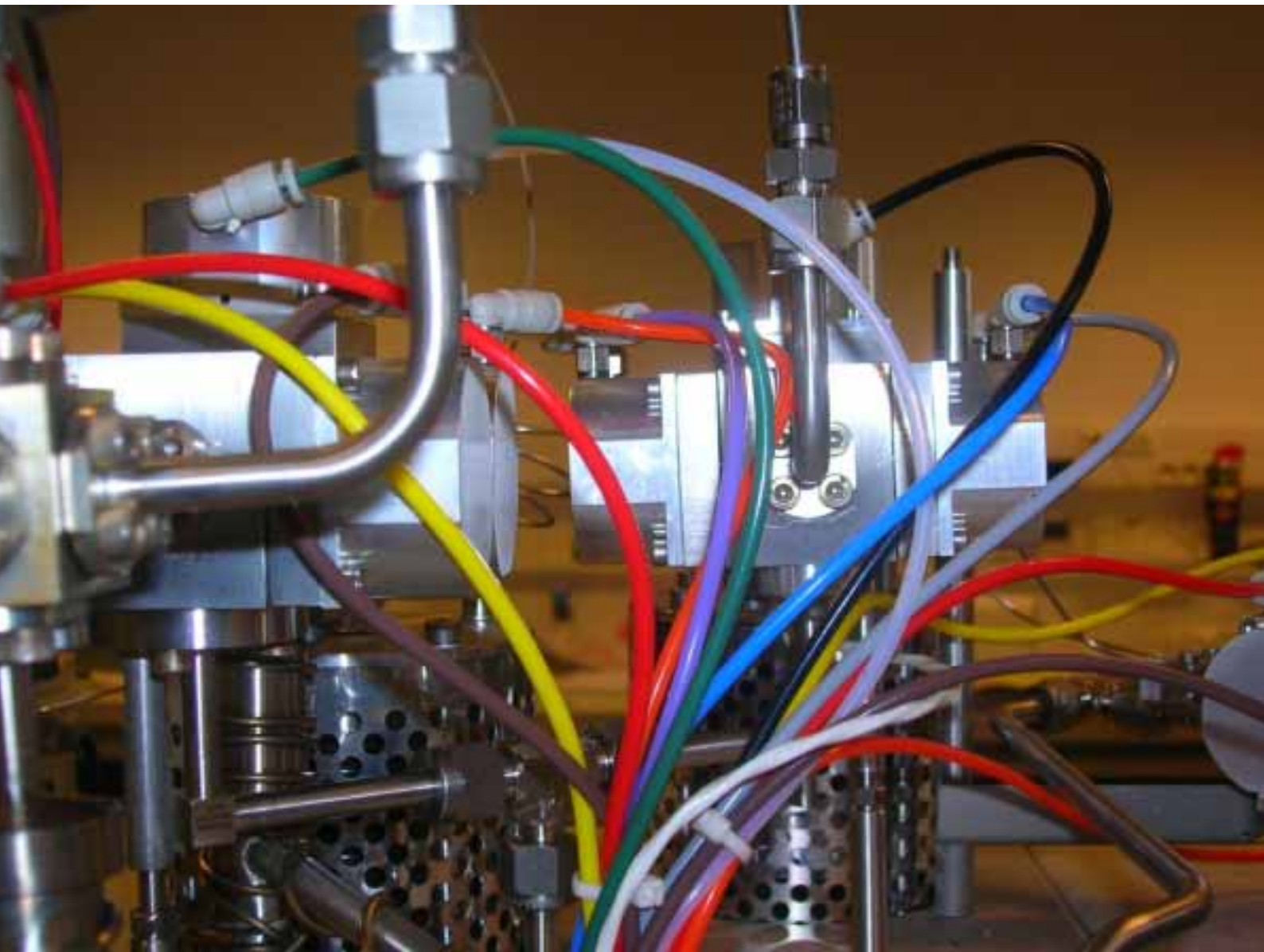
- Nothdurft LD, Webb GE (2008) Earliest diagenesis in scleractinian coral skeletons: implications for palaeoclimate-sensitive geochemical archives. *Facies* 55:161–201.
- O’Connell JF, Allen J (2004) Dating the colonization of Sahul (Pleistocene Australia–New Guinea): a review of recent research. *Journal of Archaeological Science* 31:835–853.
- Okai T, Suzuki A, Kawahata H, et al. (2002) Preparation of a new geological survey of japan geochemical reference material: coral jcp-1. *Geostandards Newsletter* 26:95–99.
- Bin Othman AS, Goh GHS, Todd PA (2010) The distribution and status of giant clams (family tridacnidae) - a short review. *Raffles Bulletin of Zoology* 58:103–111.
- Ourbak T (2006) Variations climatiques interannuelles à interdécennales dans le Pacifique Tropical telles qu’enregistrées par les traceurs géochimiques contenus dans les coraux massifs. Ph.D thesis, Université de Bordeaux I
- Owen EF, Wanamaker Jr. AD, Feindel SC, et al. (2008) Stable carbon and oxygen isotope fractionation in bivalve (*Placopecten magellanicus*) larval aragonite. *Geochimica et Cosmochimica Acta* 72:4687–4698.
- Pannella G (1976) Tidal growth patterns in recent and fossil mollusc bivalve shells: a tool for the reconstruction of paleotides. *Naturwissenschaften* 63:539–543.
- Pannella G, MacClintock C (1968) Biological and environmental rhythms reflected in molluscan shell growth. *Memoir (The Paleontological Society)* 64–80.
- Pätzold J, Heinrichs JP, Wolschendorf K, Wefer G (1991) Correlation of stable oxygen isotope temperature record with light attenuation profiles in reef-dwelling *Tridacna* shells. *Coral Reefs* 10:65–69.
- Petchev F, Anderson A, Zondervan A, et al. (2008) New marine deltaR values for the South Pacific subtropical gyre region. *Radiocarbon* 50:373–397.
- Philander SG (1990) El Niño, La Niña, and the southern oscillation. *International geophysics series* 46:193.
- Philander SG, Gu D, Halpern D, et al. (1996) Why the ITCZ is mostly north of the equator. *Journal of Climate* 9:2958–2972.
- Di Piazza A, Pearthree E (1999) The spread of the “Lapita people”: A demographic simulation. *Journal of Artificial Societies and Social Simulation* 2:1–15.
- Di Piazza A, Di Piazza P, Pearthree E (2007) Sailing virtual canoes across Oceania: revisiting island accessibility. *Journal of archaeological science* 34:1219–1225.
- Picaut J, Ioualalen M, Delcroix T, et al. (2001) The oceanic zone of convergence on the eastern edge of the Pacific warm pool: A synthesis of results and implications for El Niño-Southern Oscillation and biogeochemical phenomena. *Journal of Geophysical Research* 106:2363–2386.
- Picaut J, Ioualalen M, Menkes C, et al. (1996) Mechanism of the zonal displacements of the Pacific warm pool: Implications for ENSO. *Science* 274:1486–1489.
- Poulain C, Lorrain A, Flye-Sainte-Marie J, et al. (2011) An environmentally induced tidal periodicity of microgrowth increment formation in subtidal populations of the clam *Ruditapes philippinarum*. *Journal of Experimental Marine Biology and Ecology* 397:58–64.
- Poveda G, Rojas W, Quiñones ML, et al. (2001) Coupling between annual and ENSO timescales in the malaria-climate association in Colombia. *Environmental Health Perspectives* 109:489.
- Quinn TM, Sampson DE (2002) A multiproxy approach to reconstructing sea surface conditions using coral skeleton geochemistry. *Paleoceanography* 17:1062.
- Quinn TM, Taylor FW (2006) SST artifacts in coral proxy records produced by early marine diagenesis in a modern coral from Rabaul, Papua New Guinea. *Geophysical Research Letters*

- Rasmusson EM, Carpenter TH (1982) Variations in tropical sea surface temperature and surface wind fields associated with the Southern Oscillation/El Niño. *Monthly Weather Review* 110:354–384.
- Raymakers C, Ringuet S, Phoon N, Sant G (2003) Review of the Exploitation of Tridacnidae in the South Pacific, Indonesia and Vietnam. Technical report submitted to the European Commission, TRAFFIC Europe, Brussels, Belgium.
- Rayner NA, Parker DE, Horton EB, et al. (2003) Global analyses of sea surface temperature, sea ice, and night marine air temperature since the late nineteenth century. *Journal of Geophysical Research* 108:29 PP.
- Reimer PJ, Baillie MGL, Bard E, et al. (2009) Intcal09 and Marine09 Radiocarbon Age Calibration Curves, 0-50,000 Years Cal Bp. *Radiocarbon* 51:1111–1150.
- Ren L, Linsley BK, Wellington GM, et al. (2002) Deconvolving the $\delta^{18}\text{O}$ seawater component from subseasonal coral $\delta^{18}\text{O}$ and Sr/Ca at Rarotonga in the southwestern subtropical Pacific for the period 1726 to 1997. *Geochimica Et Cosmochimica Acta* 67:1609–1621.
- Renssen H, Seppä H, Crosta X, et al. (2012) Global characterization of the Holocene Thermal Maximum. *Quaternary Science Reviews* 48:7–19.
- Rhoads DC, Lutz RA (1980) Skeletal growth of aquatic organisms: biological records of environmental change. Plenum Press New York.
- Rhoads DC, Pannella G (1970) The use of molluscan shell growth patterns in ecology and paleoecology. *Lethaia* 3:143–161.
- Richardson CA (2001) Molluscs as archives of environmental change. *Oceanography and Marine Biology: An Annual Review* 39:103–164.
- Richerson PJ, Boyd R, Bettinger RL (2001) Was agriculture impossible during the Pleistocene but mandatory during the Holocene? A climate change hypothesis. *American Antiquity* 66:387–411.
- Richter C, Roa-Quiaoit H, Jantzen C, et al. (2008) Collapse of a new living species of giant clam in the Red Sea. *Current Biology* 18:1349–1354.
- Rind D (2000) Relating paleoclimate data and past temperature gradients: Some suggestive rules. *Quaternary Science Reviews* 19:381–390.
- Roberts WH (2007) An investigation into the causes for the reduction in the variability of the el niño southern oscillation in the early Holocene in a global climate model. Ph. D thesis, University of Washington.
- Rodbell DT, Seltzer GO, Anderson DM, et al. (1999) An ~ 15,000-year record of El Niño-driven alluviation in southwestern Ecuador. *Science* 283:516–520.
- Rodland DL, Schone BR, Baier S, et al. (2008) Changes in gape frequency, siphon activity and thermal response in the freshwater bivalves *Anodonta cygnea* and *Margaritifera falcata*. *Journal of Molluscan Studies* 75:51–57.
- Rodland DL, Schöne BR, Helama S, et al. (2006) A clockwork mollusc: Ultradian rhythms in bivalve activity revealed by digital photography. *Journal of Experimental Marine Biology and Ecology* 334:316–323.
- Romanek CS (1985) Shell growth in the small giant clam, *Tridacna maxima* revealed by microstructural and stable isotopic variations. Ph.D thesis, University of Florida.
- Ropelewski CF, Halpert MS (1987) Global and regional scale precipitation patterns associated with the El Niño/Southern Oscillation. *Monthly Weather Review* 115:1606–1626.
- Rosewater J (1965) The family Tridacnidae in the Indo-Pacific. *Indo-Pacific Mollusca* 1:347–396.
- Rosewater J (1982) A new species of *Hippopus* (Bivalvia: Tridacnidae). *Nautilus* 96:3–6.
- Sand C (2010) Lapita calédonien: archéologie d'un premier peuplement insulaire océanien.


- Société des Océanistes, Travaux & documents océanistes 2:296.
- Sandweiss DH, Maasch KA, Burger RL, et al. (2001) Variation in Holocene El Niño frequencies: Climate records and cultural consequences in ancient Peru. *Geology* 29:603.
- Sano Y, Kobayashi S, Shirai K, et al. (2012) Past daily light cycle recorded in the strontium/calcium ratios of giant clam shells. *Nature Communications* 3:761.
- Schneider RC, Smith SV (1982) Skeletal Sr content and density in *Porites* spp. in relation to environmental factors. *Marine Biology* 66:121–131.
- Schöne BR (2008) The curse of physiology—challenges and opportunities in the interpretation of geochemical data from mollusk shells. *Geo-Marine Letters* 28:269–285.
- Schwartzmann C, Durrieu G, Sow M, et al. (2011) In situ giant clam growth rate behavior in relation to temperature: A one-year coupled study of high-frequency noninvasive valvometry and sclerochronology. *Limnology and Oceanography* 56:1940.
- Seeto J, Nunn PD, Sanjana S (2012) Human-mediated prehistoric marine extinction in the Tropical Pacific? Understanding the presence of *Hippopus hippopus* (linn. 1758) in ancient shell middens on the Rove Peninsula, Southwest Viti Levu Island, Fiji. *Geoarchaeology* 27:2–17.
- Shelley C (1989) Growth, sclerochronology and development of the Tridacnidae, with particular reference to *Hippopus hippopus*. Ph.D. thesis, James Cook University of North Queensland.
- Sheppard PJ (2011) Lapita colonization across the Near/Remote Oceania boundary. *Current Anthropology* 52:799–840.
- Sims N, Howard N (1988) Indigenous tridacnid clam populations and the introduction of *Tridacna derasa* in the Cook Islands. *Giant clams in Asia and the Pacific* 34–40.
- Smith SDA (2011) Growth and population dynamics of the giant clam *Tridacna maxima* (Röding) at its southern limit of distribution in coastal, subtropical eastern Australia. *Molluscan Research* 31:37.
- Solomon S, Qin D, Manning M, et al. (2007) *Climate Change 2007: the physical science basis*. Cambridge University Press.
- Stahle DW, D'Arrigo RD, Krusic PJ, et al. (1998) Experimental dendroclimatic reconstruction of the Southern Oscillation. *Bulletin-American Meteorological Society* 79:2137–2151.
- Stott L, Cannariato K, Thunell R, et al. (2004) Decline of surface temperature and salinity in the western tropical Pacific Ocean in the Holocene epoch. *Nature* 431:56–59.
- Summerhayes GR (2007) The rise and transformations of Lapita in the Bismarck Archipelago. *From Southeast Asia to the Pacific: Archaeological perspectives on the Austronesian expansion and the Lapita cultural complex Taipei: Center for Archaeological Studies, Research Center for Humanities and Social Sciences, Academia Sinica* 129–172.
- Sun D, Gagan MK, Cheng H, et al. (2005) Seasonal and interannual variability of the Mid-Holocene East Asian monsoon in coral $\delta^{18}\text{O}$ records from the South China Sea. *Earth and Planetary Science Letters* 237:69–84.
- Surge D, Lohmann KC, Dettman DL (2001) Controls on isotopic chemistry of the American oyster, *Crassostrea virginica* : implications for growth patterns. *Palaeogeography, Palaeoclimatology, Palaeoecology* 172:283–296.
- Swart PK (1981) The strontium, magnesium and sodium composition of recent scleractinian coral skeletons as standards for palaeoenvironmental analysis. *Palaeogeography, Palaeoclimatology, Palaeoecology* 34:115–136.

- Swart PK, Burns SJ, Leder JJ (1991) Fractionation of the stable isotopes of oxygen and carbon in carbon dioxide during the reaction of calcite with phosphoric acid as a function of temperature and technique. *Chemical Geology: Isotope Geoscience section* 86:89–96.
- Swart PK, Greer L, Rosenheim BE, et al. (2010) The ^{13}C Suess effect in scleractinian corals mirror changes in the anthropogenic CO_2 inventory of the surface oceans. *Geophys Res Lett* 37:5 PP.
- Tanaka N, Monaghan MC, Rye DM (1986) Contribution of metabolic carbon to mollusc and barnacle shell carbonate 320:520–523.
- Taylor TW (1992) Quaternary vertical tectonics of the central New Hebrides island arc. *Proceedings of the Ocean Drilling Program, Initial Reports* 134:33–42.
- Trenberth KE (1976) Spatial and temporal variations of Southern Oscillation. *Quarterly Journal of the Royal Meteorological Society* 102:639–653.
- Tudhope AW, Chilcott CP, McCulloch MT, et al. (2001) Variability in the El Niño - Southern oscillation through a glacial-interglacial cycle. *Science* 291:1511–1517.
- Tyson PD, Lee-Thorp J, Holmgren K, Thackeray JF (2002) Changing gradients of climate change in southern Africa during the past millennium: implications for population movements. *Climatic Change* 52:129–135.
- Vargas G, Rutllant J, Ortlieb L (2006) ENSO tropical-extratropical climate teleconnections and mechanisms for Holocene debris flows along the hyperarid coast of western South America (17 degrees-24 degrees S). *Earth Planet Sci Lett* 249:467–483.
- Vincent DG (1994) The South-Pacific Convergence Zone (SPCZ) - a Review. *Monthly Weather Review* 122:1949–1970.
- Waliser DE, Gautier C (1993) A Satellite-derived Climatology of the ITCZ. *Journal of Climate* 6:2162–2174.
- Waliser DE, Graham NE, Gautier C (1993) Comparison of the highly reflective cloud and outgoing longwave radiation datasets for use in estimating tropical deep convection. *Journal of climate* 6:331–353.
- Walther GR, Post E, Convey P, et al. (2002) Ecological responses to recent climate change. *Nature* 416:389–395.
- Wanamaker Jr AD, Kreutz KJ, Borns Jr HW, et al. (2007) Experimental determination of salinity, temperature, growth, and metabolic effects on shell isotope chemistry of *Mytilus edulis* collected from Maine and Greenland. *Paleoceanography* 22:PA2217.
- Wang B, Wang Y (1996) Temporal structure of the southern oscillation as revealed by waveform and wavelet analysis. *Journal of Climate* 9:1586–1598.
- Wang P, Clemens S, Beaufort L, et al. (2005) Evolution and variability of the Asian monsoon system: state of the art and outstanding issues. *Quaternary Science Reviews* 24:595–629.
- Wanner H, Beer J, Butikofer J, et al. (2008) Mid- to Late Holocene climate change: an overview. *Quaternary Science Reviews* 27:1791–1828.
- Wanner H, Solomina O, Grosjean M, et al. (2011) Structure and origin of Holocene cold events. *Quaternary Science Reviews* 30:3109–3123.
- Watanabe T, Oba T (1999) Daily reconstruction of water temperature from oxygen isotopic ratios of a modern *Tridacna* shell using a freezing microtome sampling technique. *Journal of Geophysical Research* 104:PP. 20,667–20,674.
- Watanabe T, Suzuki A, Kawahata H, et al. (2004) A 60-year isotopic record from a mid-Holocene fossil giant clam (*Tridacna gigas*) in the Ryukyu Islands: physiological and paleoclimatic implications. *Palaeogeography, Palaeoclimatology, Palaeoecology* 212:343–354.

- Weber JN, Woodhead PMJ (1972) Temperature dependence of oxygen-18 concentration in reef coral carbonates. *J Geophys Res* 77:463–473.
- Weber JN, Woodhead PMJ (1971) Diurnal variations in the isotopic composition of dissolved inorganic carbon in seawater from coral reef environments. *Geochimica et Cosmochimica Acta* 35:891–902.
- Welsh K, Elliot M, Tudhope A, et al. (2011) Giant bivalves (*Tridacna gigas*) as recorders of ENSO variability. *Earth and Planetary Science Letters* 307:266–270.
- Wheeler AP (1992) Mechanisms of molluscan shell formation. *Calcification in biological systems* 179–216.
- Wirrmann D, Eagar SH, Harper MA, et al. (2011a) First insights into mid-Holocene environmental change in central Vanuatu inferred from a terrestrial record from Emaotfer Swamp, Efate Island. *Quat Sci Rev* 30:3908–3924.
- Wirrmann D, Semah AM, Chacornac-Rault M (2006) Late Holocene paleoenvironment in northern New Caledonia, southwestern Pacific, from a multiproxy analysis of lake sediments. *Quaternary Research* 66:213–232.
- Wirrmann D, Sémah A-M, Debenay J-P, Chacornac-Rault M (2011b) Mid- to late Holocene environmental and climatic changes in New Caledonia, southwest tropical Pacific, inferred from the littoral plain Gouaro-Déva. *Quaternary Research* 76:229–242.
- Woodroffe CD (2003) Mid-late Holocene El Niño variability in the equatorial Pacific from coral microatolls. *Geophysical Research Letters* 30 - GL015868
- Woodroffe CD, Gagan MK (2000) Coral microatolls from the central Pacific record Late Holocene El Niño. *Geophys Res Lett* 27:1511–1514.
- Wyrtki K (1989) Some thoughts about the west Pacific warm pool Western Pacific International meeting and workshop on TOGA COARE. J. Picaut, R. Lukas, and T. Delcroix, Eds, Nouméa, pp 99–109.
- Xie P, Arkin PA (1997) Global precipitation: A 17-year monthly analysis based on gauge observations, satellite estimates, and numerical model outputs. *Bulletin of the American Meteorological Society* 78:2539–2558.
- Xie S-P, Saito K (2001) Formation and Variability of a Northerly ITCZ in a Hybrid Coupled AGCM: Continental Forcing and Oceanic–Atmospheric Feedback. *Journal of Climate* 14:1262–1276.
- Yesner DR (2001) Human dispersal into interior Alaska: antecedent conditions, mode of colonization, and adaptations. *Quaternary Science Reviews* 20:315–327.
- Yonge CM (1975) Giant clams. *Scientific American* 232:96–105.
- Yuan D, Cheng H, Edwards RL, et al. (2004) Timing, duration, and transitions of the last interglacial Asian monsoon. *Science* 304:575–578.
- Zann LP, Ayling AM (1988) Status of giant clams in Vanuatu. *ACIAR Monograph Series* 60–6398.
- Zhang JW, Chen FH, Holmes JA, et al. (2011) Holocene monsoon climate documented by oxygen and carbon isotopes from lake sediments and peat bogs in China: a review and synthesis. *Quaternary Science Reviews* 30:1973–1987.
- Zheng W, Braconnot P, Guilyardi E, et al. (2008) ENSO at 6ka and 21ka from ocean–atmosphere coupled model simulations. *Climate Dynamics* 30:745–762.
- Zhou G, Minakawa N, Githeko AK, Yan G (2004) Association between climate variability and malaria epidemics in the East African highlands. *Proceedings of the National Academy of Sciences of the United States of America* 101:2375.



Détail d'un spectromètre de masse. UPMC, Paris, 2011. Crédit photo: N. Duprey.



**Annexe I – Réflexions sur les analyses
géochimiques de bio-carbonates (coraux, coquilles)**

J'ai prélevé au cours de ma thèse 2400 échantillons de poudre de squelette corallien et 300 échantillons de poudre de coquille de bénitiers à l'aide d'un micro-échantillonneur. Parmi ces 2700 échantillons, 960 ont été analysés sur un ICP-MS pour obtenir la composition en strontium/calcium et 1240 ont été analysés sur un spectromètre de masse pour obtenir la composition isotopique (isotopes stables de l'oxygène et du carbone). Ne sont pas inclus dans cette liste les analyses correspondant aux matériaux de référence, aux standards servant à la calibration de l'appareil et les séries répliquées pour vérification. Cette banque de donnée s'ajoute aux nombreux travaux déjà publiés dont la plupart sont accessibles via le site internet de la National Oceanic and Atmospheric Administration (NOAA) [<http://www.ncdc.noaa.gov/paleo/datalist.html>]. Il serait donc extrêmement intéressant de comparer mes données à celles obtenues au cours de travaux précédents afin d'avoir un panorama des tendances climatiques au cours de l'Holocène à l'échelle de l'Océan Pacifique. Cependant les résultats d'une étude d'inter-comparaison entre les trois différents spectromètres de masse utilisés au cours de ma thèse m'ont amené à réfléchir sur les méthodologies employées lors de l'analyse de bio-carbonates et à reconsidérer la façon d'utiliser les bases de données mises à dispositions via le net.

I. Etude de reproductibilité des analyses isotopiques

Les analyses isotopiques présentées dans ma thèse ont été réalisées sur trois modèles de spectromètres de masse différents dont les caractéristiques sont listées dans la table A-1:

Table A-1 : Caractéristiques des équipements de spectrométrie de masse utilisés dans cette étude.

	équipement # 1	équipement # 2	équipement # 3
Système de génération de CO₂	Thermo Kiel IV®	Multiprep carbonate Gilson®	Multiprep carbonate Gilson®
Spectromètre	Thermo DeltaV Advantage®	GV instrument IsoPrime®	GV instrument Optima®
Température piège à eau (°C)	-120	-70	-70
Température acide Phosphorique (°C)	70	90	90

Pour vérifier dans quelle mesure il était possible de comparer les résultats obtenus sur ces différents équipements, j'ai réalisé des tests d'inter-calibration en analysant des répliqués d'un même échantillon sur des équipements différents. La table A-2 récapitule la nature et le nombre d'échantillons analysés ainsi que l'équipement utilisé.

Table A-2 : Caractéristiques des échantillons analysés dans cette étude.

Référence	Nature	Minéralogie	Remarques	Equ. #1	Equ. #2	Equ. #3
Marceau	marbre	calcite	Réplicats du même échantillon	-	9	8
Macha	bivalve <i>Mesodesma donacium</i>	aragonite	Réplicats du même échantillon	-	10	6
Psp-07-09	corail <i>Porites sp.</i>	aragonite	Échantillons indépendants	102 ($\delta^{13}\text{C}$) 87 ($\delta^{18}\text{O}$)		-

Dans le cas des matériaux Marceau et Macha, plusieurs répliques ont été analysées. Une valeur moyenne et un écart type de $\delta^{13}\text{C}$ et de $\delta^{18}\text{O}$ ont ensuite été calculés pour chaque matériau et pour chaque équipement (Figures A-1a et A-1b). Dans le cas du matériau Psp-07-09, il s'agit d'une série d'échantillons indépendants prélevés le long d'un transect parallèle à l'axe de croissance du corail et analysés une fois avec l'équipement #1 et une seconde fois avec l'équipement #2 (Figure A-1c et A-1d).

Les résultats des inter-comparaisons pour les analyses de $\delta^{13}\text{C}$ et de $\delta^{18}\text{O}$ sont très différents. Sur les deux comparaisons effectuées, #2 vs. #3 (Figures A-1a et A-1b) et #1 vs. #2 (Figures A-1c et A-1d), le $\delta^{13}\text{C}$ montre une très bonne reproductibilité avec des résultats se trouvant sur la droite théorique ($y=x$). En revanche, les analyses de $\delta^{18}\text{O}$ affichent des résultats plus contrastés, la comparaison #1 vs. #2 (Figure A-1b) montre un décalage moyen de 0.26‰ vpdb entre les deux spectromètres, avec un décalage minimum observé pour les valeurs les plus faibles (0.15‰ vpdb) et maximum pour les valeurs les plus élevées (0.36‰ vpdb). Converti en valeurs équivalentes de température en considérant un rapport moyen de 0.2‰ par degrés Celsius (par ex., Epstein et al. 1953; McConnaughey 1989; Weber and Woodhead 1972; Wellington et al. 1996), ceci entraîne un décalage moyen de plus d'un degré Celsius avec un décalage maximum de 1.4°C. La comparaison entre les équipements #2 vs. #3 (Figure A-1d) montre que la droite théorique $y=x$ est incluse dans l'intervalle représentant l'écart-moyen de chaque analyse par rapport à la droite théorique, indiquant que les analyses de ces appareils sont reproductibles. Cependant la dispersion des répliques autour de la droite théorique est importante, ce point sera discuté par la suite.

Les résultats de cette inter-comparaison montrent que la reproductibilité des analyses de $\delta^{13}\text{C}$ sur ces trois équipements est très satisfaisante. En revanche, la reproductibilité des analyses de $\delta^{18}\text{O}$ varie selon l'équipement utilisé. Ainsi un biais systématique de 0.26‰ vpdb équivalent à un écart de température de plus de 1°C, a été observé entre les équipements #2 et #3. La présence de biais systématique entre les équipements utilisés rend extrêmement problématique toute comparaison avec des données d'études précédentes dont les conditions d'analyses ne sont pas connues. Ceci est d'autant plus vrai pour des études portant sur la variabilité climatique Holocène, cette dernière étant caractérisée par des variations de

température de l'eau de surface, à l'échelle millénaire, de faible amplitude, i.e., 1 – 3°C (par ex., Abram et al. 2009; cette étude).

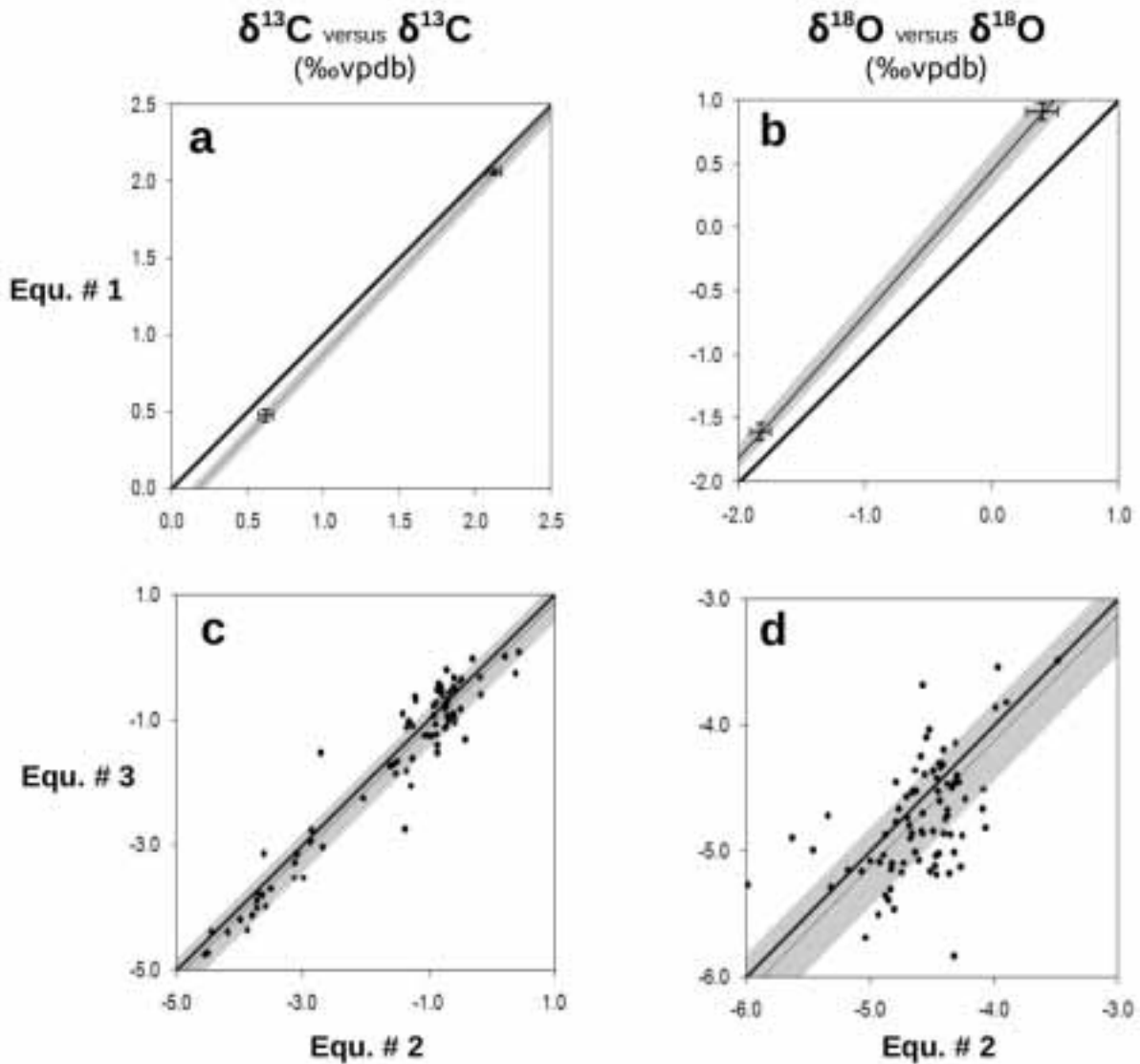


Figure A-1. Comparaison d'analyses isotopiques ($\delta^{13}\text{C}$ et $\delta^{18}\text{O}$) obtenues avec les différents équipements détaillés dans la Table A-1. Comparaison des résultats obtenus avec les équipements #1 versus #2 : **a** - rapport isotopique $\delta^{13}\text{C}$, **b** - rapport isotopique $\delta^{18}\text{O}$. L'intervalle grisé représente \pm un écart-type de part et d'autre de la droite de régression des sets de données comparés. Comparaison des résultats obtenus avec les équipements #3 versus #2 : **c** - rapport isotopique $\delta^{13}\text{C}$, **d** - rapport isotopique $\delta^{18}\text{O}$. L'intervalle grisé représente l'écart-moyen de chaque analyse par rapport à la droite théorique $y=x$.

Ces biais systématiques remettent également en cause l'utilité des fonctions de transfert établies entre un proxy géochimique et la variable qu'il représente, incluant celle produite dans le chapitre II de ma thèse (isotopes stables de l'oxygène de la coquille de bénitier vs. SST). Ainsi on peut s'interroger sur les raisons du décalage systématique d'environ 0.5‰

vpdb observé dans l'ordonnée à l'origine des fonctions de transfert $SST = f(\delta^{18}O_{shell} - \delta^{18}O_{sw})$ établies pour les bénitiers, alors que les pentes de ces fonctions sont quasiment identiques (Figure A-2). Il m'a semblé important de développer ici une réflexion sur les causes possibles des biais systématiques dans les analyses géochimiques des carbonates en m'appuyant sur les résultats précédents i.e., Figure A-1, ainsi que sur une étude bibliographique²⁸.

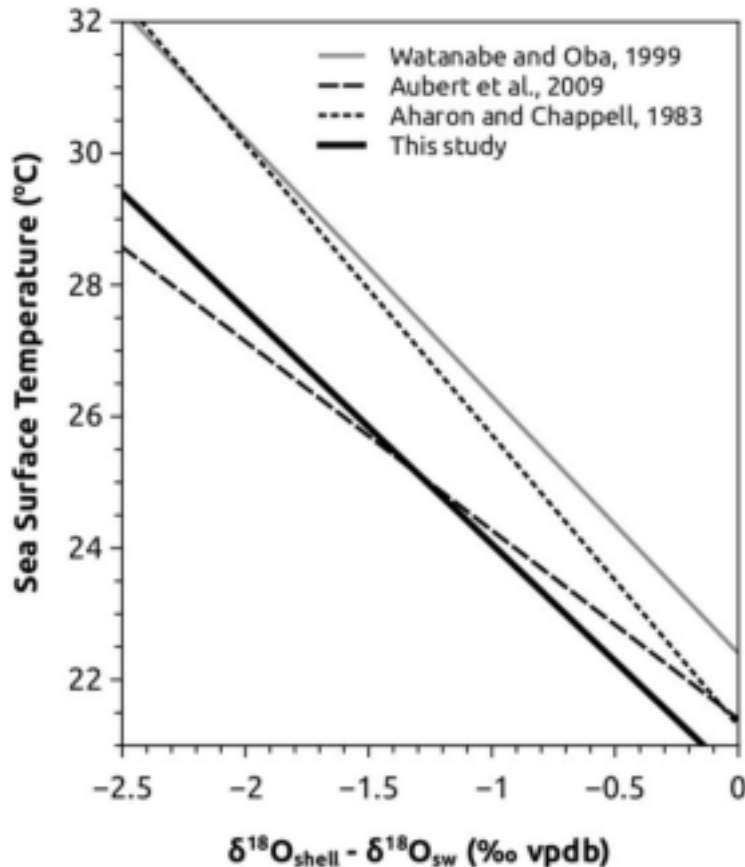


Figure A-2. Droites issues des fonctions de transfert empiriques reliant la différence ($\delta^{18}O_{shell} - \delta^{18}O_{sw}$) à la SST pour les bénitiers *Hippopus hippopus* (Aubert et al. 2009; Watanabe and Oba 1999), *Tridacna maxima* (cette étude) et une fonction calculée à partir de données obtenus sur les deux genres de bénitiers – *Hippopus* et *Tridacna* – (Aharon 1980).

II. Causes possibles des biais systématiques pour les analyses isotopiques (cas du $\delta^{18}O$)

Vapeur d'eau – Lorsque les valeurs de $\delta^{18}O$ présentent un biais alors que le $\delta^{13}C$ reste stable, comme observé dans notre étude, il y a vraisemblablement eu un échange entre le dioxyde de carbone (CO_2) issu de l'échantillon lors de la dissolution par l'acide phosphorique et l'oxygène provenant d'une molécule d'eau (H_2O). Malgré l'utilisation de pièges à eau dans le circuit du spectromètre de masse, il n'est pas exclu que des molécules d'eau persistent dans les volumes et/ou sur les surfaces du circuit de capillaires emprunté par le CO_2 . Les capillaires constituent des surfaces d'échanges privilégiées entre le dioxyde de carbone issu de la dissolution du carbonate et les molécules d'eau. La présence de molécules d'eau dans les capillaires peut s'expliquer par le fait que l'acide utilisé lors de la dissolution du carbonate (acide phosphorique) est fortement hygroscopique et a tendance à se dimériser en libérant une

²⁸ Remarque : le but recherché ici n'est pas de comparer les qualités analytiques des équipements présentés.

molécule d'eau dont l'oxygène peut potentiellement s'échanger avec l'oxygène des molécules de CO₂ issu de l'échantillon. C'est ici que la différence entre l'équipement utilisé peut intervenir. En effet, les températures de fonctionnement des pièges à eau (Table A-1) et la géométrie du circuit emprunté par le CO₂ (i.e., les volumes et surfaces des capillaires) sont différentes sur les trois équipements. De plus, les dispositifs d'extraction de CO₂ des équipements #2 et #3 ne fonctionnent pas de la même manière. Avec le dispositif #2, aucun échange avec l'atmosphère n'est possible à partir de la mise en vial²⁹ jusqu'à l'analyse. En revanche, si l'air contenu dans le vial contient de la vapeur d'eau, un échange peut survenir et ce d'autant plus que le vial est préchauffé à 90°C pendant plusieurs heures avant l'analyse. Dans le dispositif #3, les vials sont placés ouverts dans une enceinte close portée à 70°C ce qui permet un échange avec l'extérieur tant que l'analyse n'est pas réalisée. Ces différences de technologies entre les équipements #2 et #3 pourraient expliquer les biais observés sur les analyses de $\delta^{18}\text{O}$.

Température de l'acide – La différence majeure entre les technologies utilisées dans les équipements #2 et #3 réside dans la température à laquelle se déroule la réaction de dissolution du carbonate par l'acide phosphorique (Table A-1). La température de l'acide entraîne un fractionnement des isotopes de l'oxygène lors de l'attaque. Ce fractionnement, fonction de la température de travail, est en théorie connu et corrigé par le logiciel fourni par le constructeur du spectromètre de masse. Cependant, les équations reliant la température à la valeur du coefficient de fractionnement disponibles dans la littérature ont été calculées à partir de relativement peu de réplicats et les constantes de ces équations (pente et ordonnée à l'origine) diffèrent selon les études. Ainsi, la gamme de valeurs du coefficient de fractionnement de la calcite à 25°C s'étend de 10.10 à 10.52 (Kim et al. 2007). Kim et al. (2007) ont recalculé une valeur du coefficient de fractionnement de la calcite à 25°C à partir d'un nombre plus conséquent de réplicats et ont obtenu une valeur moyenne de 10.25. Les équations reliant la température à la valeur du coefficient de fractionnement possèdent donc une marge d'incertitude qui pourrait également expliquer les problèmes de reproductibilité observés.

La valeur d'usine pour le spectromètre de l'équipement #2 est 10.20. Je n'ai pas pu avoir accès aux valeurs des deux autres équipements, on peut donc s'interroger sur le type d'équation utilisé dans les deux autres spectromètres utilisés pour cette étude. Les données isotopiques disponibles sur le site de la NOAA ne comportent pas de métadonnées précisant ce type d'information, de sorte qu'il est risqué d'effectuer des comparaisons entre les différentes séries de données.

Phénomène de "vieillesse" des échantillons – La figure A-1d montre que, bien qu'il n'y ait pas de biais systématique entre les résultats donnés par les équipements #2 et #3, les valeurs des réplicats de $\delta^{18}\text{O}$ présentent une variabilité importante comparée aux réplicats de $\delta^{13}\text{C}$. Le fait que seul le $\delta^{18}\text{O}$ soit affecté suggère qu'il y a eu échange d'oxygène entre le carbonate et la vapeur d'eau. Les équipements #1 et #2 utilisent le même dispositif d'extraction de CO₂, l'échange entre carbonate et vapeur d'eau pouvant survenir lors de cette

²⁹ Nom donné au tube en verre au fond duquel se trouve la poudre de (bio) carbonate à analyser.

étape n'est donc pas en cause. En revanche une étude de Tobin et al. (2011) a montré qu'un phénomène d'altération ou "vieillessement" de la poudre de carbonate pouvait survenir au cours du temps. Ces auteurs ont ainsi observé une décroissance du rapport isotopique $\delta^{18}\text{O}$ de $-0.1\%.\text{jour}^{-1}$ pour de la poudre de carbonate stockée à 70°C pendant 24 h. La granulométrie de la poudre est un paramètre important dans ce phénomène qui a été observé pour une poudre dont le diamètre des grains était d'environ $10\ \mu\text{m}$. Aucune altération notable du rapport isotopique $\delta^{18}\text{O}$ n'a été observée pour des grains d'un diamètre d'environ $20\ \mu\text{m}$. Tobin et al. (2011) expliquent ce phénomène par un échange entre le carbonate et la vapeur d'eau survenant à la surface des grains. En effet, le volume d'une sphère augmentant plus rapidement que la surface, plus le grain est gros, moins le vieillissement de la poudre a de conséquences sur la valeur moyenne du $\delta^{18}\text{O}$. Le rôle du phénomène de vieillissement des poudres dans les biais systématiques de mesure reste cependant probablement limité car il dépend de la proportion de la fraction de poudre de l'échantillon dont le diamètre est inférieur à $10\ \mu\text{m}$. En revanche il pourrait expliquer la variabilité observée dans la série des 100 répliqués analysés sur les équipements #1 et #2.

III. Matériaux de référence : clé de voûte de la géochimie

Afin d'assurer la répétabilité et la reproductibilité d'une analyse géochimique, un (ou plusieurs) échantillon d'un matériau dont la composition géochimique est connue avec précision est analysé dans les mêmes conditions que les échantillons dont on cherche à déterminer la composition chimique. La composition chimique de ce matériau est déterminée en le faisant analyser par plusieurs laboratoires. La valeur moyenne de ces analyses est considérée comme étant la composition chimique du matériau, qui fera alors office de référence. On parle de valeur certifiée. Les valeurs mesurées sur les matériaux dont la composition est inconnue sont ensuite corrigées (si nécessaire) en fonction de la différence entre la valeur certifiée et la valeur obtenue (mesurée) du matériau de référence. Un matériau de référence doit avoir les caractéristiques suivantes :

- Il doit être de la même nature que le matériau utilisé (du carbonate si le matériau analysé est composé de carbonate etc.),
- La concentration en éléments analysés doit être dans la gamme des valeurs attendues pour le matériau à analyser,
- Il doit être composé de la même matrice que le matériau analysé. Dans le cas des carbonates, selon que l'on travaille avec un matériau minéral ou biogénique, le minéral (par ex., calcite ou aragonite) et la teneur en matière organique (par ex., marbre ou corail) peuvent varier fortement, induisant de potentiels "effets de matrice" qui contribuent à diminuer la précision de l'analyse. Par exemple, on choisira un bémolier de référence pour corriger des analyses géochimiques d'un bémolier dont on cherche la composition.

Ce sont ces matériaux de référence qui sont les garants de l'inter-comparaison des données géochimiques utilisées en paléoclimatologie. Cependant il existe des problèmes liés à la détermination de ces valeurs dites de référence et au choix du matériau de référence.

Cas des analyses de Strontium/Calcium : Pour les analyses de rapport strontium/calcium dans les coraux du genre *Porites sp.*, un des matériau de référence utilisé est le JCp-1 qui est issu du squelette d'une colonie de corail du genre *Porites sp.* collectée dans les îles Ryukyu – Japon – (Inoue et al. 2004; Okai et al. 2002). Le matériau de référence choisi est donc tout à fait adapté au matériau à analyser et le fait que le matériau de référence et le matériau à analyser soient issus d'organismes du même genre permet une correction optimale de l'effet de matrice. Le problème majeur rencontré avec ce matériau est sa valeur de référence en strontium/calcium qui n'est pas encore établie avec précision. La figure A-3 montre des valeurs de température de surface reconstruites à partir de ce matériau de référence JCp-1 analysé par 18 laboratoires différents répartis sur 4 continents.

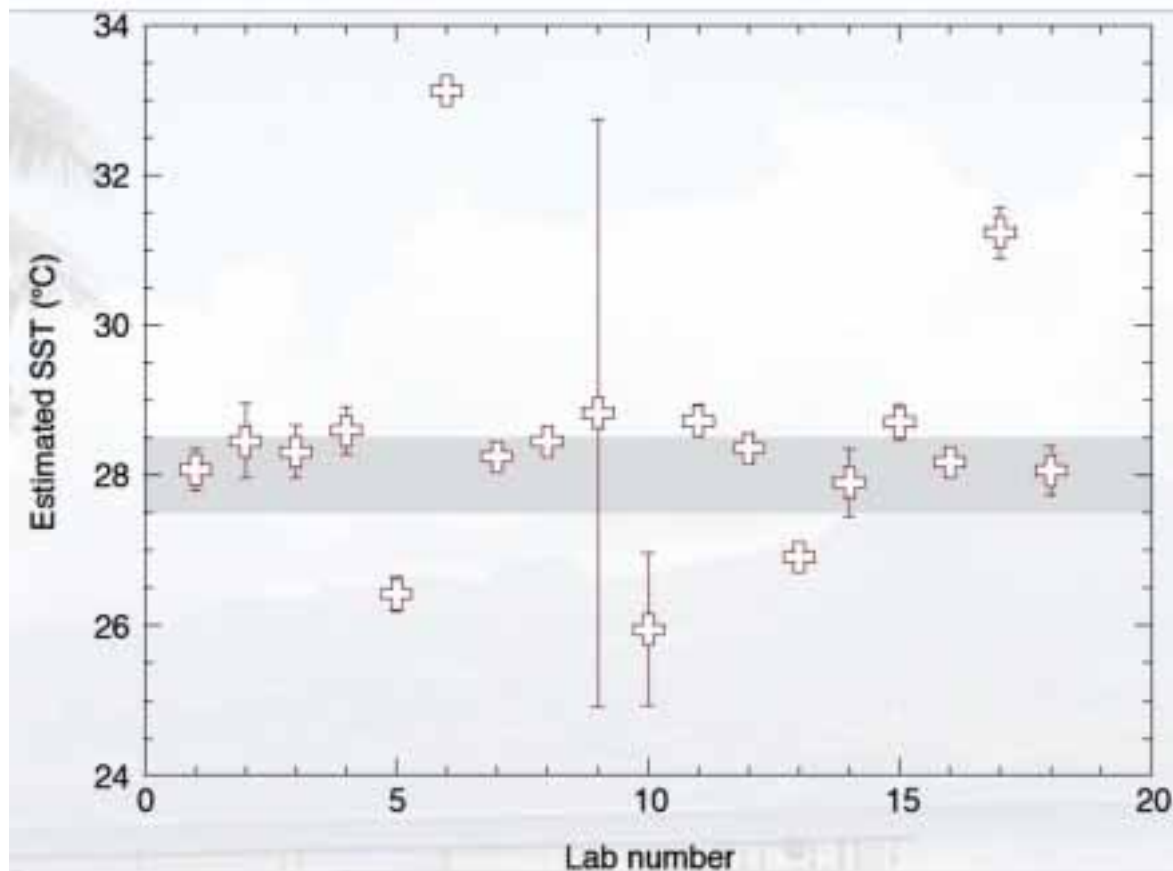


Figure A-3. Reconstruction de température des eaux de surface (SST) obtenue à partir de valeurs moyenne du matériau de référence JCp-1 (corail *Porites sp.*) analysés dans 18 laboratoires différents. Les barres d'erreur représentent l'écart-type des analyses effectuées dans les différents laboratoires. Dans certains cas ces barres d'erreurs sont plus petites que les symboles. La bande grisée représente un intervalle de correspondance à 1°C. D'après Hathorne et al. (2010).

La gamme de température obtenue est de près de 7°C, correspondant à des valeurs en Sr/Ca variant de 8.54 à 8.98 mmol/mol. Une telle différence de température reconstituée à partir d'analyses d'un même matériau est très clairement bien trop importante par rapport à la

précision nécessaire lors d'études paléoclimatiques. D'autre part, les études paléoclimatiques (reconstructions ou calibrations) basées sur des analyses de Sr/Ca précisent rarement si un matériau de référence a été utilisé ni, le cas échéant, quelle valeur certifiée a été utilisée (par ex., Abram et al. 2009; Beck 1997; Gagan et al. 1998; Kilbourne et al. 2004; McCulloch et al. 1996; Morimoto et al. 2002; Ren et al. 2002). Comme pour les fonctions de transfert établies pour les bénitiers, les fonctions calculées pour le rapport Sr/Ca et la SST dans les coraux présentent des variations importantes de l'ordonnée à l'origine alors que les pentes sont similaires (Figure A-4).

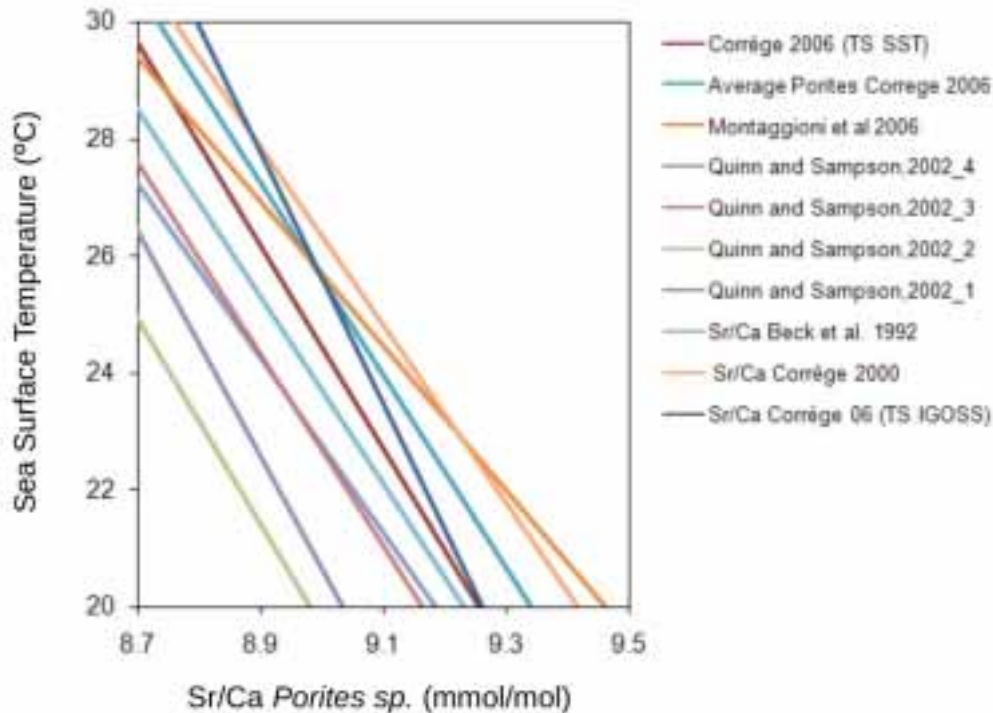


Figure A-4. Droites issues des fonctions de transfert empiriques reliant le rapport strontium-calcium à la température des eaux de surface (SST) calculées pour l'espèce de corail massif *Porites* sp. (Beck et al. 1992; Corrège 2006; Corrège et al. 2000; Montaggioni et al. 2006; Quinn and Sampson 2002)

Ceci laisse penser qu'une partie de ces erreurs pourrait être due à des biais systématiques liés 1/ à une absence d'utilisation de matériaux de référence 2/ à des valeurs certifiées non unifiées. Ceci illustre d'une part les disparités qui existent entre les laboratoires et donc l'importance d'utiliser le même matériau de référence lors d'analyses à des fins paléoclimatiques et d'autre part la difficulté à déterminer des valeurs de références certifiées.

Cas des analyses de $\delta^{18}\text{O}$: Lors de l'engouement des paléoclimatologues pour l'étude des isotopes stables de l'oxygène ($\delta^{18}\text{O}$) des archives carbonatées biogéniques dans les années 1950, un matériau de référence a été créé à partir de tests fossiles du bélemnite *Belemnitella americana* provenant de la formation géologique PeeDee en Caroline de Sud, États-Unis

(Craig 1957; Craig 1953; Epstein et al. 1953; Epstein et al. 1951). La composition isotopique de ce matériau de référence, désigné par le sigle PDB, est arbitrairement définie comme le point zéro des mesures de $\delta^{18}\text{O}$ et de $\delta^{13}\text{C}$. Lorsque ce matériau a été épuisé, il a été remplacé par d'autres matériaux calibrés par rapport au PDB lui-même : le Vienna PeeDee Belemnite et le marbre NBS-19 qui sont toujours utilisés aujourd'hui pour corriger les mesures isotopiques faites sur les bio-carbonates, incluant les coraux et les bénitiers.

Ces trois matériaux de référence sont composés de calcite alors que les coraux et les bénitiers sont composés d'aragonite : la matrice des matériaux de référence utilisés depuis 50 ans n'est donc pas la même que celle des matériaux analysés. Ceci est en contradiction avec le point numéro 3 concernant les caractéristiques des matériaux de références. Pourtant, une étude de Kim et al. (2007) montre que, lors de la dissolution par l'acide phosphorique, les coefficients de fractionnement de l'aragonite et de la calcite ne varient pas de la même façon suivant la température de l'acide (Figure A-5). Bien que les valeurs des coefficients produits par Kim et al. (2007) soient contestés par Gilg et al. (2007) ces derniers s'accordent à dire que les coefficients de fractionnement entre calcite et aragonite peuvent différer de 0.2‰. Bien que Gilg et al. (2007) considèrent cette valeur comme faible, il s'agit néanmoins d'une erreur de l'ordre de 1°C en termes de paléo-température.

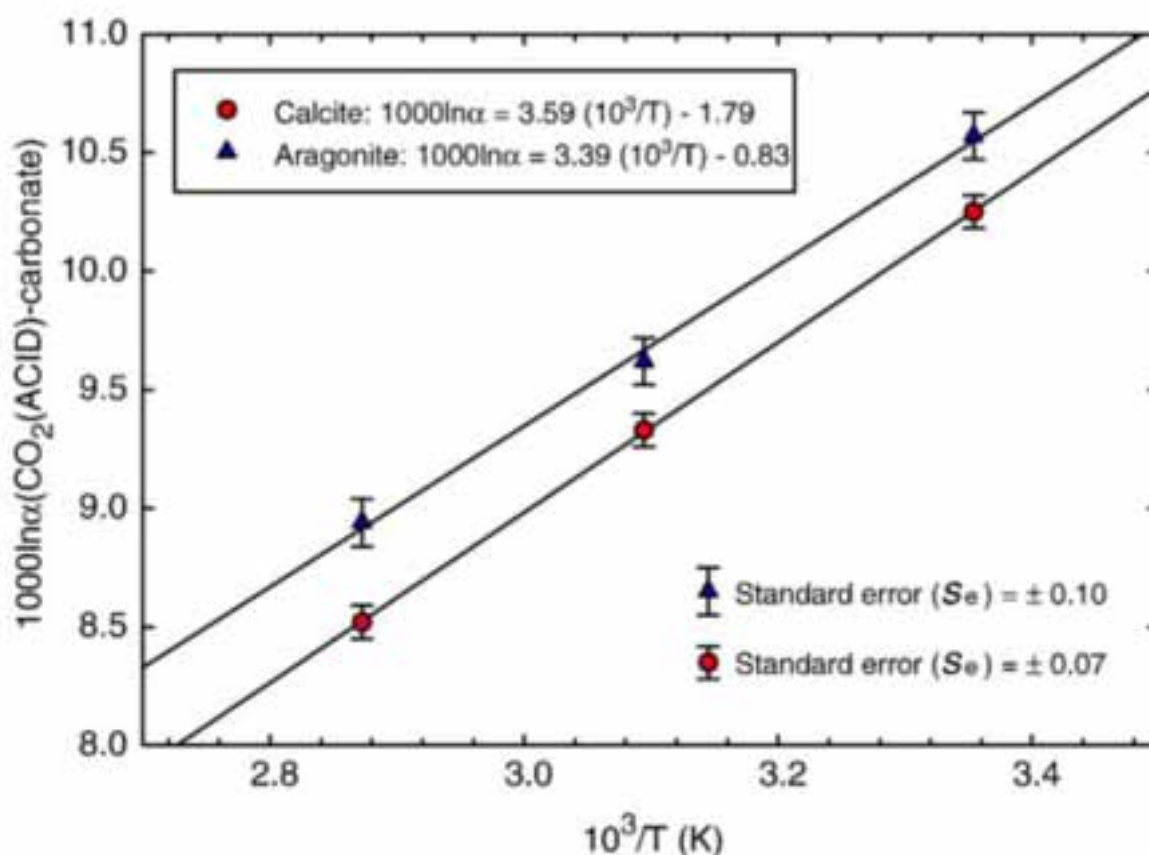


Figure A-5. Relation entre le coefficient de fractionnement de l'aragonite (triangles bleus) et de la calcite (cercles rouges) lors de la dissolution du carbonate de calcium par l'acide phosphorique, en fonction de la température de ce dernier (exprimé en 10^3 kelvin⁻¹). Les deux équations correspondantes sont également représentées. D'après Kim et al. (2007).

Parmi les 21 travaux (en 2012) qui citent le papier de Kim et al. (2007), aucun ne traite de paléo-reconstructions basées sur des analyses de corail ou de bénitiers. L'article de Gilg et al. (2007), quant à lui, n'est cité qu'une seule fois. D'autre part, il est intéressant de noter que les logiciels intégrés aux trois spectromètres utilisés dans cette étude ne permettent pas de modifier les valeurs de la relation entre les coefficients de fractionnement. Ceci montre le peu d'intérêt porté à ces problèmes d'une part par la communauté des paléo-climatologues, et d'autre part par les constructeurs des spectromètres de masse.

IV. Conclusions, Préconisations et Perspectives

Compte tenu des biais systématiques affectant potentiellement les fonctions de transfert, il n'est pas possible de comparer quantitativement des données géochimiques issues d'archives fossiles ou modernes analysées sur des équipements différents, sauf si une inter-calibration a pu être réalisée. Les données géochimiques issues de l'analyse d'archives fossiles doivent être interprétées à la lumière d'archives modernes analysées sur les mêmes équipements et non à celle de données instrumentales.

Dans le cas des bio-carbonates, il est impératif d'utiliser des matériaux de référence qui proviennent d'un organisme de la même espèce (ou au moins du même genre) afin de pouvoir corriger de manière optimale l'effet de matrice. Lorsqu'aucun matériau de référence n'existe dans le commerce, comme c'est le cas pour les analyses de $\delta^{18}\text{O}$ et de $\delta^{13}\text{C}$ pour les coraux et bénitiers, ou lorsque la valeur certifiée d'un matériau est contestée, comme c'est le cas pour le Sr/Ca pour JCp-1, il est indispensable de pallier ce manque par la création d'un matériau de référence interne pour corriger *a minima* l'effet de matrice de manière optimale. Il est également possible d'envisager une correction *a posteriori* des séries d'analyses réalisées alors que la valeur du matériau de référence ne reposait pas sur un nombre significatifs de répliqués. La création d'un matériau de référence est donc un investissement à long terme pour les laboratoires d'isotopie.

Plus généralement, il est indispensable de continuer les recherches sur l'influence de la température de l'acide phosphorique sur le coefficient de fractionnement de la calcite et de l'aragonite afin d'établir des bases robustes qui permettraient une standardisation des mesures isotopiques au niveau international. De même, ces observations soulèvent également le problème lié au manque de métadonnées concernant l'utilisation des matériaux de référence et des valeurs certifiées utilisées lors de l'analyse des données géochimiques accessibles sur internet.


Références

- Abram NJ, McGregor HV, Gagan MK, et al. (2009) Oscillations in the southern extent of the Indo-Pacific Warm Pool during the mid-Holocene. *Quaternary Science Reviews* 28:2794–2803.
- Aharon P (1980) Stable isotope geochemistry of a late quaternary coral reef sequence, New Guinea : application of high resolution data to paleoclimatology. Ph.D thesis, Australian National University
- Aubert A, Lazareth CE, Cabioch G, et al. (2009) The tropical giant clam *Hippopus hippopus* shell, a new archive of environmental conditions as revealed by sclerochronological and $\delta^{18}\text{O}$ profiles. *Coral Reefs* 28 : 989–998.
- Beck JW (1997) Abrupt changes in early Holocene tropical sea surface temperature from coral Sr/Ca thermometry. *Nature* 385 : 705–707.
- Beck JW, Edwards RL, Ito E, et al. (1992) Sea-surface temperature from coral skeletal strontium/calcium ratios. *Science* 257 : 644–647.
- Corrège T (2006) Sea surface temperature and salinity reconstruction from coral geochemical tracers. *Palaeogeography Palaeoclimatology Palaeoecology* 232 : 408–428.
- Corrège T, Delcroix T, Recy J, et al. (2000) Evidence for stronger El Niño-Southern Oscillation (ENSO) events in a mid-Holocene massive coral. *Paleoceanography* 15 : 465–470.
- Craig H (1957) Isotopic standards for carbon and oxygen and correction factors for mass-spectrometric analysis of carbon dioxide. *Geochimica et Cosmochimica Acta* 12 : 133–149.
- Craig H (1953) The geochemistry of the stable carbon isotopes. *Geochimica et Cosmochimica Acta* 3 : 53–92.
- Epstein S, Buchsbaum R, Lowenstam H, Urey HC (1951) Carbonate-water isotopic temperature scale. *Geological Society of America Bulletin* 62 : 417–426.
- Epstein S, Buchsbaum R, Lowenstam HA, Urey HC (1953) Revised carbonate-water isotopic temperature scale. *Geological Society of America Bulletin* 64 : 1315–1326.
- Gagan MK, Ayliffe LK, Hopley D, et al. (1998) Temperature and surface-ocean water balance of the mid-Holocene tropical Western Pacific. *Science* 279 : 1014–1018.
- Gilg H, Taubald H, Struck U (2007) Phosphoric acid fractionation factors for aragonite between 25 and 72°C with implications on aragonite-calcite oxygen isotope fractionation. *Geochimica Cosmochimica Acta* 71 : A323.
- Hathorne E, Adkins J, Asami R, et al. (2010) An inter-laboratory study of coral Sr/Ca and other element/Ca ratios. 10th International Conference on Paleoceanography, ICP 10
- Inoue M, Nohara M, Okai T, et al. (2004) Concentrations of trace elements in carbonate reference materials coral JCp-1 and giant clam JCT-1 by inductively coupled plasma-mass spectrometry. *Geostandards and Geoanalytical Research* 28 : 411–416.
- Kilbourne KH, Quinn TM, Taylor FW, et al. (2004) El Niño-Southern Oscillation-related salinity variations recorded in the skeletal geochemistry of a *Porites* coral from Espiritu Santo, Vanuatu. *Paleoceanography*
- Kim ST, Mucci A, Taylor BE (2007) Phosphoric acid fractionation factors for calcite and aragonite between 25 and 75 C : revisited. *Chemical Geology* 246 : 135–146.
- McConnaughey T (1989) C-13 and O-18 isotopic disequilibrium in biological carbonates.2. invitro simulation of kinetic isotope effects. *Geochimica Et Cosmochimica Acta* 53 : 163–171.
- McCulloch M, Mortimer G, Esat T, et al. (1996) High resolution windows into early Holocene climate : Sr/Ca coral records from the Huon Peninsula. *Earth and Planetary Science Letters* 138 : 169–178.

- Montaggioni LF, Le Cornec F, Corrège T, Cabioch G (2006) Coral barium/calcium record of mid-Holocene upwelling activity in New Caledonia, South-West Pacific. *Palaeogeography Palaeoclimatology Palaeoecology* 237 : 436–455.
- Morimoto M, Abe O, Kayanne H, et al. (2002) Salinity records for the 1997–98 El Niño from Western Pacific corals. *Geophysical Research Letters* 29 : 4 PP.
- Okai T, Suzuki A, Kawahata H, et al. (2002) Preparation of a New Geological Survey of Japan Geochemical Reference Material : Coral JCp 1. *Geostandards Newsletter* 26 : 95–99.
- Quinn TM, Sampson DE (2002) A multiproxy approach to reconstructing sea surface conditions using coral skeleton geochemistry. *Paleoceanography* 17 : 1062.
- Ren L, Linsley BK, Wellington GM, et al. (2002) Deconvolving the delta O-18 seawater component from subseasonal coral delta O-18 and Sr/Ca at Rarotonga in the southwestern subtropical Pacific for the period 1726 to 1997. *Geochimica Et Cosmochimica Acta* 67 : 1609–1621.
- Tobin TS, Schauer AJ, Lewarch E (2011) Alteration of micromilled carbonate $\delta^{18}\text{O}$ during Kiel Device analysis. *Rapid Communications in Mass Spectrometry* 25 : 2149–2152.
- Watanabe T, Oba T (1999) Daily reconstruction of water temperature from oxygen isotopic ratios of a modern *Tridacna* shell using a freezing microtome sampling technique. *Journal of Geophysical Research* 104 : PP. 20,667–20,674.
- Weber JN, Woodhead PMJ (1972) Temperature dependence of oxygen-18 concentration in reef coral carbonates. *J Geophys Res* 77 : 463–473.
- Wellington GM, Dunbar RB, Merlen G (1996) Calibration of stable oxygen isotope signatures in Galapagos corals. *Paleoceanography* 11 : 467–480.



Session Paléocéanographie et Paléoclimatologie de la conférence de l'American Geophysical Union, lors de la présentation des résultats du chapitre III et de l'étude suivante – annexe 2 (posters.) San Francisco, É.U. Décembre 2011. Crédit photo: N. Duprey.



Annexe II – article: Digital correction of computed x-radiographs for coral densitometry

Ce chapitre est publié dans la revue *Journal of Experimental Marine Biology and Ecology*.

Remarque : l'article est présenté sous le format de la revue



Contents lists available at SciVerse ScienceDirect

Journal of Experimental Marine Biology and Ecology

journal homepage: www.elsevier.com/locate/jembe

Digital correction of computed X-radiographs for coral densitometry

Nicolas Duprey^{a,*}, Hugues Boucher^a, Carlos Jiménez^{b,1}^a IPSL/LOCEAN, UPMC/CNRS/IRD/MNHN, IRD Bondy, 93143, France^b Centro de Investigación en Ciencias del Mar y Limnología (CIMAR), Universidad de Costa Rica, San Pedro, 11501-2060 San José, Costa Rica

ARTICLE INFO

Article history:

Received 25 July 2011

Received in revised form 7 September 2012

Accepted 17 September 2012

Available online xxxx

Keywords:

Calcification rate

Coral densitometry

Coral skeleton

Density

Porites sp.*Siderastrea siderea*

ABSTRACT

The recent increase in sea surface temperature and ocean acidification raises major concerns about the evolution of the coral calcification rate. Digitized X-radiographs have been used for coral skeleton density measurements since the 1980s. The main limitation of coral densitometry from digitized X-radiographs is the X-ray intensity heterogeneity due to spherical spreading (inverse square law) and heel effect. Until now, extra X-ray images or aluminum standards have been used to correct X-radiographs. However, such corrective methods may be constraining when working with a high number of coral samples. Here, we present an inexpensive, straightforward, and accurate digital detrending (DD) method to correct the heterogeneities of the X-ray irradiation that affect X-radiographs. The X-radiograph is corrected against the irradiation imprint recorded by its own background using a kriging interpolation method, thus allowing reliable optical density measurements directly on the corrected X-ray image. This digital detrending (DD) method was validated using skeletal bulk density measurements and computerized tomography (CT). Coral densitometry using DD corrected X-radiographs does not require the destruction of the coral sample and provides high-resolution measurements. Since DD does not require extra aluminum standards to correct X-radiographs, this method optimizes the working space available on the X-ray image. Moreover, it corrects the entire X-radiograph, thus larger samples or numerous samples can be X-rayed at the same time.

© 2012 Elsevier B. . All rights reserved.

1. Introduction

Recent changes evidenced in global sea surface temperature (SST) and oceans' pH, raise major concerns about the future of coral reefs (IPCC, 2007; Kleypas, 1999; Pandolfi et al., 2011). A major consequence of ocean pH decrease is the diminution of the aragonite saturation state (Ω_{arag}). A compilation of data documenting calcification response to the Ω_{arag} decrease among individual coral species, coral mesocosms and *in situ* reef communities, showed that this response was consistently negative (Pandolfi et al., 2011). Since the early 1990's an unprecedented declining trend of the coral calcification rate (product of the annual extension rate and the coral skeleton density) has been observed in Great Barrier Reef records, most probably due to the recent increase in SST and to ocean acidification (Cooper et al., 2008; De'ath et al., 2009). Conversely, coral response to combined ocean warming and pH decrease appears highly variable and often non-linear. Moreover, coral response is also greatly influenced by other factors such as nutrients, pollutants or salinity so that projecting the future of coral reefs in a global warming and ocean acidification context is still uncertain (Pandolfi et

al., 2011). As stated by the IPCC report (2007) "acidification is an emerging issue with potential for major impacts in coastal areas, but there is little understanding of the details. It is an urgent topic for further research, especially programs of observation and measurement". Documenting the long term trends in coral calcification is crucial in understanding the mechanisms and implications of ocean acidification on coral reefs, in order to predict coral reef future.

Coral calcification rate (CR) is calculated by $CR = ER \times d$, where (ER) is the annual extension rate and (d) is the coral skeleton density. Whereas extension rate can be directly measured from the banding pattern revealed by X-radiography, many methods have been developed since the 1970s to measure skeletal density. Direct measurements have been performed based on mercury displacement (Dustan, 1975), water displacement (Hughes, 1987) and coral pore volume calculation (Carricart-Ganivet et al., 2000). Although these methods provide reliable measurements, they are time consuming, imply the destruction of the sample and provide low measurement resolution (generally performed by sampling annual growth increments). Methods that do not require the destruction of the coral sample, such as gamma densitometry (Chalker and Barnes, 1990) or medical X-ray computerized tomography (CT) (Bosscher, 1993) are quick and provide higher resolutions (less than one millimeter, i.e., monthly resolution or higher). However, these methods rely on specialized and expensive equipment, not always easily accessible. Alternative methods for coral skeleton density measurement are based on digitized X-radiographs (Carricart-Ganivet and Barnes,

* Corresponding author at: Institut de Recherche pour le Développement IRD, 32 Avenue Henri aragnat, 93140 Bondy France. Tel.: +33 688932745; fax: +33 148025554.

E-mail address: nicolas_duprey@yahoo.fr (N. Duprey).

¹ Present address: Energy, Environment and Water Research Center (EEWRC) of The Cyprus Institute. P.O. Box 27456, CY-1645 Nicosia, Cyprus.

2007; Chalker et al., 1985; Helmle et al., 2000). Optical densities (OD)² of X-radiographs are measured on film or on digital images and converted into density values using OD reference standards (e.g., *Tridacna maxima* shells and/or aluminum wedges).

An important drawback is that X-radiographic instruments do not provide uniform irradiation of the entire area covered by the X-ray film and may therefore result in misleading density measurements. Two reasons account for such irradiation heterogeneities: the heel effect which is defined by an irradiation gradient along the anode–cathode axis and the inverse square law which states that the irradiation is inversely proportional to the square of the distance from the X-ray source (Carricart-Ganivet and Barnes, 2007; Chalker et al., 1985; Helmle et al., 2000; Meredith and Massey, 1971). The irradiation gradient caused by the heel effect may lead to biases in density measurements up to 26% (Chalker et al., 1985), which is similar to the seasonal density variations that are reported for massive corals *Montastrea annularis* (20% – Carricart-Ganivet and Barnes, 2007), *Porites* sp. (15% – this study) and *Siderastrea siderea* (30% – this study). Several alternative methods have been proposed to overcome such miscalculations. For example, Helmle et al. (2002) performed paired X-radiographs (using the same settings) of a coral sample and an aluminum plate. Therefore, it was possible to correct the coral sample image from the irradiation heterogeneities recorded by the aluminum plate's X-radiograph. However, considering that each X-radiograph has to be taken twice, this technique becomes expensive and time-consuming when a high number of samples have to be analyzed. Carricart-Ganivet and Barnes (2007) proposed a simple way for correcting the heel effect. The correction is based on the measurement of OD variations on an aluminum bar located beside the coral sample along the anode–cathode axis. The heel effect-related distortions are then measured, and extrapolated over coral samples. The method provides a reliable one-dimensional correction along the anode–cathode axis. Unfortunately, the extrapolation of this correction to the whole X-radiograph image may only be applied upon particular settings (X-ray source to film distance and film dimension).

In the present study, we introduce a digital detrending (DD) method which corrects the heterogeneously irradiated X-radiographs. This method is inexpensive, straightforward and accurate. The DD method uses the X-ray irradiation imprint, recorded by the X-radiograph's background, to reconstruct a full image of the irradiation pattern. The X-radiograph's background is defined here as the image area without any objects or graphical information such as letters or numbers. The resulting modeled image is then subtracted from the original X-ray image, therefore enabling reliable optical density measurements from the corrected X-ray image. This method provides a correction of X-ray irradiation heterogeneities on the whole X-radiograph, which means a two-dimensional correction. The digital detrending (DD) method was used for densitometry measurements on samples of widely studied massive corals *Porites* sp. and *S. siderea* (De'ath et al., 2009; Guzman and Tudhope, 1998; Lough and Cooper, 2011).

2. Materials and methods

2.1. Computed X-radiography

Experiments were performed using a medical computed radiography (CR) device. CR produces digitized images obtained directly from an imaging plate (IP) instead of a conventional photo sensitive film. IP is placed beneath coral slabs before being irradiated (Fig. 1a). The final result is an 8 bits digitized image (pixel values comprised between 0 and 255). Such an image can be used for optical density

(OD) measurements and be easily modified with conventional image-processing software. CR is affected by heterogeneous X-ray irradiation just like conventional radiography.

The CR device was a Super Contact® X-ray device (General Electric Company). X-radiographs were acquired with Fuji® imaging plates made of photosensitive phosphorus. Digitized images were then obtained using an IP reader (Fuji® FCR 5000). The resolution of this device is lower than conventional X-radiography.

2.2. X-ray irradiation heterogeneities

2.2.1. Heel effect

The heel effect is responsible for the irradiation intensity gradient along the anode–cathode axis: the electrons emitted from the cathode interact with the anode resulting in a high exposure at the cathode side of the IP and a decrease toward the anode side (Fig. 1b).

2.2.2. Inverse square law

The inverse square law models the three-dimensional spherical spreading of the X-ray beam: irradiation intensity is attenuated by a factor proportional to the inverse of the squared distance from the X-ray source to the IP surface. As IP is generally centered beneath the X-ray source, the irradiation pattern shows over-exposed area at the center of the image, decreasing toward the edges (Fig. 1b). The influence of spherical spreading on the irradiation pattern gets lower with increasing source–subject distance.

The inverse square law specifies that the ratio of X-ray intensity on the IP (I_1) to intensity on the subject surface (I_2) is:

$$\frac{I_1}{I_2} = \frac{(S_p - s)^2}{(S_p)^2} \quad (1)$$

where S_p = source to IP distance and s = sample thickness.

2.3. Computed tomography

Computed tomography (CT), with its high-contrast resolution, allows accurate and reliable density measurements, as this method is not influenced by the X-ray beam distortion phenomena that usually affect computed radiography. A CT-scan was used to compare density profiles measured on DD corrected images to the density profile of the CT scan. The computerized tomography device used was a Phillips Brilliance 40®. CT density values are expressed as Hounsfield units.

2.4. Reference materials

We used two massive corals slabs as reference samples. Reference slab R_s was cut off a core drilled in 2008 from a living colony of the reef-building species *S. siderea* at Cahuita reef (9°44'N–82°48'W), Limón, Costa Rica. R_s size was 280 × 70 mm; slab thickness (s) was 5 mm. Reference slab R_p was cut off from a living colony of the reef-building species *Porites* sp. at the *Fausse Passe de Uitoé* reef (22°17'S–166°10'E), New-Caledonia, France, in 2010. This coral was collected alive and transferred into an aquarium in 2008. R_p size was 150 × 150 mm and the slab thickness (s) was 10 mm. For coral density measurements, a reference transect for both slabs was set along the maximum growth axis, perpendicular to the growth increments. For R_s , the reference transect tr_s was 87 mm long and encompassed 15 couplets of high and low density bands; for R_p , the reference transect tr_p was 130 mm long and encompassed 13 couplets of high and low density bands. In order to avoid as much as possible intra-corallite density variations, the width of the density transects was 10 mm to include approximately three *S. siderea* corallites (polyps mean diameter ~3 mm) and ten *Porites* sp. corallites (polyps mean diameter ~1 mm).

² In the following study the Optical Density (OD) refers to the gray level from 0 to 255 corresponding to the 8 bits coding of the digital images.

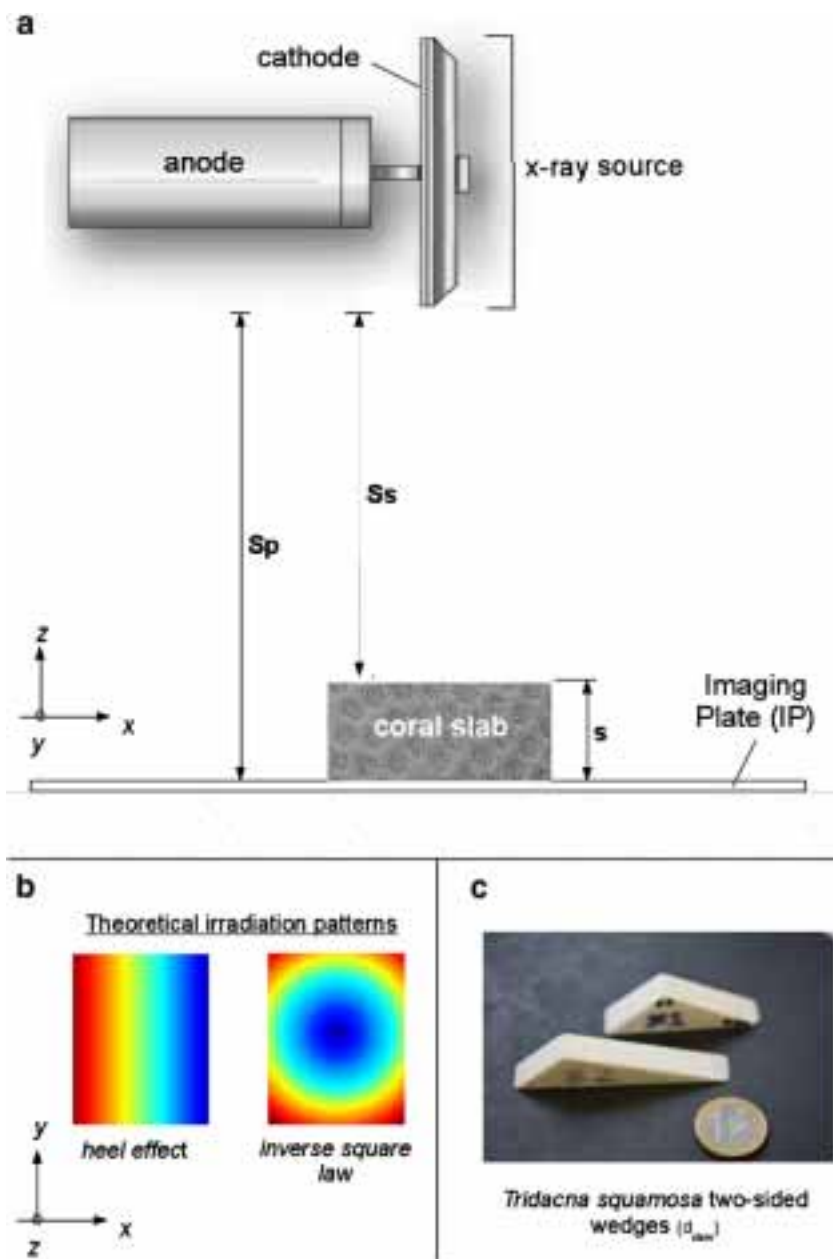


Fig. 1. Computed radiography (CR). a – scheme of the settings used in this study: the anode–cathode axis is along the x axis, S_p is the X-ray source to IP surface distance, S_s is the X-ray source to coral sample surface and s is the sample thickness. b – theoretical irradiation patterns that affect CR, the color scale shows the attenuation of the irradiation; blue: no attenuation, red: high attenuation. c – photograph of the two giant clam wedges (d_{clam}) used for the density calibration, scale is given by the one Euro money coin. (For interpretation of the references to color in this figure legend, the reader is referred to the web version of this article.)

2.5. Density scaling

Density scaling is based on two, two-sided wedges (d_{clam} – Fig. 1c) cut from the internal layer of a giant clam's shell *Tridacna squamosa*. One wedge is 17.4 mm high and 54.2 mm long with slopes of 26.6° and 41.2°. The second wedge is 15.9 mm high and 71.8 mm long with slopes of 43.4° and 16.0°. The bulk densities of the wedges were obtained by weighing with a hydrostatic balance.

Care should be given when cutting a wedge into a giant clams' shell as it is composed of three distinct aragonitic layers (internal layer, external layer and hinge layer) which present their distinct density and crystallographic structure (N. Duprey, unpublished data). To avoid any measurement bias, wedges must be cut into either external or internal shell layer. X-radiographs revealed that the density of the whole shell's internal layer (d_{shell}) was homogeneous.

To ensure the consistency of the density scaling, another scaling standard (d_{powder}) was added on some X-radiographs for comparison purposes. Standard d_{powder} is composed of 14 plastic cubes filled with *Porites sp.* coral aragonite powder (grain size < 200 μm). Each cube was filled with a carefully weighted amount of powder to obtain a density scale from 0 to 3 for an equivalent sample thickness of 12 mm.

Both plastic cubes filled with coral powder and wedges have a similar range of density values. However, wedges were favored for their small sizes because these optimize the space available on the X-radiograph, so that more coral samples can be X-rayed at the same time.

2.6. X-radiographs

All the X-radiographs and their characteristics are listed in Table 1. For this study, we used eight X-radiographs made with the CR device

Table 1
Characteristics of the computed X-radiographs used in this study.

Group	Label	Samples orientation ^a	Sp (cm)	Reference samples ^b	Density standard ^c	k	mAs	date
A	A1	Perpendicular	130	R _s + R _p	d _{clam}	73	8.0	04–2012
	A2	Parallel						
	A3	Diagonal						
B	B1	Perpendicular	80	R _s + R _p	d _{clam}	70	6.4	04–2012
	B2	Parallel						
	B3	Diagonal						
C	C1	Perpendicular	100	R _s	d _{powder}	73	8.0	07–2010
	C2	Perpendicular		R _p + coral cubes	d _{powder} + d _{clam}	73	8.0	11–2010

^a Along the anode–cathode axis.

^b R_s: *Siderastrea siderea*; R_p: *Porites* sp.

^c d_{clam}: *Tridacna squamosa* two-sided wedges; d_{powder}: plastic cubes filled with coral powder.

previously described. The main purpose of these X-radiographs was to test the reliability of the digital detrending method depending on the distance Sp and sample orientation along the anode–cathode axis. Therefore, coral reference samples were placed along three directions with regard to the anode–cathode axis: perpendicular, parallel and diagonal. Selected distances (Sp) were 130 cm, 100 cm and 80 cm. X-radiographs were acquired over a two-year period, providing the opportunity to test the DD method against a potential machine drift over time.

Merely considering the inverse square law and the IP size (355 × 428 mm), the minimum exposures at image edges would be 11.8%, 8.1% and 5.0% less than the exposures at the center for Sp = 80 cm, Sp = 100 cm and Sp = 130 cm, respectively.

X-radiograph C2 was used to test the density calibration of the two density standards (d_{powder} and d_{clam}). For that purpose we used 13 *Porites* sp. cubes (~2 cm³) which bulk densities were determined by weighting with a hydrostatic balance. Coral cube density ranged from 1.21 to 1.39 g·cm⁻³.

2.7. Digital detrending procedure

The first stage of the digital detrending (DD) process is the background area selection. This area is used as a recorder of the irradiation pattern. The background area selection aims to remove all saturated margins, all pixels corresponding to samples and optical density scale or information, from the original X-radiograph (Fig. 2a). This background extraction is made using the *magic stick* tool of the image processing software GIMP® (or equivalent). This step leaves empty areas corresponding to objects' locations (Fig. 2b). Missing OD values are interpolated using a kriging interpolation from the dacefit MATLAB® toolbox (Lophaven et al., 2002). The result is a complete image of OD variations (Fig. 2c) following the overall pattern presented by the original background area. The corrected image is obtained by subtracting the modeled background to the original image (Fig. 2d).

The DD method initially supposes that the X-ray intensity at the IP surface is similar to the X-ray intensity at the sample surface. However, X-ray source to sample surface distance (Ss) is smaller than X-ray source to IP surface distance (Sp). Considering Eq. (1), it can be stated that the spherical spreading causes the X-ray intensity to be higher at the sample surface than at the IP surface. This may generate a small bias in measurement, thereafter referred as thickness bias, leading to a slightly overestimated density. This bias can be reduced by decreasing the sample thickness and corrected during the DD process by dividing corresponding background values with the ratio I₁/I₂.

X-ray attenuation in air may also account for the difference between X-ray intensities at sample and IP surfaces. Coral densitometry studies are usually performed on samples with thickness less than 10 mm. According to the air mass attenuation coefficient table from the National Institute of Standards and Technology, X-ray attenuation for a 10 mm air layer is negligible (Table 2).

2.8. Digital detrending evaluation

In order to optimize the DD procedure we had to test first if the X-ray irradiation imprint on the IP remains identical while maintaining the X-ray source settings and the Sp distance constant (α). If this last assumption is true, then a standard correction could be used within a group of X-radiographs made with the same settings. Therefore, the DD procedure would be simplified and faster. If not, each X-radiograph should be corrected with the irradiation record of its own background. By taking pair-wise images, α was tested using the mean relative difference of OD (ΔOD_(i,j)).

The relative difference of OD (δOD_(i,j,k)) at point k for images i and j is defined as:

$$\delta OD_{i,j,k} = \frac{|(OD_i(x_{(k)},y_{(k)}) - OD_j(x_{(k)},y_{(k)}))|}{OD_i(x_{(k)},y_{(k)})} \quad (2)$$

where OD_i(x_(k),y_(k)) is the OD value at image coordinates (x_(k),y_(k)) for image i and OD_j(x_(k),y_(k)) is the OD value at image coordinates (x_(k),y_(k)) for image j.

The mean relative difference of OD (ΔOD_(i,j)) for images i and j is:

$$\Delta OD_{i,j} = \frac{1}{n} \times \sum_{k=1}^n \delta OD_{i,j,k} \quad (3)$$

where n is the number of pixel coordinates shared by image i and j backgrounds.

Considering the causes of the X-ray irradiation heterogeneities, the reliability of the digital detrending process had to be tested through two other assumptions.

The DD method corrects and preserves the density information of the sample independently of:

- (β) – the sample orientation along the anode–cathode axis
- (γ) – the distance S_p.

The density information of the coral samples refers to the density variability (qualitative information) and to the density value (quantitative information). β was tested by measuring the coral density profiles (tr_s and tr_p) on sample set perpendicularly, parallel and diagonally to the anode/cathode axis, while the other settings remained unchanged. Intra-group A density transect comparisons evaluated the ability of the DD method to correct the irradiation heterogeneities mainly caused by the heel effect (independently of the sample orientation along the anode–cathode axis). Intra-group B density transect comparisons evaluated the correction of both the heel effect and the inverse square law heterogeneities (independently of the sample orientation along the anode–cathode axis). γ was tested by inter-group (A and B) comparisons. The comparison of inter-groups (A, B and C) was used to assess the ability of the DD method to cope with a potential machine

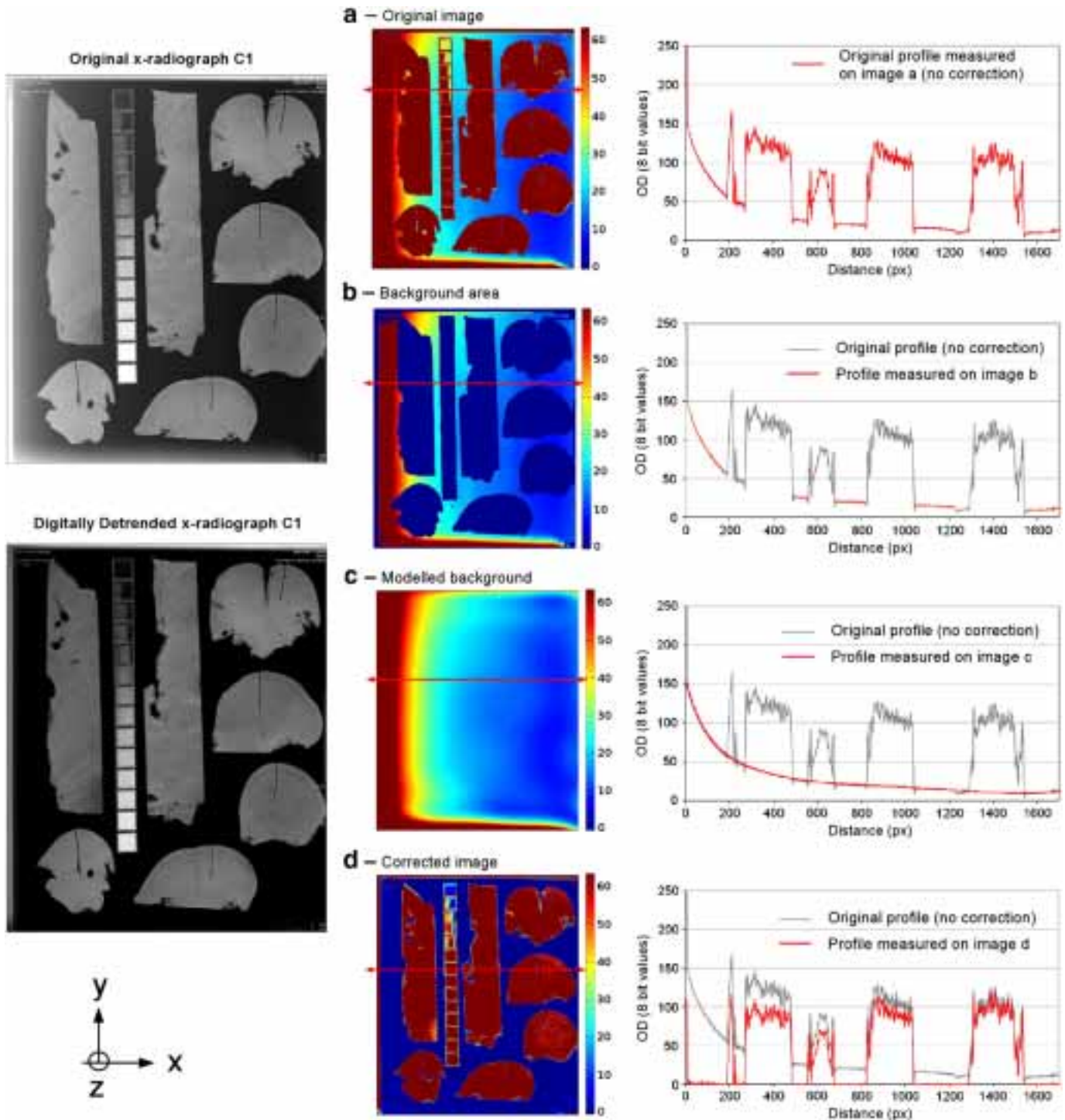


Fig. 2. X-radiograph C1 left: original and digitally detrended image in black and white right: optical density (OD) variations on the whole image (false colors) and along the red transect (graph). a – original image: note the heterogeneities affecting the background, resulting on both effects of inverse square law and heel effect. b – original background area: saturated margin, sample objects or graphical information have been removed. c – modeled background d – detrended image: i.e., (b) minus (d). (For interpretation of the references to colour in this figure legend, the reader is referred to the web version of this article.)

drift over time. Finally, to ensure that the DD method yields the same density variations as other density measurement techniques, the density measurements made on a DD corrected image were compared to computed tomography scanning measurements.

To test the previous assumptions, density values were measured along tr_s and tr_p for each X-radiograph. The correlation between the density profiles was tested using the regression coefficient R^2 . Furthermore, relative standard deviations (RSD) were calculated at each point along transects of the compared X-radiographs and

averaged in order to compile the results. These mean relative standard deviation (RSD) values were used to evaluate the precision (reproducibility) of density measurements.

The mean relative standard deviation (RSD) for compared transects is defined as:

$$RSD = \frac{1}{p} \times \sum_{i=1}^p rsd_i \quad (4)$$

Table 2

X-photon energy attenuation for 1 cm air layer and a 30–150 ke energy range. Data from National Institute of Standards and Technology [www.nist.gov].

X-photon energy (ke)	Energy attenuation for 1 cm air layer (%)
30	0.043
40	0.030
50	0.025
60	0.023
80	0.020
100	0.019
150	0.016

where p is the number of points along the compared transects [$p(\text{tr}_s) = 439$ and $p(\text{tr}_p) = 666$] and rsd_i represents the relative standard deviation of the density at point i .

2.9. Density calibration

OD values were converted into densities using the two, two-sided wedges cut from the internal layer of a giant clam's shell *T. squamosa*. The OD values on DD corrected X-radiographs were measured along the two sides of both wedges using the ImageJ® software. As giant clam shell also contains organic matter, which influences bulk density, wedge thicknesses had to be corrected in order to obtain equivalent thicknesses, corresponding to wedges made of pure aragonite. Thereafter, a wedge's equivalent thickness was defined as T_{w100} .

The equivalent thickness scaling at each point along a wedge was calculated by:

$$T_{w100} = \frac{T_x \times d_{\text{shell}}}{d_{\text{arag}}} \quad (5)$$

where T_x = measures wedge thickness, d_{shell} = shell wedge density ($\text{g} \cdot \text{cm}^{-3}$) and d_{arag} = density of pure aragonite ($2.930 \text{ g} \cdot \text{cm}^{-3}$).

OD values were then paired with corresponding equivalent thicknesses (T_{w100}) calculated along the wedges. Paired OD and T_{w100} values from the two wedges were pooled and fitted by a quadratic polynomial function:

$$\text{OD} = a \cdot T_{w100}^2 + b \cdot T_{w100} + c \quad (6)$$

where a , b and c constants are the coefficients determined by the polynomial fitting for the studied X-radiograph.

Eq. (6) obtained from the wedges' data was then reversely used to convert OD values of coral samples into pure aragonite equivalent thicknesses (T_{s100}). Subsequently, coral sample density values (d) were obtained from T_{s100} :

$$d = \frac{T_{s100}}{T_s} \cdot d_{\text{arag}} \quad (7)$$

where d = coral sample density ($\text{g} \cdot \text{cm}^{-3}$), T_{s100} = pure aragonite equivalent thickness for coral sample, T_s = measured coral sample thickness and d_{arag} = density of pure aragonite ($2.930 \text{ g} \cdot \text{cm}^{-3}$).

2.10. Calibration's validation

In order to validate our density calibration using *T. squamosa* wedges, OD measurements were performed on coral cubes and plastic cubes filled with coral powder on the detrended X-radiograph C1. OD values were converted into densities using previous Eqs. (5) to (7). These values were regressed against bulk density measurements performed on the same coral and plastic cube standards.

Table 3

Optical density mean relative difference ΔOD (%) of the X-radiograph background area.

Groups compared	ΔOD range (%) ^a
Intra-group A	8–77
Intra-group B	15–164
Intra-group C	59–290
A vs. B	25–147
A vs. C	41–223
B vs. C	64–198

^a Pairs of pixels compared: $9.2 \cdot 10^5 < n < 2.3 \cdot 10^6$.

The relative error (re_i) of X-radiograph density measurements was calculated for each coral cube:

$$\text{re}_i = 100 \cdot \frac{|d_{\text{calc.}(i)} - d_{\text{bulk.}(i)}|}{d_{\text{bulk.}(i)}} \quad (8)$$

where $d_{\text{calc.}(i)}$ is the density of coral cube i calculated from OD after digital detrending ($\text{g} \cdot \text{cm}^{-3}$) and $d_{\text{bulk.}(i)}$ is the bulk density ($\text{g} \cdot \text{cm}^{-3}$) of coral cube i .

The mean relative error (RE) of X-radiograph density measurements was evaluated by averaging the relative errors (re_i) of coral cubes:

$$\text{RE} = \frac{1}{n} \times \sum_{i=1}^n \text{re}_i \quad (9)$$

where $n = 14$ is the number of coral cubes (*Porites* sp.).

3. Results

3.1. Reproducibility of the irradiation imprint (α)

The background area of the eight X-radiographs viewed in false colors show a strong OD gradient along the anode–cathode axis, with low OD at the anode side increasing toward the cathode side. This pattern is a characteristic of the heel effect (Fig. 1a). A concentric OD pattern, characteristic of the spherical spreading, is noticeable on some images. As expected, X-radiographs with high distance Sp (groups A) present a less marked concentric pattern than X-radiographs with low distance Sp (group B). OD mean relative difference (ΔOD) of X-radiographs backgrounds ranges from 8% up to 290% (Table 3). Intra-group and inter-group comparisons lead to similar ΔOD : most X-radiographs present highly variable background OD values: assumption α is thus not valid within our experimental settings.

3.2. Influence of the sample orientation along the anode–cathode axis (β) and of the Sp distance (γ)

Density profiles measured on corrected X-radiographs of groups A and B are well correlated (Table 4). Inter-group and intra-group correlation coefficient values (R^2) are significant and have a similar range from 0.90 to 1.00 ($p < 0.001$).

Inter-group mean relative standard deviation and intra-group mean relative standard deviation (RSD) of densities measured on

Table 4

Correlation coefficient R^2 range ($p < 0.001$) for transects tr_s and tr_p made on the corrected X-radiographs of groups A, B and C.

Corrected X-radiographs	tr_s	tr_p
Intra-group A	$0.90 < R^2 < 0.98$	$0.99 < R^2 < 1.00$
Intra-group B	$0.96 < R^2 < 0.98$	$0.95 < R^2 < 0.99$
Inter-groups (A and B)	$0.90 < R^2 < 0.99$	$0.97 < R^2 < 1.00$
All X-radiographs	$0.85 < R^2 < 0.99$	$0.95 < R^2 < 1.00$

Table 5
RSD measured along tr_s and tr_p using the uncorrected and corrected X-radiographs.

	RSD (%) uncorrected	RSD (%) DD corrected
Intra-group A	10.1	4.8
Intra-group B	13.1	4.3
Inter-groups (A and B)	16.0	5.5
All X-radiographs	16.1	6.8

uncorrected images range from 10.1 to 16.0% (Table 5). Density profiles measured on corrected images show a RSD reduced by a factor of 2 to 3. No differences are noticed between the inter-group RSD and intra-group RSD, which are both around 4–5%.

The variations and the precision of density measurements from the corrected images show no difference regarding the sample orientation along the anode–cathode axis (β) or the Sp distance (γ). Assumptions β and γ are thus validated within our experimental settings.

3.3. Density measurement precision on DD corrected images

RSD calculated over all uncorrected X-radiographs (groups A, B and C, 14 transects = $7 \times tr_s$ and $7 \times tr_p$) reaches 16.1% (Table 5). RSD

calculated over all DD corrected X-radiographs is 6.8%. These values include measurements made on X-radiographs of two coral samples of different genus, set on three different ways along the anode–cathode axis, with three different distances (Sp), made across a two-year period.

3.4. Density variations

The tr_s and tr_p density profiles, measured on uncorrected images, shown as examples in Fig. 3, present seasonal density variations comprised around 30 and 15% respectively. Profile tr_s measured on the uncorrected image presents an increasing trend with a maximum density difference reaching 50%. The mean profile tr_s from DD corrected images does not present any remarkable trend. This mean profile tr_s shows density variations identical to the CT scan density profile variations (Fig. 3a). This correlation is a robust result as each of the seven density profiles tr_s , measured on corrected X-radiographs, is significantly correlated with the density profile made on the CT scan ($0.89 < R^2 < 0.96$; $p < 0.001$; Table 6). The DD method thus eliminates the density trend caused by the X-ray heterogeneities. Conversely, the magnitude of the seasonal density variations is not affected by the DD correction.

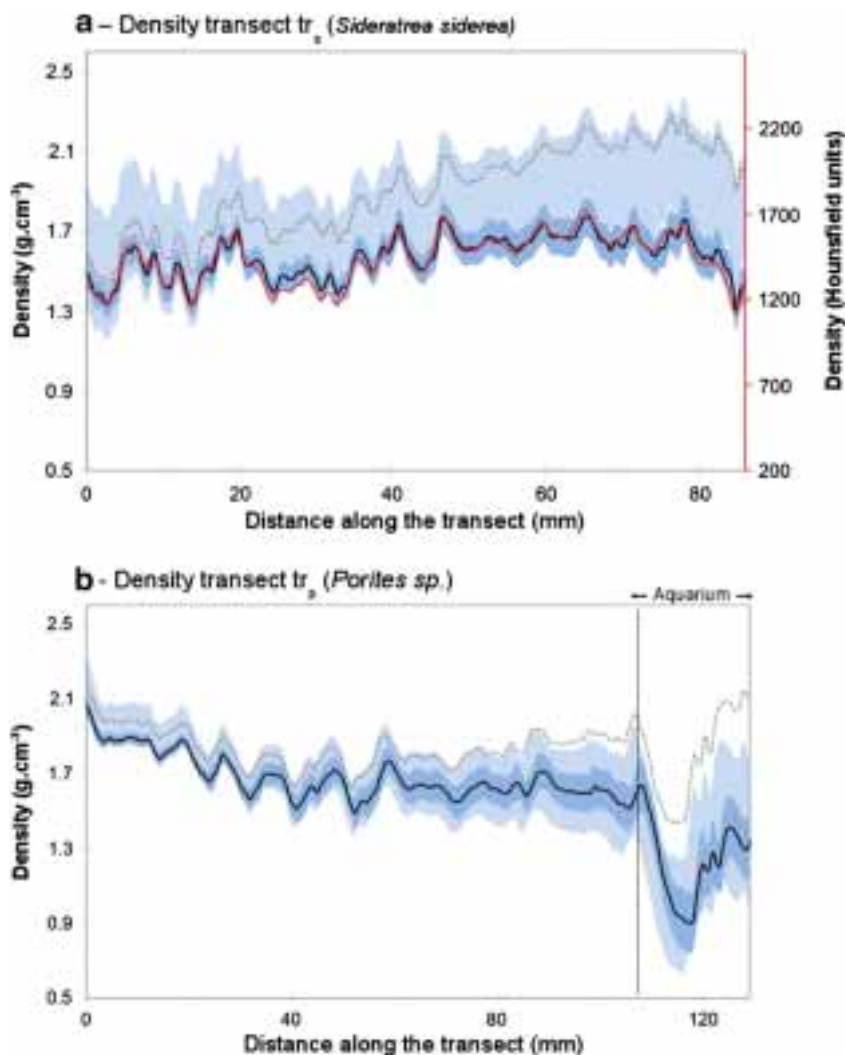


Fig. 3. Density measured along the reference transects tr_s (a) and tr_p (b). Black curve is the mean density calculated from the seven corrected images with one standard deviation interval (dark blue). The red curve is the density measured on the CT scan (values are expressed in Hounsfield units). The light blue areas correspond to standard deviation of mean densities calculated from the uncorrected images (1σ). Examples of density transects from uncorrected images are shown (dotted line). (For interpretation of the references to color in this figure legend, the reader is referred to the web version of this article.)

Table 6
Correlation coefficient R^2 of transects tr_s made on the corrected X-radiographs versus the measurements made on the CT-scan.

Corrected X-radiographs	R^2 ($p < 0.001$)
A1	0.93
A2	0.96
A3	0.95
B1	0.93
B2	0.94
B3	0.96
C1	0.89

Profile tr_p from the uncorrected image (Fig. 3b) displays a density drop that matches with the transfer of sample R_p from the reef to the aquarium. This profile also displays a parabolic trend with a maximum density difference reaching 50%. The DD method removes the parabolic trend of the profile tr_p , and highlights a linear declining trend with density difference reaching 40%. The density drop (sample R_p transfer) is not affected by the DD correction.

3.5. Density calibration

The four sides of the two, two-sided *T. squamosa* wedges (Fig. 1c) returned identical OD versus T_{w100} profiles ($R^2 = 0.9998$, $p < 0.001$, Fig. 4). Density values, calculated from corrected X-radiograph C2, are regressed against the bulk density values (coral cubes and plastic cubes filled with coral powder – Fig. 5). This regression presents a significant correlation coefficient ($R^2 = 0.99$; $p < 0.001$; $n = 27$). Comparison between bulk densities of the 14 *Porites sp.* coral cubes and the calculated density values show that the mean relative error (RE – Eq. (9)) is 3.32%.

4. Discussion

Computed X-radiographs commonly show an uneven exposure due to both the heel effect and the spherical spreading. Such irradiation heterogeneities may lead to variations in coral density up to 50% (Fig. 3). These density variations exceed the seasonal variations commonly observed in massive coral: 30% for *S. siderea*, 15% for *Porites sp.* and about 20% for *Montastrea annularis* (Carricart-Ganivet and Barnes, 2007). These variations in density may lead to biased

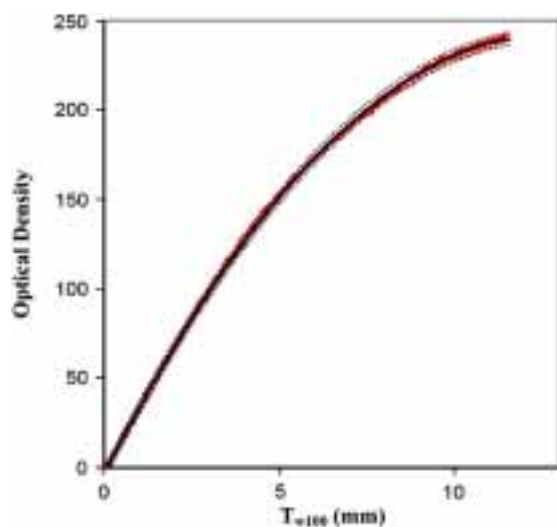


Fig. 4. OD from detrended X-radiograph C2 plotted versus wedge's equivalent thickness (T_{w100}). Red dots: (OD, T_{w100}) pooled dataset. Black line corresponds to a quadratic polynomial fitting. Dashed lines indicate 99% confidence interval. (For interpretation of the references to color in this figure legend, the reader is referred to the web version of this article.)

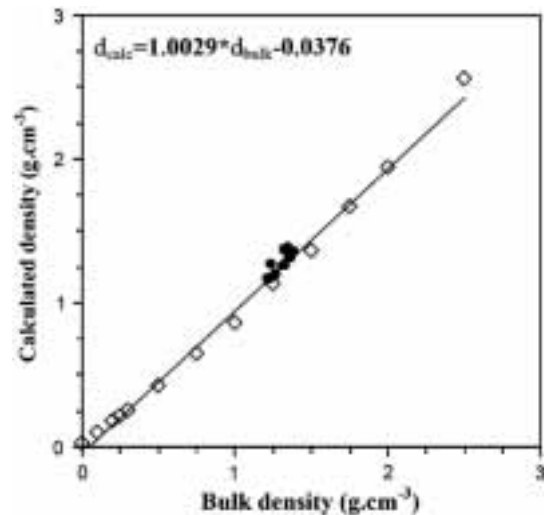


Fig. 5. Plot of bulk densities (d_{bulk}) of cubes filled with coral powder (squares, $n = 14$) and coral cubes (circles, $n = 13$) versus densities (d_{calc}) calculated from digitally detrended C1.

calcification rate calculation and thus to wrong environmental interpretations.

The digital detrending method, presented here, aimed to correct the irradiation heterogeneities that affect conventional and computed X-radiography. X-radiographs were corrected against the irradiation pattern recorded by the background of the image. The first step of this study was to test if the X-ray irradiation imprint on the imaging plates (IP) remains identical while maintaining the X-ray source settings and the Sp distance constant. Our results showed that the X-ray irradiation imprint recorded by the IP was highly variable, even with constant X-ray source settings and Sp distance. X-ray irradiation records must be considered as unique and thus cannot be transposed to another X-radiograph, even within constant settings. These results are in accordance with previous studies (Carricart-Ganivet and Barnes, 2007; Chalker et al., 1985). The X-ray irradiation records may be affected by several factors including the X-ray device stability, the X-ray tube aging and also the recording abilities of the IP or film sensitiveness (Carricart-Ganivet and Barnes, 2007).

Density profiles from DD corrected X-radiographs were highly correlated to the density profile measured on the computed tomography scan. These R^2 correlation values were not affected by the orientation of the sample along the anode–cathode axis and the distance from the X-ray source (Table 6). The DD method was thus able to correct X-radiographs of coral samples, showing strong irradiation heterogeneities; independently of the sample orientation along the anode–cathode axis and the distance from the X-ray source. Furthermore, this study revealed that the coral intrinsic density variations (e.g., seasonal density variations or punctual events) contained by the X-radiograph are preserved during the DD process (Fig. 3).

The mean relative error on density measurements of 14 coral cubes of *Porites sp.*, using giant clam *T. squamosa* wedges as density standard (Eq. (9)), was 3.32%. Causes of such an error may be related to the IP sensitiveness (i.e., signal to noise ratio) and to the chemical composition differences between giant clam shell and coral skeleton that could induce a bias up to 2% in density measurements (Chalker et al., 1985). Carbonate structure differences between coral slabs and shell wedges may also contribute to this error, potentially generating diffusion and/or diffraction of the incident X-ray.

Enhancing the number of density measurements from 14 up to 7735 measured points (439×7 tr_s values and 666×7 tr_p values), the overall precision of the coral densitometry from DD corrected X-radiographs reaches 6.8% (Table 5 and Fig. 3). It is important to notice that this value includes the error intrinsic to X-radiography

device (noise of the recorded X-ray signal and potential machine drift over time), the error related to the DD correction itself and the error of the density calibration process. This value is noteworthy compared to the biases in density measurements, caused by uncorrected irradiation heterogeneities that reach up to 50%. In addition, the overall error on density measurement is below the range of the seasonal density variations reported previously for massive coral skeleton.

The efficiency of our DD method relies on the X-ray irradiation pattern recorded by the background. As a result, it is necessary to optimize the background area all over the X-radiograph: samples must be scattered all over the IP with spacing of a few centimeters in between and from the plate edges. We recommend to space X-rayed objects by more than 1 cm between each and to keep a two centimeter margin from the edges. Consequently, larger samples or numerous samples can be X-rayed at the same time and compared on the same image as shown on X-radiograph C1 (Fig. 2). The DD method is straightforward, as it does not rely on specific radiography device settings and does not need any prior assumption on the causes of X-ray beam heterogeneities. DD method saves time as it does not require extra X-radiographs to correct the irradiation heterogeneities. Our detrending method could also be applied onto digitized conventional X-radiographs. The DD method applied to such X-radiographs would provide the opportunity to perform qualitative density measurements on X-radiographs from previous studies. Quantitative density measurements would be even possible for X-radiographs acquired with a density scale.

The digital detrending method is a powerful tool for monitoring the impact of ocean acidification and global warming on coral calcification rates. This cheap, inexpensive, quick and straightforward method is appropriate for large scale studies. This method could also be applied on paleo-environmental/climatic studies.

Acknowledgments

The authors thank the radiology staff of Jean Erdier hospital (Bondy, Seine Saint Denis, France) for their professional help and patience with computerized X-radiographs and CT scans. We thank Claire E. Lazareth, Henning Kuhnert, Ruth Gingold, Marielle Dumestre, Christine Omuombo, Mercedes Mendez-Millan and two anonymous reviewers for their relevant corrections and comments.

Coral sample R_s was drilled with funds provided by the ice-rectory of Research of the University of Costa Rica (project

808-A8-602) during an internship (N.D.), facilitated by the exchange program of the University of La Rochelle and the University of Costa Rica a program supported by the “Bourse régionale de la découverte” (région Poitou-Charentes). Coral sample R_p was collected during a field trip done in the framework of the HOLBECO project, supported by the French INSU-EC2CO program (managed by the IFREMER Institute). [RH]

References

- Boscher, H., 1993. Computerized-tomography and skeletal density of coral skeletons. *Coral Reefs* 12, 97–103.
- Carricart-Ganivet, J.P., Barnes, D.J., 2007. Densitometry from digitized images of X-radiographs: methodology for measurement of coral skeletal density. *J. Exp. Mar. Biol. Ecol.* 344, 67–72.
- Carricart-Ganivet, J.P., Beltran-Torres, A.U., Merino, M., Ruiz-Zarate, M.A., 2000. Skeletal extension, density and calcification rate of the reef building coral *Montastraea annularis* (Ellis and Solander) in the Mexican Caribbean. *Bull. Mar. Sci.* 66, 215–224.
- Chalker, B.E., Barnes, D.J., 1990. Gamma densitometry for the measurement of skeletal density. *Coral Reefs* 9, 11–23.
- Chalker, B.E., Barnes, D.J., Isdale, P., 1985. Calibration of X-ray densitometry for the measurement of coral skeletal density. *Coral Reefs* 4, 95–100.
- Cooper, T.F., De'Ath, G., Fabricius, K.E., Lough, J.M., 2008. Declining coral calcification in massive *Porites* in two nearshore regions of the northern Great Barrier Reef. *Glob. Chang. Biol.* 14, 529–538.
- De'Ath, G., Lough, J.M., Fabricius, K.E., 2009. Declining coral calcification on the Great Barrier Reef. *Science* 323, 116.
- Dustan, P., 1975. Growth and form in reef-building coral *Montastrea annularis*. *Mar. Biol.* 33, 101–107.
- Guzman, H.M., Tudhope, A.W., 1998. Seasonal variation in skeletal extension rate and stable isotopic (¹³C/¹²C and ¹⁸O/¹⁶O) composition in response to several environmental variables in the Caribbean reef coral *Siderastrea siderea*. *Mar. Ecol. Prog. Ser.* 166, 109–118.
- Helmle, K.P., Dodge, R.E., Ketcham, R.A., 2000. Skeletal architecture and density banding in *Diploria strigosa* by X-ray computed tomography. Proceedings 9th International Coral Reef Symposium, Bali, Indonesia 23–27 October 2000 1, pp. 365–371.
- Helmle, K.P., Kohler, K., Dodge, R.E., 2002. Relative optical densitometry and the Coral X-radiograph Densitometry System: Coral XDS. International Society of Reef Studies European Meeting, Cambridge, England.
- Hughes, T.P., 1987. Skeletal density and growth form of corals. *Mar. Ecol. Prog. Ser.* 35, 259–266.
- Kleypas, J.A., 1999. Geochemical consequences of increased atmospheric carbon dioxide on coral reefs. *Science* 284, 118–120.
- Lophaven, S.N., Nielsen, H.B., Søndergaard, J., 2002. A Matlab Kriging Toolbox.
- Lough, J.M., Cooper, T.F., 2011. New insights from coral growth band studies in an era of rapid environmental change. *Earth Sci. Rev.* 108, 170–184.
- Meredith, W.H., Massey, J.B., 1971. *Fundamental Physics of Radiology*, 2nd edn. John Wright Sons Ltd, Bristol. (661 pp.).
- Pandolfi, J.M., Connolly, S.R., Marshall, D.J., Cohen, A.L., 2011. Projecting coral reef futures under global warming and ocean acidification. *Science* 333, 418–422.
- Solomon, S., Qin, D., Manning, M., et al. (Eds.), 2007. *Climate Change 2007: The Physical Science Basis*. Cambridge University Press.